UNIVERSIDADE D
COIMBRA

Maria Mafalda Santos Costa

Mycobacterial Methylmannose Polysaccharides' Biosynthesis

Tese no âmbito do Doutoramento em Biologia Experimental e Biomedicina, ramo de Biologia Molecular, Celular e do Desenvolvimento, orientada pelo Doutor Nuno Miguel da Silva Empadinhas e coorientada pelo Doutor Pedro José Barbosa Pereira e pela Doutora Sandra Morais Cardoso e apresentada ao Instituto de Investigação Interdisciplinar da Universidade de Coimbra.

Fevereiro de 2019

Instituto de Investigação Interdisciplinar da Universidade de Coimbra

Mycobacterial Methylmannose Polysaccharides' Biosynthesis

Maria Mafalda Santos Costa

Tese no âmbito do Doutoramento em Biologia Experimental e Biomedicina, ramo de Biologia Molecular, Celular e do Desenvolvimento, orientada pelo Doutor Nuno Miguel da Silva Empadinhas e coorientada pelo Doutor Pedro José Barbosa Pereira e pela Doutora Sandra Morais Cardoso e apresentada ao Instituto de Investigação Interdisciplinar da Universidade de Coimbra.

Fevereiro de 2019

UNIVERSIDADE D
COIMBRA

AGRADECIMENTOS

Em primeiro lugar gostaria de agradecer ao Doutor Nuno Empadinhas por me ter desafiado a arriscar nesta aventura, confiando no meu trabalho e na minha determinação para o fazer. Sempre disponível para debater ideias e acreditando neste projeto desde início, ajudou a tornar-me mais resiliente e com maior sentido crítico.

Ao meu coorientador, Doutor Pedro Pereira pela prontidão demonstrada ao longo deste percurso, disponibilizando recursos necessários ao progresso deste trabalho em momentos mais conturbados. Agradeço ainda ao seu grupo pela colaboração neste trabalho, nomeadamente pela disponibilidade em debater possíveis ideias e estratégias a seguir.

À Doutora Sandra Morais Cardoso por assumir a responsabilidade interna da tese.

À Doutora Rita Ventura por me ter aberto as portas do seu laboratório e me ter recebido tão bem, providenciando sempre toda a ajuda e ferramentas necessárias (incluindo material, reagentes, solventes e afins) para o progresso deste trabalho. Obrigada por estar constantemente disponível, por confiar no meu trabalho e por ter permitido explorar o meu gosto por química orgânica que já vinha da licenciatura!

Aos meus pilares no laboratório: "chefinha" Su, embora o primeiro impacto após ter partido uma TLC do Vítor não tenha sido o melhor, a minha opinião depressa mudou depois de começar a trabalhar contigo! Tornaste-te na minha companheira de sorrisos e de lágrimas, de abraços e de palavras, bastando muitas vezes um olhar para comunicarmos e lermos os pensamentos uma da outra! Ajudaste-me a crescer a todos os níveis, foste as minhas braçadeiras para me manter à superfície e ter-te ao meu lado todos os dias, partilhando os bons e maus momentos, foi fundamental para chegar aqui! "Levo-te comigo prá vida!" ♥

"Mini-chefe" Ana, em 2011 fui a tua primeira aprendiza a quem começaste a transmitir a tua paixão pela ciência e pelas micobactérias e agora sou a "tua" primeira doutoranda que acompanhaste sempre de perto! Muitas vezes foste os remos do meu barco, ultrapassando comigo as lutas diárias e marés de resultados negativos com palavras sábias, ajudas imprescindíveis, ideias fundamentais, mantendo-me sempre à tona sem me deixar afogar! Agradeço-te por tudo e nesta última fase pela ajuda e tempo dispensado a este manuscrito.

PS: Não me irei esquecer da história do sistema de filtração! Prontinho a usar e tu desmontas super rápido pecinha a pecinha, borrachinha a borrachinha e dizes "vá agora monta tu!". E aos "novos aprendizes" já explicas muito calmamente e eles nem precisam de o montar outra vez! O eterno trauma de ter sido a tua primeira "cobaia"! Ahah ♥

A todos os colegas/amigos que fazem/fizeram parte do grupo: Diogo, Daniela, Ritinha (o FPLC nunca mais foi o mesmo sem ti!), Cristina (minha Tininha), Ana Monteiro (minha despassarada), Adele, Xaroca, Pau, Catarina, Beatriz, Antonella, Inês e Mariana…cada um deixou a sua marca ao longo deste percurso, cultivando sempre o espírito de entreajuda, a boa disposição e também as brincadeiras no laboratório!

À Fundação para a Ciência e a Tecnologia por me ter concedido o apoio financeiro através de uma Bolsa de Doutoramento (SFRH/BD/101191/2014) e pelo suporte financeiro para realização do trabalho experimental através dos projetos EU-FEDER Programa COMPETE POCI-01-0145-FEDER-007440 (UID/NEU/04539/2013), FCOMP-01-0124-FEDER-028359 (PTDC/BIA-MIC/2779/2012) e POCI-01-0145-FEDER-029221 (PTDC/BTM-TEC/29221/2017).

À maltinha do ITQB por estarem sempre disponíveis a ajudar-me, a esclarecerem as minhas dúvidas e também a evitarem que eu pudesse "explodir com o laboratório" ao tentar torná-lo numa indústria e a querer produzir gramas (ou quilos!) de compostos! Em especial, à Eva e à Vanessa por TODA a paciência e tempo dispensado em me explicar tudinho, inclusivamente comecei a gostar da magia dos protões e carbonos a falarem entre si e uns com outros em uníssono! Tenho saudades do teu carinho, Eva: "olha para isto tudo torto e queimado, MCê! Vai fazer outro! Rápido!!" ou dos nossos duetos musicais Vanessa, em lados opostos do laboratório sempre muito afinados! Ahah Foram apenas quatro meses, mas parecia que já vos conhecia há anos! Obrigada pela ajuda e por todo o apoio! ♥

Ao Doutor Bruno Manadas e à Vera por toda a disponibilidade e ajuda prestada nas análises de espectrometria de massa, principalmente pelo desafio de não serem proteínas, mas sim polissacáridos de manose!

À Prof. Isaura Simões e à Prof. Paula Veríssimo que me acompanham desde a licenciatura e são duas grandes referências para mim! Estiveram sempre disponíveis para ajudar e discutir ideias ao longo de todo o meu percurso, fazendo-me acreditar mais em mim e a arriscar! Sou-lhes profundamente grata por isso!

Às pessoas do 1º piso do CNC, em especial às técnicas que sem o vosso auxílio, o nosso trabalho seria muito mais difícil e demorado, e à maltinha do almoço na biblioteca, que muitas vezes me ajudaram a desanuviar e a carregar baterias.

Aos meus AMIGOS: vocês são os andaimes da minha vida! Ajudaram a reerguer-me e a tornar-me uma pessoa melhor e mais forte, acompanhando sempre por perto todo este percurso, sem nunca me deixar desistir! Cada um à sua maneira e muitas vezes sem o saber, foi essencial no apoio e paciência!! Não irei esquecer as palavras, os gestos, os sorrisos, os abraços, as lágrimas, as alegrias, as mensagens, as dores musculares, as superações, as deslocações até

Coimbra (#amigosdelésalés), os passeios de fim de semana, os jantares, as noitadas…eu sei lá! Vocês são o meu suporte!! Não vos vou nomear, vocês sabem quem são!! ♥ Deixo só um agradecimento especial à minha Olguinha, à Matilde, à Camila, ainda com meses de vida, as fotos com um teu sorriso contagiante foram como lufadas de ar fresco matinais, e à Dani, minha ajuda preciosa na ilustração e edição de imagens!

A toda a minha família, agradeço o apoio, as palavras e a preocupação em que as "minhas bichas" continuassem a crescer e que os "meus açúcares" se mantivessem docinhos! Em especial, às minhas piratinhas que sem saber e em visitas rápidas conseguiram muitas vezes carregar as minhas baterias e me deram muita força para continuar! ♥

Ao meu Tó Peixe, andamos às turras desde que eu me lembro e podemos agora até passar uns dias sem nos falarmos, mas quando tudo desaba somos o porto de abrigo um do outro!! Foste a minha grua, ouviste-me vezes sem conta e muitas delas sem perceberes o meu mundo de enzimas que cortam e outras que juntam, mas nunca me deixaste afundar! És grande (e não só em tamanho) e tenho um enorme orgulho na pessoa que és! ♥

Aos meus pais, que merecem uma estátua, principalmente pela paciência destes últimos meses! Ainda tive receio que me pusessem as malas à porta! Ahah Sempre com palavras de incentivo e por vezes sem perceberem muito bem este universo "onde nada se vê a acontecer", acreditaram sempre em mim e não me deixaram vacilar em momentos de maior aperto! ♥

A todos, MUITO OBRIGADA! "Tenho mais sorte do que juízo!"

TABLE OF CONTENTS

ABSTRACT

In recent years, there has been an increasing number of mycobacterial infections caused by nontuberculous mycobacteria (NTM) mostly associated with comorbidities such as HIV infection, underlying pulmonary diseases or diabetes. Moreover, the urgency to fight mycobacterial diseases is intensified by their drug resistance and lack of specific antibiotics against NTM.

A major adaptive advantage of members of the *Mycobacterium* genus stems from the composition and arrangement of their cell envelope that confers the ability to persist and survive under adverse conditions, contributing to their virulence and pathogenicity. Additionally, mycobacteria possess two unusual intracellular polymethylated polysaccharides (PMPS) of 6-*O*-methylglucose (MGLP) and 3-*O*-methylmannose (MMP). These are distributed differently through mycobacterial species, MGLP appears to be synthetized by all known mycobacteria and MMP was only isolated from rapidly growing mycobacteria (RGM). PMPS were proposed to modulate mycobacterial fatty-acid metabolism and indirectly the assembly of cell envelope lipids and glycoconjugates, but the importance of MMP for mycobacterial fitness in the environment or during infection has raised important issues. Since PMPS are considered potential drugs targets, it is crucial to expand the knowledge of their functions and details of their biosynthetic pathways.

A biosynthetic pathway for MMP was proposed in 1984 where MMP polymerization would occurs through alternating mannosylation and methylation reactions catalysed by a mannosyltransferase and a methyltransferase, respectively. Recently, an alternative pathway was proposed wherein mannosyltransferase activity would be independent of mannose methylation, allowing the addition of successive mannose units prior to methylation. However, the genes and enzymes involved in MMP biosynthesis are unknown.

In this work, a mycobacterial gene cluster, composed by four genes, was proposed to be responsible for MMP biosynthesis. Of the four enzymes, three were biochemically characterized as a MMP hydrolase (MmpH), as an α-(1→4)-mannosyltransferase (ManT) and as a 1-*O*-methyltransferase (MeT1), strongly indicating their involvement in MMP biosynthesis. Moreover, the three-dimensional structure of MeT1 was determined. The identification of these genes, the features of each of the enzymes and their *in vitro* cooperation favour their commitment to the MMP biosynthetic pathway herein described, which contributes to further the knowledge about this polysaccharide. These results can now be used to better understand the physiological role of MMP in mycobacteria as well as its possible involvement in growth, resilience and pathogenesis.

Keywords: Mycobacteria, methylmannose polysaccharide (MMP), biosynthesis, mannosyltransferase, hydrolase, methyltransferase, metabolism

RESUMO

Ao longo dos últimos anos tem-se verificado um aumento de infeções provocadas por micobactérias não-tuberculosas (NTM), principalmente associadas a comorbidades como infeção por HIV, doenças pulmonares subjacentes ou diabetes. Para além disso, a resistência das micobactérias aos anti-micobacterianos existentes e a falta de antibióticos específicos para NTM intensifica a necessidade de combater estas bactérias.

Uma grande vantagem adaptativa do género *Mycobacterium* deriva da composição e organização da sua parede celular, conferindo-lhe a capacidade de persistir e sobreviver em condições adversas e, assim, também contribuir para a sua virulência e patogenicidade. Adicionalmente, as micobactérias possuem dois polissacáridos polimetilados intracelulares (PMPS) raros de 6-*O*-metilglucose (MGLP) e 3-*O*-metilmanose (MMP). Os PMPS encontram-se distribuídos de forma distinta pelas diferentes espécies de micobactérias, sendo que o MGLP parece ser sintetizado por todas as micobactérias enquanto que o MMP apenas foi isolado de micobactérias de crescimento rápido (RGM). A função destes polímeros está relacionada com a modulação do metabolismo dos ácidos gordos em micobactérias e, indiretamente, com a síntese de lípidos e glicoconjugados do envelope celular. Contudo, a importância do MMP na capacidade adaptativa das RGM a condições ambientais desfavoráveis ou durante o desenvolvimento de infeções tem sido alvo de questões importantes. Assim, os PMPS são considerados potenciais alvos terapêuticos, sendo essencial expandir o conhecimento acerca da sua função e das vias de biossíntese.

A via de biossíntese dos MMP foi proposta em 1984, onde a polimerização ocorreria através de reações alternadas de manosilação e de metilação catalisadas por uma manosiltransferase e uma metiltransferase, respetivamente. Recentemente, foi proposta uma via alternativa onde a atividade de uma manosiltransferase seria independente da metilação das manoses por uma metiltransferase, permitindo adicionar sucessivamente unidades de manose antes da sua metilação. Todavia, não existem mais evidências acerca da síntese de MMP nem dos genes ou das enzimas envolvidas no processo.

Neste trabalho propomos um conjunto de quatro genes que identificámos no genoma de micobactérias e que é responsável pela síntese de MMP. Das quatro enzimas, três foram caracterizadas bioquimicamente, designadamente uma MMP hidrolase (MmpH), uma α-(1→4)-manosiltransferase (ManT) e uma 1-*O*-metiltransferase (MeT1), demonstrando-se assim o seu envolvimento na biossíntese do MMP. A estrutura tridimensional da MeT1 foi também determinada. Assim, a identificação dos genes, a determinação das propriedades de cada enzima e a sua cooperação *in vitro* a favor da síntese de MMP aqui descritas contribuem para melhorar o conhecimento sobre este polissacárido, fornecendo pistas cruciais para a compreensão da função fisiológica de MMP bem como do seu possível envolvimento no crescimento, resiliência e patogénese das micobactérias que o sintetizam.

Palavras-chave: Micobactérias, polissacarídeo de metilmanose (MMP), biossíntese, manosiltransferase, hidrolase, metiltransferase, metabolismo

ABBREVIATIONS

^{13}C-NMR	carbon-13 nuclear magnetic resonance
^{1}H-NMR	proton nuclear magnetic resonance
4Å MS	4Å molecular sieves
AcOEt	ethyl acetate
AG	arabinogalactan
AIDS	acquired immunodeficiency syndrome
AMMP	acetylated MMP
Ar	aromatic
Ara*f*	D-arabinofuranosyl
ATR	attenuated total reflectance
BCG	bacillus Calmette-Guérin
BLAST	basic local alignment search tool
C_q	quaternary carbon
Ct	control
CUR	curtain gas
d	doublet
DAT	di-acyltrehaloses
DBU	1,8-diazabicycloundec-7-ene
dd	doublet of doublets
DIPEA	*N*,*N*-diisopropylethylamine
DMAP	4-dimethylaminopyridine
DMF	dimethylformamide
DPA	decaprenylphosphoryl-D-arabinose
DR	drug resistance
DST	drug susceptibility testing
DTNB	5,5′-dithiobis-2-nitrobenzoic acid, Ellman's Reagent
DTT	dithiothreitol
EDTA	ethylenediaminetetraacetic acid
FA	fatty acids
FAS	fatty acid synthetase
FTIR	Fourier-transform infrared spectroscopy
Gal*f*	D-galactofuranosyl
GDP	guanosine diphosphate
GG	glucosylglycerate
GlcNAc	*N*-acetylglucosamine acid

GPL	glycopeptidolipids
GS1	nebulized gas 1
GT	glycosyltransferases
Hex	hexane
HIV	human immunodeficiency virus
IPTG	β-D-1-thiogalactopyranoside
J	coupling constant
KEGG	Kyoto encyclopaedia of genes and genomes
LAM	lipoarabinomannans
LB	lysogeny broth
LM	lipomannans
LOS	lipooligosaccharides
LTBI	latent tuberculosis infection
m	multiplet
M1P	mannose-1-phosphate
M6P	mannose-6-phosphate
MA	mycolic acids
mAGP	mycolyl-arabinogalactan-peptidoglycan complex
Man	D-mannose
Man_1A	octyl 3-*O*-methyl-mannose (substrate used in Xia et al., 2012)
Man_1B	octyl mannose (substrate used in Xia et al., 2012)
Man_2	4α-mannobiose
Man_2A	octyl 3,3'-di-*O*-methyl-4α-mannobiose (substrate used in Xia et al., 2012)
Man_2B	octyl mannose-4α-3-*O*-methyl-mannose (substrate used in Xia et al., 2012)
Man_3A	octyl 3,3',3''-tri-*O*-methyl-4α-mannotriose (substrate used in Xia et al., 2012)
Man_3B	octyl mannose-4α-3,3'-di-*O*-methyl-mannobiose (substrate used in Xia et al., 2012)
Man_4A	octyl 3,3',3'',3'''-tetra-*O*-methyl-4αmannotetraose (substrate used in Xia et al., 2012)
Man_4B	octyl mannose-4α-3,3',3''-tri-*O*-methyl-mannotriose (substrate used in Xia et al., 2012)
Man_4C	octyl 4α-mannotetraose (substrate used in Xia et al., 2013)
Man_5A	octyl 3,3',3'',3''',3''''-penta-*O*-methyl-4α-mannopentaose (substrate used in Xia et al., 2012)

Man_5B	octyl mannose-4α-3,3',3'',3'''-tetra-*O*-methyl-mannotetraose (substrate used in Xia et al., 2012)
ManT	α-(1→4)-mannosyltransferase
MDR-TB	multi-drug resistant TB
MeT1	1-*O*-methyltransferase
$Met_{1,3}Man_1$	1,3-di-*O*-methyl-mannose (substrate used in Weisman et. al,1984b)
$Met_{1,3}Man_{12}$	1,3,3',3'',3''',3'''',3''''',3'''''',3''''''',3'''''''',3''''''''',3'''''''''',3''''''''''-trideca-*O*-methyl-dodecamannose (substrate used in Weisman et al., 1984b)
$Met_{1,3}Man_3$	1,3,3',3''-tetra-*O*-methyl-4α-mannotriose (substrate used in Weisman et al., 1984b)
$Met_{1,3}Man_4$	1,3,3',3'',3'''-penta-*O*-methyl-4α-mannotetraose (substrate used in Weisman et al., 1984b)
$Met_{1,3}Man_6$	1,3,3',3'',3''',3'''',3'''''-hepta-*O*-methyl-4α-mannohexaose (substrate used in Weisman et al., 1984b)
MGLP	methylglucose lipopolysaccharide
MGP	deacylated MGLP
MMP	methylmannose polysaccharide
MmpH	methylmannose polysaccharide hydrolase
MS	mass spectrometry
MTase	methyltransferase
Mtb	*Mycobacterium tuberculosis*
MurNAc	*N*-acetylmuramic acid
MurNGly	*N*-glycolylmuramic acid
NCBI	National Center for Biotechnology Information
NTM	nontuberculous mycobacteria
PAT	poly-acyltrehaloses
PEP	phosphoenolpyruvate
PDIM/DIM	phthiocerol dimycocerosate
PG	peptidoglycan
Ph	phenyl
pHBAH	*p*-hydroxybenzoic acid hydrazide
PI	phosphatidyl-*myo*-inositol
PIM	phosphatidyl-*myo*-inositol mannosides
PK/LDH	pyruvate kinase and lactate dehydrogenase
pManT	putative mannosyltransferase
pMeT3	putative 3-*O*-methyltransferase
PMPS	polymethylated polysaccharides

pMTase	putative methyltransferases
PPM	polyprenol-phosphate-mannose
RGM	rapidly growing mycobacteria
rpm	revolutions per minute
rt	room temperature
s	singlet
SAH	*S*-adenosylhomocysteine
SahH	*S*-adenosylhomocysteine hydrolase
SAM	*S*-adenosylmethionine
SGM	slowly growing mycobacteria
SL	sulfolipids
$sMan_3$	synthetic propyl 4α-mannotriose
$sMan_4$	synthetic propyl 4α-mannotetraose
$sMet_{1,3}Man_2$	synthetic 1,3,3'-tri-*O*-methyl-4α-mannobiose
sMetMan	synthetic 3-*O*-methylmannose
$sMetMan_2$	synthetic 3,3'-di-*O*-methyl-4α-mannobiose
$sMetMan_3$	synthetic propyl 3,3',3''-tri-*O*-methyl-4α-mannotriose
$sMetMan_4$	synthetic propyl 3,3',3'',3'''-tetra-*O*-methyl-4α-mannotetraose
t	triplet
TB	tuberculosis
TBDMSOTf	tert-butyldimethylsilyl triflate
TEV	*tobacco etch virus* protease
TDM	trehalose dimycolates
TDR-TB	totally-drug resistant TB
TGF-β	transforming growth factor beta
THF	tetrahydrofuran
TLC	thin-layer chromatography
TMM	trehalose monomycolates
TMSOTf	trimethylsilyl trifluoromethanesulfonate
U	unit
UDP	uridine diphosphate
WT	wild-type
XDR-TB	extensively-drug resistant TB
$β\text{-}Man_2$	4β-mannobiose
$β\text{-}Man_3$	4β-mannotriose
$β\text{-}Man_4$	4β-mannotetraose
δ	chemical shift

LIST OF FIGURES

Chapter 4: Two methyltransferases identified in the MMP gene cluster

Chapter 5: General Discussion

LIST OF TABLES

Chapter 1:
General Introduction

1. The mycobacterial world

The *Mycobacterium* genus was, until recently, a heterogenous group of bacteria comprised by nearly two hundred species (http://www.bacterio.net/mycobacterium), including obligate intracellular pathogens and environmental saprophytic species, commonly designated nontuberculous mycobacteria (NTM) (Simner et al., 2016). Very recently, comparative genomic analysis and molecular signatures identified different clades that were distributed by five novel genera, namely an emended *Mycobacterium* genus with the "Tuberculosis-Simiae" clade, including all major human pathogens (*M. tuberculosis*, *M. bovis*, *M. africanum*, *M. microti*, *M. caprae*, *M. pinnipedii*, *M. mungi*, *M. canetti*, *M. orygis* and *M. suricattae*) that can cause tuberculosis in humans and animals, and *Mycobacterium leprae*, the ethological agent of leprosy (Esteban and Muñoz-Egea, 2016; Nunes-Costa et al., 2016; Simner et al., 2016), as well as the novel genera *Mycolicibacterium*, *Mycolicibacter*, *Mycolicibacillus* and *Mycobacteroides* in which all other NTM species were now included (Gupta et al., 2018). These genera belong to the suborder *Corynebacterineae* of the class *Actinobacteria*, being phylogenetically related to the genera *Corynebacterium*, *Nocardia*, *Gordonia* and *Rhodococcus*, which are industrially, clinically or environmentally relevant (Hartmans et al., 2006). NTM have been progressively emerging as important opportunistic pathogens, especially in hosts where the immune system surveillance is impaired as a consequence of HIV infection, lung disease or in the chronically ill or in the elderly (Nunes-Costa et al., 2016; Wassilew et al., 2016; Claeys and Robinson, 2018). Comparisons between mycobacterial genomes show an evolutionary divergence between NTM and strict pathogens, while some studies propose that the latter derive from a common ancestor with phenotypic similarities to *M. canetti* (Supply et al., 2013; Gagneux, 2018).

Mycobacteria are traditionally divided in two groups: the slowly growing mycobacteria (SGM) and the rapidly growing mycobacteria (RGM). This classification is traditionally based on the time required by each species to form visible colonies on solid medium. While RGM species need less than seven days, SGM species require more than seven days, sometimes weeks, to form visible colonies on agar plates (Nunes-Costa et al., 2016). The phylogenetic grouping based on 16S rRNA gene sequences also corroborates this division, with some exceptions, and studies argue that RGM are ancestors of SGM (Claeys and Robinson, 2018). Although SGM have always received more attention as human pathogens, there is no proven relationship between growth rate and pathogenicity, being that both SGM and RGM are capable of causing serious opportunistic infections. Indeed, SGM such as *M. avium*, *M. kansasii*, *M. haemophilum*, *M. xenopi* and *M. marinum,* as well as RGM such as *M. abscessus*, *M. chelonae* and *M. fortuitum* are among the most common causes of NTM diseases (Simner et al., 2016; Wassilew et al., 2016; Brown-Elliott and Philley, 2017).

Hence, SGM are now distributed across the genera *Mycobacterium*, *Mycolicibacter* and *Mycolicibacillus* (Gupta et al., 2018). On the other hand, the *Mycobacteroides* genus aggregates the RGM strains of the abscessus-chelonae clade, while the remaining RGM species now included in the *Mycolicibacterium* genus, e.g., *Mycolicibacterium smegmatis*, *Mycolicibacterium vanbaalenii* and *Mycolicibacterium hassiacum* (Gupta et al., 2018).

1.1. Tuberculosis

Tuberculosis (TB) is still a disease estimated to latently infect a quarter of the world's population. In 2017, TB was responsible for about 1.3 million deaths (WHO, 2018).

The persistence of TB is associated to an easy dissemination of its etiological agent, *Mycobacterium tuberculosis* (*Mtb*), by infected people that cough or sneeze and release droplets carrying the bacilli (Ehrt et al., 2018). Inside the lungs, the immune system is activated to phagocytize the invader that leads to the formation of a compact and organized structure called granuloma, which is an hallmark structure of TB infection (Machelart et al., 2017). However, *Mtb* manipulates the immune system to its own advantage, creating a protected niche where it can persist and replicate, since it can inhibit vacuolar acidification in macrophages, block phagolysosomal maturation and disrupt apoptosis and autophagy mechanisms (Ernst, 2018). The granuloma structure is capable of keeping *Mtb* inside the alveoli without clinical symptoms, radiological abnormalities or microbiological evidences and this state is designated as latent TB infection (LTBI) (Lee, 2016; Behr et al., 2018).

Human immunodeficiency virus (HIV) is a burden in LTBI progression to active TB and, in recent years, there has been an increase in co-infection cases due to an impairment of immune competence in acquired immunodeficiency syndrome (AIDS) patients and, consequently, a decrease of the protective responses to TB (Procop, 2017). Diabetes and other chronic diseases, malnutrition, smoke exposure (and smoking habits) and anaemia are also risk factors that contribute for development of active TB (Bastos et al., 2018). The only vaccine approved against TB was developed in the early 20th century from an attenuated strain of *M. bovis*, the bacillus Calmette-Guérin (BCG) (Russell et al., 2010). However, BCG vaccine has a very limited efficacy in adults, making it a poor solution on hopes of TB eradication. Once a first TB infection is established, the treatment guidelines require two phases totalizing six months: an initial course of isoniazid, ethambutol, rifampicin and pyrazinamide for two months, and the remaining four months of treatment with isoniazid and rifampicin (Trofimov et al., 2017). Inadequate prescription plans and incomplete treatment courses, as well as the lack of a rapid diagnosis leading to ineffective initial responses to TB infection, have contributed for drug resistance (DR), hampering disease eradication in many cases (Seaworth and Griffith, 2017; Hameed et al., 2018). Indeed, three degrees of DR have been identified in TB: multi-drug resistant (MDR-TB), extensively-drug

resistant (XDR-TB) and totally-drug resistant (TDR-TB). MDR-TB is characterized by *Mtb* resistance to rifampicin and isoniazid, which requires second line injectable drugs (amikacin, capreomycin or kanamycin) or fluoroquinolones (levofloxacin, moxifloxacin and gatifloxacin). When resistance both to first-line drug and also to second-line drugs is detected, the strains are designated XDR-TB (Seaworth and Griffith, 2017; Hameed et al., 2018). All drugs mentioned above date from the 20th century and only two new drugs, bedaquiline and delamanid, have been approved recently (Seaworth and Griffith, 2017). Despite some initial controversy about the associated severe side-effects (Field, 2015; Seaworth and Griffith, 2017), bedaquiline has gained some importance and is currently recommended for the treatment of MDR- and XDR-TB (Pontali et al., 2016).

1.2. NTM infections

NTM are frequently isolated from environments with which humans and animals frequently contact namely soil, water and dust (Falkinham III, 2018). These mycobacteria are oligotrophs (able to grow with very low concentrations of nutrients), have a high tolerance to extreme temperatures and pH, are capable of forming biofilms and can easily adapt to adverse conditions (Falkinham III, 2018). It was considered that one of the distinguishing features of NTM infection, in relation to TB infection, was the lack of human to human transmission, however the first cases of human to human transmission of *M. abscessus* were reported in patients with cystic fibrosis (Martiniano and Nick, 2015).

NTM have gained attention, since they are opportunistic pathogens that can cause an array of human diseases in immunocompromised patients, including those with HIV-AIDS or with other chronic diseases that fragilize the immune system, namely diabetes, or in those undergoing immunosuppressive therapy due to transplants. Underlying chronic lung diseases are also predisposing factors for NTM infection, as is alcoholism, smoking or even pregnancy (Simner et al., 2016; Wassilew et al., 2016; Brown-Elliott and Philley, 2017). Clinically, the most relevant NTM are members of the *M. avium* complex, *M. abscessus*, *M. kansasii*, *M. malmoense* and *M. xenopi*, because these are the most frequently associated to humans diseases (Falkinham III, 2009; Simner et al., 2016). However, NTM also cause diseases in immunocompetent individuals, namely in women without evident immune defects but that seemingly have a phenotypic predisposition to develop NTM lung disease (Chan and Iseman, 2010, 2013; Mirsaeidi and Sadikot, 2015). This phenotype is more associated to thin and elderly (postmenopausal) women with some thoracic abnormalities such as scoliosis and mitral valve prolapse, possibly due to an alteration on adipokines (leptin and adiponectin), sex hormones (oestrogen) and/or transforming growth factor beta (TGF-β) expression, which could affect its

functional roles and increase their susceptibility to NTM infection (Chan and Iseman, 2010, 2013; Mirsaeidi and Sadikot, 2015).

Besides pulmonary TB-like infection, NTM can also cause extrapulmonary infections in skin, bones and joints but infections of the central nervous system and ocular infections were also reported (Brown-Elliott and Philley, 2017; Holt and Kasperbauer, 2018). Some of the extrapulmonary infections are often associated to a nosocomial origin after surgeries and due to inadequate sterilization and disinfection of equipment. The use of contaminated solutions, syringes and catheters or reutilization of injection devices or haemodialysis filters are also frequent vehicles of infections (Brown-Elliott and Philley, 2017; Sood and Parrish, 2017). *Mycobacterium chelonae*, for example, is associated with skin, bone and soft-tissue infections while *M. ulcerans* causes Buruli ulcer, the third most common mycobacterial disease worldwide and an endemic disease in many developing countries but rare in western societies (Holt and Kasperbauer, 2018). This serious pathogen infects the cutis and produces a necrotizing toxin that leads to destruction of skin and muscle, possibly also involving bone corrosion (O'Brien et al., 2019).

The huge obstacles for control/eradication of NTM diseases are the identification of the environmental source and the correct diagnosis and treatment due to symptom ambiguity and lack of appropriate antibiotics (Raju et al., 2016; Wassilew et al., 2016; Basille et al., 2018). Water is considered the main source of NTM infections, since mycobacteria are not eliminated from drinking water distribution systems with standard water treatment strategies involving chlorination. In fact, this strategy eliminates microbial competitors and naturally select for these bacteria that are resistant to other disinfectants as well, allowing them to adapt to the oligotrophic water distribution systems and to form and enrich biofilms. Furthermore, human activity in agriculture such as discharging biocides, the overuse of antibiotics and disinfection also select for and favours NTM survival (Sood and Parrish, 2017; Claeys and Robinson, 2018; Falkinham III, 2018). For example, NTM are frequently identified in hospital water systems, namely members of the *M. avium* complex, *M. abscessus*, *M. chelonae*, *M. fortuitum* and *M. mucogenicum* (Simner et al., 2016). In addition to their resistance to chlorination, many NTM are significantly heat-resistant and biofilms adhere to pipe surfaces, making recirculating hot water plumbing systems, such as the ones usually found on hospitals, ideal habitats for high numbers of NTM from where they can be easily aerosolized. It has been suggested that, for better control of NTM numbers in water distribution systems, it is important to raise water heater temperatures to at least 55 °C, to install filters to retain bacteria, to drain and refill hot water heaters periodically and to frequently disinfect or replace showerheads (Falkinham III, 2015).

The clinical symptoms of NTM lung infection are similar to TB infection and, in cases of extrapulmonary infections, the disease assumes a range of nonspecific or variable

manifestations that are difficult to distinguish from other pathologies with similar clinical presentation without molecular testing (Griffith et al., 2007). Since treatment plans for TB or NTM infection are different and NTM are differently resistant to antibiotics, correct diagnosis and antimicrobial susceptibility testing are essential. However, as molecular techniques underlying a correct diagnosis and drug susceptibility testing (DST) are often time consuming, in order not to delay the initial response to the detected infection, an empirical treatment plan is often initiated, which may also represent a risk for development of drug resistance (Raju et al., 2016; Wassilew et al., 2016; Basille et al., 2018). Moreover, since NTM exhibit natural resistance to antimicrobials, a delayed or incorrect diagnosis can lead to treatment failure (Wassilew et al., 2016; Basille et al., 2018). Thus, it is urgent to develop direct, rapid and sensitive methods for NTM detection, which will have a high impact in aiding first response and also in minimizing resistance acquisition.

2. Cell envelope of mycobacteria

Mycobacteria have a remarkable lipid-rich cell envelope filled with complex carbohydrates that is determinant to their antibiotic and disinfectant resistance phenotypes, contributing also to pathogenicity and survival in inhospitable environments (Abrahams and Besra, 2018; Singh et al., 2018). The mycobacterial cell envelope is a dynamic structure divided in three layers: a capsule, a cell wall core and a plasma membrane (figure 1.1) (Jankute et al., 2015). The capsule is the outermost layer and, consequently, provides the first interaction with the host, being involved in immune modulation and mycobacterial virulence (van de Weerd et al., 2016). This structure is constituted by polysaccharides and proteins, but the exact composition varies between mycobacterial species, since the major constituents in *Mtb* capsule are polysaccharides, whereas in *M. smegmatis* and *M. phlei*, the main capsule components are proteins (Daffé, 2015; Jankute et al., 2015). The main polysaccharide of the *Mtb* capsule is an α-D-glucan composed by α-(1→4) glucose residues branched every five or six units with α-(1→6)-glucosylpyranose, sharing structural features with the intracellular glycogen (Daffé, 2015). The cell wall core extends from the plasma membrane outward in layers and is constituted by peptidoglycan (PG), arabinogalactan (AG) and mycolic acids (MA), covalently linked thus forming a strong impermeable complex, designated mAGP (Jankute et al., 2015). The plasma membrane is a basic structure organized as a lipid bilayer similarly to other biological membranes and is composed by phospholipids including phosphatidylglycerol, diphosphatidylglycerol, cardiolipin, phosphatidylethanolamine and phosphatidyl-*myo*-inositol (PI), as well as a variety of mannosylated PI (phosphatidyl-*myo*-inositol mannosides (PIM), lipomannans (LM) and lipoarabinomannans (LAM) (Berg et al., 2007; Daffé et al., 2014; Daffé, 2015).

2.1. Cell wall core

The cell wall core contains the major amount of lipids and the mAGP is associated to the atypical mycobacterial resilience to hydrophilic drugs and to survival inside macrophages, contributing to their pathogenicity and virulence (Abrahams and Besra, 2018).

The mycobacterial PG confers shape and rigidity to the mycobacterial cell, counteracting the outer osmotic pressure, and contributes for a crucial balance in bacteria growth and survival (Abrahams and Besra, 2018). This layer is composed by alternating units of *N*-acetylglucosamine acid (GlcNAc) and *N*-acetylmuramic acid (MurNAc) linked via β-(1→4) linkages, where some of these are hydroxylated into *N*-glycolylmuramic acid (MurNGly) (Abrahams and Besra, 2018). This modification is present in all mycobacteria, providing them an increase in PG robustness and a decrease in susceptibility to lysozyme degradation when compared to other microorganisms (Jankute et al., 2015). AG is constituted by D-arabinofuranosyl (Ara*f*) and D-galactofuranosyl residues (Gal*f*), forming a linear chain of Gal*f* units linked by alternating β-(1→5) and β-(1→4) bonds and branched of the 8^{th}, 10^{th} and 12^{th} Gal*f* with D-arabinan chains comprised of 22 or 23 Ara*f* units (Jankute et al., 2015).

MA form a mycomembrane of α-alkyl-β-hydroxyl fatty acids (C_{60-90}) with asymmetric bilayer organization, playing key roles in impermeability to drugs and disinfectants and in the ability to form biofilms and to adapt the membrane fluidity in response to environmental conditions, which, consequently, contribute to mycobacterial survival and virulence (Abrahams and Besra, 2018; Ghazaei, 2018; Singh et al., 2018). About 60% of the mycobacterial cell wall dry weight is due to MA that are classified in three distinct types: α-mycolates, keto-mycolates and methoxy-mycolates, differing in the configuration of cyclopropane rings (Ghazaei, 2018; Singh et al., 2018). The MA cyclopropane rings have great importance in the structural integrity of the cell wall and they also contribute to bacterial protection inside the infected host, since a *Mtb* mutant lacking the cyclopropane ring of keto-mycolates showed reduced growth within macrophages (Takayama et al., 2005; Ghazaei, 2018; Singh et al., 2018). In the outermost leaflet, MA were also found as free esters of trehalose, as part of structures called trehalose monomycolates (TMM) and trehalose dimycolates (TDM), which are essential in infection processes and in the modulation of mycobacterial resistance to antimicrobial drugs (Daffé et al., 2014; Nobre et al., 2014; Ghazaei, 2018). Intercalated with MA esters, an assortment of free phenolic glycolipids (phthiocerol dimycocerosate (PDIM/DIM)), lipoglycans (PIM, LM and LAM) and other trehalose-esters (di- and poly-acyltrehaloses (DAT and PAT), sulfolipids (SL) and lipooligosaccharides (LOS)) are also present in the outermost leaflet of the cell wall. Overall these components play crucial roles in the maintenance of cell wall architecture, act as a permeability barrier and modulate the pathogenicity and virulence of mycobacteria (Daffé et al., 2014; Gago et al., 2018; Singh et al., 2018).

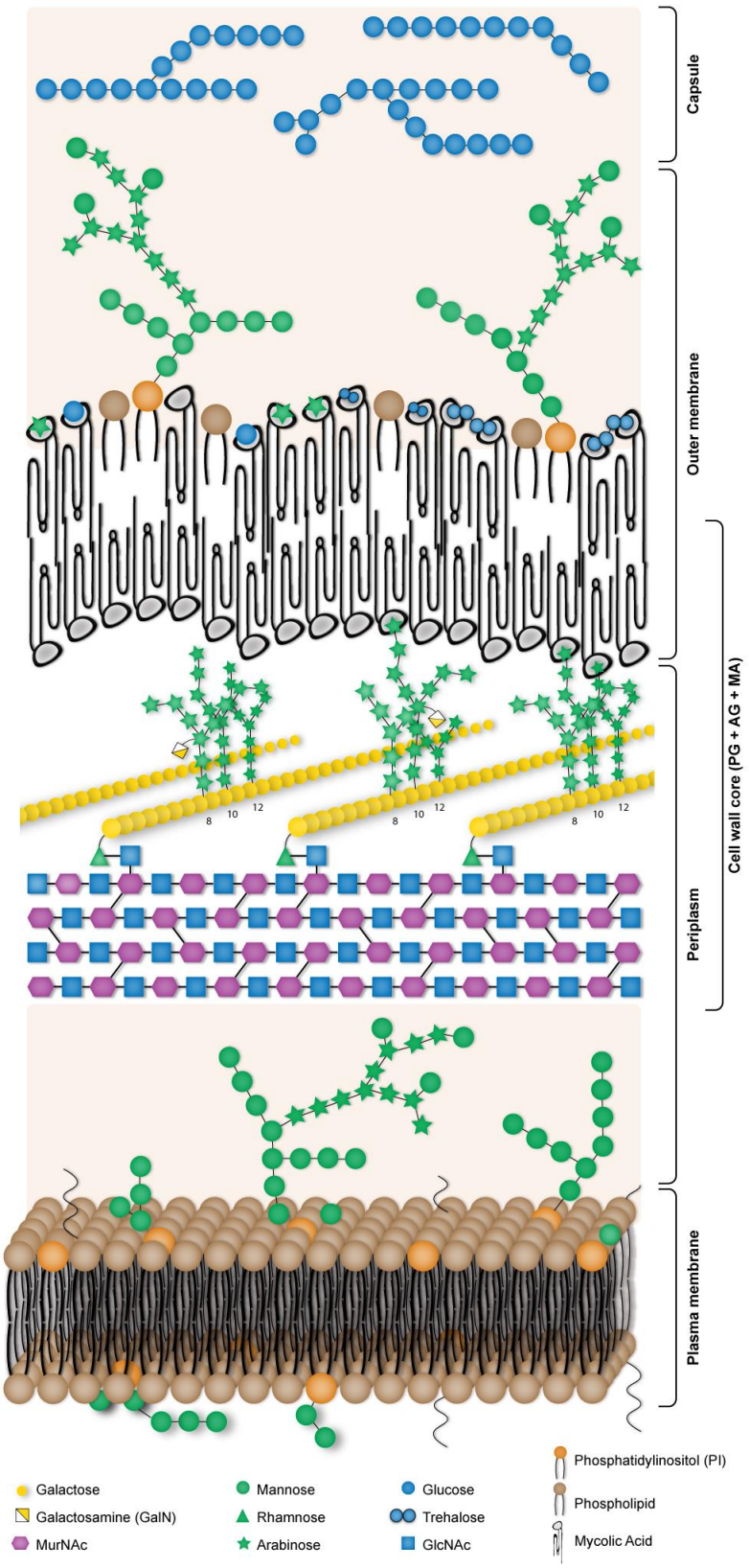

Figure 1.1 – Schematic representation of the mycobacterial cell envelope. The envelope is divided in plasma membrane, cell wall core and capsule, highlighting lipoglycans (PIM, LM and LAM) present in the periplasm and in the outer membrane. The overall schematic and individual structures are not drawn to scale and the symbols and colours used for carbohydrates were based on https://www.ncbi.nlm.nih.gov/glycans/snfg.html. MurNAc, *N*-acetylmuramic acid; GlcNAc, *N*-acetylglucosamine acid.

2.2. PIM, LM and LAM and key-mannosyltransferases in their biosynthesis

Lipoglycans were initially identified by Ballou and co-workers (Ballou et al., 1963; Lee and Ballou, 1965), attracting increasing interest due to their antigenicity features and proposed involvement in mycobacterial pathogenicity (Weber and Gray, 1979; Hunter et al., 1983; Cao and Williams, 2010). PIM, LM and LAM are present in mycobacterial cell envelopes (figure 1.1) (Ortalo-Magné et al., 1996) and, although all share a common lipid, the PI, they are noncovalently anchored to the inner or the outer membranes, appearing to be embedded in the cell envelope (Pitarque et al., 2008). PIM are simple but heterogeneously mannosylated glycolipids comprising mannose residues attached to the *myo*-inositol ring of phosphatidyl-*myo*-inositol. They exist as mono-, di-, tri-, tetra-, penta- and hexamannosides with different degrees of acylation, having been identified four possible acylation sites: at positions 1 and 2 of the glycerol, position 3 of *myo*-inositol and at position 6 of one of the mannoses (figure 1.2 A) (Sancho-Vaello et al., 2017; Abrahams and Besra, 2018). These glycolipids play essential roles in permeability, inner membrane integrity and control of cell septation and division (Parish et al., 1997; Patterson et al., 2003; Morita et al., 2005). LM and LAM are extended forms of PIM and possess a similar backbone constituted by 21 to 34 mannoses linked by α-(1→6) linkages and branched in 5-10 units with α-(1→2)-mannose (figure 1.2 B and C) (Jankute et al., 2015; Abrahams and Besra, 2018). Additionally, LAM are more complex structures, containing ramifications of about 50-80 Ara*f* units bound through α-glycosidic linkages and, depending on the species, can also have a capping motif (figure 1.2 C) (Berg et al., 2007; Singh et al., 2018). In pathogenic strains such as *M. tuberculosis*, *M. leprae* and *M. marinum*, LAM are capped with 1 to 3 mannoses bound by α-(1→2)-linkages (figure 1.2 C), whereas rapid growers such as *M. smegmatis* and *M. fortuitum* show a PI linked to the LAM terminals, despite the fact that some species like *M. chelonae* do not exhibit any capped motif (Stoop et al., 2013). There is a relation between the presence of LAM mannose caps and mycobacterial virulence, since they are important in pathogenicity, having additional important roles in the maintenance of cell wall integrity and a critical influence in growth (Fukuda et al., 2013; Stoop et al., 2013). However, there is still some divergence about the actual effects of these lipoglycans in the inflammatory response mounted by the immune system in macrophages and dendritic cells and some experimental discrepancies make it difficult to reach define conclusions (Källenius et al., 2016).

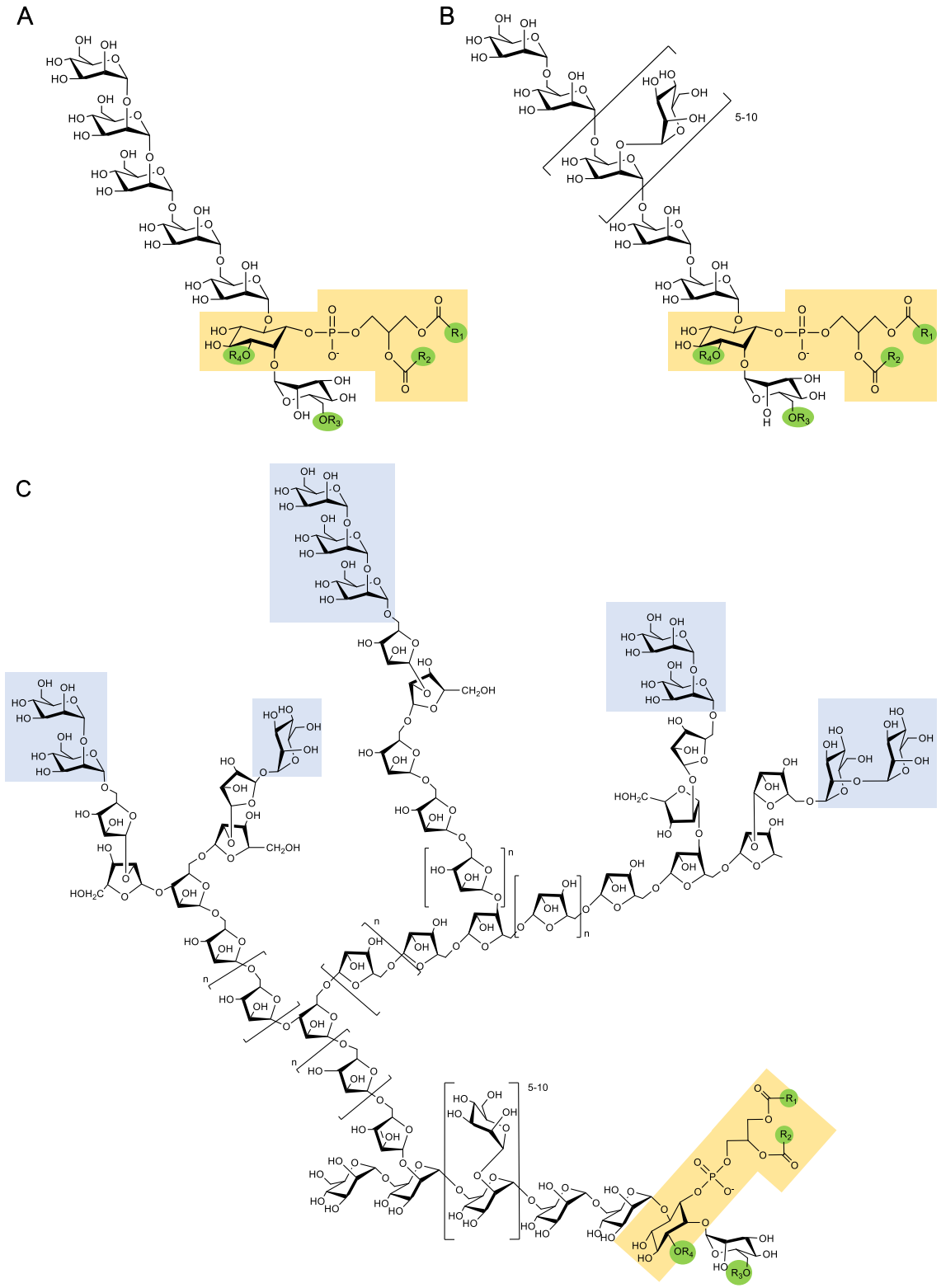

Figure 1.2 – Chemical structure of mycobacterial mannoglycans. A) PIM_6, one of the most abundant lipoglycans in mycobacteria and the last in the PIM biosynthetic pathway. B) LM. C) LAM capped with mannosyl units. The yellow boxes identify the phosphatidyl-*myo*-inositol group present in the three glycans and the green circles indicated possible acylation sites. The blue boxes evidence the mannosyl units of LAM capping motifs present in pathogenic species such as *Mtb*. (n) indicates variable number of residues according to species. Adapted from Cao and Williams, 2010, Mishra et al., 2011 and Sancho-Vaello et al., 2017.

The first biosynthetic studies regarding these lipoglycans (PIM, LM, LAM) were performed in the 60's (Brennan and Ballou, 1967, 1968). Not surprisingly, since they possess the same backbone, the initial steps for the synthesis of the three polymers are similar and catalysed by the same enzymes, having a branch-point where the synthesis diverges for the different pathways (Guerin et al., 2007). The synthesis is initiated from PI with addition of mannosyl residues to positions 2 and 6 of the *myo*-inositol ring by PimA (α-(1→2)-mannosyltransferase, Rv2610c) and PimB' (α-(1→6)-mannosyltransferase, Rv2188), respectively, producing PIM_2 (figure 1.3) (Korduláková et al., 2002; Lea-Smith et al., 2008; Guerin et al., 2009). PimA and PimB' are essential for mycobacterial growth and the fact that a signal sequence is absent from their amino acid sequences and that these enzymes use guanosine diphosphomannose (GDP-mannose) as donor substrate (as opposed to membrane bound polyprenolphosphate), suggests that these initial steps could occur in the cytoplasm or close to the inner leaflet of the plasma membrane (Korduláková et al., 2002; Morita et al., 2004; Lea-Smith et al., 2008; Guerin et al., 2009). One of the acylation reactions was already identified and is catalysed by an acyltransferase (AcylT, Rv2611c) that adds a palmitic acid to the C6 of the first mannose of the *myo*-inositol ring (Korduláková et al., 2003). However, this enzyme uses PIM_1 (intermediate product of the PimA reaction) and PIM_2 as substrates, which leads to two possible pathways for the initial steps of the biosynthesis: the PI can either be mannosylated two times before being acylated or, alternatively, the addition of palmitic acid occurs between both mannosylation reactions (Korduláková et al., 2003). Both pathways can co-exist in mycobacteria but the first is favoured (figure 1.3) (Guerin et al., 2009).

The third mannosylation step was identified in *Mtb* CDC1551 and is carried out by the enzyme PimC, an α-(1→6)-mannosyltransferase that transfers a mannosylpyranose unit from GDP-mannose to Ac_3PIM_2, forming Ac_3PIM_3 (Kremer et al., 2002). The absence of this gene in *Mtb* H37Rv, allied to the fact that its disruption does not affect mycobacterial growth nor the total amount of lipoglycans when compared to the wild-type (WT), suggests the presence of other enzyme with compensatory activity (Kremer et al., 2002). The remaining acylations and the fourth mannosylation were not identified yet, but $AcPIM_4$/Ac_2PIM_4 is considered the synthesis branch-point where PIM, LM or LAM biosynthesis diverges, because the subsequent mannoses are added through different types of glycosidic bonds: the fifth and sixth mannoses of PIM are bound by α-(1→2)-linkages, whereas LM and LAM are extended by α-(1→6)-bonds (figure 1.3) (Patterson et al., 2003; Morita et al., 2004, 2006).

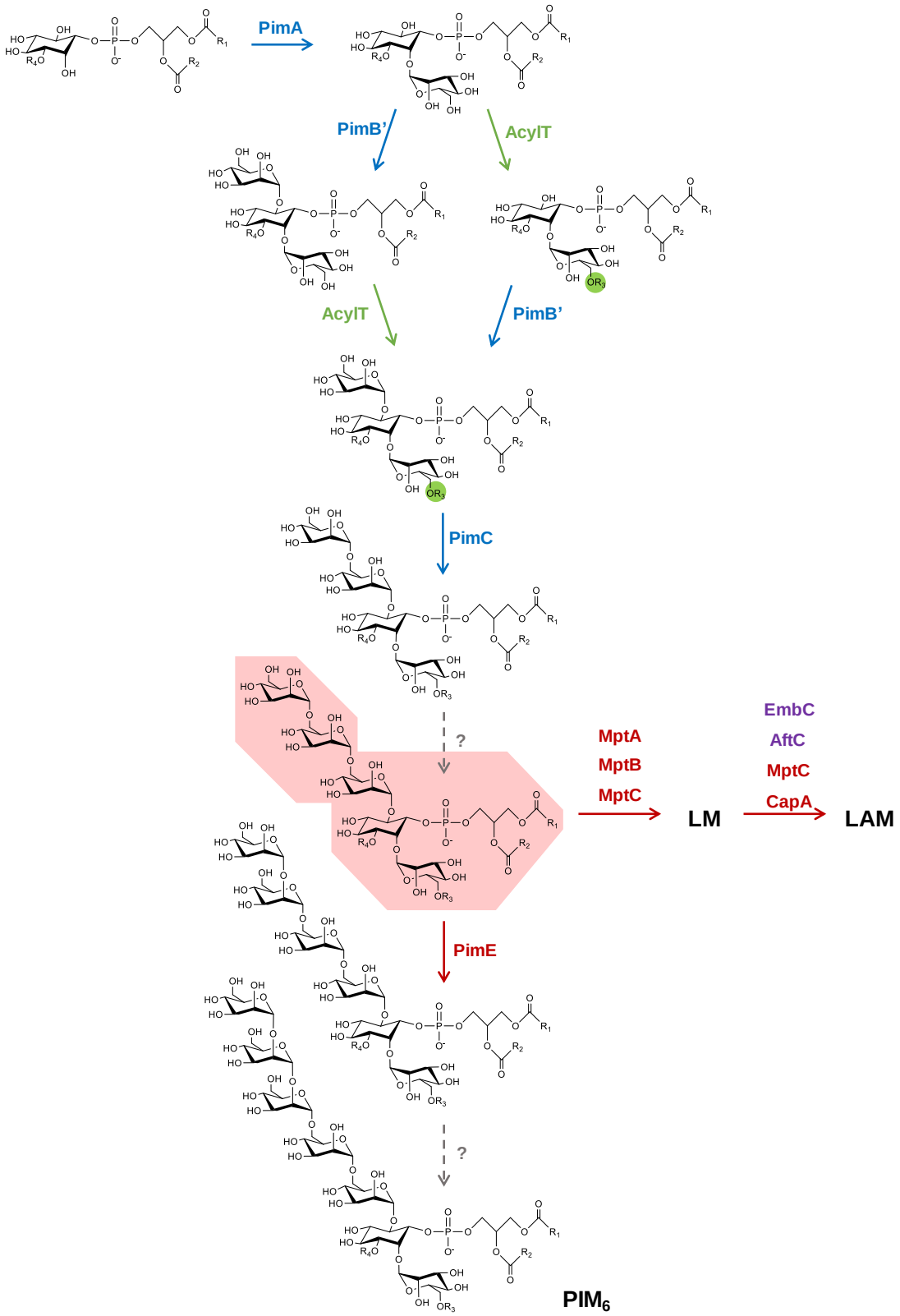

Figure 1.3 – Pathway for the synthesis of PIM, LM and LAM in mycobacteria. Mannosyltransferases depending on GDP-mannose are identified in blue, whereas mannosyltransferases that use polyprenol-phosphate-mannose (PPM) as mannose donor group are in red. The pink box highlights the branch-point of the pathway where the biosynthesis diverges between PIM, LM or LAM. The enzymes involved in the synthesis of the arabinan domain of LAM are indicated in purple. Dashed grey lines indicate unknown mannosyltransferases putatively involved in the pathway. Adapted from Korduláková et al., 2003, Cao and Williams, 2010 and Guerin et al., 2010.

To complete the PIM biosynthetic pathway an α-(1→2)-mannosyltransferase, PimE (Rv1159), catalyses the fifth mannosylation reaction in the periplasmic side of the membrane, and the mannose donor is polyprenol-phosphate-mannose (PPM) and not the cytosolic GDP-mannose (figure 1.3) (Besra et al., 1997; Morita et al., 2004, 2006). The last step in PIM synthesis leading to $AcPIM_6/Ac_2PIM_6$ has not been identified yet, although this form and $AcPIM_2/Ac_2PIM_2$ are the most abundant PIM forms in the mycobacterial cell wall (Morita et al., 2006).

As mentioned above, LM and LAM biosynthesis progress from the branch point after the production of $AcPIM_4/Ac_2PIM_4$ (selected in pink in figure 1.3) in the periplasmic side of the plasma membrane, using PPM as a donor group. Two α-(1→6)-mannosyltransferases elongate the main backbone, MptA (Rv2174) and MptB (Rv1459c), which are responsible for the synthesis of the distal and proximal ends of the mannan cores, respectively (figure 1.3) (Kaur et al., 2007; Mishra et al., 2007, 2008). LM and LAM are branched with a single mannosyl unit, catalysed by MptC (Rv2181), an α-(1→2)-mannosyltransferase that is also involved in the addition of mannose to the capping motif of LAM in pathogenic mycobacteria, together with CapA (Rv1635c), an α-(1→5)-mannosyltransferase (figure 1.3) (Dinadayala et al., 2006; Kaur et al., 2006, 2008; Mishra et al., 2011). The arabinan domain of LAM is similar to that of AG. One elongating enzyme identified in LAM biosynthesis is EmbC (Rv3793) that adds 12-16 Ara*f* residues with α-(1→5)-linkages, using decaprenylphosphoryl-D-arabinose (DPA) as donor group, and AftC (Rv2673) that adds α-(1→3)-Ara*f* units in specific steps of the pathway, allowing the initiation of the branching in the structure of the LAM arabinan domain (figure 1.3) (Shi et al., 2006; Birch et al., 2008; Alderwick et al., 2011). There have been speculations about other enzymes potentially involved in the arabinan domain biosynthetic pathway, but the unavailability of substrates hinders the identification and study of the complete enzymatic process (Abrahams and Besra, 2018).

3. Mycobacterial intracellular glycans

Mycobacteria are able to synthesize several intracellular carbohydrates and derivatives, including glycogen, trehalose and unique polymethylated polysaccharides, all of which are involved direct or indirectly in the maintenance of cell envelope composition and structure, which emphasizes their importance in mycobacterial growth and survival.

Glycogen is a large glucose polymer composed of a main chain of approximately 90% α-(1→4)-glucopyranosyl residues and branched with α-(1→6)-linkages (Chandra et al., 2011). This α-glucan is an energy source in many organisms and in mycobacteria shows structural similarity to capsular α-glucan (Sambou et al., 2008). Trehalose is a glucose disaccharide

synthesized by numerous species of the three domains of the Tree of Life, except in mammals, and in addition to its metabolic roles as carbon source and as storage carbohydrate, it also serves protective and adaptive functions as compatible solute (Murphy et al., 2005). In mycobacteria, trehalose is the major free sugar in the cytoplasm, as well as a major structural component of glycolipids in the cell envelope, e.g., trehalose monomycolates (TMM), trehalose dimycolate (TDM), diacyltrehaloses (DAT) and pentacyltrehalose (PAT) (Murphy et al., 2005; Nobre et al., 2014). The absence of biosynthetic pathways for this sugar in mammals make the mycobacterial routes and their intervening enzymes attractive targets for antimycobacterial therapeutics (Nobre et al., 2014). The importance of these carbohydrates in mycobacteria is highlighted by the existence of three different biosynthetic pathways for trehalose, namely the OtsA-OtsB, TreY-TreZ and TreS pathways (Nobre et al., 2014), and by related synthesis mechanisms involving glycogen, trehalose and maltose, which despite functional redundancy, reflect the crucial contribution of α-glucans in mycobacteria survival (Elbein et al., 2010; Kalscheuer et al., 2010; Nobre et al., 2014).

3.1. Polymethylated polysaccharides: methylglucose lipopolysaccharide (MGLP) and methylmannose polysaccharide (MMP)

Mycobacteria synthetize two intracellular polymethylated polysaccharides (PMPS): the methylglucose lipopolysaccharide (MGLP) and the methylmannose polysaccharide (MMP). These molecules were identified in the 1960s by Ballou and co-workers (Lee, 1966; Gray and Ballou, 1971) and quickly raised a great deal of interest due to their particular composition and features directly associated to the modulation of mycobacterial fatty acids (FA) metabolism (Ilton et al., 1971).

MGLP is a glucan constituted by a main chain of glucose and 6-*O*-methylglucose units, some of which differentially acylated with acetate, propionate, isobutyrate, succinate and octanoate (Saier and Ballou, 1968a, 1968b). The MGLP reducing end is composed of glyceric acid linked through an α-(1→2) linkage to the first glucose unit in the polysaccharide to form glucosylglycerate (GG). GG is in turn linked to a second glucose through an α-(1→6) linkage, initiating the main α-(1→4) MGLP chain. The 1st and 3rd glucoses of the α-(1→4) main chain are branched with β-(1→3)-linked glucoses, whereas a 3-*O*-methylglucose unit represents the nonreducing terminus of MGLP (figure 1.4) (Tuffal et al., 1998; Mendes et al., 2012; Maranha et al., 2015).

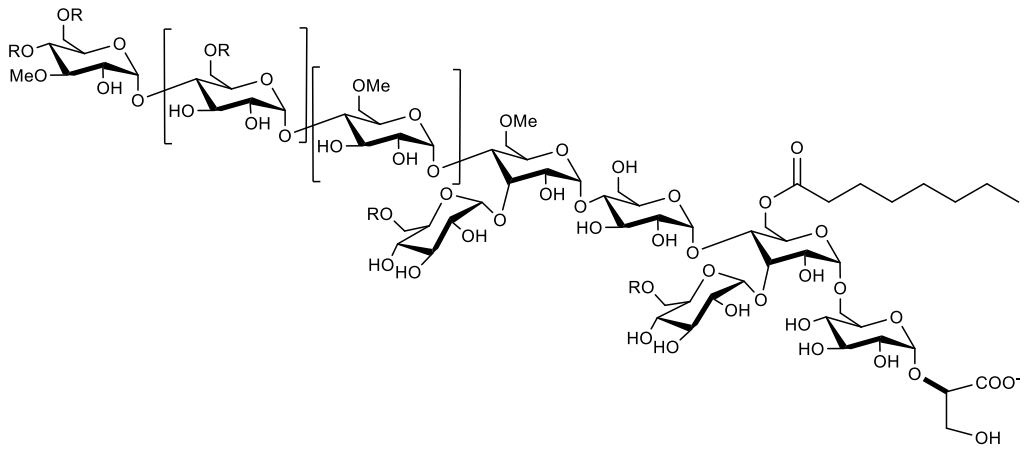

Figure 1.4 – Chemical structure of mycobacterial MGLP. R's correspond to the position of acyl groups (acetate, propionate, isobutyrate, succinate) Adapted from Maranha et al., 2015.

The MMP basic unit, 3-*O*-methylmannose, is a relatively rare molecule in nature and the first monomers were identified in *Streptomyces griseus* (Candy and Baddiley, 1966), followed by isolation and characterization of a polysaccharide composed of this methylated sugar from *M. phlei* and *M. smegmatis* (Gray and Ballou, 1971; Maitra and Ballou, 1977). Mycobacterial MMP is composed of 11 to 14 non-acylated 3-*O*-methylmannoses, forming an α-(1→4) linked linear chain with the reducing end blocked by a methyl aglycon, whereas the nonreducing end mannose is unmethylated (figure 1.5) (Maitra and Ballou, 1977). A striking difference between the mycobacterial and the *Streptomyces* spp. MMP is that in the latter has esterified acetyl moieties at position 6 of some of the 3-*O*-methylmannose residues, hence it was designated acetylated MMP (AMMP) (Candy and Baddiley, 1966; Harris and Gray, 1977; Kari and Gray, 1979).

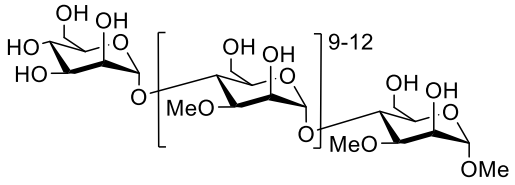

Figure 1.5 – Chemical structure of mycobacterial MMP. Adapted from Mendes et al., 2012.

MGLP has been isolated from all examined mycobacteria (SGM and RGM) and several related *Nocardia* species (Lee, 1966; Hunter et al., 1986; Pommier and Michel, 1986) whereas MMP has only been detected in and purified from RGM species and from the related *S. griseus* (table 1.1) (Gray and Ballou, 1971; Harris and Gray, 1977; Tian et al., 2000).

Table 1.1 – PMPS distribution in mycobacteria and in strains of related genera.

Species	Growth	MGLP	MMP	Reference
M. tuberculosis	SGM	+	-	(Lee, 1966; Stadthagen et al., 2007)
M. bovis		+	n.d.	(Tuffal et al., 1998)
M. leprae		+	n.d.	(Hunter et al., 1986)
M. xenopi		+	n.d.	(Tuffal et al., 1995)
M. smegmatis	RGM	+	+	(Kamisango et al 1987; Bergeron et al. 1975)
M. phlei		+	+	(Ilton et al., 1971; Weisman and Ballou, 1984b)
M. vaccae		+	n.d.	(Tian et al., 2000)
M. parafortuitum		+	+	(Weisman and Ballou, 1984b)
M. aurum		+	+	(Weisman and Ballou, 1984b)
M. chitae		+	+	(Weisman and Ballou, 1984b)
Streptomyces griseus		n.d.	+	(Candy and Baddiley, 1966)
Nocardia otitidis-caviarum		+	n.d.	(Pommier & Michel 1986)
Nocardia brasiliensis		+	n.d.	(Pommier & Michel 1986)
Nocardia farcinica		+	n.d.	(Pommier & Michel 1986)
Nocardia kirovani		+	n.d.	(Pommier & Michel 1986)

+: detected; -: not detected; n.d.: not determined

The first structural studies conducted regarding MGLP and MMP proposed that they would adopt different conformations in solution, with MGLP likely assuming a helical structure and MMP producing a cyclic form (Lee, 1966; Gray and Ballou, 1971). However, upon revision of MMP structure, it was proposed that both would adopt a helical structure in solution with the methyl groups facing the helix interior and the free hydroxyl groups exposed to the exterior, forming a hydrophobic tunnel similar to cyclodextrins (Machida et al., 1973; Bergeron et al., 1975; Yabusaki et al., 1979). Allied to this particular structural conformation, these molecules have been demonstrated to form 1:1 complexes with FA, preferring the long-chain acyl-CoAs between C_{16-22}, being palmitoyl-CoA the favourite, in detriment of short-chain derivatives with C_{10-14} or non CoA FA such as palmitate (Machida and Bloch, 1973; Bergeron et al., 1975). Moreover, binding of palmitoyl-CoA induced conformational changes in MMP that could be inferred from techniques such as optical rotation, NMR (^{1}H and ^{13}C) and thermodynamics (Bergeron et al., 1975; Yabusaki et al., 1979; Maggio, 1980; Ballou, 1981; Kiho and Ballou, 1988). Recently, one study casted doubt about the conformation and mode of interaction of MMP with FA, suggesting that MMP would not assumes a helical structure and that the 3-*O*-methyl groups would be solvent exposed as well the hydroxyl groups with neither actually sequestering FA. NMR results and molecular docking simulations support the existence of disordered complexes and a significant role of carbohydrate-lipid interactions in stabilizing the MMP-FA complex (Liu et al., 2016).

Several studies have demonstrated that the presence of methyl groups is crucial to sequester the long-chain acyl CoA derivatives, since the capacity to form complexes was hindered after demethylation of MGLP and improved with methylation of α-cyclodextrins (Machida et al., 1973; Bergeron et al., 1975). This inclusion and protection of FA by PMPS further allow the polysaccharides to prevent acyl-CoA hydrolysis, protecting them from degradation by cytoplasmic lipolytic enzymes (Yabusaki and Ballou, 1978, 1979).

PMPS were described as causing a stimulatory effect on FA synthesis, showing a reduction of the K_m of fatty acid synthetase (FAS) around nine-fold and four-fold for acetyl-CoA and malonyl-CoA, respectively, when present in the reactions (Ilton et al., 1971; Goren, 1972; Vance et al., 1973). However, the stimulatory effect of PMPS was affected by acetyl-CoA concentrations, being negligible at high acetyl-CoA concentrations (300 μM) but markedly high at low acetyl-CoA concentrations (20 μM). MMP is more effective at stimulating FAS-I than MGLP (Vance et al., 1973), allowing FA synthesis to occur at low acetyl-CoA concentrations. This stimulatory effect toward FAS is associated with its ability to form complexes with the acyl-CoA substrate. When binding long chain acyl-CoA, PMPS relieve the inhibition mechanism of the enzyme caused by the end product, allowing its diffusion into the intracellular aqueous environment and accelerating the overall of FA synthesis (Vance et al., 1973). After a huge initial burst rate of FA synthesis, MMP allows maintenance of the high levels of production by FAS in steady state, reducing significantly the K_m for acetyl-CoA and avoiding the rate-limiting step verified in the absence of MMP (Banis et al., 1977; Wood et al., 1977). Moreover, MMP influences the transacylation reaction that is the transfer of the CoA group to the acyl produced, increasing ten-fold the production of long acyl chains (C_{24}-CoA), since in the absence of MMP only C_{16}-CoA acyl chains or smaller are produced (Peterson and Bloch, 1977). Thus, mycobacterial PMPS are associated to the large stimulation of *de novo* synthesis and elongation of FA (Konrad, 1977).

3.1.1. Biosynthesis of MMP

The first steps towards elucidating PMPS biosynthesis initiated by Ballou and co-workers led to the identification of some enzymatic activities involved in MGLP and MMP biosynthetic pathways (Ferguson and Ballou, 1970). MGLP received substantially more attention, because it is the only of two polysaccharides found in pathogenic mycobacteria such as *Mtb*, and as such they could provide targets for therapeutic strategies (Jackson and Brennan, 2009; Mendes et al., 2012). Hence, the pathway was studied in detail in the last years and at least five gene clusters involved in MGLP synthesis were identified in *Mtb* H37Rv (Mendes et al., 2012). Some genes and enzymes were extensively studied, their functions identified and characterized and, in some cases, the three dimensional structures determined (Stadthagen et al., 2007;

Empadinhas et al., 2008; Pereira et al., 2008; Kaur et al., 2009; Mendes et al., 2011; Alarico et al., 2014; Maranha et al., 2015; Cereija et al., 2017). MGLP is a α-(1→4)-glucan sharing similarities with other α-glucans mentioned above and, curiously, some of the biosynthetic enzymes are related with glycogen biosynthetic enzymes, revealing compensatory activities (Stadthagen et al., 2007; Sambou et al., 2008).

The biosynthetic pathway for MMP was initially proposed in 1984 by Ballou and co-workers, suggesting that MMP polymerization would occurs through alternating mannosylation and methylation reactions catalysed by a mannosyltransferase and a methyltransferase (MTase), respectively (Weisman and Ballou, 1984a, 1984b). In this pathway, a mannosyltransferase would catalyse the transfer of mannose from GDP-mannose to a terminal 3-*O*-methylmannose, alternating with a MTase for the transfer of methyl groups from *S*-adenosylmethionine (SAM) to the growing mannose chain (figure 1.6 A). In these studies, mannosyltransferase activity was detected in cell membrane extracts of *M. smegmatis* and was active in the presence of methylated tetra- to dodeca-mannosides ($Met_{1,3}Man_4$-$Met_{1,3}Man_{12}$) with a sharp decrease in affinity over $Met_{1,3}Man_6$ (Weisman and Ballou, 1984b). This was not surprising since when working in the isolation of *M. smegmatis* MMP, the smaller MMP intermediates found were pentamannosides, suggesting that the early biosynthetic steps could involve mechanisms other than elongation reactions (Yamada et al., 1979; Weisman and Ballou, 1984b). On the other hand, MTase activity was detected in soluble extracts and showed broader activity, capable of methylating oligomannosides ranging from two to eleven mannose residues, despite the fact that the enzymatic extract was more active with smaller acceptors between tri and pentamannosides (Weisman and Ballou, 1984a). These authors also proposed that MTase would be involved in MMP termination with an unmethylated mannose, since the affinity towards the longer mannosylated acceptors decreased progressively (Weisman and Ballou, 1984a). Furthermore, the presence of palmitoyl-CoA could induce the formation of complexes with the newly formed MMP molecule, diminishing the affinity of MTase to methylate the last mannose (Weisman and Ballou, 1984a). All oligomannosides tested in these assays were obtained through Smith degradation and methanolysis from a mixture of mature $MMP_{11\text{-}14}$. Selected precursors had different polymerization degrees but all of them had a methyl group at the 1-OH position (Yamada et al., 1979; Weisman and Ballou, 1984a, 1984b).

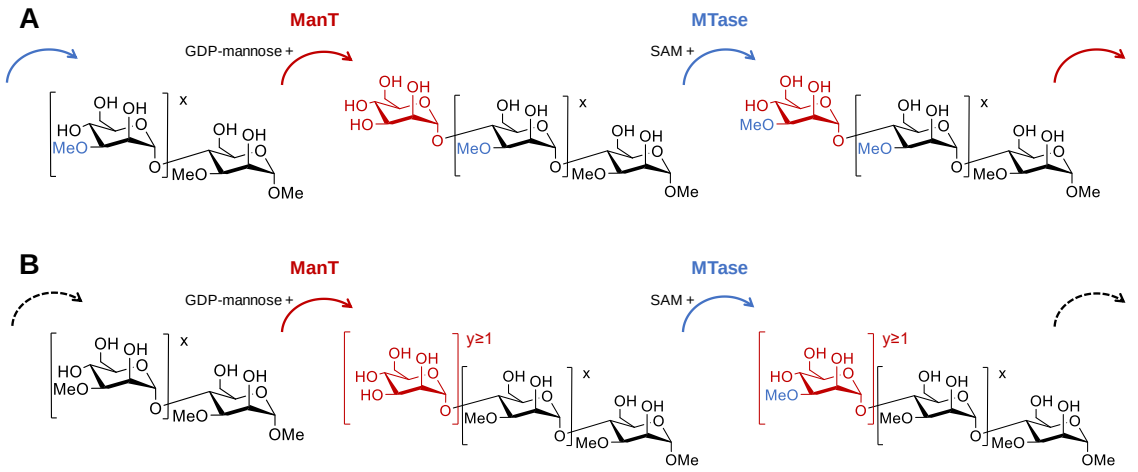

Figure 1.6 – Schematic representation of the proposed MMP biosynthetic pathway. A) Weisman and Ballou in 1984 proposed a mechanism with alternating mannosylation and methylation reactions. B) Xia and colleagues suggested that mannosylation and methylation reactions are independent. ManT, mannosyltransferase; MTase, methyltransferase. The mannose groups added by ManT are highlighted in red and the methylation reactions in position 3 catalysed by MTase are in blue. Adapted from Xia et al., 2012.

Twenty-eight years later, an alternative pathway was postulated wherein ManT activity would be independent of mannose methylation, allowing the addition of successive mannose units prior to methylation (figure 1.6 B) (Xia et al., 2012). These authors were also able to detect an α-(1→4)-mannosyltransferase (ManT) activity in the membrane fraction of *M. smegmatis* using synthetic oligomannosides ranging from one to five mannoses (Man_{1-5}) with different degrees of 3-*O*-methylation (Xia et al., 2012). Independently of methylation, they observed ManT activity in membrane extracts of *M. smegmatis* from trimannosides and considered the tetramannosides as the preferential acceptors (Xia et al., 2012). To compare the influence of methylations, these authors further synthesized an unmethylated tetramannoside, showing that ManT activity decreased in the absence of methyl groups (Xia, 2013). The draft genome of *M. hassiacum* (Tiago et al., 2012) allowed us to identify the cluster of genes for the synthesis of MMP, a discovery that was the subject of a grant application funded by the Foundation for Science and Technology that the same year (https://app.dimensions.ai/details/grant/grant.3534321). Shortly thereafter, the *manT* gene identity in *M. smegmatis* was also reported based on bioinformatic studies but the recombinant enzyme was not purified (Xia, 2013). Still, *E. coli* extracts containing the *M. smegmatis* recombinant ManT were successfully used to confirm the enzyme's substrate specificity, showing that it mostly produced hexa- and heptamannoside from 3-*O*-methylated tetramannosides (Xia, 2013).

Since this polysaccharide seems to be exclusively produced in RGM, it is crucial to understand its physiological role and the likely important relation with FA metabolism, as well as its importance on cell envelope dynamics and impact on mycobacterial growth rate.

4. Objectives

Since the discovery of the mycobacterial MMP in the early 1970's, this polysaccharide has been isolated from environmental opportunistic NTM. Due to its absence from *M. tuberculosis* and from closely related pathogens, MMP did not attract as much attention as its counterpart MGLP, which appears to be produced by all mycobacteria, including the more pathogenic species. However, in recent years, with the increasing number of NTM infections it was deemed crucial to explore some of the particular features of these remarkable microorganisms and interrogate the MMP function and its apparently scattered distribution, namely by examining if the presence of both MGLP and MMP in some species can impact mycobacterial fitness in the environment or during infection. Hence, the major aim of this work was to identify the genes for the MMP biosynthetic pathway and to characterize the corresponding enzymes, which could be used as targets for development of innovative therapeutics to replace the dated and largely ineffective antibiotics in use against NTM diseases. Symbiosis between microbiology, enzymology, synthetic chemistry and crystallography was essential for the development of the activities in this thesis.

Chapter 2:
A unique MMP recycling mechanism by a novel hydrolase

1. Introduction

Mannose is a simple sugar and an epimer of glucose found in all organisms as a monomer, in a glycan or as a glycoconjugate, and involved in several metabolic and cell recognition processes (Ladevèze et al., 2017). Mannosyl units can be attached to the nitrogen of asparagine residues or the hydroxyl oxygen of serine and threonine residues of proteins, forming *N*-glycans or *O*-glycans, respectively (Ladevèze et al., 2017; Poole et al., 2018). This protein glycosylation mechanism is present not only in eukaryotes, but also in bacteria, often associated to bacterial pathogenicity and interaction with hosts (Poole et al., 2018). The outermost layers of fungal cell walls possess several *N*-mannosylated proteins containing large amounts of mannosyl units, about 100-150 in *Candida albicans* and 150 in *Saccharomyces cerevisiae*, linked by α-(1→6) linkages and branched chains composed of α-(1→2), α-(1→3), α-(1→6) and β-(1→2) bonds (Shibata and Okawa, 2010; Ladevèze et al., 2017). These organisms also have *O*-glycoproteins with mannose short chains with up to five units linked by α-(1→2) and α-(1→3) bonds (Buurman et al., 1998; Ladevèze et al., 2017). In pathogenic fungal species, such as *C. albicans*, mannoproteins are involved in host recognition and interaction processes such as adhesion, immune-surveillance and immune-modulation, contributing to their virulence (Buurman et al., 1998; Shibata and Okawa, 2010). Curiously, some archaea also have *N*-glycosylated proteins in their outer surface: *Methanothermus fervidus*, for example, has a carbohydrate moiety containing mannose and 3-*O*-methylmannose as well as *N*-acetylgalactosamine (Karcher et al., 1993; Ladevèze et al., 2017).

O-glycoproteins containing mannosyl residues were also found in mycobacteria, such as MPB83 (Mb2898) and Apa (Rv1860) that play roles of host adhesion and mycobacterial pathogenicity (Dobos et al., 1995, 1996; Michell et al., 2003; Ragas et al., 2007; Chen et al., 2012; Nandakumar et al., 2013). In these proteins, the mannosyl moieties are attached to threonine residues in Pro-rich domains, but show different number of mannoses and types of glycosyl bonds (Dobos et al., 1996; Michell et al., 2003). The Apa protein has one to three α-(1→2)-mannosyl units attached to four threonines, whereas MPB83 of *M. bovis* possesses three mannopyranose residues bound by α-(1→3)-linkages in two threonines (Dobos et al., 1996; Michell et al., 2003). Furthermore, the *O*-mannosylation of Apa was already observed using cell-free extracts from *M. smegmatis* (Cooper et al., 2002). Through bioinformatic tools, an *O*-mannosyltransferase (Rv1002c) was identified (VanderVen et al., 2005) and a *Mtb* mutant lacking a functional *Rv1002c* gene was highly attenuated in its pathogenicity and severely impaired on *in vitro* growth, which showed that *O*-mannosylation is also essential for *Mtb* virulence (Liu et al., 2013).

Mannose can also be organized in polymers designated mannans, which are found in eukaryotes and prokaryotes. In the cell wall of plants, mannans are the main components of

hemicellulose and are classified into four subfamilies according to their sugar composition: linear mannans, glucomannans, galactomannans and galactoglucomannans (Moreira and Filho, 2008; Malgas et al., 2015). All these molecules have a β-(1→4)-linked main chain either composed only by mannose or by a mixture of manno- and glucopyranose units and both can be α-(1→6)-branched with galactose (Moreira and Filho, 2008; Malgas et al., 2015). Recently, a polysaccharide was isolated from *Oligotropha carboxidovorans* with approximately 35-40 units of 3-*O*-methylmannose linked by α-(1→2)-glycosidic bonds, but its function in this bacterium is unknown (Komaniecka et al., 2017).

Actinobacteria are not an exception in having diverse extra and intracellular structures containing mannopyranose units, namely the phosphatidylinositol mannosides (PIM), lipomannans (LM), lipoarabinomannans (LAM) and methylmannose polysaccharide (MMP) (Ballou et al., 1963; Lee and Ballou, 1965; Harris and Gray, 1977; Maitra and Ballou, 1977; Lea-Smith et al., 2008; Cashmore et al., 2017). Mannosyl residues in PIM, LM and LAM are mostly linked through α-(1→2) and α-(1→6)-glycosidic bonds (Guerin et al., 2010) but, curiously, the mannose units in the intracellular polymethylated MMP are connected by unusual α-(1→4)-linkages that, so far, have not been found in nature in other mannans (Maitra and Ballou, 1977; Moreira and Filho, 2008). In addition, mannose is essential for mycobacterial growth and viability, as demonstrated with a mutant lacking the phosphomannose isomerase gene (*manA*), which caused an alteration of the mannose metabolism in the absence of exogenously added mannose (Patterson et al., 2003). The enzyme encoded by *manA* catalyses the interconversion of fructose-6-phosphate and mannose-6-phosphate, the unique pathway for *de novo* synthesis of mannose (Patterson et al., 2003). This mutation had consequences on processes involved in septation and cell division, hampering the growth rate of *M. smegmatis*, which could be rescued in the presence of exogenous mannose (Patterson et al., 2003). Moreover, the synthesis rate of the abovementioned mannose polymers also decreased when compared to WT *M. smegmatis* (Patterson et al., 2003).

As mannosides are ubiquitous in nature, the existence of enzymes that can degrade them is crucial and several have been isolated from the microbial world. Two types of mannoside-degrading enzymes were identified: the mannosidases, which hydrolyse the nonreducing terminal of a mannoside to release mannosyl units, and the mannanases (endo-mannanases or endo-mannosidases) whose cleavage site in a mannan backbone is internal (Chauhan and Gupta, 2017; Srivastava and Kapoor, 2017). These enzymes are part of the CAZY database of glycosyl hydrolases (http://www.cazy.org/Glycoside-Hydrolases.html) with diverse types of both α- and β-mannosidases, as well as different β-(1→4)-mannanases, many of which identified in bacteria and fungi (Cantarel et al., 2009; Chauhan and Gupta, 2017; Srivastava and Kapoor, 2017). However, the same is not true for the α-mannanases characterized thus far, which seem

to be more restricted and were only characterized in *Bacilllus circulans* and *Bacteroides thetaiotaomicron* (α-(1→6)-mannanases), in a strain of *Flavobacterium* (α-(1→3)-mannanase) and in *Bacteroides* species and *Shewanella amazonensis* (α-(1→2)-mannanases) (Nakajima et al., 1976, 1996; Maruyama and Nakajima, 2000; Matsuda et al., 2011; Thompson et al., 2012).

2. Methods

2.1. Extraction and purification of MMP

MMP was isolated from *M. smegmatis*, following the protocols described in Tuffal et al., (1995) and Stadthagen et al., (2007) with some modifications. *M. smegmatis* was grown in a glycerol-based medium at pH 7.0 (20 g/L glycerol, 5 g/L casamino acids (Difco), 1 g/L fumaric acid, 1 g/L K_2HPO_4, 0.3 g/L $MgSO_4$, 0.02 g/L $FeSO_4$ and 2 g/L Tween 80) (Brennan and Ballou, 1968) and total lipids, including the amphiphilic polymethylated polysaccharides (PMPS), were extracted with chloroform:methanol (1:2) for three hours under constant agitation. After centrifugation (8000 rpm, 30 min, room temperature (rt)), the supernatant was recovered and evaporated, followed by another extraction step with chloroform:methanol (2:1). The aqueous phase was retrieved, concentrated by evaporation and purified by reverse phase chromatography on Resource RPC column (GE Healthcare). MMP was eluted with 30% (v/v) methanol in water and fractions were analysed by thin-layer chromatography (TLC) using chloroform:methanol:water (55:40:10, v/v/v) as the solvent system. The TLC plate was stained by spraying with α-naphtol-sulfuric acid solution, followed by charring at 120 °C (Jacin and Mishkin, 1965). Residual methanol from the RPC purification was evaporated in a centrifugal vacuum concentrator (Thermo Fisher) and fractions containing MMP were pooled and further purified on a HiPrep 16/60 Sephacryl S-200 HR column (GE Healthcare), equilibrated in water. The fractions collected were analysed by TLC as described above, and those containing MMP were pooled and lyophilized (Scanvac CoolSafe, Labogene).

2.2. Mass spectrometry analysis of MMP variants

The MMP sample was suspended and/or diluted in a solution containing 50% (v/v) acetonitrile and 0.1% (v/v) formic acid and analysed in a Triple TOF™ 5600 or Triple TOF™ 6600 System (Sciex) by direct infusion. The flow rate was set to 10 µL/min and the ionization source (ESI DuoSpray™ Source) was operated in either the positive mode (ion spray voltage of 5500 V) or negative mode (ion spray voltage of -4500 V) and set at 25 psi for nebulizer gas 1 (GS1), 25 psi for the curtain gas (CUR). The acquisition was performed in full scan mode (TOF-MS mode) and product ions were obtained using collision energy ramping. The samples were analysed by mass spectrometry (MS) at the CNC/UC Proteomics Facility.

2.3. Identification of the MMP biosynthesis operon in *M. hassiacum*

Based on the proposed biosynthetic pathway for MMP (Weisman and Ballou, 1984a, 1984b; Xia et al., 2012), we identified a 4-gene cluster in the *M. hassiacum* genome encoding a putative glycosyltransferase, two putative *S*-adenosylmethionine (SAM)-dependent methyltransferases and a protein of unknown function (Empadinhas et al., 2012; Tiago et al., 2012). The amino acid

sequences of the four enzymes were retrieved from the *M. hassiacum* genome and used in BLAST analysis (https://blast.ncbi.nlm.nih.gov/Blast.cgi) in order to detect homology with other species of mycobacteria and related organisms.

2.4. Recombinant expression and purification of MMP hydrolase (MmpH)

The protein of unknown function identified in the cluster was annotated at the NCBI database as a putative prenyltransferase but bioinformatic analysis revealed that it possesses a glycosyl hydrolase domain, hence we sought to investigate its function. For recombinant expression of the gene, herein designated *mmpH*, we selected the sequence from *M. hassiacum* (WP_110570796.1) and a synthetic sequence optimized for *E. coli* expression was obtained (GenScript). The gene was cloned between the *NdeI* and *HindIII* restriction sites of the expression vector pET30a and the construction was transferred to *E. coli* BL21 star. *E. coli* cells were grown in lysogeny broth (LB) medium supplemented with 30 µg/mL kanamycin at 37 °C until $OD_{600} \approx 0.8$, when the incubation temperature was decreased to 25 °C and recombinant protein expression was induced by addition of 0.5 mM isopropyl β-D-1-thiogalactopyranoside (IPTG). After overnight growth, 3 L of cell culture were harvested by centrifugation (9000 rpm, 15 min, 4 °C), suspended in 20 mL buffer A (20 mM sodium phosphate pH 7.4, 0.5 M NaCl, 20 mM imidazole) and frozen at -20 °C.

After thawing the cell pellets, 20 µg/mL DNAse I and 5 mM $MgCl_2$ were added and the cells were disrupted by sonication on ice with three 40 Hz pulses of 20 s (10 s pause between pulses) per 7 mL of lysate. The supernatant was clarified by centrifugation (17000 rpm, 30 min, 4 °C), filtered through a 0.45 µm pore low protein binding filter (Millipore) and loaded onto a 5 mL HisTrap HP column (GE Healthcare), previously equilibrated with buffer A. The protein of interest was eluted with 200 mM imidazole in buffer B (20 mM sodium phosphate pH 7.4, 0.5 M NaCl, 500 mM imidazole) and its purity assessed by SDS-PAGE. Fractions containing recombinant MmpH were pooled and concentrated using a 10 kDa molecular weight cutoff centrifugal ultrafiltration device (Millipore). To further purify the protein, the sample was loaded onto a HighPrep 16/60 Sephacryl S-200 and MmpH was eluted in 20 mM BTP pH 7.5 and 200 mM NaCl. Following purity assessment by SDS-PAGE, the fractions containing pure recombinant enzyme were pooled and concentrated as described above. The protein content was determined with the Bradford assay kit (BioRad).

2.5. Substrate specificity of MmpH and analysis of reaction products

The substrate specificity of MmpH acting as a glycosyl hydrolase was determined using maltotetraose, maltopentaose, maltohexaose, maltoheptaose, maltooctaose (Sigma), synthetic 4α-mannosides (see chapter 3, section 3.3), MMP, MGLP and deacylated MGLP (MGP)

(obtained by Ana Maranha), β-(1→4)-mannans (Megazyme) and the enzymes' own reaction products after purification (see below). The reaction mixtures containing pure MmpH (5.1 nM), 25 mM BTP pH 7.5 and 2.5 mM of different sugars were incubated at 37 °C during 2 h. Product formation was initially monitored by TLC on silica gel 60 plates (Merck) with a solvent system composed of chloroform:methanol:water (55:40:10, v/v/v) and revealed with α-naphtol solution as described above. To analyse the formation of reaction products, assays with MMP were performed in the same reaction conditions with different incubation times (5, 15, 30 min) at 37 °C and analysed by TLC.

The purification of MmpH products was performed by reverse phase chromatography using a Resource RPC column. The products were obtained in 2 mL reaction with 50 mM BTP pH 6.5, 1.5 mM MMP and 15.8 nM MmpH at 45 °C for 4 h. The reaction was diluted in water and injected in a RPC column and the products were eluted in 30-40% (v/v) methanol in water. The fractions were analysed by TLC as described above and pure fractions containing the same sugar were pooled and lyophilized (Scanvac CoolSafe, Labogene). The samples were analysed by MS at the CNC/UC Proteomics Facility. Each sample was suspended and/or diluted with a solution containing 50% (v/v) acetonitrile and analysed in Triple TOF™ 5600 or Triple TOF™ 6600 System (Sciex) by direct infusion. The flow rate was set to 10 µL/min and the ionization source (ESI DuoSpray™ Source) was operated in the positive mode (ion spray voltage of 5500 V) and negative mode (ion spray voltage of -4500 V), 25 psi for GS1, 25 psi for the CUR. The acquisition was performed in full scan mode (TOF-MS mode) and product ions were obtained using collision energy ramping.

2.6. Biochemical characterization of MmpH

MmpH activity was characterized by a discontinuous method through a highly sensitive reducing-sugar assay using *p*-hydroxybenzoic acid hydrazide (pHBAH), as previously described (Lever, 1972; Mellitzer et al., 2012), which reacts with reducing sugars and allows their quantification. The pHBAH stock solution 5% (w/v) in 0.5 M HCl was prepared and the working solution was obtained by diluting the stock with 0.5 M NaOH 1:4 (v/v), prepared freshly each day for measurement (Lever, 1972; Mellitzer et al., 2012). The assays were initiated by addition of 1.3 nM MmpH to reaction mixtures containing the appropriate buffer and 1.5 mM MMP. Cooling on ethanol-ice stopped the reaction and inactivation of the enzyme was achieved by addition of 150 µL of pHBAH working solution, followed by addition of 25 µL of 100 mM BTP pH 7.5. The quantification mixture was incubated 5 min at 95 °C and absorbance at 415 nm registered, after transferring the mixture to 96-well microtiter plates. The effect of pH was determined at 45 °C in 50 mM MES (pH 5.5 to 6.5) or BTP (pH 6.5 to 8.5) buffers and the temperature profile was determined between 25 and 65 °C in 50 mM BTP pH 7.5. The enzyme

activity dependence of divalent cations was examined by incubating the reaction mixture with the chloride salts of Mg^{2+}, Mn^{2+}, Ca^{2+}, Cu^{2+}, Fe^{2+}, Co^{2+} and Zn^{2+} (2.5 mM) and without cations, or in the presence of 10 mM ethylenediaminetetraacetic acid (EDTA) at 37 °C for 30 min. These reactions were analysed by TLC as described above. All experiments were performed in triplicate.

2.7. Kinetic parameters

The kinetic parameters for MmpH were determined under optimal conditions at 37 °C and 45 °C through a discontinuous method as described above. The K_m and V_{max} values were determined for MMP in reaction mixtures containing 50 mM BTP pH 6.5 and 1.3 nM enzyme. All experiments were performed in triplicate with appropriated controls. Kinetic parameters were calculated with GraphPad Prism software (version 5.00).

3. Results

3.1. Purification of MMP and analysis by mass spectrometry

The purification of MMP with a two-step chromatographic strategy allowed obtaining circa 3.5 mg of a pure MMP sample per litre of *M. smegmatis* cell culture. The sample was a mixture of MMP with different polymerization degrees, at least three, as shown in TLC (three adjacent spots at the bottom) (figure 2.1 A). This result matched a previous MMP extraction from *M. smegmatis*, where heterogeneous MMP differing on one methylated mannose were isolated (Maitra and Ballou, 1977; Yamada et al., 1979). To ascertain how many different degrees of polymerization of MMP were present in solution, the sample was analysed by MS. The spectrum acquired in positive mode showed four peaks of $[M+2H]^+$ ions that can be assigned to molecules with a total of 11 to 14 mannoses with different methylation, corresponding to different polymerization degrees of MMP (figure 2.1 B). In these ions, the mass/charge values of each molecule are reduced by half, since two charges are added to the molecules (table 2.1).

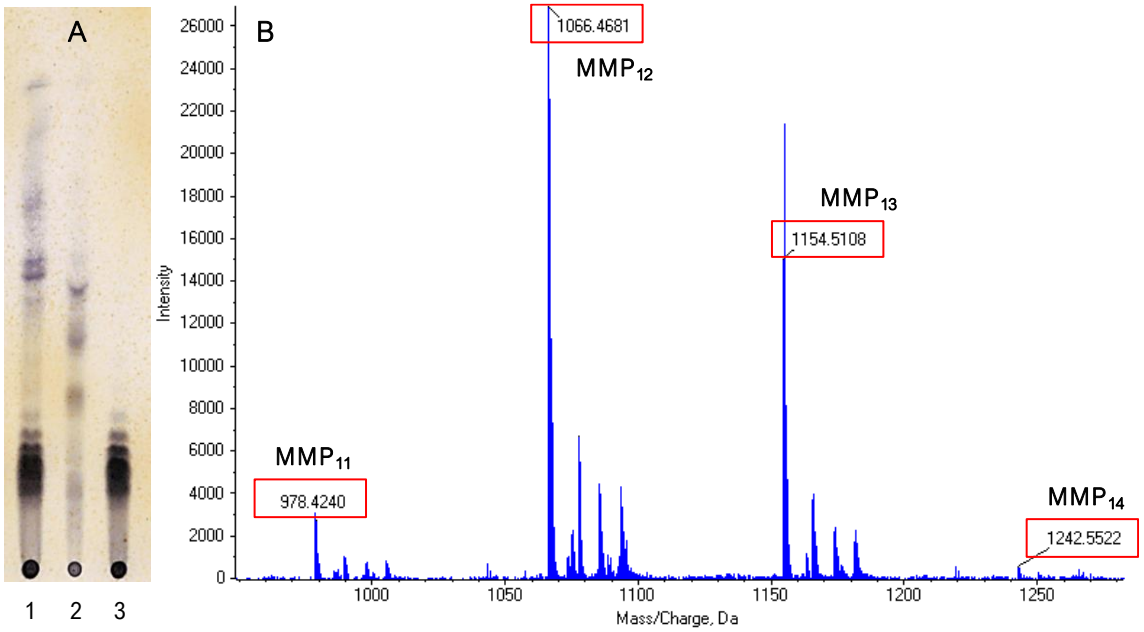

Figure 2.1 – MMP isolated from *M. smegmatis*. A) TLC plate with MMP separation by a two-step purification strategy: lane 1 – MMP-containing fractions pooled after reverse phase chromatography; lane 2 – impurities of MMP sample separated by gel filtration; 3 – pure MMP mixture obtained by gel filtration. B) ESI-TOF spectra of pure MMP sample acquired in positive ion mode. $[M-2H]^+$ ions are in a red box.

Table 2.1 – Calculated exact masses and corresponding ions formed in MS analysis for MMP_{11-14}.

Molecules	Exact mass (g/mol)	$[M-2H]^+$ (m/z)	Spectrum peak (m/z)
MMP_{11}	1954.77	978.39	978.42
MMP_{12}	2130.84	1066.43	1066.46
MMP_{13}	2306.91	1154.46	1154.51
MMP_{14}	2482.98	1242.50	1242.57

The molecular weights of these molecules correspond to MMP structures that Ballou and co-workers described for a polysaccharide with a reducing end blocked with a methyl aglycon, a main backbone of methylated mannoses, including the first mannose of the reducing end methylated in positions 1 and 3, and a nonreducing end with an unmethylated mannose residue (figure 2.2). As expected, each molecule detected differs in one methylated mannose, ranging from MMP_{11} with nine 3-*O*-methyl mannoses plus the reducing and nonreducing end terminal mannoses, to MMP_{14} with twelve 3-*O*-methyl mannoses plus the terminal mannoses. We tried to separate the $MMP_{11\text{-}14}$ heterogeneous mixture resorting to several chromatographic methods without success. However, the structural information resulting from MS analysis is restricted, not confirming the correct position of methyl groups, and only allowing matching the molecular weight to methylated mannose units (Zaia, 2004).

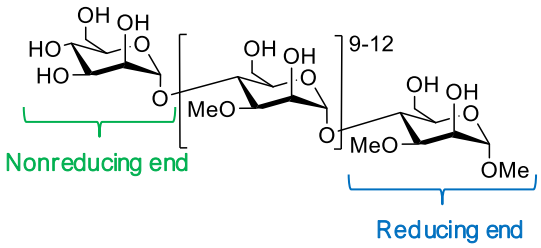

Figure 2.2 – Chemical structure of mycobacterial MMP. Reducing and nonreducing ends are identified. Adapted from Mendes et al., 2012.

To aid validation of the ions identified during MS analysis and attributed to MMP, the precursor ions of $MMP_{11\text{-}13}$ were subjected to MS/MS tandem fragmentation. Tandem MS breaks down a selected precursor ion into product ions (fragments) and the resulting pattern of fragmentation reveals certain aspects of the precursor ion chemical structure. In MS/MS of protonated large saccharides, ions deriving from glycosidic bond cleavages are likely to predominate, resulting in limited structural information. High-mannose oligosaccharides tend to produce product-ions from successive losses of hexose residues, resulting in a uniform product ion pattern (Zaia, 2004). Peaks corresponding to the loss of the nonreducing end mannose and two to three methylated mannoses (figure 2.3 A, peak 1411) are visible in the fragmentation spectra, as well is the successive loss of the glycosidic bond between the methylated mannoses in MMP (figure 2.3 A, peaks 1265, 1089, etc.; difference of 176 u). During the fragmentation process, the two charges ($2H^+$) that MMP molecules acquired during ionization are lost and the m/z displayed in the spectra are equal to the exact mass of the ion formed plus one proton, due to acquisition on positive ion mode. The fragments identified for each MMP correspond to mannosides containing the MMP reducing end and ranging from one to nine methylated mannoses, which match MMP's main backbone and corroborate the MMP proposed structure (table 2.2 and figure 2.3).

Table 2.2 – Calculated exact masses and corresponding ions formed in MS/MS analysis of MMP_{11-13}.

Molecules	Exact mass (g/mol)	$[M-H]^+$ (m/z)	Spectrum peak (m/z)
$Met_{1,3}Man$	208.09	209.10	209.09
$Met_{1,3}Man_2$	384.16	385.17	385.16
$Met_{1,3}Man_3$	560.23	561.24	561.22
$Met_{1,3}Man_4$	736.30	737.31	737.28
$Met_{1,3}Man_5$	912.37	913.38	913.34
$Met_{1,3}Man_6$	1088.44	1089.45	1089.40
$Met_{1,3}Man_7$	1264.51	1265.52	1265.46
$Met_{1,3}Man_8$	1440.58	1441.59	1441.52
$Met_{1,3}Man_9$	1616.65	1617.66	1617.58

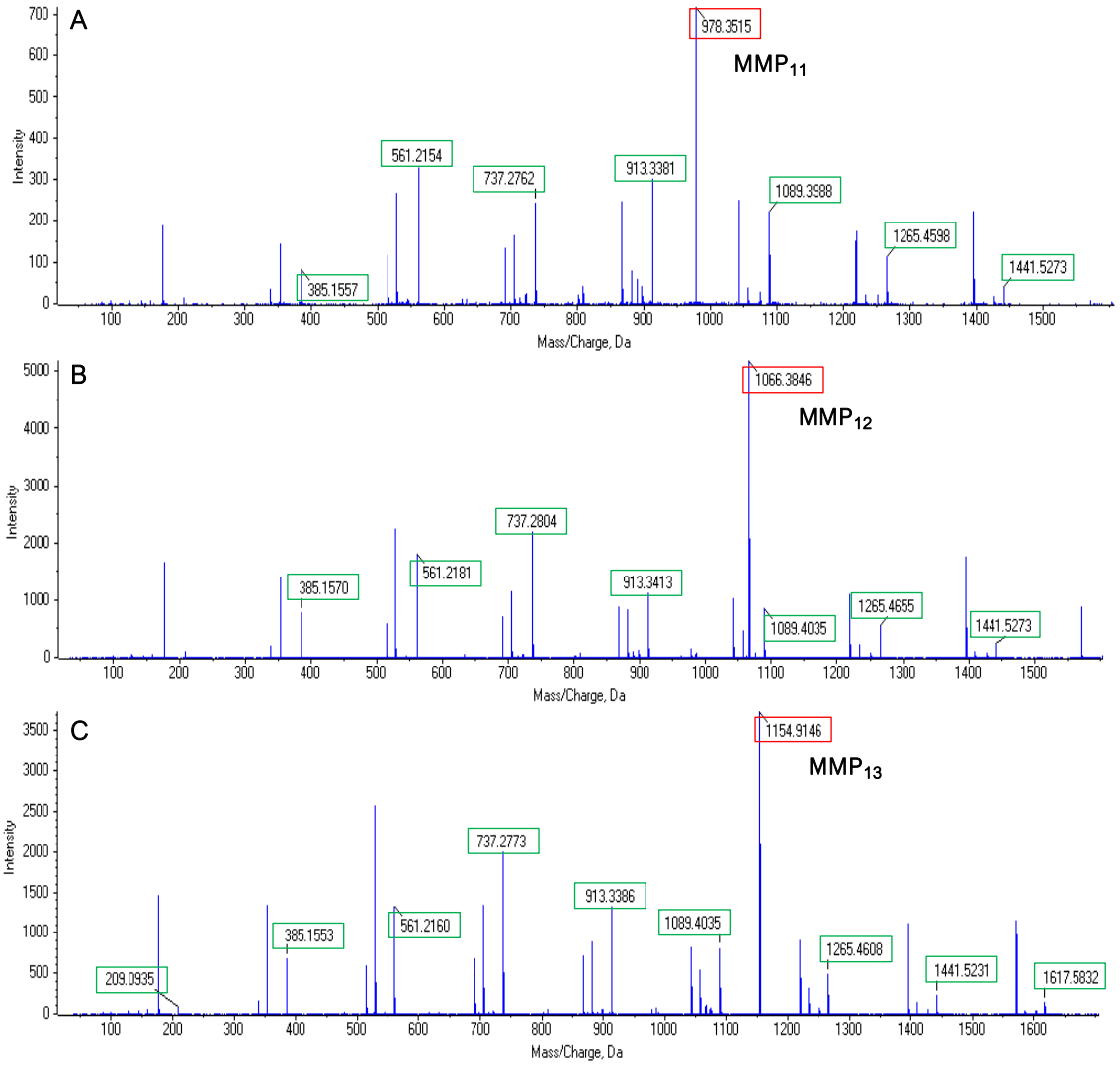

Figure 2.3 – MS/MS analysis of MMP_{11} (A), MMP_{12} (B) and MMP_{13} (C) acquired in positive ion mode. The red boxes identify the precursor $[M-2H]^+$ ions corresponding to MMP and the green boxes highlight the $[M-H]^+$ ions of the fragment formed in MS/MS fragmentation.

3.2. Identification of the MMP genetic cluster and the *mmpH* gene

A 4-gene cluster (figure 2.4) encoding a putative mannosyltransferase, two putative SAM-dependent methyltransferases and a protein of unknown function was identified in several NTM genomes (https://mycobrowser.epfl.ch/), some of which are known to produce MMP (table 1.1, chapter 1) (Gray and Ballou, 1971; Weisman and Ballou, 1984b; Kamisango et al., 1987; Tian et al., 2000). Similar clusters were detected in related actinobacteria, namely *Streptomyces griseus* and *Nocardia otitidiscaviarum*, although the former produces an acylated form of MMP and the latter has not been confirmed to synthesize MMP (figure 2.4). Although so far, the presence of MMP has only been reported in rapidly growing mycobacteria (RGM), similar clusters were detected in the genomes of several slowly growing mycobacteria (SGM), namely in some strains of *M. ulcerans* and *M. avium*, as well as in *M. xenopi* (figure 2.4). MMP biosynthetic gene clusters were not detected in genomes of members of the *M. tuberculosis* complex, in agreement with previous reports of the absence of MMP from these pathogens (Stadthagen et al., 2007).

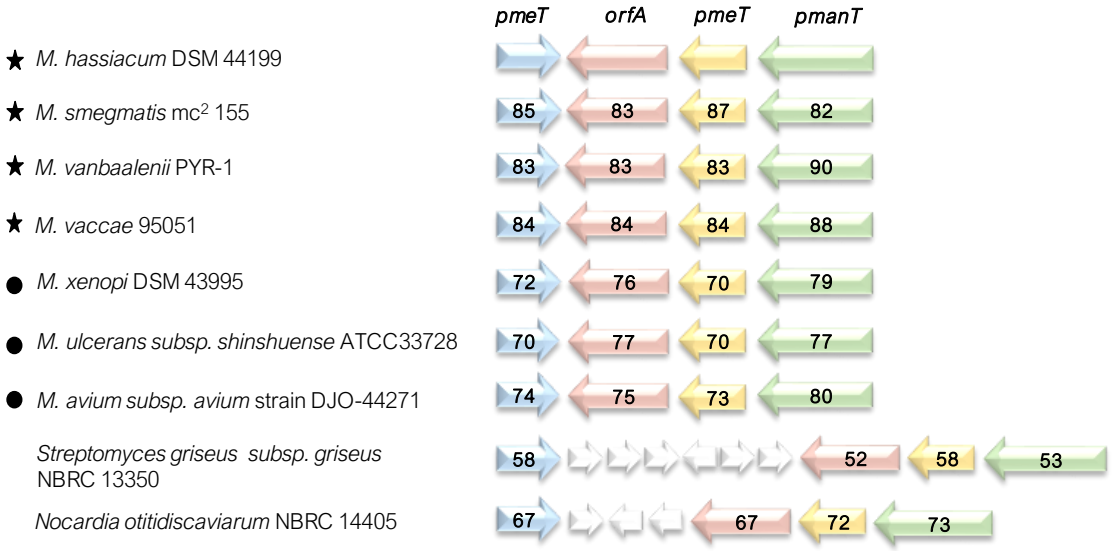

Figure 2.4 – Genomic organization of the MMP cluster in *Actinobacteria*. Cluster constituted by four genes (arrows) drawn to scale. *pmeT* (blue and yellow) are putative methyltransferases likely to add methyl groups in the 1-OH and 3-OH positions of mannose units. *orfA* (pink) protein of unknown function with a glycoside hydrolase domain. *pmanT* (green) putative mannosyltransferase. Black star, RGM; Black circle, SGM. The percentage of amino acid identity in relation to the *M. hassiacum* protein sequences is indicated inside the arrows.

The protein of unknown function identified in the 4-gene cluster was annotated as a prenyltransferase but possessed a glycosyl hydrolase domain, which aroused our interest, because a MMP hydrolase had never been reported. Thus, the enzyme encoded by the corresponding 1077 bp *M. hassiacum* gene (accession number WP_018354040.1) was purified

to homogeneity (figure 2.5) as a His-tagged recombinant protein from cell-free *E. coli* extracts in bioactive form at approximately 3 mg protein per litre of culture.

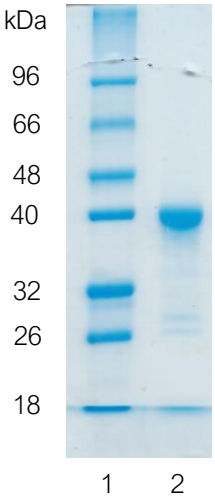

Figure 2.5 – SDS-PAGE analysis of the purified recombinant protein. Lane 1 – molecular weight marker; lane 2 – purified recombinant MmpH from *M. hassiacum*.

3.3. Substrate specificity of MmpH and analysis of reaction products

The protein of unknown function hydrolysed the purified mixture of MMP into oligomannosides and was thus designated MMP hydrolase (MmpH). The hydrolysis was observed by TLC through the appearance of two spots migrating above the MMP substrate. In these conditions, shorter substrates tend to migrate further in TLC, in relation to the point of origin, than substrates with a higher degree of polymerization (figure 2.6). MmpH did not present hydrolytic activity with β-mannans or other synthetic 4α-oligomannosides (chapter 3, section 3.3) or with its own reaction products (figure 2.7 B). Furthermore, the glucose counterparts of MMP, the acetylated and deacetylated forms of MGLP were also tested as possible substrates, as well as several maltooligosaccharides, but none of the glucose polysaccharides were substrates for the enzyme. The reaction products obtained after MMP hydrolysis were purified by reverse phase chromatography (figure 2.7 A). Despite several attempts to optimize the separation, a better separation of the products only allowed to obtain pure products in very little quantities after each purification round and most purification fractions were contaminated with the subsequent purified product (figure 2.7 A).

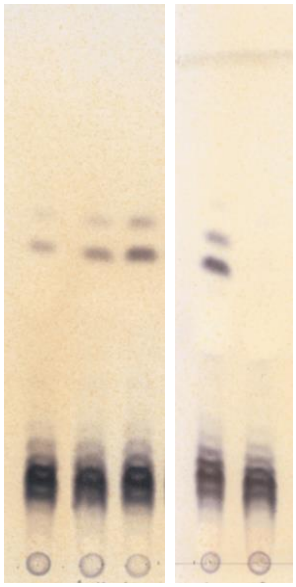

Figure 2.6 – TLC analysis of the hydrolytic activity of MmpH over time. Lane 1 – 5 min reaction; lane 2 – 15 min reaction; lane 3 – 30 min reaction; lane 4 – 2 h reaction; lane Ct- – control without enzyme. Reactions containing MmpH (5.1 nM), 25 mM BTP pH 7.5 and 2.5 mM MMP were incubated at 37 °C.

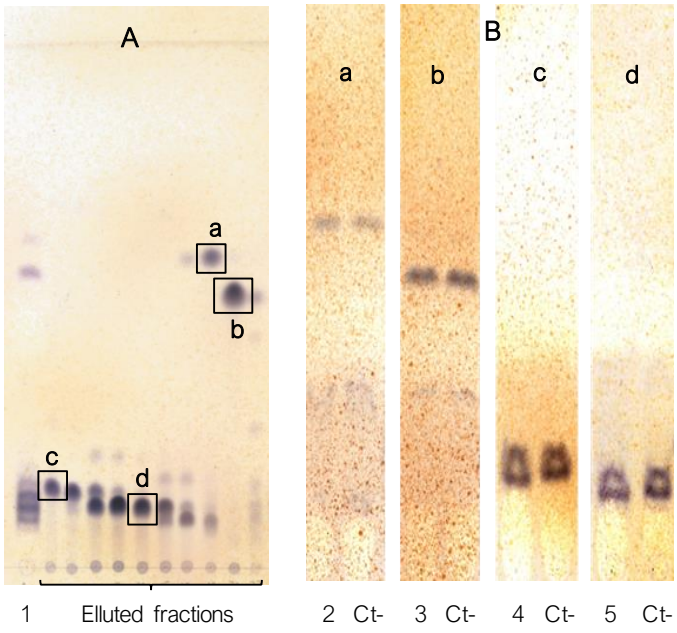

Figure 2.7 – A) TLC analysis of eluted fractions after purification of MmpH products. B) TLC analysis of MmpH activity using with its own reaction products **a** to **d** as substrates. **a** to **d** correspond to the purest hydrolytic products selected. Lane 1 – MmpH reaction with MMP for 2 h; lane 2 – MmpH reaction with product **a**; lane 3 – MmpH reaction with product **b**; lane 4 – MmpH reaction with product **c**; lane 5 – MmpH reaction with product **d**; lane Ct- – control without enzyme.

The purest fractions of the four main hydrolytic products were selected for MS analysis (figure 2.7 A **a**-**d**), revealing oligosaccharides differing in the number of mannose units and methylations. Product **a** (figure 2.8 A) corresponds to an oligosaccharide of four mannoses all methylated at position 3 and one also at position 1, whereas mass of product **b** corresponds to five methylated mannoses in the same position (figure 2.8 B). MS analysis of product **c** revealed an oligosaccharide constituted by seven mannoses in which six are methylated at position 3 and the last one is an unmethylated mannose (figure 2.8 C). Product **d** is very similar to product **c** with the addition of one methylated mannose at position 3 (figure 2.8 D). Despite several purifications, it was not possible to analyse the remaining products either due to obtaining insufficient product amounts or being unable to separate contaminants. It is important to highlight again that the methylation positions of four oligomannosides were not confirmed by MS, but were assumed from the original positions on the MMP structure proposed by Maitra and Ballou (Maitra and Ballou, 1977).

The MS precursor ions for each of the oligomannosides correspond to their calculated exact mass plus a Na^+ ion ($[M\text{-}Na]^+$, table 2.3), which were fragmented by MS/MS in order to confirm their proposed structures (figure 2.9 A-D). The fragmentation pattern observed for these samples was compatible with the loss of glycosyl bonds with successive loss of hexoses, which did not allow for the assignment of methylation positions but enabled interpretation of the general structures of the products formed. The fragmentation spectra (figure 2.9 A-D) for products **a** and **b** show successive loss of methylated mannoses, corresponding to a mass variation of 176 u, allowing to observe the m/z corresponding to the monosaccharide $Met_{1,3}Man$. In contrast, for the products **c** and **d**, we could detect ions that correspond to the loss of only the unmethylated mannose (162 u) and progressive reduction of one methylated mannose (table 2.3), most notoriously the monosaccharide MetMan.

Table 2.3 – Calculated exact masses and corresponding ions formed in MS/MS analysis of hydrolytic products.

Molecules	Exact mass (g/mol)	$[M\text{-}Na]^+$ (m/z)	Spectrum peak (m/z)	Molecules	Exact mass (g/mol)	$[M\text{-}Na]^+$ (m/z)	Spectrum peak (m/z)
$Met_{1,3}Man$	208.09	231.08	231.09	MetMan	194.08	217.07	217.08
$Met_{1,3}Man_2$	384.16	407.15	407.17	$MetMan_2$	370.15	393.14	393.16
$Met_{1,3}Man_3$	560.23	583.22	583.25	$MetMan_3$	546.22	569.21	569.23
$Met_{1,3}Man_4$ (Product **a**)	736.30	759.29	759.30	$MetMan_4$	722.29	745.28	745.31
$Met_{1,3}Man_5$ (Product **b**)	912.37	935.36	935.37	$MetMan_5$	898.36	921.35	921.39
Man-$MetMan_6$ (Product **c**)	1236.48	1259.47	1259.57	$MetMan_6$	1074.43	1097.42	1097.47
Man-$MetMan_7$ (Product **d**)	1412.55	1435.54	1435.66	$MetMan_7$	1250.50	1273.49	1273.56

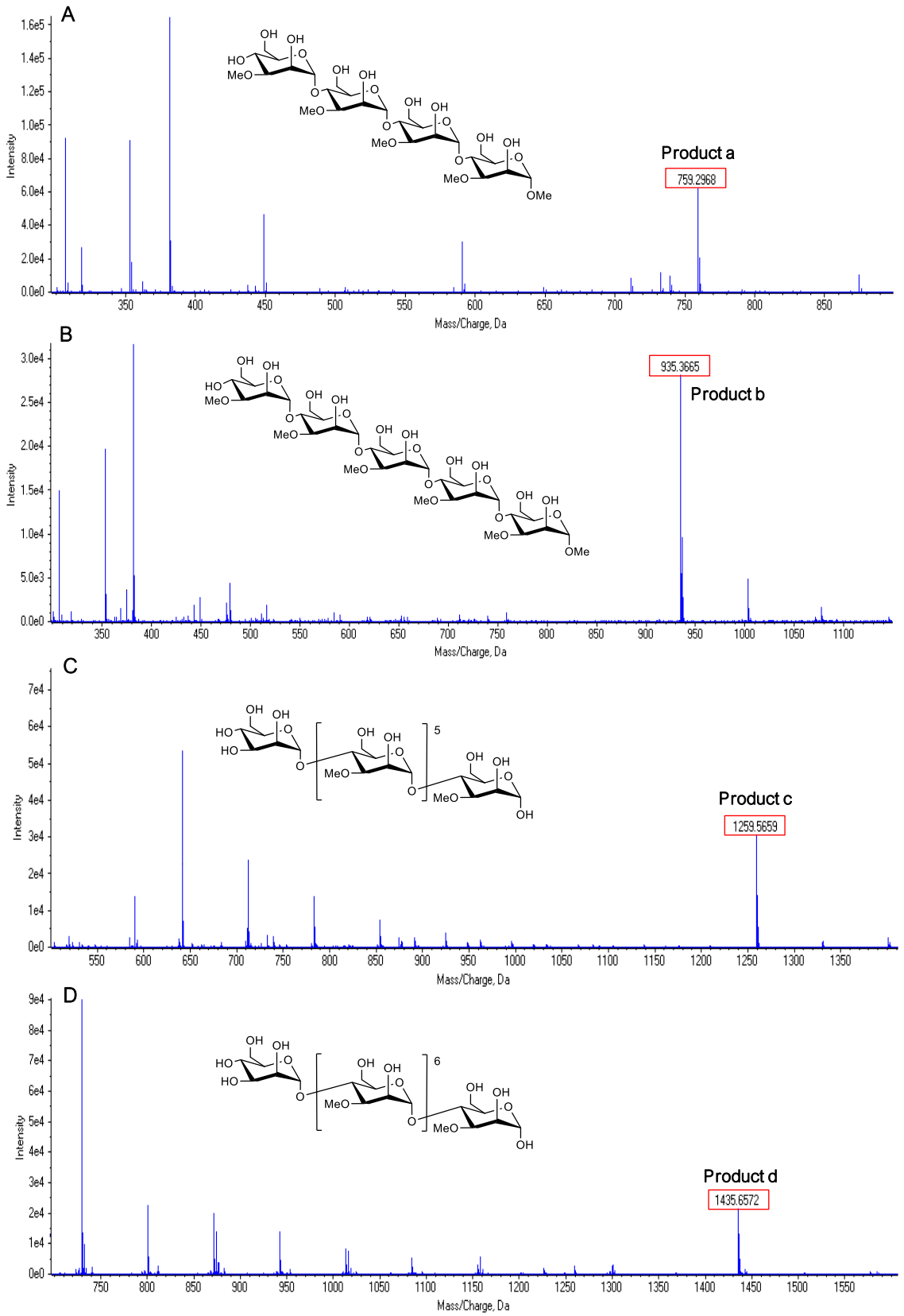

Figure 2.8 – MS analysis of purified oligosaccharide products after hydrolysis of MMP with recombinant MmpH. A – D) ESI-TOF spectra acquired in positive ion mode of samples **a** to **d**. Identified in a red box for each sample is the $[M\text{-}Na]^+$ ion. The chemical structure overlaid on spectrum correspond to the molecule identified in each sample.

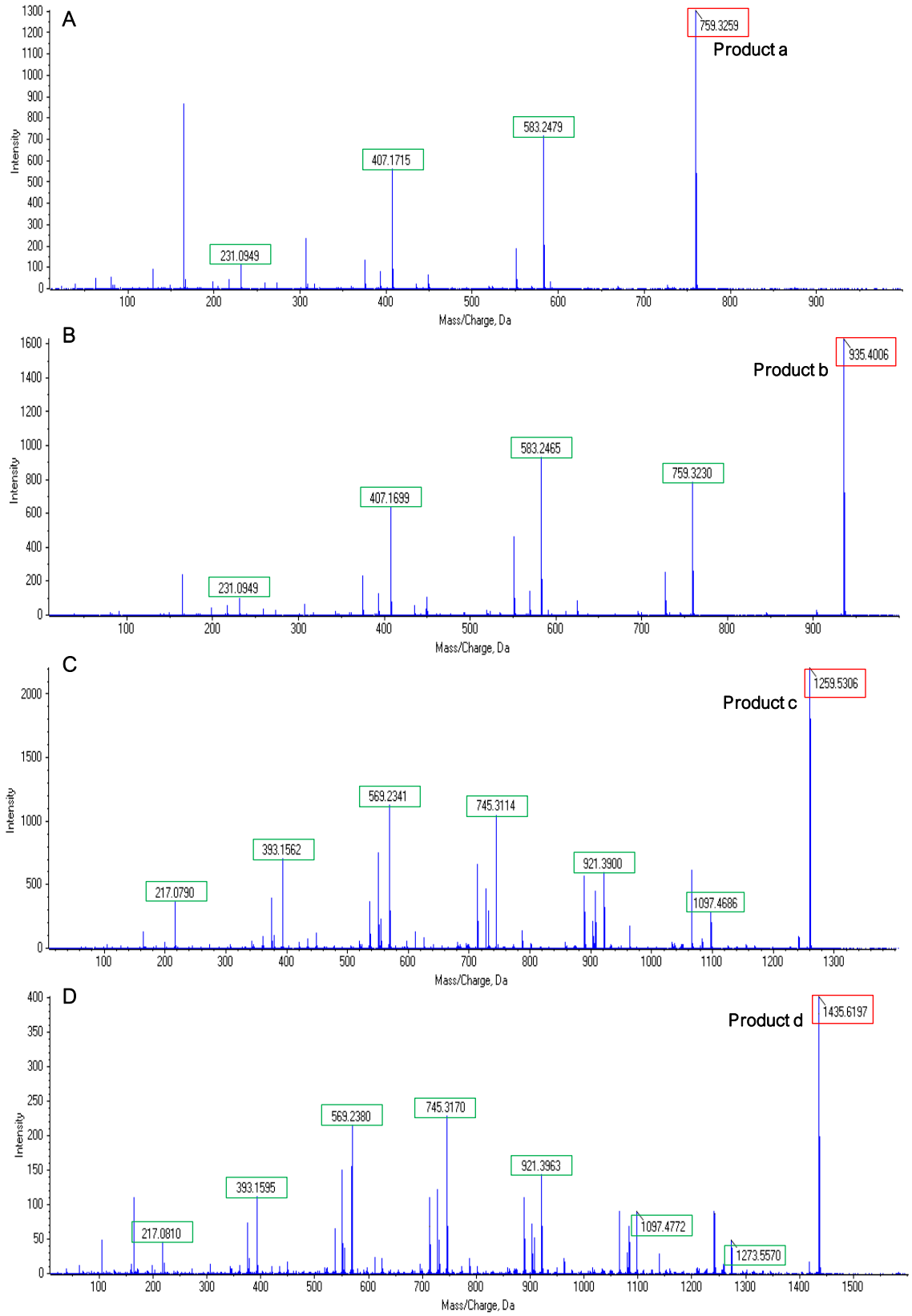

Figure 2.9 – MS/MS analysis of hydrolytic products' ions. A) Spectrum of product **a**. B) Spectrum of product **b**. C) Spectrum of product **c**. D) Spectrum of product **d**. Spectra acquired in positive ion mode. The red boxes indicate the precursor $[M\text{-}Na]^+$ ions and the green boxes highlight the $[M\text{-}Na]^+$ ions of each fragment formed from MS/MS fragmentation.

Based on MS results, we can conclude that products **a** and **b** retain the reducing end of MMP and products **c** and **d** match the nonreducing end of MMP, suggesting that the cleavage mechanism of MmpH is internal in regard to the MMP structure, acting as an α-(1→4)-mannanase. However, the presence of different degrees of polymerization of MMP hamper identification of the exact hydrolytic mechanism of MmpH, due to the possible formation of multiple products. In order to try to discern the hierarchy of product formation, reaction incubation time was decreased to 5 min, allowing to observe that product **b** was the first to be produced and that during the reaction time ranging from 5 min to 2 hours, the production of **b** is more pronounced than that of **a**, which is mirrored in the intensity of the spot of product **b** in relation to product **a** (figure 2.6). This also indicates that the pentamannoside **b** seems to be preferably produced and that eventually it might also be the preferentially produced *in vivo*. After several purifications, the octamannoside **d** was consistently purified in higher quantity than heptamannoside **c**.

3.4. Biochemical and kinetic properties of MmpH

Recombinant *M. hassiacum* MmpH was active between 25 and 65 °C, with maximum activity observed at 45 °C (figure 2.10 A) and between pH 5.5 and 8.5, showing an activity peak at pH 6.5 in BTP buffer (figure 2.10 B). MmpH activity was independent of divalent metal ions, retaining activity in the presence of EDTA.

The kinetic characterization of MmpH was performed with varying concentrations of previously purified MMP at 37 and 45 °C, exhibiting Michaelis-Menten behaviour (figure 2.10 C and D). The enzyme was more efficient at 45 °C than 37 °C, which was expected since this was the temperature at which the enzyme was maximally active. The apparent K_m was higher at 45 °C than at 37 °C, the calculated V_{max} and enzyme turnover (k_{cat}) were half of those determined at 45 °C (table 2.4). Catalytic efficiency was also higher at 45 °C.

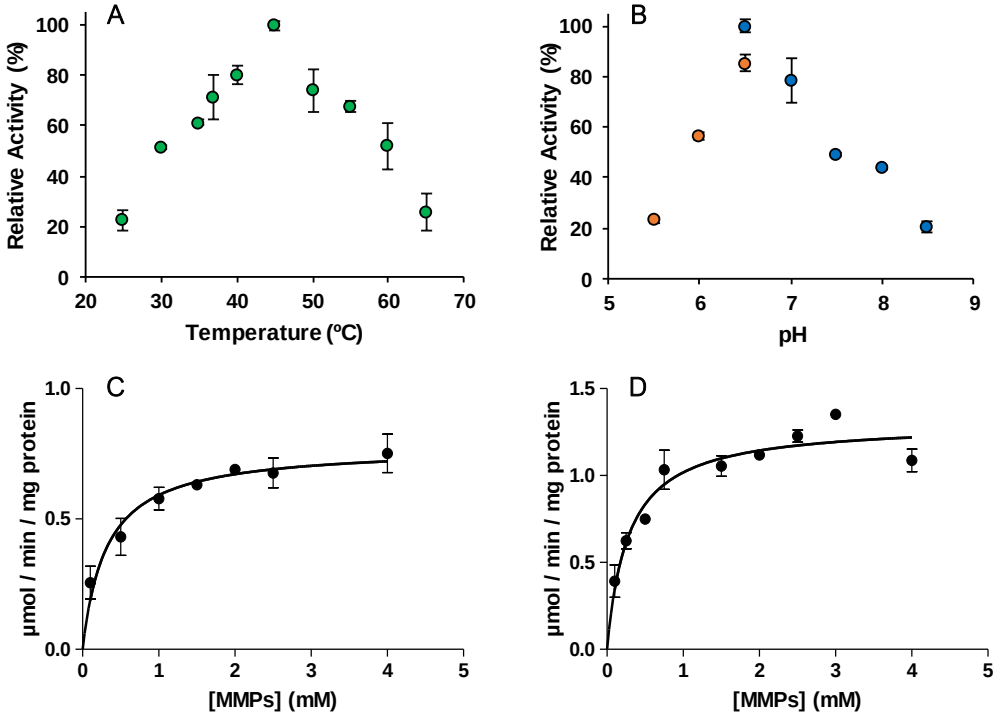

Figure 2.10 – Biochemical and kinetic properties of recombinant MmpH. A) Temperature profile. B) pH dependence in the presence of MES (orange) and BTP (blue) buffers. C) Michaelis-Menten curve for MmpH activity at 37 °C. D) Michaelis-Menten curve for MmpH activity at 45 °C. Error bars represent standard deviation (A and B) or standard error of the mean (C and D).

Table 2.4 – Kinetic parameters of recombinant MmpH from *M. hassiacum.*

Substrate	T (°C)	K_m (mM)	V_{max} (µmol/min/mg)	k_{cat} (min^{-1})	k_{cat}/K_m ($min^{-1}.mM^{-1}$)
MMP	37	0.32 ± 0.09	0.78 ± 0.05	0.68 ± 0.04	2.14 ± 0.63
	45	0.39 ± 0.07	1.46 ± 0.07	1.27 ± 0.06	3.24 ± 0.60

4. Discussion

PMPS were firstly isolated in the 1960's from *M. phlei* and *M. smegmatis* (Lee, 1966; Gray and Ballou, 1971; Maitra and Ballou, 1977; Kamisango et al., 1987) and so far MMP has only been isolated from NTM, in contrast to MGLP that appears to be synthetized in all mycobacteria. Bloch and co-workers proposed their involvement in lipid synthesis, directly modulating fatty acids metabolism and thus indirectly involved in the assembling of cell wall lipids (Machida and Bloch, 1973; Bloch and Vance, 1977). However, despite many attempts there is still a lack of understanding of their *in vivo* functions and about the biological meaning of their differential distribution among mycobacteria. The biosynthetic pathway for MGLP has been the subject of many studies, since MGLP is present in strictly pathogenic mycobacteria such as *M. tuberculosis*, and some enzymes are encoded by genes considered essential for growth (Sassetti et al., 2003; Mendes et al., 2012). On the other hand, MMP has been overlooked for a long time, but the increasing numbers of NTM infections prompted the study of this polysaccharide in more detail, from the identification of the genes and enzymes involved to its role in mycobacterial physiology and lifestyle (Wassilew et al., 2016; Claeys and Robinson, 2018). A few attempts to unravel its biosynthetic pathway were unsuccessful (Weisman and Ballou, 1984b, 1984a; Xia et al., 2012; Xia, 2013). Herein, we have identified a 4-gene gene cluster likely involved in MMP biosynthesis (figure 2.4). This cluster possesses genes for a putative mannosyltransferase, for two putative SAM-dependent methyltransferases and a gene coding for a protein with unknown function.

The enzyme of unknown function is annotated as a prenyltransferase, but its glycosyl hydrolase domain led us to speculate that it could be involved in the hydrolysis of MMP with production of a lower-order intermediate. Indeed, after a few unsuccessful attempts with a number of oligosaccharides as possible substrates, MMP itself was tested and the MMP hydrolase activity was uncovered. This MMP hydrolase, herein designated MmpH, was able to hydrolyse the mixture of MMP purified from *M. smegmatis*, cleaving internally the polysaccharides' structure into oligomannosides that correspond to the opposing ends of MMP and acting, therefore, as an α-(1→4)-mannanase (figure 2.8). This is, to our knowledge, an unprecedented mannanase activity, which emphasizes its importance. This enzyme shows high amino acid identity with homologues from other mycobacteria and related actinobacteria (figure 2.4). However, MmpH has low similarity with characterized α-mannanases or with β-(1→4)-mannanases, displaying 30-40% amino acid sequence identity and query score below 20% in BLAST analysis, underlying its uniqueness.

MmpH was very specific for MMP mixture, lacking the ability to hydrolyse β-(1→4)-bonds of the β-mannans or the α-(1→4)-bonds of the maltooligosaccharides tested. Moreover, the similar polysaccharide MGLP, which in its deacetylated form possesses a glucose main chain with

methylations in the 6-OH position instead of 3-*O*-methylmannoses, was also not a substrate. Furthermore, this enzyme was not able to hydrolyse its own reaction products (figure 2.7 B) or have a reverse activity that could re-establish the ligation between the oligomannosides produced, as detected for other hydrolases in certain conditions (Lundemo, 2015). The maximum activity *in vitro* was detected at 45 °C (figure 2.10 A), near the optimal temperature for *M. hassiacum* growth (50 °C) (Tiago et al., 2012), and the pH range for activity was slightly acidic (figure 2.10 B), which could suggest that this enzyme is active under stress conditions (Roxas and Li, 2009).

Due to the heterogenous nature of the substrate utilized, it was difficult deciphering the hydrolytic mechanism of MmpH, but different incubation periods allowed the formation of reaction products over time (figure 2.6). In the first few minutes of the reaction, production of oligomannoside **b**, the pentamannoside with a reducing end was favoured and, although both the tetramannoside **a** and pentamannoside **b** were produced over time, **b** was continuously favoured over **a**. Thus, although the two products with reducing ends have been isolated *in vitro*, the pentamannoside **b** seems to be preferably produced and, hypothetically, its production might be preferred *in vivo*. Yamada and Ballou reported that when isolating MMP and its precursors the smaller precursor isolated was a pentamannoside (Yamada et al., 1979), which in light of our results can lead to the hypothesis that these precursors are the result of MmpH activity. However, because MmpH is also capable of producing tetramannosides that were until now regarded as the first biosynthetic step in the MMP pathway, the primer for MMP biosynthesis *in vivo* remains to be unequivocally identified (Weisman and Ballou, 1984b; Xia et al., 2012). Regarding the oligomannosides with a nonreducing end, octamannoside **d** was always obtained after several purifications of MmpH products and at higher levels than heptamannoside **c**, which could reflect preference for octamannoside **d** production.

Although we cannot correlate peak intensity of the MS spectra (figure 2.1 B, 2.3 A-C, 2.8 A-D and 2.9 A-D) with the abundance of each molecule analysed and we do not know are unsure which MMP size is prevalent in our mixture, we can speculate that given the two predominantly produced products (pentamannoside **b** and octamannoside **d**), MMP_{13} is hydrolysed preferentially. Moreover, the hydrolysis of other MMP sizes in solution is most likely occurring, since combining product **b** plus **c** equals MMP_{12} and the combination of tetramannoside **a** with products **c** or **d** gives rise to MMP_{11} or MMP_{12}, respectively. Following the same logic, the nonreducing oligomannosides containing six and nine mannoses could derive from hydrolysis of MMP_{11} and MMP_{14}, unfortunately these mannosides' presence could only be tested by TLC due to elution in the low purity fractions obtained during the purification of MmpH products (figure 2.7 A), which hindered their identification and/or analysis by MS. The ideal approach to establish a correct correlation between each MMP size and the hydrolytic product produced by MmpH

would have been to hydrolyse each size separately, but repeated unsuccessful attempts to separate the different MMP did not allow performing individual assays.

The mechanism of the enzyme suggests that MmpH might have a crucial recycling role in MMP biogenesis, where each “old MMP” is degraded into two smaller fragments that themselves are used as substrates for elongation to produce new MMP polysaccharides.

Purification of MMP was essential for the identification and functional characterization of MmpH and the method optimized in our laboratory will be crucial to finally discover if these polysaccharides are indeed produced in SGM as *M. avium* and *M. ulcerans*, which possess similar gene clusters for MMP synthesis. Although we were not able to obtain a homogenous form of MMP, the purification of an endo-(1→4)-mannanase and the identification of the oligomannoside products confirms that this enzyme was most likely misannotated as a prenyltransferase.

Chapter 3:

A key α-(1→4)-mannosyltransferase for elongation of mycobacterial MMP

1. Introduction

Mycobacteria have a high content of carbohydrate either as components of their robust and impermeable cell wall or as intracellular glycans, which depend on the existence of a huge diversity of glycosyltransferases (GT) involved in the biosynthetic pathways of very diverse sugars such as PG, AG, trehalose, glycogen, LAM, PMPS, among others (Berg et al., 2007). GT are grouped in 106 families based on amino acid sequence homology (http://www.cazy.org/GlycosylTransferases.html) and are further classified according to their different folds in three super families: GT-A, GT-B and GT-C (Berg et al., 2007; Cantarel et al., 2009; Breton et al., 2012). GT-A and GT-B comprise mainly enzymes that use NDP-sugar and transfer saccharides through inverting or retaining mechanisms (Lairson et al., 2008; Breton et al., 2012; Liang et al., 2015), while GT-C contains transmembrane enzymes that use polyprenyl-linked sugar donors (Lairson et al., 2008; Breton et al., 2012; Liang et al., 2015).

Capsular glucan, glycogen and the polymethylated polysaccharide MGLP are glucose polymers with similar backbones linked by α-(1→4)-glycosidic bonds. A few years ago, two glucosyltransferases, Rv3032 and GlgA (Rv1212c), were found to be involved in the elongation step of these glucans (Stadthagen et al., 2007; Sambou et al., 2008). Despite acting upon different substrates, the enzymes seem to have compensatory activity, since in a Rv3032 mutant MGLP synthesis could not be totally abolished and in a GlgA mutant with diminished glycogen synthesis, normal levels could be restored by an episomal copy of *Rv3032* (Stadthagen et al., 2007; Sambou et al., 2008).

Biosynthesis of mycobacterial mannoglycans such as PIM, LM and LAM involves at least eight different mannosyltransferases (table 3.1). These mannosyltransferases differ essentially in the type of glycosidic bonds created and in the donor group used, since mycobacteria have two possible mannose donors, the cytoplasmatic GDP-mannose and the membrane bound polyprenol-phosphate-mannose (PPM) (Yokoyama and Ballou, 1989; Berg et al., 2007; Guerin et al., 2010).

Table 3.1 – Mannosyltransferases involved in PIM, LM and LAM synthesis.

Mannosyl-transferases	Type of glycosidic bond	Mannose Donor		Reference
		GDP-mannose	PPM	
PimA	α-(1→2)-ManT	✓	x	(Korduláková et al., 2002)
PimB'	α-(1→6)-ManT	✓	x	(Guerin et al., 2009)
PimC	α-(1→6)-ManT	✓	x	(Kremer et al., 2002)
PimE	α-(1→2)-ManT	x	✓	(Morita et al., 2006)
MptA	α-(1→6)-ManT	x	✓	(Kaur et al., 2007; Mishra et al., 2007)
MptB	α-(1→6)-ManT	x	✓	(Mishra et al., 2008)
MptC	α-(1→2)-ManT	x	✓	(Kaur et al., 2006, 2008)
CapA	α-(1→5)-ManT	x	✓	(Appelmelk et al., 2008)

MMP differs from the other mannosylated mycobacterial structures, because it is the only known polysaccharide with α-(1→4)-linked mannoses, which unlike the hyper branched LM and LAM, has a linear chain, rendering the key biosynthetic α-(1→4)-mannosyltransferase (ManT) likely unique from the functional, mechanistic and possibly structural points of view. While searching for the biosynthetic enzymes for MMP, the activity of ManT was detected in membrane extracts of *M. smegmatis* and an elongation mechanism for MMP through alternating mannosylation and methylation reactions was proposed (Weisman and Ballou, 1984b). In ManT activity assays, some oligomannosides resulting from Smith degradation and methanolysis of mature MMP were used, which gave rise to substrates with different sizes ($Met_{1,3}Man_1$-$Met_{1,3}Man_{12}$, figure 3.1 A) all methylated at position 1-OH and 3-OH, confirming that the enzyme used preferentially $Met_{1,3}Man_4$ but could also use longer substrates, while it was not active with lower order mannosides (<$Met_{1,3}Man_3$) (Yamada et al., 1979; Weisman and Ballou, 1984b).

Recently, a different mechanism was suggested for MMP elongation, wherein mannosylation activity would be independent of methylation reactions or of the methyl groups present on the oligomannosides (Xia et al., 2012; Xia, 2013). ManT activity was tested in membrane extracts of *M. smegmatis* using synthetic oligomannosides ranging from one to five mannoses, blocked at position 1-OH with an octyl group and with different degrees of 3-*O*-methylations, some totally methylated (Man_{1-5}A, figure 3.1 B) and others with a terminal unmethylated mannose (Man_{1-5}B, figure 3.1 B) (Xia et al., 2012).

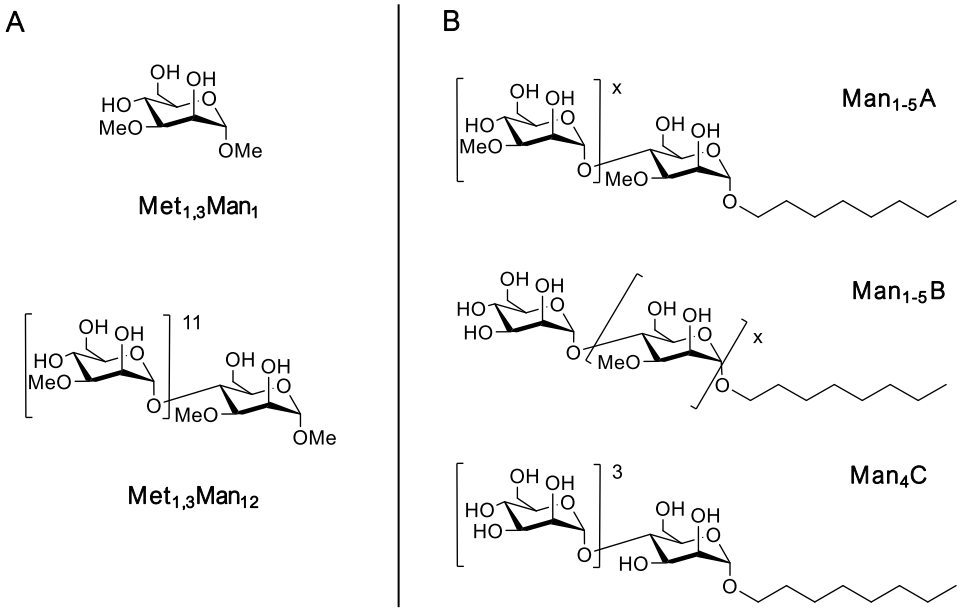

Figure 3.1 – Chemical structures of mannosides used to probe ManT activity with membrane extracts of *M. smegmatis*. A) substrates used by Weisman et al. B) substrates used by Xia et al. (**x**) indicates the number of mannoses, varying from 0 to 4. Adapted from Weisman et al., 1984b and Xia et al., 2012 and 2013.

These authors verified that the ManT was active from trimannosides of both sets of oligomannosides (Man_3A and Man_3B), independently of the methylations (Xia et al., 2012). Although the activity in the presence of pentamannosides (Man_5A and Man_5B) had been similar to the tetramannosides, Man_4A and Man_4B were considered as the preferential substrates and observed that hexa- and heptamannosides were mostly produced from Man_4A while penta- and hexamannosides were obtained from Man_4B (Xia et al., 2012; Xia, 2013). They further synthesized a Man_4 without methylations also blocked at position 1-OH with a octyl group (Man_4C, figure 3.1 B) and, although ManT was active with this substrate, its preference was for the methylated ones (Xia, 2013). These authors also identified the *manT* gene in *M. smegmatis* through bioinformatics tools, but were faced with some difficulties in the purification process and were only able to analyse the substrate specificity by overexpressed ManT in *E. coli* extracts (Xia, 2013). They used Man_4A as substrate and confirmed the production of hexa- and heptamannosides, as previously determined in membrane extracts (Xia et al., 2012; Xia, 2013). Hence, not only the elongation mechanism but the ManT enzyme itself remained largely enigmatic due an inability to obtain the enzyme in pure form.

2. Methods

2.1. Identification of *manT* in the MMP cluster in *M. hassiacum* genome

The 4-gene cluster we proposed to be involved in MMP biosynthesis contains a putative mannosyltransferase gene (*manT*), whose role in MMP synthesis we sought to investigate. The amino acid sequence (WP_005631138.1) was initially retrieved from the draft *M. hassiacum* genome before publication (Tiago et al., 2012). The ManT sequence was used as template for BLAST searches in the available mycobacterial genomes (https://blast.ncbi.nlm.nih.gov/Blast.cgi) and amino acid sequences of ManT homologues were retrieved from the KEGG database (https://www.genome.jp/kegg/).

2.2. Recombinant expression and purification of ManT

For recombinant expression of the *manT* gene, the sequence from *M. hassiacum* (WP_005631138.1) was selected and a synthetic gene sequence optimized for *E. coli* expression was obtained from GenScript. In a first approach, the gene was cloned between the *NdeI* and *HindIII* restriction sites of the expression vector pET30a. The stop codon was removed from the reverse primer to allow translation of a C-terminal vector-encoded 6xHis-tag, followed by transformation into *E. coli* BL21 Star. Cells were cultured in LB medium supplemented with 30 µg/mL kanamycin at 37 °C until $OD_{600} \approx 0.8$, when the incubation temperature was decreased to 25 °C. Recombinant protein expression was induced by addition of 0.5 mM IPTG. Unfortunately, after cell disruption by sonication as described below, it was not possible to obtain soluble protein due to inclusion bodies formation. Faced with this, the 6xHis-tag was transferred to the N-terminus using the same synthetic sequence optimized for *E. coli* expression and inserted between the *XhoI* and *EcoRI* restriction sites of vector pET30a also transformed into *E. coli* BL21 Star. Cells were cultured under the conditions described above and after overnight growth, the culture was harvested by centrifugation (9000 rpm, 15 min, 4 °C), and suspended in 20 mL buffer A (20 mM sodium phosphate pH 7.4, 0.5 M NaCl, 20 mM imidazole), followed by disruption through sonication on ice with three 40 Hz pulses of 20 s (10 s pause between pulses) per 7 mL of lysate in the presence of 20 µg/mL DNAse I and 5 mM $MgCl_2$. The supernatant was clarified by centrifugation (17000 rpm, 30 min, 4 °C), filtered through a 0.45 µm pore low protein binding filter (Millipore) and loaded onto a 5 mL HisTrap HP column (GE Healthcare), previously equilibrated with buffer A. The target protein was eluted with 350 and 500 mM imidazole in buffer B (20 mM sodium phosphate pH 7.4, 0.5 M NaCl, 500 mM imidazole) and its purity assessed by SDS-PAGE. However, the purified ManT was unstable and precipitated after a few hours on ice.

In close collaboration with the Biomolecular Structure and Function Group at IBMC/i3S/UP (Porto), an alternative strategy was designed to clone the *manT* artificial gene between the *NcoI* and *EcoRI* restriction sites of the expression vector pETM11, which allowed engineering a TEV

protease recognition cleavage to allow removal of the histidine tag from the recombinant ManT after its purification (by Jorge Ripoll-Rozada). The construction was transferred into *E. coli* BL21 (DE3) and cells were grown in LB medium supplemented with 50 μg/mL kanamycin at 37 °C until $OD_{600} \approx 0.6$, then the incubation temperature was decreased to 25 °C and recombinant protein expression was induced by addition of 1 mM IPTG. After overnight growth, 3 L of cell culture were harvested by centrifugation (9000 rpm, 15 min, 4 °C), suspended in 20 mL buffer C (20 mM sodium phosphate pH 8, 0.5 M NaCl, 20 mM imidazole, 5 mM β-mercaptoethanol and 0.1% (v/v) Triton X-100) and frozen at -20 °C. The cell pellets were disrupted by sonication on ice with three 40 Hz pulses of 20 s (10 s pause between pulses) per 7 mL of lysate followed by the addition of 0.3 mg/mL lysozyme, 20 μg/mL DNAse I, 5 mM $MgCl_2$ and 1% (w/v) PMSF. The supernatant clarified by centrifugation (17000 rpm, 30 min, 4 °C) was filtered through a 0.45 μm pore low protein binding filter (Millipore) and loaded onto a 5 mL HisTrap HP column (GE Healthcare), equilibrated with buffer C. Bound proteins were eluted with 250 mM imidazole in buffer D (20 mM sodium phosphate pH 8, 0.5 M NaCl, 500 mM imidazole, 5 mM β-mercaptoethanol and 0.1% (v/v) Triton X-100) and their purity assessed by SDS-PAGE. Fractions containing recombinant ManT were pooled and concentrated, using a 30 kDa molecular weight cutoff centrifugal ultrafiltration device (Millipore). The histidine tag was removed by digestion with *Tobacco etch virus* (TEV) protease through overnight dialysis at 4 °C against 20 mM sodium phosphate pH 8, 0.5 M NaCl, 0.5 M EDTA, 1 mM dithiothreitol (DTT) and 0.1% (v/v) Triton X-100. After the second affinity chromatography with the HisTrap column, the enzyme was loaded into the same column under the conditions mentioned above, showing that tag had not been removed, possibly, because the recognition sequence (ENLYFQ/S) was inaccessible to TEV. To increase enzyme purity, the sample was loaded onto a HighPrep 16/60 Sephacryl S-200 and ManT was eluted in 20 mM sodium phosphate pH 8, 0.5 M NaCl, 1 mM DTT and 0.1% (v/v) Triton X-100. Fractions containing recombinant ManT were pooled and concentrated as abovementioned, flash frozen in liquid nitrogen and stored at -80 °C. The protein content was determined with the Bradford assay kit (BioRad).

2.3. Chemical synthesis, purification and NMR analysis of 4α-oligomannosides

Due to the very specific nature of these substrates and their commercial unavailability, it was necessary to chemically synthesize the putative acceptor substrates, which we accomplished in collaboration with the Bioorganic Chemistry Group at the ITQB NOVA (Oeiras). In total, four mannosides with different polymerization and methylation degrees were synthetized: propyl 4α-mannotriose ($sMan_3$), propyl 3,3',3''-tri-*O*-methyl-4α-mannotriose ($sMetMan_3$), propyl 4α-mannotetraose ($sMan_4$) and propyl 3,3',3'',3'''-tetra-*O*-methyl-4α-mannotetraose ($sMetMan_4$).

In most chemical reactions, the products were purified through preparative flash columns chromatography using silica gel Merck 60H and the analytical TLCs were performed in aluminium-backed silica gel Merck 60 F254 and eluted with the adequate eluent for each reaction, mentioned below for each synthetic compound. Reagents and solvents were purified and dried according to the literature (Armarego and Chain, 2003). All ^{1}H-NMR spectra were obtained at 400 MHz in $CDCl_3$, MeOH or D_2O with chemical shift values (δ) in ppm downfield from tetramethylsilane in the case of $CDCl_3$, and ^{13}C-NMR spectra were obtained at 100.61 MHz in $CDCl_3$, MeOH or D_2O. Assignments are supported by 2D correlation NMR studies. The specific rotations ($[\alpha]_D^{20}$) were measured using an automatic polarimeter. The chemical schemes are illustrated in detail in schemes 1-4 of section 3.2 and all data about the compounds' characterization ($[\alpha]_D^{20}$, NMR, MS and FTIR) are described in Annex 1, including the NMR spectra.

Allyl α-D-mannopyranoside (5)

D-mannose (20.00 g, 0.111 mol) was dissolved in distilled allyl alcohol (133.4 mL, 1.96 mol) and camphorsulfonic acid was added (133.4 mg, 0.58 mmol). The mixture was maintained under reflux, overnight. The solvent was removed under vacuum and the crude product was purified by flash column chromatography (9:1 CH_2Cl_2:MeOH, v/v) to afford compound **5** (19.4 g, 80%, α anomer) as a colourless oil.

Allyl 4,6-*O*-benzylidene-α-D-mannopyranoside (6)

To a solution of **5** (18.9 g, 86 mmol) in dry THF (62.5 mL), benzaldehyde dimethyl acetal (25.8 mL, 172 mmol) and camphorsulfonic acid, in a catalytic amount, were added. The mixture was stirred and refluxed for 5 h. The mixture was quenched with a saturated aqueous $NaHCO_3$ solution (30 mL) and extracted with AcOEt (3x30 mL). The combined organic layers were dried with Na_2SO_4, filtered and concentrated under vacuum. The residue was purified by recrystallization (9:1 hexano:ethyl acetate (Hex:AcOEt), v/v) to afford the compound **6** (18.7 g, 75%, α anomer) as a white solid.

Allyl 2,3-di-*O*-acetyl-4,6-*O*-benzylidene-α-D-mannopyranoside (7)

To a solution of **6** (6.2 g, 19.4 mmol) in dry pyridine (30 mL) at 0 °C, acetic anhydride (5.6 mL, 58.2 mmol) and a catalytic amount of DMAP were added. The mixture was stirred at 0 °C for 5 min and warmed to room temperature (rt). After 2 h, the mixture was quenched with water (30 mL) and extracted with AcOEt (3x30 mL). The combined organic layers were dried with Na_2SO_4, filtered and then concentrated under vacuum. The crude product was purified by flash column chromatography (7:3 Hex:AcOEt, v/v) to afford compound **7** (6.7 g, 88%, α anomer) as a colourless oil.

Allyl 2,3-di-*O*-acetyl-6-*O*-benzyl-α-D-mannopyranoside (8)

To a solution of **7** (6.69 g, 17.05 mmol) in dry THF (61 mL) at 0 °C, $NaBH_3CN$ (13.8 g, 0.2 mol) was added. The mixture was stirred at 0 °C and a solution of HCl in dry Et_2O (64 mL, 2M) was added dropwise until the reaction was completed by TLC. The solvent was removed under vacuum, re-dissolved in water (20 mL) and extracted with CH_2Cl_2 (3x20 mL). The combined organic layers were dried with anhydrous Na_2SO_4, filtered and concentrated under vacuum. The crude product was purified by flash column chromatography (7:3 to 1:1 Hex:AcOEt, v/v) to afford compound **8** (5.95 g, 88%, α anomer) as a colourless oil.

Allyl 2,3-di-*O*-acetyl-6-*O*-benzyl-4-*O*-*tert*-butyldimethylsilyl-α-D-mannopyranoside (9)

To a solution of **8** (5.81 g, 14.73 mmol) in dry dichloromethane (80 mL) at 0 °C and dry DIPEA (7.17 mL, 41.16 mmol) and TBDMSOTf (6.7 mL, 29.4 mmol) were added sequentially. The mixture was stirred for 20 min at 0 °C. TLC (7:3 Hex:AcOEt, v/v) indicated that the reaction was completed. The mixture was washed with an aqueous solution of $NaHCO_3$ (saturated) and extracted with CH_2Cl_2. The organic layer was dried with Na_2SO_4, filtered and concentrated. Purification of the reaction crude by flash column chromatography (eluent from 100% Hex (v/v) to 9:1 Hex:AcOEt, v/v) afforded **9** (4.13 g, 55%, α anomer) as a colourless oil.

2,3-di-*O*-acetyl-6-*O*-benzyl-4-*O*-*tert*-butyldimethylsilyl-α-D-mannopyranoside (10)

To a solution of **9** (3.96 g, 7.77 mmol) in dry methanol (36 mL), $PdCl_2$ (0.275 g, 1.55 mmol) was added. The mixture was stirred at rt for 2 h and then the mixture was filtered through celite and washed with methanol. The filtrate was concentrated under vacuum and purified by flash column chromatography (7:3 to 1:1 Hex:AcOEt, v/v) to afford compound **10** (2.28 g, 63%, α anomer) as a colourless oil.

2,3-di-*O*-acetyl-6-*O*-benzyl-4-*O*-*tert*-butyldimethylsilyl-α-D-mannopyranosyl trichloroacetamidate (11)

To a solution of **10** (2.28 g, 4.85 mmol) in dry CH_2Cl_2 (30 mL) at 0 °C, DBU (0.32 mL, 2.13 mmol) and trichloroacetonitrile (2.4 mL, 24.3 mmol) were added. The mixture was stirred for 10 min at 0 °C, warmed to rt and stirred for 2h. The solvent was evaporated under vacuum and the crude product was purified by flash column chromatography (7:3 Hex:AcOEt, v/v) to afford compound **11** (1.94 g, 65%) as a colourless oil.

Allyl 2,3-di-*O*-acetyl-6-*O*-benzyl-4-*O*-*tert*-butyldimethylsilyl-α-D-mannopyranosyl-(1→4)-2,3-di-*O*-acetyl-6-*O*-benzyl-α-D-mannopyranoside (12)

A suspension of **11** (1.88 g, 3.07 mmol), **8** (1.21 g, 3.07 mmol) and 4Å MS in CH_2Cl_2 (30 mL) was stirred at rt for 30 min. TMSOTf (0.556 mL, 3.07 mmol) was added at -20 °C and the mixture was stirred until 0 °C. After 30 min, saturated $NaHCO_3$ aqueous solution (30 mL) was added and

the mixture was extracted with CH_2Cl_2 (3x10 mL). The combined organic phases were dried with anhydrous Na_2SO_4, filtered and concentrated under vacuum. The crude product was purified by flash column chromatography (7:3 Hex:AcOEt, v/v) to afford compound **12** (0.174 g, 7%, α anomer) as a colourless oil.

Allyl 2,3-di-*O*-acetyl-6-*O*-benzyl-α-D-mannopyranosyl-(1→4)-2,3-di-*O*-acetyl-6-*O*-benzyl-α-D-mannopyranoside (13)

A suspension of **11** (1.88 g, 3.07 mmol), **8** (1.21 g, 3.07 mmol) and 4Å MS in dry CH_2Cl_2 (30 mL) was stirred at rt for 30 min. TMSOTf (0.556 mL, 3.07 mmol) was added at -20 °C and the mixture was stirred until 0 °C. After 30 min, saturated $NaHCO_3$ aqueous solution (30 mL) was added and the mixture was extracted with CH_2Cl_2 (3x10 mL). The combined organic phases were dried with anhydrous Na_2SO_4, filtered and concentrated under vacuum. The crude product was purified by flash column chromatography (7:3 Hex:AcOEt, v/v) to afford compound **13** (1.88 g, 84%, α anomer) as a colourless oil.

Allyl 2,3,4-tri-*O*-acetyl-6-*O*-benzyl-α-D-mannopyranosyl-(1→4)-2,3-di-*O*-acetyl-6-*O*-benzyl-α-D-mannopyranoside (14)

To a solution of **13** (0.98 g, 1.34 mmol) in dry pyridine (8 mL) at 0 °C, acetic anhydride (194 µL, 2.05 mmol) and a catalytic amount of DMAP were added. The mixture was stirred at 0 °C for 5 min and warmed to rt. After 2 h, the mixture was quenched with water (5 mL) and extracted with AcOEt (3x10 mL). The combined organic layers were dried with anhydrous Na_2SO_4, filtered and the concentrated under vacuum. The crude product was purified by flash column chromatography (7:3 Hex:AcOEt, v/v) to afford compound **14** (0.92 g, 89%, α anomer) as a colourless oil.

2,3,4-tri-*O*-acetyl-6-*O*-benzyl-α-D-mannopyranosyl-(1→4)-2,3-di-*O*-acetyl-6-*O*-benzyl-α-D-mannopyranoside (15)

To a solution of **14** (0.92 g, 1.19 mmol) in dry methanol (17.5 mL), $PdCl_2$ (42.2 mg, 0.238 mmol) was added. The mixture was stirred at rt for 2 h and then the mixture was filtered through celite and washed with methanol. The filtrate was concentrated under vacuum and purified by flash column chromatography (7:3 to 1:1 Hex:AcOEt, v/v) to afford compound **15** (0.778 g, 89%, α anomer) as a colourless oil.

2,3,4-tri-*O*-acetyl-6-*O*-benzyl-α-D-mannopyranosyl-(1→4)-2,3-di-*O*-acetyl-6-*O*-benzyl-α-D-mannopyranosyl trichloroacetamidate (16)

To a solution of 15 (0.693 g, 0.945 mmol) in dry CH2Cl2 (6 mL) at 0 °C, DBU (62 µL, 0.416 mmol) and trichloroacetonitrile (0.474 mL, 4.73 mmol) were added. The mixture was stirred for 10 min at 0 °C, warmed to rt and stirred for 2 h. The solvent was evaporated under vacuum and

the crude product was purified by flash column chromatography (6:4 Hex:AcOEt, v/v) to afford compound **16** (0.666 g, 80%) as a colourless oil.

Allyl 2,3,4-tri-*O*-acetyl-6-*O*-benzyl-α-D-mannopyranosyl-(1→4)-2,3-di-*O*-acetyl-6-*O*-benzyl-α-D-mannopyranosyl-(1→4)-2,3-di-*O*-acetyl-6-*O*-benzyl-α-D-mannopyranosyl-(1→4)-2,3-di-*O*-acetyl-6-*O*-benzyl-α-D-mannopyranoside (17)

A suspension of **16** (0.597 g, 0.68 mmol), **13** (0.497 g, 0.68 mmol) and 4Å MS in dry CH_2Cl_2 (15 mL) was stirred at rt for 30 min. TMSOTf (0.123 mL, 0.68 mmol) was added at -20 °C and the mixture was stirred until 0 °C. After 30 min, saturated $NaHCO_3$ aqueous solution (10 mL) was added and the mixture was extracted with CH_2Cl_2 (3x10 mL). The combined organic phases were dried with anhydrous Na_2SO_4, filtered and concentrated under vacuum. The crude product was purified by flash column chromatography (7:3 Hex:AcOEt, v/v) to afford compound **17** (0.798 g, 80%, α anomer) as a colourless oil.

Allyl 6-*O*-benzyl-α-D-mannopyranosyl-(1→4)-6-*O*-benzyl-α-D-mannopyranosyl-(1→4)-6-*O*-benzyl-α-D-mannopyranosyl-(1→4)-6-*O*-benzyl-α-D-mannopyranoside (18)

To a solution of **17** (0.798 g, 0.55 mmol) in MeOH (7 mL), MeONa (17.8 mg ,0.33 mmol) was added. After complete conversion of the starting material, previously activated Dowex H^+ resin was added until neutral pH. After filtration with MeOH, the solvent was removed under vacuum to give compound **18** (0.561 g, quantitative, α anomer) as a colourless oil.

Propyl α-D-mannopyranosyl-(1→4)-α-D-mannopyranosyl-(1→4)-α-D-mannopyranosyl-(1→4)-α-D-mannopyranoside (1)

Compound **18** (0.520 g, 0.51 mmol) in AcOEt/EtOH (2:1 – 3 mL) was hydrogenated at 50 psi in the presence of Pd/C 10% (0.25 equiv). After 7 h, the reaction mixture was filtered through celite and the solvent was removed under vacuum to afford compound **1** (0.179 g, 52%, α anomer) as a viscous colourless foam.

Allyl 2,3,4-tri-*O*-acetyl-6-*O*-benzyl-α-D-mannopyranosyl-(1→4)-2,3-di-*O*-acetyl-6-*O*-benzyl-α-D-mannopyranosyl-(1→4)-2,3-di-*O*-acetyl-6-*O*-benzyl-α-D-mannopyranose (19)

A suspension of **11** (78.8 mg, 0.13 mmol), **13** (94 mg, 0.13 mmol) and 4Å MS in dry CH_2Cl_2 (3 mL) was stirred at rt for 30 min. TMSOTf (23.3 µL, 0.13 mmol) was added at -20 °C and the mixture was stirred until 0 °C. After 30 min, saturated $NaHCO_3$ aqueous solution (10 mL) was added and the mixture was extracted with CH_2Cl_2 (3x10 mL). The combined organic phases were dried with anhydrous Na_2SO_4, filtered and concentrated under vacuum. The crude product was purified by flash column chromatography (7:3 Hex:AcOEt, v/v) to afford compound **19** (92 mg, 67%, α anomer) as a colourless oil.

Allyl 6-*O*-benzyl-α-D-mannopyranosyl-(1→4)-6-*O*-benzyl-α-D-mannopyranosyl-(1→4)-6-*O*-benzyl-α-D-mannopyranoside (20)

To a solution of **19** (70 mg, 0.108 mmol) in MeOH (2 mL), MeONa (2.12 mg, 39.3 µmol) was added. After complete conversion of the starting material, previously activated Dowex H^+ resin was added until neutral pH. After filtration with MeOH, the solvent was removed under vacuum to give compound **20** (46 mg, 87%, α anomer) as a colourless oil.

Propyl-α-D-mannopyranosyl-(1→4)-α-D-mannopyranosyl-(1→4)-α-D-mannopyranoside (2)

Compound **20** (46 mg, 56.4 µmol) in AcOEt/EtOH (2:1 – 3 mL) was hydrogenated at 50 psi in the presence of Pd/C 10% (0.25 equiv). After 7 h, the reaction mixture was filtered through celite and the solvent was removed under vacuum to afford compound **2** (30 mg, quantitative, α anomer) as a viscous colourless foam.

Allyl 4,6-*O*-benzylidene-3-*O*-methyl-α-D-mannopyranoside (21)

To a solution of **6** (7.2 g, 23.4 mmol) in dry methanol (30 mL), dibutyltin oxide (6.7 g, 26.9 mmol) was added. The mixture was stirred under reflux for 3 h and the solvent was removed under vacuum. The crude product was re-dissolved in dry DMF (45 mL) and iodomethane (7.3 mL, 117 mmol) was added and the mixture was heated at 50 °C, overnight. The solvent was first removed under vacuum, then the mixture was re-dissolved in CH_2Cl_2 (30 mL) and the white solid formed was filtered. The solvent was removed under vacuum and the reaction mixture was purified by flash column chromatography (7:3 to 1:1 Hex:AcOEt, v/v) to afford compound **21** (4.83 g, 58%, α anomer) as a yellow oil.

Allyl 2,4-di-*O*-acetyl-4,6-*O*-benzylidene-3-*O*-methyl-α-D-mannopyranoside (22)

To a solution of **21** (4.39 g, 13.6 mmol) in dry pyridine (30 mL) at 0 °C, distilled acetic anhydride (1.93 mL, 20.4 mmol) and a catalytic amount of DMAP were added. The mixture was stirred at 0 °C for 5 min and warmed to rt. After 2 h, the mixture was quenched with water (30 mL) and extracted with AcOEt (3x30 mL). The combined organic layers were dried with Na_2SO_4, filtered and the concentrated under vacuum. The crude product was purified by flash column chromatography (7:3 Hex:AcOEt, v/v) to afford compound **22** (4.52 g, 92%, α anomer) as a colourless oil.

Allyl 2-*O*-acetyl-6-*O*-benzyl-3-*O*-methyl-α-D-mannopyranoside (23)

To a solution of **22** (4.5 g, 12.4 mmol) in dry THF (35 mL) at 0 °C, $NaBH_3CN$ (9.36 g, 0.15 mol) was added. The mixture was stirred at 0 °C, and a solution of HCl in dry Et_2O (51 mL, 1M) was added dropwise until the reaction was completed by TLC. The solvent was removed under vacuum, re-dissolved in water (20 mL) and extracted with CH_2Cl_2 (3x20 mL). The combined organic layers were dried with Na_2SO_4, filtered and concentrated under vacuum. The crude

product was purified by flash column chromatography (7:3 to 1:1 Hex:AcOEt, v/v) to afford compound **23** (3.54 g, 78%, α anomer) as a colourless oil.

Allyl 2-*O*-acetyl-6-*O*-benzyl-4-*O*-*tert*-butyldimethylsilyl-3-*O*-methyl-α-D-mannopyranoside (24)

To a solution of **23** (4.37 g, 11.9 mmol) in dry dichloromethane (0 mL) at 0 °C, dry DIPEA (5.8 mL, 33.3 mmol) and TBDMSOTf (3 mL, 13.1 mmol) were added sequentially. The mixture was stirred for 90 min at 0 °C. TLC (7:3 Hex:AcOEt, v/v) indicated that the reaction was completed. The mixture was washed with an aqueous solution of $NaHCO_3$ (saturated) and extracted with CH_2Cl_2. The organic layer was dried with Na_2SO_4, filtered and concentrated. Purification of the reaction crude by flash column chromatography (eluent from 100% (v/v) Hex to 9:1 Hex:AcOEt, v/v) afforded **24** (3.65 g, 64%, α anomer) as a colourless oil.

2-*O*-acetyl-6-*O*-benzyl-4-*O*-*tert*-butyldimethylsilyl-3-*O*-methyl-α-D-mannopyranoside (25)

To a solution of **24** (3.2 g, 6.65 mmol) in dry methanol (30 mL), $PdCl_2$ (0.236 g, 1.33 mmol) was added. The mixture was stirred at rt for 2 h and then the mixture was filtered through celite and washed with methanol. The filtrate was concentrated under vacuum and purified by flash column chromatography (7:3 to 1:1 Hex:AcOEt, v/v), to afford compound **25** (1.47 g, 50%, α anomer) as a colourless oil.

2-*O*-acetyl-6-*O*-benzyl-4-*O*-*tert*-butyldimethylsilyl-3-*O*-methyl-α-D-mannopyranoside trichloroacetamidate (26)

To a solution of **25** (0.714 g, 1.62 mmol) in dry CH_2Cl_2 (7 mL) at 0 °C, DBU (110 µL, 0.71 mmol) and trichloroacetonitrile (0.474 mL, 4.73 mmol) were added. The mixture was stirred for 10 min at 0 °C, warmed to rt and stirred for 2 h. The solvent was evaporated under vacuum and the crude product was purified by flash column chromatography (8:2 Hex:AcOEt, v/v) to afford compound **26** (0.54 g, 57%) as a colourless oil.

Allyl 2,4-di-*O*-acetyl-6-*O*-benzyl-3-*O*-methyl-α-D-mannopyranoside (27)

To a solution of **23** (1.72 g, 4.68 mmol) in dry pyridine (5 mL) at 0 °C, acetic anhydride (0.66 mL, 7.02 mmol) and a catalytic amount of DMAP were added. The mixture was stirred at 0 °C for 5 min, warmed to rt and stirred for 90 min. The mixture was quenched with water (20 mL) and extracted with AcOEt (3x20 mL). The combined organic layers were dried with Na_2SO_4, filtered and concentrated under vacuum. The crude product was purified by flash column chromatography (7:3 Hex:AcOEt, v/v) to afford **27** (1.26 g, 83%, α anomer) as a colourless oil.

2,4-Di-*O*-acetyl-6-*O*-benzyl-3-*O*-methyl-(α/β)-D-mannopyranoside (28)

To a solution of **27** (1.23 g, 3.02 mmol) in dry methanol (10 mL), $PdCl_2$ (0.107 g, 0.604 mmol) was added. The mixture was stirred at rt for 2 h and then the mixture was filtered through celite and washed with methanol. The filtrate was concentrated under vacuum and purified by flash column chromatography (7:3 to 1:1 Hex:AcOEt, v/v) to afford compound **28** (0.99 g, 89%, α anomer) as a colourless oil.

2,4-Di-*O*-acetyl-6-*O*-benzyl-3-*O*-methyl-α-D-mannopyranosyl trichloroacetamidate (29)

To a solution of **28** (0.96 g, 2.6 mmol) in dry CH_2Cl_2 (10 mL) at 0 °C, DBU (0.171 mL, 1.14 mmol) and trichloroacetonitrile (1.3 mL, 13 mmol) were added. The mixture was stirred for 10 min at 0 °C, warmed to rt and stirred for 2 h. The solvent was evaporated under vacuum and the crude product was purified by flash column chromatography (7:3 Hex:AcOEt, v/v) to afford compound **29** (1.27 g, 70%) as a colourless oil.

Allyl 2-*O*-acetyl-6-*O*-benzyl-3-*O*-methyl-α-D-mannopyranosyl-(1→4)-2-*O*-acetyl-6-*O*-benzyl-3-*O*-methyl-α-D-mannopyranoside (30)

A suspension of **26** (0.51 g, 0.87 mmol), **23** (0.35 g, 0.87 mmol) and 4Å MS in dry CH_2Cl_2 (30 mL) was stirred at rt for 30 min. TMSOTf (0.16 mL, 0.87 mmol) was added at -20 °C and the mixture was stirred until 0 °C. After 30 min, saturated $NaHCO_3$ aqueous solution (30 mL) was added and the mixture was extracted with CH_2Cl_2 (3x10 mL). The combined organic phases were dried with anhydrous Na_2SO_4, filtered and concentrated under vacuum. The crude product was purified by flash column chromatography (7:3 Hex:AcOEt, v/v) to afford compound **30** (0.274 g, 48%, α anomer) as a colourless oil.

Allyl 2,4-di-*O*-acetyl-6-*O*-benzyl-3-*O*-methyl-α-D-mannopyranosyl-(1→4)-2-*O*-acetyl-6-*O*-benzyl-3-*O*-methyl-α-D-mannopyranoside (31)

A suspension of **29** (0.91 g, 1.77 mmol), **23** (0.65 g, 1.77 mmol) and 4Å MS in CH_2Cl_2 (10 mL) was stirred at rt for 30 min. TMSOTf (319 µL, 1.77 mmol) was added at -20 °C and the mixture was stirred until 0 °C. After 30 min, saturated $NaHCO_3$ aqueous solution (10 mL) was added and the mixture was extracted with CH_2Cl_2 (3x10 mL). The combined organic phases were dried with Na_2SO_4, filtered and concentrated under vacuum. The crude product was purified by flash column chromatography (7:3 Hex:AcOEt, v/v) to afford compound **31** (0.81 g, 65%, α anomer) as a colourless oil.

2,4-Di-*O*-acetyl-6-*O*-benzyl-3-*O*-methyl-α-D-mannopyranosyl-(1→4)-2-*O*-acetyl-6-*O*-benzyl-3-*O*-methyl-α-D-mannopyranose (32)

To a solution of **31** (0.78 g, 1.09 mmol) in MeOH (5 mL), $PdCl_2$ (38.7 mg ,0.22 mmol) was added. After 2 h at rt, the mixture was filtered through celite and washed with MeOH. The crude

product was purified by flash column chromatography (1:1 Hex:AcOEt, v/v) to afford compound **32** (0.54 g, 73%, α anomer) as a colourless oil.

2,4-Di-*O*-acetyl-6-*O*-benzyl-3-*O*-methyl-α-D-mannopyranosyl-(1→4)-2-*O*-acetyl-6-*O*-benzyl-3-*O*-methyl-α-D-mannopyranosyl trichloroacetamidate (33)

To a solution of **32** (0.59 g, 0.87 mmol) in dry CH_2Cl_2 (7 mL) at 0 °C, DBU (110 µL, 0.71 mmol) and trichloroacetonitrile (0.474 mL, 4.73 mmol) were added. The mixture was stirred for 10 min at 0 °C, warmed to rt and stirred for 2 h. The solvent was evaporated under vacuum and the crude product was purified by flash column chromatography (8:2 Hex:AcOEt, v/v) to afford compound **33** (0.504 g, 68%) as a colourless oil.

Allyl 2,4-di-*O*-acetyl-6-*O*-benzyl-3-*O*-methyl-α-D-mannopyranosyl-(1→4)-2-*O*-acetyl-6-*O*-benzyl-3-*O*-methyl-α-D-mannopyranosyl-(1→4)-2-*O*-acetyl-6-*O*-benzyl-3-*O*-methyl-α-D-mannopyranosyl-(1→4)-2-*O*-acetyl-6-*O*-benzyl-3-*O*-methyl-α-D-mannopyranoside (34)

A suspension of **33** (0.304 g, 0.371 mmol), **30** (0.25 g, 0.371 mmol) and 4Å MS in dry CH_2Cl_2 (8 mL) was stirred at rt for 30 min. TMSOTf (70 µL, 0.371 mmol) was added at -30 °C and the mixture was stirred until 0 °C. After 30 min, saturated $NaHCO_3$ aqueous solution (10 mL) was added and the mixture was extracted with CH_2Cl_2 (3x10 mL). The combined organic phases were dried with anhydrous Na_2SO_4, filtered and concentrated under vacuum. The crude product was purified by flash column chromatography (7:3 Hex:AcOEt, v/v) to afford compound **34** (0.423 g, 86%, α anomer) as a colourless oil.

Allyl 6-*O*-benzyl-3-*O*-methyl-α-D-mannopyranosyl-(1→4)-6-*O*-benzyl-3-*O*-methyl-α-D-mannopyranosyl-(1→4)-6-*O*-benzyl-3-*O*-methyl-α-D-mannopyranosyl-(1→4)-6-*O*-benzyl-3-*O*-methyl-α-D-mannopyranoside (35)

To a solution of **34** (408 mg, 0.304 mmol) in MeOH (5 mL), MeONa (9.84 mg, 0.18 mmol) was added. After complete conversion of the starting material, previously activated Dowex H^+ resin was added until neutral pH. After filtration with MeOH, the solvent was removed under vacuum to give compound **35** (285 mg, 84%, α anomer) as a colourless oil.

Propyl 3-*O*-methyl-α-D-mannopyranosyl-(1→4)-3-*O*-methyl-α-D-mannopyranosyl-(1→4)-3-*O*-methyl-α-D-mannopyranosyl-(1→4)-3-*O*-methyl-α-D-mannopyranoside (3)

Compound **35** (246 mg, 219 µmol) in AcOEt/EtOH (2:1 – 3 mL) was hydrogenated at 50 psi in the presence of Pd/C 10% (0.25 equiv). After 7 h, the reaction mixture was filtered through celite and the solvent was removed under vacuum to afford compound **3** (160 mg, quantitative, α anomer) as a viscous colourless foam.

Allyl 2,4-di-*O*-acetyl-6-*O*-benzyl-3-*O*-methyl-α-D-mannopyranosyl-(1→4)-2-*O*-acetyl-6-*O*-benzyl-3-*O*-methyl-α-D-mannopyranosyl-(1→4)-2-*O*-acetyl-6-*O*-benzyl-3-*O*-methyl-α-D-mannopyranoside (36)

A suspension of **30** (207 mg, 0.252 mmol), **23** (92.4 mg, 0.252 mmol) and 4Å MS in dry CH_2Cl_2 (4 mL) was stirred at rt for 30 min. TMSOTf (45.7 µL, 0.13 mmol) was added at -30 °C and the mixture was stirred until 0 °C. After 30 min, saturated $NaHCO_3$ aqueous solution (10 mL) was added and the mixture was extracted with CH_2Cl_2 (3x10 mL). The combined organic phases were dried with anhydrous Na_2SO_4, filtered and concentrated under vacuum. The crude product was purified by flash column chromatography (7:3 Hex:AcOEt, v/v) to afford compound **36** (219 mg, 85%, α anomer) as a colourless oil.

Allyl 6-*O*-benzyl-3-*O*-methyl-α-D-mannopyranosyl-(1→4)-6-*O*-benzyl-3-*O*-methyl-α-D-mannopyranosyl-(1→4)-6-*O*-benzyl-3-*O*-methyl-α-D-mannopyranoside (37)

To a solution of **36** (111 mg, 0.108 mmol) in MeOH (2 mL), MeONa (3.5 mg, 65 µmol) was added. After complete conversion of the starting material, previously activated Dowex H^+ resin was added until neutral pH. After filtration with MeOH, the solvent was removed under vacuum to give compound **37** (70 mg, 76%, α anomer) as a colourless oil.

Propyl 3-*O*-methyl-α-D-mannopyranosyl-(1→4)-3-*O*-methyl-α-D-mannopyranosyl-(1→4)-3-*O*-methyl-α-D-mannopyranoside (4)

Compound **37** (50 mg, 58.3 µmol) in AcOEt/EtOH (2:1 – 3 mL) was hydrogenated at 50 psi in the presence of Pd/C 10% (0.25 equiv). After 7 h, the reaction mixture was filtered through celite and the solvent was removed under vacuum to afford compound **4** (37 mg, quantitative, α anomer) as a viscous colourless foam.

2.4. Substrate specificity of ManT

The substrate specificity of ManT was determined using guanosine diphosphomannose (GDP-mannose), guanosine diphosphoglucose (GDP-glucose, Sigma), guanosine diphosphofucose (GDP-fucose, Carbosynth), mannose-1-phosphate (M1P) and mannose-6-phosphate (M6P, Sigma) as possible donors and D-glucose, D-mannose (Man), 3-*O*-methyl-D-glucose, methyl D-glucose, methyl D-mannose (Sigma), maltose, maltotetraose, maltotriose (Carbosynth), 4α-mannobiose (Man_2, Dextra), 3-*O*-methyl-mannose (sMetMan, synthesis described in chapter 4), 3,3'-di-*O*-methyl-4α-mannobiose ($sMetMan_2$, synthesis described in chapter 4), 1,3,3'-tri-*O*-methyl-4α-mannobiose ($sMet_{1,3}Man_2$, synthesis described in chapter 4), $sMan_3$, $sMetMan_3$, $sMan_4$, $sMetMan_4$ (all synthesized at ITQB NOVA), 4β-mannobiose (β-Man_2, Carbosynth), 4β-mannotriose (β-Man_3) and 4β-mannotetraose (β-Man_4, Megazyme) as possible acceptors groups.

Biological substrates available were also tested: the polymethylated polysaccharide MGLP and its deacylated form MGP (obtained by Ana Maranha) and the enzymatic products of MmpH (**a-d**, chapter 2).

The reaction mixtures containing pure ManT (2.1 μM), 25 mM BTP pH 7.5, 5 mM of donor substrates and 5 mM of acceptor substrates were incubated at 37 °C for 2 h. Product formation was monitored by TLC on silica gel 60 plates (Merck) with a solvent system composed of butanol:ethanol:water (4:4:2, v/v/v) and stained by spraying with α-naphtol-sulfuric acid solution, followed by charring at 120 °C (Jacin and Mishkin, 1965).

2.5. Biochemical characterization

Biochemical properties of ManT activity were examined by a discontinuous method through indirect quantification of the GDP released, as previously described (Mendes et al., 2010). A series of discontinuous assays were performed to determine the pH and temperature profiles and the effect of divalent cations, salt (NaCl) and detergent (Triton X-100) on ManT activity. The assays were initiated by the addition of ManT (0.52 μM) to reaction mixtures containing the appropriate buffer (50 mM), 1.5 mM sMetMan$_4$, 2.5 mM GDP-mannose, 5 mM $MgCl_2$, 0.1% (v/v) Triton X-100 and 25 mM NaCl. Cooling on ethanol-ice stopped the reaction and inactivation of the enzyme was achieved by sequential addition of 1.25 μL of 5 N HCl and 1.25 μL of 5 N NaOH. After this, the quantification mixture containing 2 mM phosphoenolpyruvate (PEP), 2.5 mM KCl, 800 μM NADH (Sigma) and 1 unit (U) of pyruvate kinase and lactate dehydrogenase (PK/LDH, Sigma) was added. The reactions were incubated at 37 °C for 15 min and the absorbance at 340 nm registered.

The effect of pH was determined at 37 °C in 50 mM BTP (pH 6.5 to 9.0) or CAPSO (pH 9.0 to 10.0) buffers and the temperature profile was determined between 20 and 55 °C in 50 mM BTP pH 8.5. The effect of divalent cations on enzyme activity was examined by incubating the reaction mixture with the chloride salts of Mg^{2+}, Mn^{2+}, Ca^{2+}, Cu^{2+}, Fe^{2+}, Co^{2+}, Zn^{2+} (5 mM) and without cations, or in the presence of 10 mM EDTA, at 37 °C for 30 min. These reactions were analysed by TLC as described above and ManT activity was quantified in the presence of $MgCl_2$ at concentrations between 0.1 and 20 mM. The influence of NaCl and Triton X-100 on ManT activity was measured with 0 to 50 mM NaCl and 0 to 0.5% (v/v) Triton X-100. All experiments were performed in triplicate.

2.6. Kinetic parameters

The kinetic parameters for ManT activity were determined under optimal conditions at 37 °C using a continuous method. The assays were performed in 96-well microtiter plates and reaction mixtures were prepared with 50 mM BTP pH 8.5, 7.5 mM $MgCl_2$, 5 mM NaCl, 0.1% (v/v) Triton

X-100, 2 mM PEP, 800 μM NADH, 2.5 mM KCl and 1 U PK/LDH. Reactions were initiated by the addition of enzyme (0.52 μM) and product formation was monitored by measuring the amount of GDP released at 340 nm.

The K_m and V_{max} values for GDP-mannose, $sMetMan_4$ or $sMan_4$ were determined using a fixed saturating concentration of GDP-mannose donor (2.5 mM in assays with $sMetMan_4$ and 5 mM in $sMan_4$ reactions) and of $sMetMan_4$ or $sMan_4$ acceptors (1.5 mM for $sMetMan_4$ and 2.5 mM for $sMan_4$). All experiments were performed in triplicate with appropriate controls (reactions without ManT or only with GDP-mannose) to ensure that the quantified GDP resulted of ManT activity and not of substrate degradation. Kinetic parameters were calculated with GraphPad Prism software (version 5.00).

2.7. Examining possible hydrolytic properties of ManT

In certain conditions, many glycosyltransferases can hydrolyse their own donor substrates during the glycosylation reaction (Lairson et al., 2008). This ability was analysed in the presence of ManT with reactions in the absence of acceptors and it was both qualitatively analysed by TLC and quantified by continuous method, as described above. The substrates used were: GDP-mannose, GDP-glucose, GDP-fucose, M1P and M6P.

2.8. Analysis of reaction products by MS

For the analysis of reaction products of $MetMan_4$ and Man_4 by MS, compounds were separated from the reaction components by TLC as previously described (Maranha et al., 2015). The products were produced in 1 mL reactions with 50 mM BTP pH 8.5, 2.5 mM GDP-mannose, 1.5 mM $sMetMan_4$ or 2.5 mM $sMan_4$, 7.5 mM $MgCl_2$ and 13 nM ManT, for 2 h at 37 °C. The reactions were spotted on TLC plates and separated with a solvent system composed of butanol:ethanol:water (4:4:2, v/v/v). After staining the marginal lanes of the TLC plates and identifying the product spots, the corresponding region in the inner unstained lanes of the TLC plate were scraped and each product extracted from silica gel using ultrapure water.

The isolated samples were analysed by MS at the CNC/UC Proteomics Facility. Each sample was suspended and/or diluted with a solution containing 50% (v/v) acetonitrile and analysed in Triple TOF™ 5600 or Triple TOF™ 6600 System (Sciex) by direct infusion. The flow rate was set to 10 μL/min and the ionization source (ESI DuoSpray™ Source) was operated in the positive mode (ion spray voltage of 5500 V) and negative mode (ion spray voltage of -4500 V), 25 psi for nebulizer gas 1 (GS1), 25 psi for the curtain gas (CUR). The acquisition was performed in full scan mode (TOF-MS mode) and product ions were obtained by collision energy ramping.

2.9. ManT activity with products of MmpH

Enzymatic activity of ManT was also quantified in presence of the biological oligomannosides produced by MmpH activity (products **a-d**, chapter 2) and of the synthetic mannosides through the continuous method described above. The assays were initiated by addition of enzyme (0.52 μM) to reaction mixtures containing 50 mM BTP pH 8.5, 1.5 mM acceptor substrate, 2.5 mM GDP-mannose, 7.5 mM $MgCl_2$, 5 mM NaCl, 0.1% (v/v) Triton X-100, 2 mM PEP, 800 μM NADH, 2.5 mM KCl and 1 U PK/LDH. Product formation was monitored at 340 nm, as described above. All experiments were performed in triplicate with appropriate controls.

3. Results

3.1. Identification of ManT in the MMP cluster in *M. hassiacum* genome

The gene cluster identified and proposed to be involved in MMP biosynthesis has a putative glycosyltransferase gene, whose true function we here confirmed. The *M. hassiacum* 1233 bp gene (WP_005631138.1), herein designated *manT*, encodes a rare α-(1→4)-mannosyltransferase with a calculated molecular mass of 48.2 kDa and a theoretical isoelectric point of 6.58.

ManT has high amino acid sequence identity with putative glycosyltransferases present in other NTM (>75%) and related actinobacteria that may also synthetize a similar polysaccharide, namely *Streptomyces griseus* (53%) and *Nocardia otitidiscaviarum* (73%), although MMP has not been detected in the latter. On the other hand, this enzyme revealed low amino acid sequence identity (<30%) with other mannosyltransferases involved in the synthesis of mannoglycans of the mycobacterial cell wall. However, although these mannosyltransferases transfer mannose units, they catalyse the formation of glycosidic bonds other than the α-(1→4) linkage formed by ManT (table 3.1, section 1), which could be the reason for their low homology with ManT. Mycobacteria possess other glycans very similar to MMP that are also mostly linear and contain α-(1→4)-linkages, but these are composed of glucosyl units, which can also explain the low amino acid sequence identity (between 28 and 33%) with two other α-(1→4)-glycosyltransferases (Rv3032 and Rv1212c) identified.

The purification of soluble and bioactive recombinant ManT was difficult and required the addition of reducing agents (β-mercaptoethanol or DTT) and of a detergent (Triton X-100) to all buffers throughout the purification procedures. Although the strategy to produce an enzyme without a histidine tag, resorting to TEV protease, has not resulted, this approach allowed to purify soluble ManT instead of a precipitated form, possibly due to presence of detergent Triton. Approximately 2 mg of pure recombinant ManT (figure 3.2) were obtained per litre of culture.

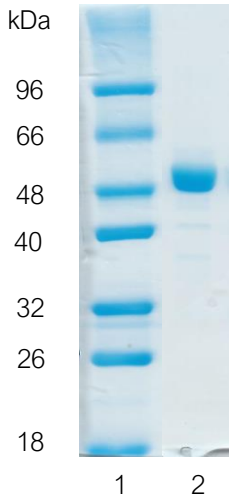

Figure 3.2 – SDS-PAGE analysis of the purified recombinant protein through reducing conditions. Lane 1 – molecular weight marker; lane 2 – purified recombinant ManT from *M. hassiacum*.

3.2. Chemical synthesis of 4α-oligomannosides

Since 4α-oligomannosides are commercially unavailable, four mannosides $sMan_4$ (**1**), $sMan_3$, (**2**), $sMetMan_4$ (**3**) and $sMetMan_3$ (**4**), each differing in selective methylation in 3-OH position, were synthesized in order to ascertain the substrate specificity of ManT (figure 3.3). For the synthesis of any oligosaccharide, it is necessary to establish a glycosylation reaction between two precursors: a glycosyl donor and a glycosyl acceptor (Davis and Fairbanks, 2002). The glycosyl donor must have in its anomeric carbon a leaving group such as a halide, trichloroacetamidate, thioglycoside, acetate, phosphite, etc., and the glycosyl acceptor must possess a free hydroxyl group so that it can react with the anomeric carbon of the donor (Davis and Fairbanks, 2002). As other sugars, mannose has several hydroxyl groups with very similar reactivity, difficulting the regioselective reaction of only one of the hydroxyl groups. Thus, the synthesis of the oligomannosides posed three main challenges: 1) selective methylation of the 3-OH position; 2) differentiation of position C-4 for selective construction of the α-(1→4)-glycosidic bond in the glycosyl acceptor; and 3) differentiation of the anomeric position in the glycosyl donor for subsequent activation.

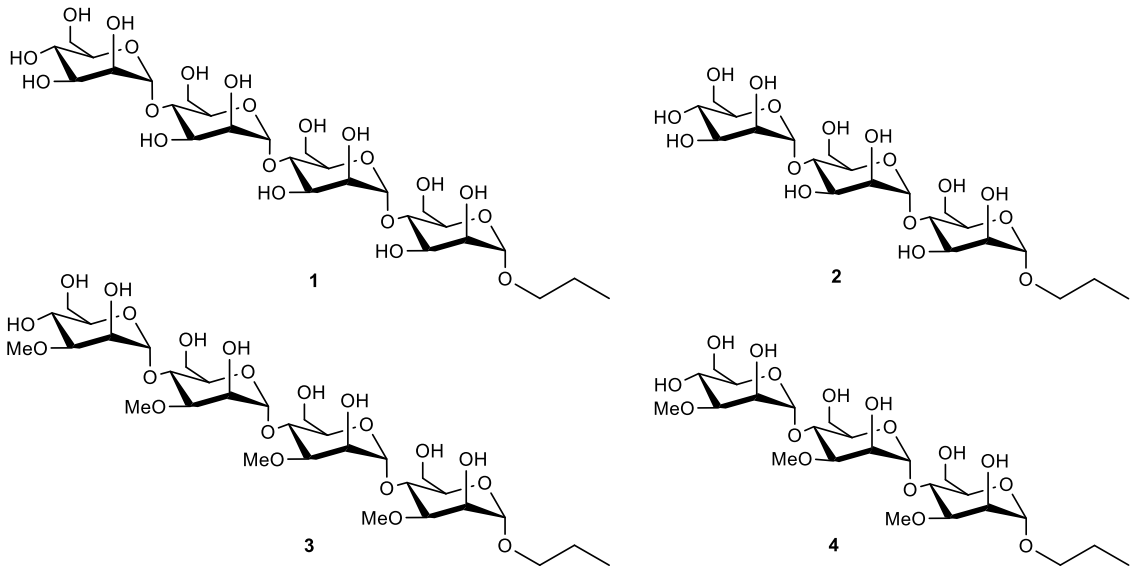

Figure 3.3 – Structures of synthetic oligomannosides: $sMan_4$ (**1**), $sMan_3$, (**2**), $sMetMan_4$ (**3**) and $sMetMan_3$(**4**).

The synthesis of the unmethylated mannoside **7** (scheme 1) was accomplished by a process already described (Liao and Lu, 1996; Chen and Kong, 2003; Poláková et al., 2009; Ripoll-Rozada et al., 2019). The selective opening of the benzylidene acetal was performed with sodium cyanoborohydride, affording alcohol **8** (scheme 1), which will be used as the glycosyl acceptor in the glycosylation reaction. To obtain the glycosyl donor, the 4-OH position of alcohol **8** was protected with TBDMSOTf in dichloromethane, followed by the removal of the allyl group using $PdCl_2$ in methanol and the synthesis of mannosyl trichloroacetamidate **11** (scheme 1). The glycosylation reaction between donor **11** and acceptor **8**, using TMSOTf, resulted in dimannoside

12 (totally protected) and 13 (4-OH position is free) in 7% and 84% yield, respectively (scheme 1). Using the dimannoside 13 deprotected in 4-OH position, it was possible to convert it in the donor dimannoside 16 for the next glycosylation reaction through acetylation of the C-4, followed by the addition of trichloroacetamidate after removal of the allyl group at the anomeric position with 65% yield (scheme 1).

Scheme 1

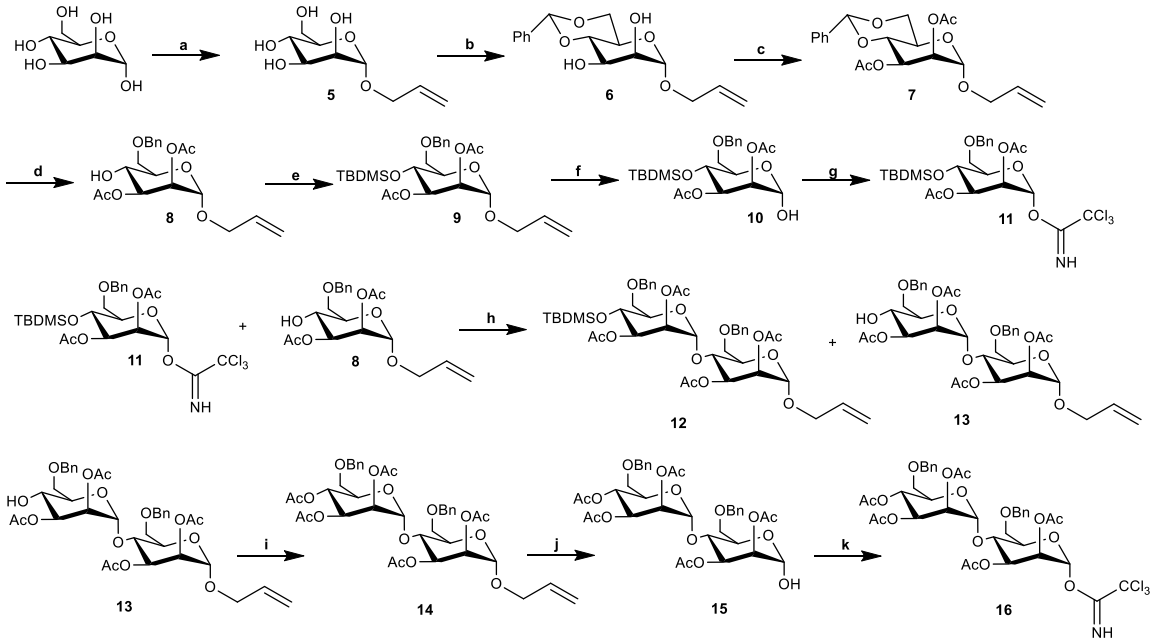

a) Allyl alcohol, reflux, 80%; b) $PhCH(OMe)_2$, THF, reflux, 75%; c) Ac_2O, DMAP, pyridine, 88%; d) $NaBH_3CN$, $HCl.Et_2O$, 0 °C, 88%; e) TBDMSOTf, DIPEA, CH_2Cl_2, 0 °C to rt, 55%; f) $PdCl_2$, MeOH, rt, 63%; g) CCl_3CN, DBU, CH_2Cl_2, 0 °C to rt, 65%; h) TMSOTf, CH_2Cl_2, 4Å MS, -20 °C, 80%; i) Ac_2O, DMAP, pyridine, 89%; j) $PdCl_2$, MeOH, rt, 89%; k) CCl_3CN, DBU, CH_2Cl_2, 0 °C to rt, 80%.

To prepare the tetramannoside 17, another glycosylation reaction was performed using the trichloroacetamidate 16 and acceptor 13 with a very good yield (80%), following sequential deprotection reactions to obtain the final $sMan_4$ 1 (scheme 2). This strategy also enabled the synthesis of the trimannoside 19 through a glycosylation reaction between trichloroacetamidate 11 and acceptor 13 (scheme 3) and the sequential removal steps of protective groups resulted in $sMan_3$ 2 (scheme 3).

Scheme 2

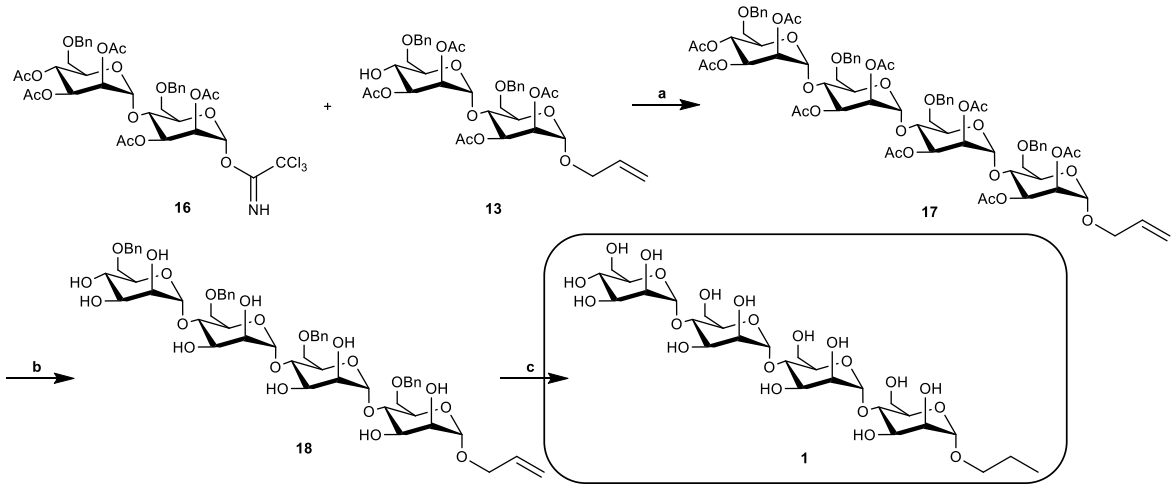

a) TMSOTf, CH_2Cl_2, 4Å MS, -20 °C, 80%; b) MeONa, MeOH, 0 °C to rt, quant.; c) H_2, Pd/C, AcOEt, 50 psi, 52%.

Scheme 3

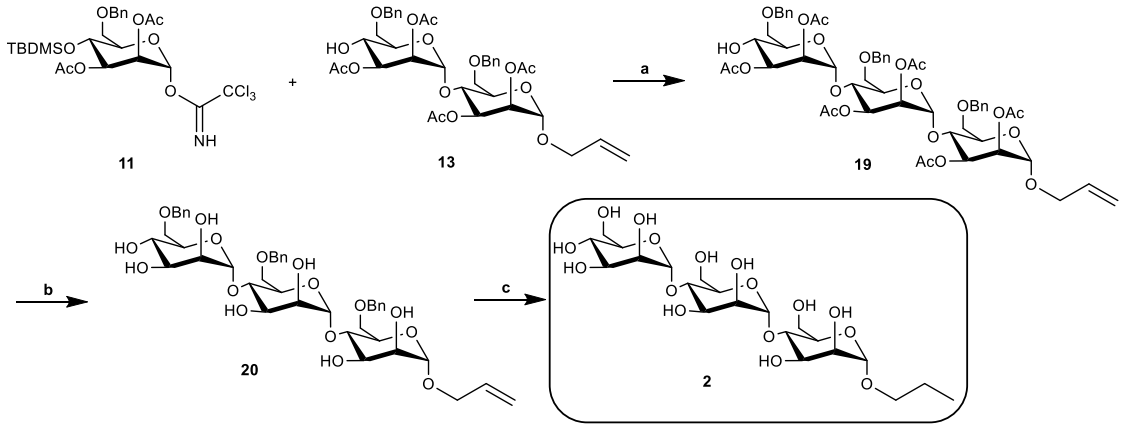

a) TMSOTf, CH_2Cl_2, 4Å MS, -20 °C, 67%; b) MeONa, MeOH, 0 °C to rt, 67%; c) H_2, Pd/C, AcOEt, 50 psi, quant.

The strategies for synthesis of the methylated mannosides are similar to the procedures adopted for the unmethylated one, but the selective introduction of the methyl group at C-3 was necessary, after protection of position C-1 with allyl and C-4 and C-6 positions with benzylidene acetal (scheme 4) (Ripoll-Rozada et al., 2019). In monomer **6**, the methyl group was added, followed by the acetylation of the free 2-OH group and the selective opening of the benzylidene acetal as described above, resulting in glycosyl acceptor **23** (scheme 4). To produce the glycosyl donor, the sugar **23** was protected at the 4-OH position using two strategies: with TBDMSOTf and with AcOEt (Ripoll-Rozada et al., 2019), affording the intermediates **24** and **27**, respectively (scheme 4). In both donors, the allyl group was removed and the mannosyl trichloroacetamidates **26** and **29** were synthesized (scheme 4).

Scheme 4

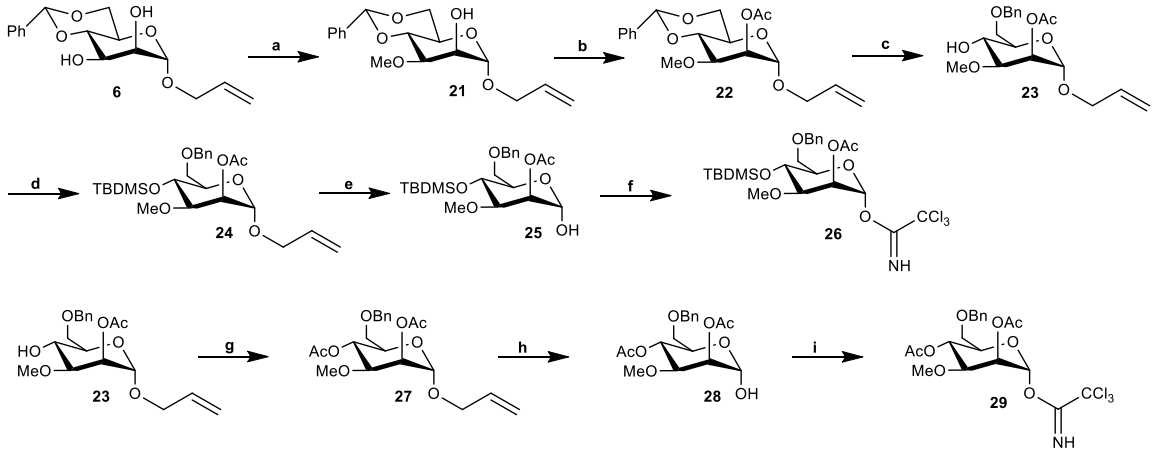

a) i. Bu_2SnO, MeOH, reflux; ii. MeI, DMF, 50 °C, 58%; b) Ac_2O, DMAP, pyridine, rt, 92%; c) $NaBH_3CN$, HCl.Et_2O, 0 °C, 78%; d) TBDMSOTf, DIPEA, CH_2Cl_2, 0 °C to rt, 64%; e) $PdCl_2$, MeOH, rt, 50%; f) CCl_3CN, DBU, CH_2Cl_2, 0 °C to rt, 57%; g) Ac_2O, DMAP, pyridine, rt, 83%; h) $PdCl_2$, MeOH, rt, 89%; i) CCl_3CN, DBU, CH_2Cl_2, 0 °C to rt, 70%.

The synthesis of methylated dimannosides **30** and **31** were performed separately, using the same acceptor **23** and trichloroacetamidate **26** and **29**, respectively, in the presence of TMSOTf (scheme 5). For the synthesis of tetramannoside $sMetMan_4$ **3** (scheme 5), the methylated dimannoside **31** was converted in a glycosyl donor and the methylated tetramannoside **34** was synthesized using the tricloroacetamidate **33** and the acceptor **30** with a very good yield (86%, scheme 6), followed by the deprotection steps (scheme 6).

Scheme 5

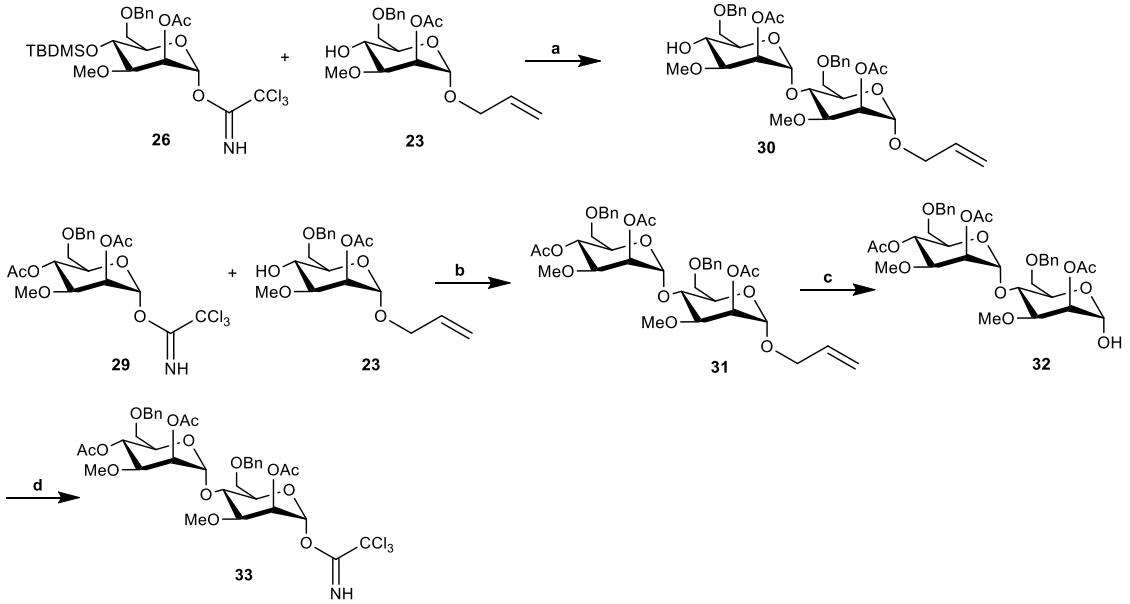

a) TMSOTf, CH_2Cl_2, 4Å MS, -20 °C, 48%; b) TMSOTf, CH_2Cl_2, 4Å MS, -20 °C, 65%; c) $PdCl_2$, MeOH, rt, 73%; d) CCl_3CN, DBU, CH_2Cl_2, 0 °C to rt, 68%.

Scheme 6

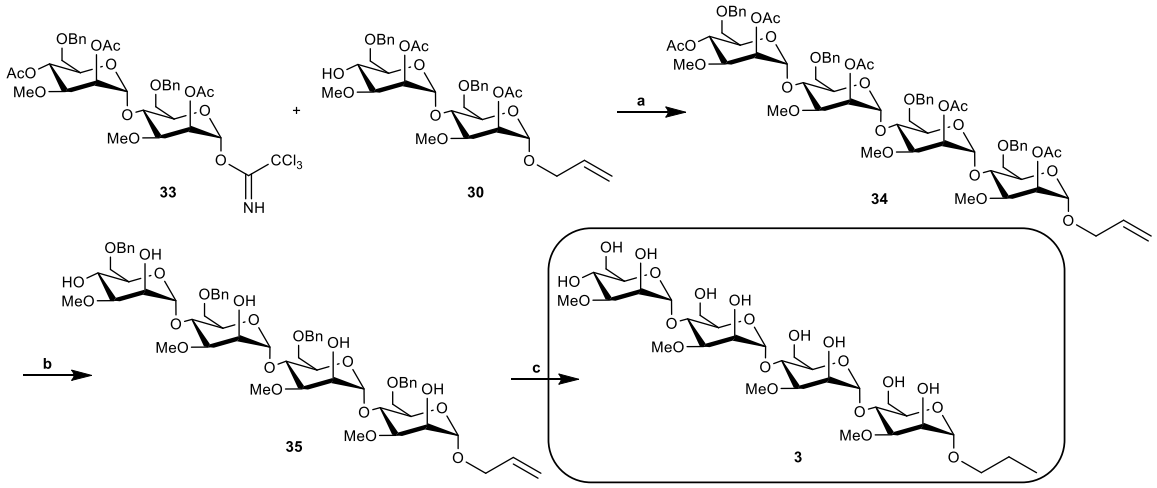

a) TMSOTf, CH_2Cl_2, 4Å MS, -20 °C, 86%; b) MeONa, MeOH, 0 °C to rt, 84%; c) H_2, Pd/C, AcOEt, 50 psi, quant.

To prepare the methylated trimannoside **36**, a glycosylation reaction between the donor **30** and acceptor **23** was performed and the final structure trimannoside $sMetMan_3$ **4** was obtained after the deprotection reactions (scheme 7).

Scheme 7

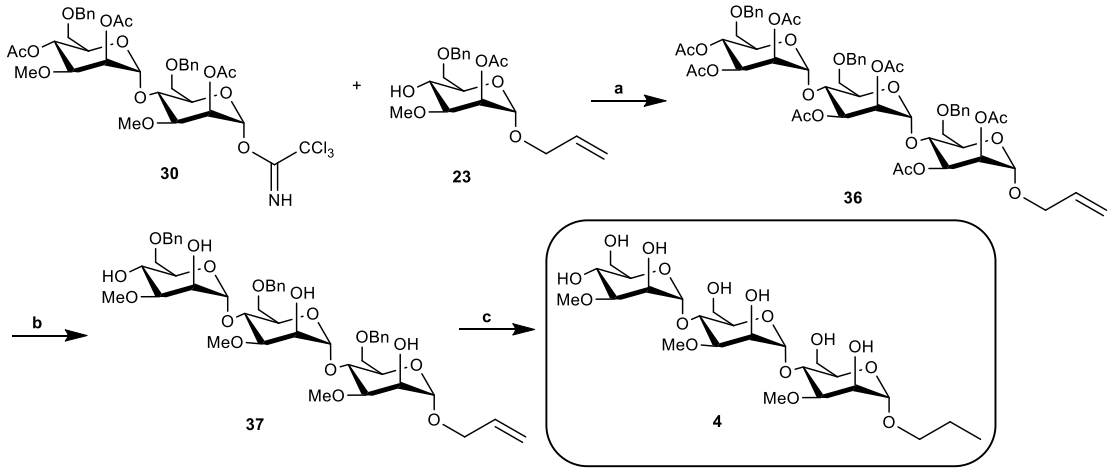

a) TMSOTf, CH_2Cl_2, 4Å MS, -20 °C, 85%; b) MeONa, MeOH, 0 °C to rt, 76%; c) H_2, Pd/C, AcOEt, 50 psi, quant.

3.3. ManT is a rare α-(1→4)-mannosyltransferase

The *M. hassiacum* ManT was highly specific towards the polymerization degree of the acceptor sugar, only using trimannosides (figure 3.4 A and C) and tetramannosides (figure 3.4 B and C), from the range of oligomannosides tested. Differentially methylated mono- and dimannosides (1-OH and/or 3-OH) were also tested as possible acceptors, but these were not used as substrates, in accordance to what had been already described in earlier studies (Weisman and Ballou, 1984b; Xia et al., 2012). Indeed, ManT was more active with tetramannoside $sMetMan_4$, followed by

trimannoside sMetMan$_3$ and, lastly, with both the corresponding unmethylated mannosides, revealing a substantially higher preference for methylated substrates. We determined that ManT to be six-fold more active with methylated than with unmethylated substrates (figure 3.5). Moreover, this enzyme was very selective for mannosyl acceptors, not using different sized maltooligosaccharides, MGP or MGLP. The enzyme was also very specific for the α-configuration the glycosidic bonds of mannosides and did not show activity with the β-(1→4)-mannosides (β-Man$_2$, β-Man$_3$ and β-Man$_4$) tested.

Regarding donor group utilization, GDP-mannose was the exclusive donor substrate identified with no other sugars being transferred from other guanosine diphosphates tested. M1P and M6P were also tested as possible mannose donors but the enzyme was unable to transfer mannose from these compounds. However, other NDP-mannose donors such as UDP-mannose and ADP-mannose were not tested, because they are not commercially available. The hydrolytic properties of ManT in the presence of these donor groups and in absence of acceptors were also tested, but the enzyme was unable to hydrolyse them.

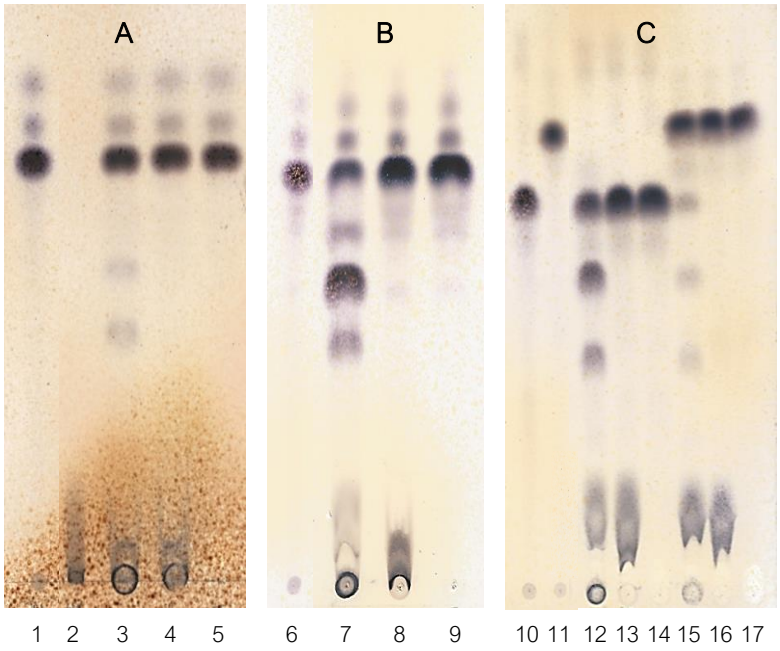

Figure 3.4 – TLC analysis of ManT activity with tri- and tetramannosides. A) Reaction with sMetMan$_3$. B) Reaction with sMetMan$_4$. C) Reaction with unmethylated sMan$_3$ and sMan$_4$. Lane 1 – standard sMetMan$_3$; lane 2 – GDP-mannose; lane 3 – ManT reaction with sMetMan$_3$; lane 4 – Ct reaction without enzyme; lane 5 – Ct reaction without GDP-mannose; lane 6 – standard sMetMan$_4$; lane 7 – ManT reaction with sMetMan$_4$; lane 8 – Ct reaction without enzyme; lane 9 – Ct reaction without GDP-mannose; lane 10 – standard sMan$_4$; lane 11 – standard sMan$_3$; lane 12 – ManT reaction with sMan$_4$; lane 13 – Ct reaction without enzyme; lane 14 – Ct reaction without GDP-mannose; lane 15 – ManT reaction with sMan$_3$; lane 16 – Ct reaction without enzyme; lane 17 – Ct reaction without GDP-mannose.

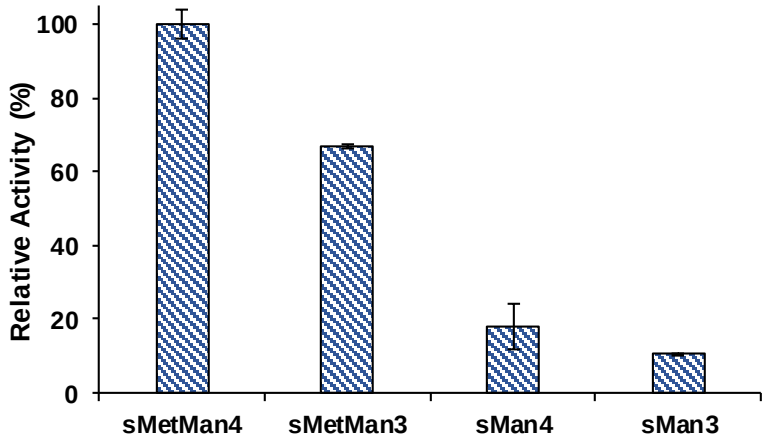

Figure 3.5 – ManT activity tested in the presence of different 3-*O*-methylated and unmethylated mannosides. ManT activity was determined by a discontinuous method through indirect quantification of the GDP released, as described previously (Mendes et al., 2010). Error bars represent standard deviation.

3.4. Biochemical and kinetic properties of ManT

Recombinant *M. hassiacum* ManT was active between 20 and 55 °C with maximum activity observed at 40 °C (figure 3.6 A). The enzyme was active between pH 6.5 and 10, showing an activity peak at pH 8.5 in BTP buffer (figure 3.6 B). However, because the relative activity at 37 °C was about 95% of maximum activity and mycobacterial infections occur at human physiological temperature, characterization of ManT was performed at 37 °C. ManT activity was independent of metal ions, showing activity in the presence of EDTA, although it was significantly (~ five-fold) improved in the presence of 7.5 mM $MgCl_2$ (figure 3.6 C). Furthermore, Triton X-100 (0.1%, v/v) enhanced ManT activity (figure 3.6 D), which is not surprising, since this detergent was essential to stabilize the enzyme in solution throughout all purification procedures and, most likely mimics the hydrophobic environment found in the membrane fraction where the enzyme activity was previously detected (Weisman and Ballou, 1984b; Xia et al., 2012). The effect of NaCl in ManT activity was also tested. The ManT activity increased in the presence of NaCl, possibly, because it acts a stabilizing agent (figure 3.6 E).

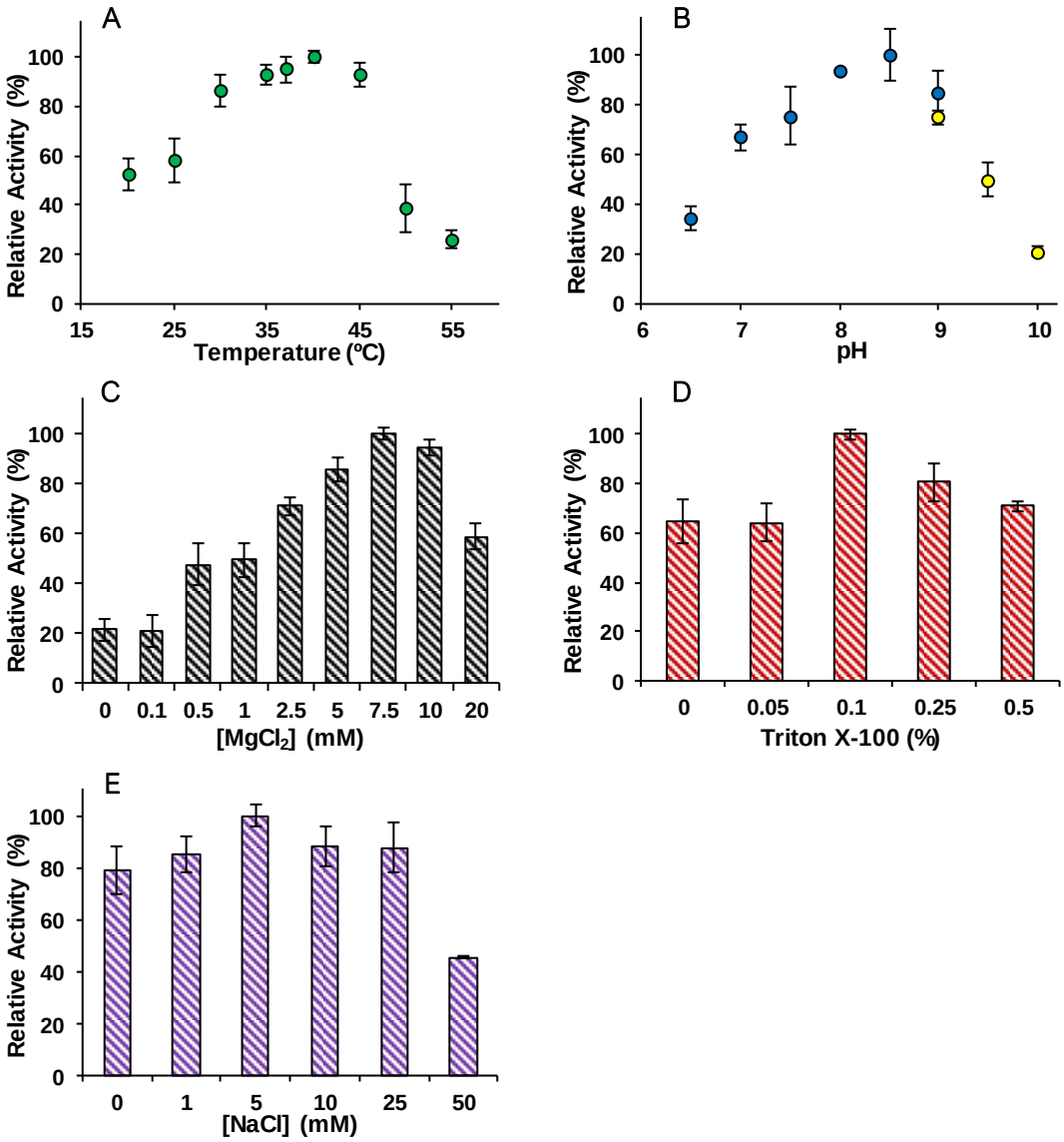

Figure 3.6 – Biochemical properties of ManT with the tetramannoside acceptor sMetMan$_4$. A) Temperature profile. B) pH dependence examined in BTP (blue) and CAPSO buffers (yellow). C) ManT activity in the presence of $MgCl_2$. D) Effect of Triton X-100 on ManT activity. E) Effect of NaCl on ManT activity. Error bars represent standard deviation.

Kinetic characterization of ManT performed with varying concentrations of GDP-mannose and with both the unmethylated and 3-*O*-methylated tetramannosides at 37 °C revealed that recombinant ManT exhibited Michaelis-Menten behaviour (figure 3.7). The K_m obtained for sMetMan$_4$ (0.128 ± 0.026 mM) was twenty-two times lower than the value for unmethylated sMan$_4$ (2.84 ± 0.56 mM) (table 3.2) and the V_{max} value was also higher for the methylated sugar, which suggests a higher affinity and, consequently, preference of the ManT for methylated substrates. Indeed, this is corroborated by the catalytic efficiencies (k_{cat}/K_m) and enzyme turnover (k_{cat}) calculated for both acceptors (0.047 ± 0.001 s^{-1} for sMetMan$_4$ and 0.025 ± 0.001 s^{-1} for sMan$_4$), evidencing once again a preference of ManT for sMetMan$_4$.

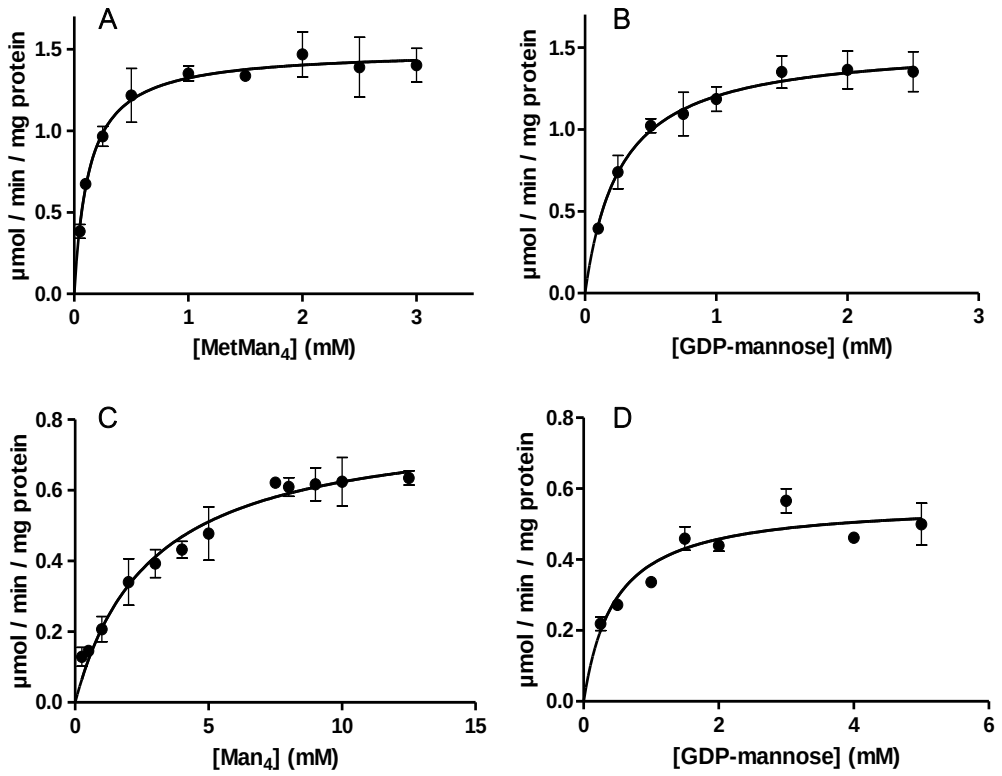

Figure 3.7 – Kinetic properties of recombinant ManT at 37 °C. A and B) Michaelis-Menten curve of ManT activity as a function of $sMetMan_4$ and GDP-mannose, respectively. C and D) Michaelis-Menten curve of ManT activity as a function of unmethylated $sMan_4$ and GDP-mannose, respectively. Error bars represent standard error of the mean.

Table 3.2 – Kinetic parameters of recombinant ManT from *M. hassiacum*.

T (°C)	Substrate	K_m (mM)	V_{max} (µmol/min/mg)	k_{cat} (s^{-1})	k_{cat}/K_m ($mM^{-1}.s^{-1}$)
37	$sMetMan_4$	0.128 ± 0.026	1.49 ± 0.054	0.047 ± 0.001	0.37 ± 0.07
	GDP-mannose	0.269 ± 0.064	1.52 ± 0.08	0.048 ± 0.002	0.18 ± 0.04
	$sMan_4$	2.84 ± 0.56	0.8 ± 0.053	0.025 ± 0.001	0.009 ± 0.002
	GDP-mannose	0.45 ± 0.11	0.56 ± 0.031	0.017 ± 0.001	0.04 ± 0.01

3.5. Analysis of reaction products by MS

The TLC analysis of ManT reactions with synthetic tetramannosides revealed the synthesis of three reaction products (RP1 to RP3) in the presence of $sMetMan_4$ (figure 3.8 A) and the formation of only two products (RP4 and RP5) with unmethylated $sMan_4$ (figure 3.8 B). Each product was isolated, purified and analysed by MS, confirming that ManT catalyses the sequential addition of mannose units to its substrates. Ions assigned to RP1, RP2 and RP3 products are in the $[M+Na]^+$ form (figure 3.9 A-C and table 3.3) and correspond to oligomannosides with one, two and three additional mannoses when compared to the original substrate ($sMetMan_4$), which confirms the

formation of penta- (figure 3.9 A), hexa- (figure 3.9 B) and heptamannosides (figure 3.9 C). Regarding the reaction products obtained with unmethylated $sMan_4$, it was only possible to confirm the identity of the RP4 product by MS due to very poor ionization of the RP5 product. RP4 corresponds to the $[M+Na]^+$ ion, which coincides with the addition of one mannose to unmethylated $sMan_4$, yielding a pentamannoside (figure 3.9 D). However, differences in one mannose unit are easily distinguishable in TLC analysis (figure 3.8 B), especially by comparison with the sequentially added mannoses at $sMetMan_4$. Thus, we can assume that the same sequential mannose additions occur in the presence of $sMan_4$ and, consequently, RP5 would be the product of two added mannoses to $sMan_4$, forming a hexamannoside.

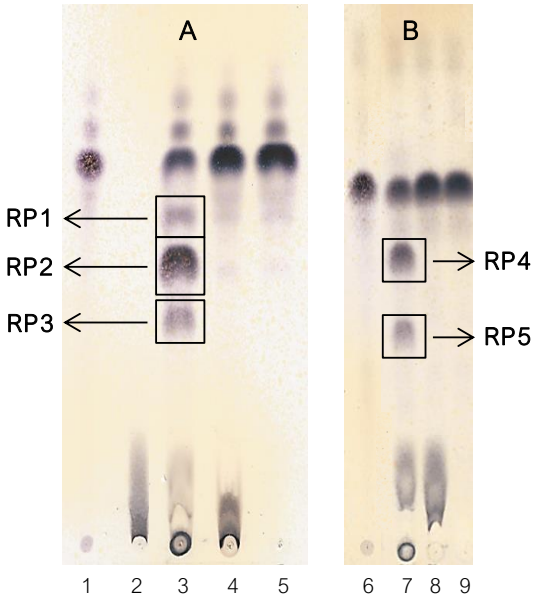

Figure 3.8 – TLC analysis of ManT activity with the tetramannosides $sMetMan_4$ and unmethylated $sMan_4$. A) Reactions with $sMetMan_4$. B) Reactions with unmethylated $sMan_4$. Lane 1 – standard $sMetMan_4$; lane 2 – GDP-mannose; lane 3 – ManT reaction with $sMetMan_4$; lane 4 – Ct reaction without enzyme; lane 5 – Ct reaction without GDP-mannose; lane 6 – standard unmethylated $sMan_4$; lane 7 – ManT reaction with $sMan_4$; lane 8 – Ct reaction without enzyme; lane 9 – Ct reaction without GDP-mannose. RP1 to RP5 correspond to ManT products obtained in the presence of either synthetic tetramannosides.

Table 3.3 – Exact masses and corresponding spectra peaks and ions of ManT reaction products and MS/MS fragmentation.

Molecules	Exact mass (g/mol)	$[M-Na]^+$ (m/z)	Spectrum peak (m/z)	Molecules	Exact mass (g/mol)	$[M-Na]^+$ (m/z)	Spectrum peak (m/z)
$MetMan_2$	412.19	435.18	435.19	Man_3-$MetMan_4$ (**RP3**)	1250.49	1273.48	1273.48
$MetMan_3$	588.26	611.25	611.26	Man_2	384.17	407.16	407.15
$MetMan_4$	764.33	787.32	787.33	Man_3	546.22	569.21	569.20
Man-$MetMan_4$ (**RP1**)	926.38	949.37	949.39	Man_4	708.27	731.26	731.25
Man_2-$MetMan_4$ (**RP2**)	1088.44	1111.43	1111.43	Man_5 (**RP4**)	870.32	893.31	893.31

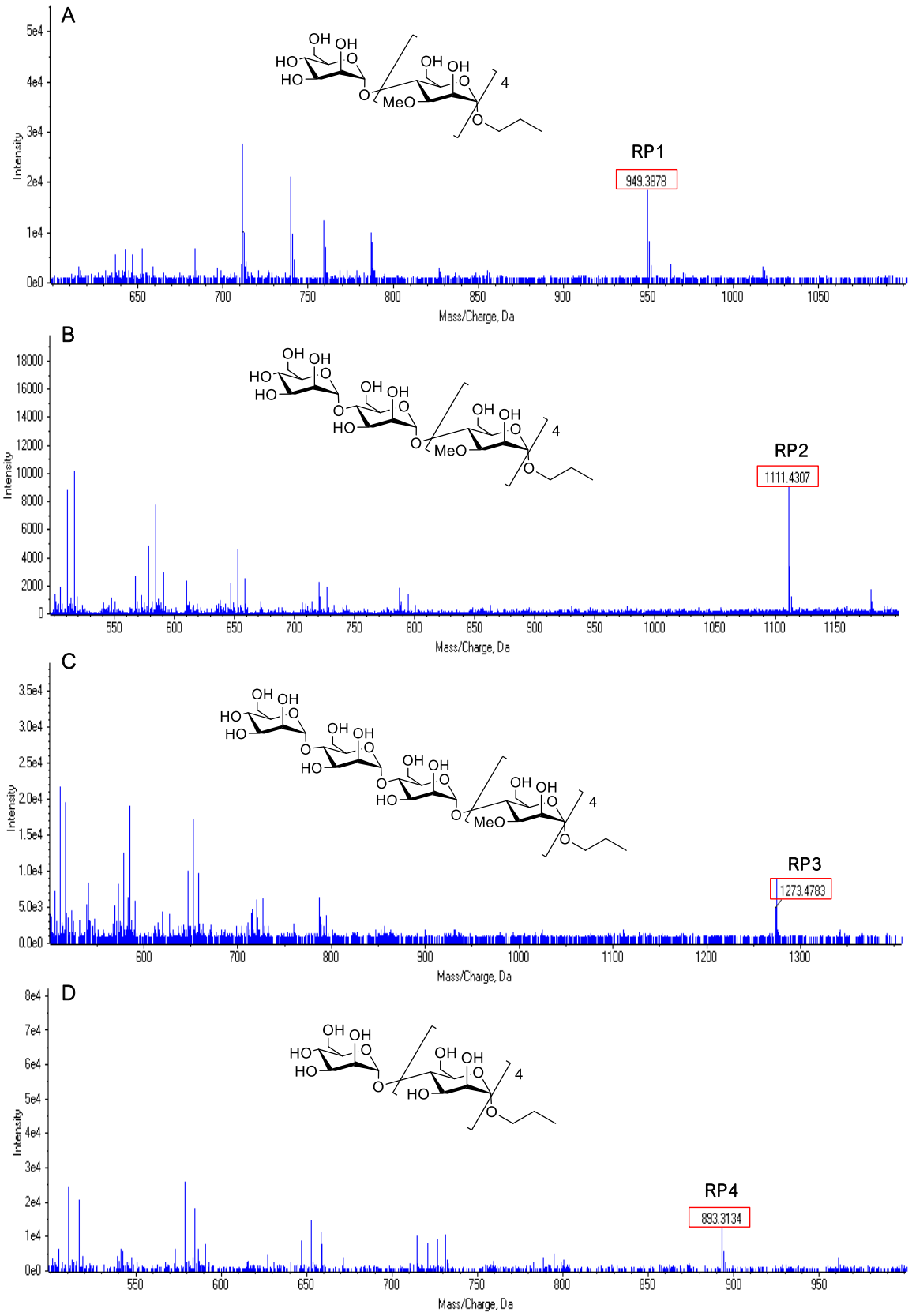

Figure 3.9 – MS analysis of purified products obtained after ManT activity with synthetic tetramannosides. A – D) ESI-TOF spectra acquired in positive ion mode of samples RP1 to RP4. Identified in a red box for each sample is the $[M\text{-}Na]^+$ ion. The chemical structure above each spectrum corresponds to the molecules identified in each sample.

All ions identified as ManT reaction products were further confirmed by MS/MS fragmentation and the spectra (figure 3.10 A-D) showed a successive loss of one mannose. In the spectra of products RP1 to RP3, it is possible to identify the loss of unmethylated mannoses (loss of 162.05 u) and of methylated mannoses (176.07 u), whereas in product RP4 the sequential loss of 162.05 u corresponds to the loss of an unmethylated mannose (figure 3.10 A-D and table 3.3).

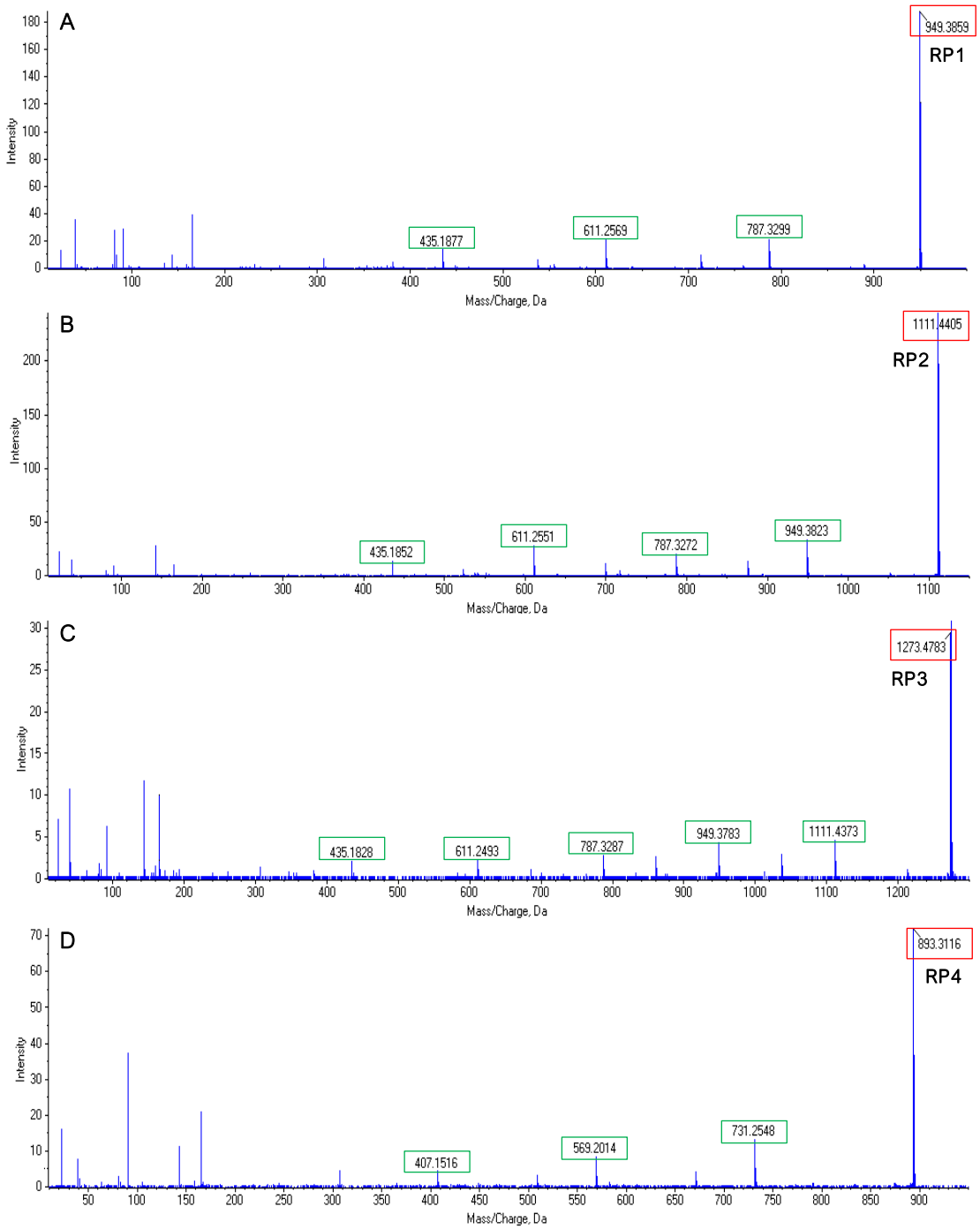

Figure 3.10 – MS/MS analysis of ManT reaction products ions. A) Spectrum of RP1. B) Spectrum of RP2. C) Spectrum of RP3. D) Spectrum of RP4. Spectra acquired in positive ion mode and the red boxes identify the $[M\text{-}Na]^+$ ions correspondent to ManT reaction products and the green boxes highlight the $[M\text{-}Na]^+$ ions of each fragment formed from MS/MS fragmentation.

3.6. ManT activity with the natural reaction products of MmpH

Recombinant *M. hassiacum* ManT is active with the four hydrolytic products **a**-**d** (figure 3.11 A) obtained with MmpH from purified MMP, as evidenced in a TLC with MmpH products being consumed in the presence of ManT (figure 3.11 B). ManT preference for shorter mannosides was examined in the presence of synthetic and biological substrates, using the chemically synthesized mannosides (schemes 1-7) and the natural MmpH products (chapter 2). Although both $sMetMan_4$ and tetramannoside **a** have four methylated mannoses (figure 3.11 A), the enzyme had 20% lower activity with tetramannoside **a** and obvious preference for the synthetic $sMetMan_4$ and the five methyl mannose-containing product **b** (figure 3.12). Furthermore, ManT had low activity with product **d** and similar low activity with the synthetic unmethylated substrates ($sMan_4$ and $sMan_3$).

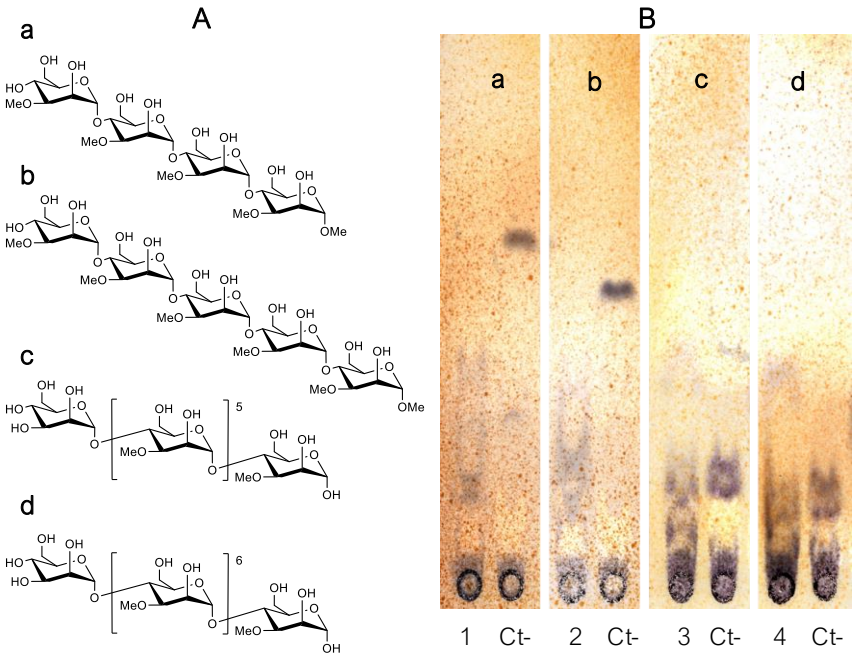

Figure 3.11 – A) Structure of MmpH products **a**-**d** with MMP as substrate. B) TLC analysis of ManT activity with MmpH products as substrates (**a**-**d**). Lane 1 – ManT reaction with product **a**; lane 2 – ManT reaction with product **b**; lane 3 – ManT reaction with product **c**; lane 4 – ManT reaction with product **d**; lane Ct- – control without enzyme.

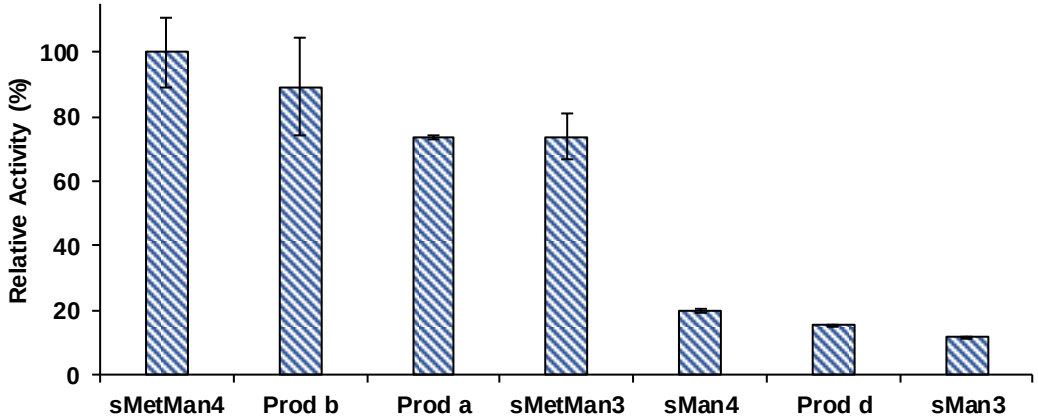

Figure 3.12 – ManT activity with synthetic and biological (MmpH products) 4α-oligomannosides as substrates. Error bars represent standard deviation.

4. Discussion

A putative mannosyltransferase (ManT) is present in the gene cluster proposed to encode the proteins responsible for MMP biosynthesis, which is, to the best of our knowledge, the only ManT that catalyses the transfer of mannose residues with concomitant formation of C1-C4 α-glycosidic bonds. This type of linkage between mannose units is rare in nature (Moreira and Filho, 2008), since among the mannosides identified in plants the β-(1→4) linkage prevails and in fungi and bacteria mannan chains are essentially α-(1→2), α-(1→3) and α-(1→6) and branched, thus more intricate than MMP (Shibata and Okawa, 2010; Malgas et al., 2015; Komaniecka et al., 2017).

Although the consensual definition of mannosyltransferase is an enzyme that transfers mannose groups, the ManT identified here has low amino acid sequence identity with other known mycobacterial mannosyltransferases as those involved in PIM, LM and LAM synthesis, which highlights the uniqueness of the linkage described here. On the other hand, the enzymes Rv3032 and Rv1212c are α-(1→4)-glucosyltransferases known to be involved in MGLP and glycogen biosynthesis (Stadthagen et al., 2007; Sambou et al., 2008; Kalscheuer et al., 2010) and they transfer glucose units from NDP-glucose to an α-(1→4)-D-glucosyl nascent chain. Despite the mechanistic resemblance, the amino acid sequence identity between these enzymes and ManT is limited, most likely due to substantial differences in the structures of the acceptor groups (Maranha et al., 2015). Moreover, donor group utilization is expectedly different, since ManT had no activity with NDP-glucose, the substrate used by Rv3032 to elongate short chain maltosyl substrates (Stadthagen et al., 2007). However, these were preliminary studies performed on cell free extracts and there was no mention of the possible utilization of other NDP-sugars such as GDP-mannose.

ManT transferred mannose groups from GDP-mannose to four synthetic mannosides tested, preferentially using methylated substrates $sMetMan_4$ and $sMetMan_3$. This preference was also observed in a previous study with membrane extracts of *M. smegmatis* where the activity of unmethylated tetramannoside and two tetramannosides with different methylation degrees was compared (Xia, 2013). However, ManT was not active in the presence of mono- and dimannosides with different combinations of methyl decorations at position 1-OH or/and 3-OH. The kinetic parameters of enzyme activity (K_m = 0.128 ± 0.026 mM for $sMetMan_4$ and K_m = 2.84 ± 0.56 mM for $sMan_4$) suggested a higher affinity for methylated sugars and showed that $sMetMan_4$ is in fact the preferred substrate, in accordance with previous works (Weisman and Ballou, 1984b; Xia et al., 2012). Curiously, the biochemical properties of ManT determined in this study were similar to those obtained by Weisman and Ballou in reactions using *M. smegmatis* membrane extracts (Weisman and Ballou, 1984b), where the activity was optimal at pH 8.2 and enhanced in the presence of $MnCl_2$, $MgCl_2$ and $CaCl_2$ (10 mM). In our study with pure recombinant ManT, maximum activity was obtained at pH 8.5 and it was also stimulated in the presence of 7.5

mM of $MgCl_2$. The addition of Triton X-100 to the purification buffers and to all enzymatic reactions was a stabilizing element that significantly enhanced ManT activity. However, despite the fact that the mannosylation activity had been associated to membrane extracts in previous studies (Weisman and Ballou, 1984b; Xia et al., 2012), ManT was purified in soluble form from *E. coli* cell-free extracts and used GDP-mannose as donor group, a substrate described as cytoplasmatic mannose donor in mycobacteria (Yokoyama and Ballou, 1989). How does ManT transiently attach to the plasma membrane remains unknown.

In addition to the synthetic substrates, this enzyme also had activity with four hydrolytic products of MmpH, showing an equivalent relative activity with the pentamannoside **b** and with synthetic $sMetMan_4$, which was unexpected seeing that product **a** has the same number of methylated mannoses and is the most similar to $sMetMan_4$. Curiously, the relative activity of ManT with tetramannoside **a** was quite similar to that with $sMetMan_3$ (figure 3.12). One possible reason for these apparent discrepancies might be related to the presence of the propyl group at the reducing end of the synthetic substrates, since this group could occupy the position of an additional mannose inside the enzyme's active site pocket for the acceptor, mimicking the presence of one additional mannose. Thus, $sMetMan_4$ would be recognized as a pentamannoside by ManT and $sMetMan_3$ as a tetramannoside, which would explain the similar relative activity that pairs $sMetMan_4$ with product **b** and $sMetMan_3$ with product **a**. However, the allyl group is essential to block the reactive C1 during synthesis of substrates and despite several attempts, it was not possible to remove it and produce deprotected tri- and tetramannosides at position 1-OH, because sugars were cleaved possibly due to HCl production during this chemical reaction step. This hypothesis for synthetic versus biological substrate utilization could be better understood with the aid of the three-dimensional structure of ManT. ManT activity towards oligomannosides with nonreducing ends, namely octamannoside **d**, was low and similar to the activity observed with the synthetic unmethylated substrates $sMan_4$ and $sMan_3$. The activity was not tested with product **c**, because it was obtained in minute quantities, but we would expect that the result should be identical to product **d**, as indicated by TLC analysis (figure 3.11 B). As these products are biological, this approach was an attempt to mimic the *in vivo* activity of ManT and, despite the unexpected preference for oligomannoside **b**, this result strengthens the hypothesis that this hydrolytic product mediates a MMP recycling mechanism, in which ManT initiates the synthesis of new MMP molecules from fragments of a pre-existing MMP hydrolysed by MmpH.

On the other hand, speculation about substrate recognition by ManT raises some questions about the utilization of trimannosides as enzymatic acceptors in earlier studies. In the first assays, Weisman and Ballou used a methylated trimannoside in both 1-OH and 3-OH positions and did not verify ManT activity in membrane extracts of *M. smegmatis* with this compound (Weisman and Ballou, 1984b). In a more recent study, Xia and colleagues could observe ManT activity with

methylated trimannosides but these were synthetic substrates in which position 1-OH was blocked by an octyl group (five extra carbons in relation to the propyl used in our study) (Xia et al., 2012) that could also mimic one more mannose units inside the active site pocket, allowing the enzyme to act in the presence of trimannosides. Xia and colleagues also tested a dimannoside blocked with an octyl group that, by the same logic, could be recognized as a trimannoside, however ManT was not active in the presence of this substrate (Xia et al., 2012). Whether this means that a trimannoside is not a substrate for ManT, in agreement with the results of Ballou and colleagues with membrane extracts of *M. smegmatis,* will require further confirmation with non-blocked substrates more similar to the physiological mannosides and analysis of the three-dimensional structure of the enzymes.

With MS and TLC analysis of ManT products, we observed that this enzyme can add up to three mannoses to $sMetMan_4$, producing penta-, hexa- and heptamannosides, whereas in the presence of $sMan_4$ only two products were detected, the penta- and hexamannosides. Hence, ManT catalyses the sequential elongation of its substrates and the its affinity towards methylated substrate is also reflected by number of products synthetized with $sMetMan_4$. This difference in reaction products was also observed when Xia et al. compared the products that resulted from tetramannosides that differed only in one methylation, since when using a totally methylated tetramannoside, it was mostly produced hexa- and heptamannosides, whereas with the compound with a latter unmethylated mannose was formed penta- and hexamannosides (Xia et al., 2012).

The results obtained in this study are in accordance with the mechanism recently proposed for ManT elongation (Xia et al., 2012; Xia, 2013), where mannosylation reactions can also occur in the absence of methyl groups at position 3-OH. However, the alternating mannosylation and methylation hypothesis of Ballou (Weisman and Ballou, 1984a) cannot be discarded, because ManT products longer than hexa- or heptasaccharide were not found and both oligomannosides can be considered as precursors of MMP when compared to the eleven to fourteen mannose units of mature MMP. Therefore, the progress of the synthesis may be dependent on methylation of individual or a block of mannoses added, and it may be that *in vivo* the mannosylation reactions are not completely dependent of methylation, but the methylation of oligomannosaccharides could be necessary for continued ManT activity or, eventually, another mannosyltransferase could be involved in the following elongation steps.

In summary, the second enzyme of the 4-gene cluster proposed to encode the enzymes necessary for MMP biosynthesis was identified and characterized as a novel and unusual α-(1→4)-ManT responsible for elongation of hydrolytic products of MmpH. Furthermore, this work contributes to further our knowledge on MMP biosynthesis, highlighting a new mannosylation reaction, hardly ever found in nature.

Chapter 4:
Two methyltransferases of the MMP gene cluster

This Chapter is partly published in:

J. Ripoll-Rozada[a], M. Costa[a], J. A. Manso, A. Maranha, V. Miranda, A. Sequeira, M. R. Ventura, S. Macedo-Ribeiro, P. J. B. Pereira[b], N. Empadinhas[b]; Biosynthesis of mycobacterial methylmannose polysaccharide requires a unique 1-*O*-methyltransferase specific for 3-*O*-methylated mannosides *Proc. Natl. Acad. Sci. U. S. A.* 2019, 116 (3), 835-844.

[a]Co-first authors; [b]Co-corresponding authors.

1. Introduction

Methylation is a modification widely found in proteins, influencing protein-protein interactions, stability, localisation and enzymatic activity and it is also commonly found in DNA and RNA molecules, playing fundamental roles in epigenetic mechanisms such as imprinting, X-inactivation, oncogenesis, inflammatory and immunological processes (Staudacher, 2012). However, this modification is much less common in carbohydrates (Staudacher, 2012).

Complementing the panoply of different components of the mycobacterial cell wall, some mycolic acids are methylated by *S*-adenosylmethionine (SAM)-dependent methyltransferases (MTases) and this modification is critical for their function and structural diversity, being associated with mycobacterial virulence (Barry III et al., 1998). Furthermore, methylations also occur in glycopeptidolipids (GPL) present on the cell wall, whose structural heterogeneity in species, such as *M. avium* and *M. intracellulare,* is reflected in their colony morphology and virulence levels (Naka et al., 2011; Staudacher, 2012).

In the *Mtb* H37Rv genome, circa 121 MTases were identified and about 70% of those are SAM-dependent enzymes (Grover et al., 2016). SAM-dependent methylation represents a major class of biological processes and includes methyl group transfer from SAM, yielding *S*-adenosyl-L-homocysteine (SAH) and a methylated molecular target (Walsh et al., 2018). Twenty of the 61 MTases whose functions have been identified act on RNA or DNA, 10 are involved in the methylation of mycolic acids and the remaining participate in diverse metabolic pathways (Grover et al., 2016). Interestingly, opportunistic and non-pathogenic NTM possess 10-20% less MTases than strictly pathogenic mycobacterial species (Grover et al., 2016).

Both intracellular PMPS are methylated but show different methylation patterns. In MMP, the entire molecule is methylated in the 3-OH positions of each mannose, from the reducing end to the main backbone, except the last mannosyl residue, and the first mannose that has an additional methylation in the 1-OH position (Gray and Ballou, 1971; Maitra and Ballou, 1977). MGLP is methylated in the 6-OH positions in the main backbone glucoses and also in the 3-OH position of the last glucose (Lee, 1966; Gray and Ballou, 1971; Mendes et al., 2012). The methylation of PMPS was proposed to be crucial for the function played by these polysaccharides, since they were postulated to assume a helical conformation in solution, forming a hydrophobic “tunnel” with inward facing methyl groups to stabilize the inclusion of long-chain FA and hydroxyl groups on the exterior face (Bergeron et al., 1975). However, a recent study suggested that, although MMP methylations are essential to bind FA, they can be orientated to the same side as hydroxyl groups and, consequently, MMP may not assumes a helical structure as proposed (Liu et al., 2016).

Two putative MTase genes from *M. tuberculosis*, *Rv3030* and *Rv3037c*, were proposed to be involved in MGLP biosynthesis and the disruption of the *Rv3030* orthologue (*MSMEG_2349*)

in *M. smegmatis* resulted in a phenotype with decreased MGLP levels, which confirmed its involvement in MGLP biosynthesis. Due to the residual MGLP content found in the *ΔMSMEG_2349* mutant, it was postulated that a MTase compensatory activity must be present, most likely encoded by *Rv3037* (Stadthagen et al., 2007). In what concerns MMP synthesis, in 1984 Ballou and co-workers detected a MTase activity in *M. smegmatis* extracts and proposed that the MMP termination of elongation was related to the decrease in affinity by the MTase to increasingly longer substrates, giving rise to the terminal unmethylated mannose (Weisman and Ballou, 1984a). In the cluster that we here propose to be responsible for MMP biosynthesis, two putative MTases are present, which are possibly involved in methylation at the C3 positions in the main backbone mannoses and at the C1 position of the MMP reducing end.

2. Methods

2.1. Identification of genes for MTases in the MMP gene cluster

In the 4-gene cluster proposed to be responsible for the MMP biosynthetic pathway, two putative MTases are present, both annotated as probable SAM-dependent MTases, which we considered to encode a 1-*O*-methyltransferase (MeT1) and a 3-*O*-methyltransferase (MeT3). Both amino acid sequences (WP_005631133.1 and WP_005631136.1) were retrieved from the *M. hassiacum* genome and used in BLAST analysis (https://blast.ncbi.nlm.nih.gov/Blast.cgi).

2.2. Expression and purification of the MTases

The genes encoding *M. hassiacum* MeT1 (WP_005631133.1) and MeT3 (WP_005631136.1) were selected for recombinant expression and the sequences were codon optimized (GenScript) for expression in *E. coli* and cloned between either the *NdeI* and *HindIII* (for *meT1*) or *XhoI* and *EcoRI* (for *meT3*) restriction sites of the expression vector pET30a (Novagen). Removal of the native stop codon yielded a C-terminal His6-tag MeT1, while MeT3 was expressed with a N-terminal His6-tag. Both were overexpressed in *E. coli* BL21 (DE3). Briefly, *E. coli* cells were grown in LB medium supplemented with 50 µg/mL kanamycin at 37 °C until OD_{600} ≈ 0.8, when the incubation temperature was decreased to 25 °C and recombinant protein expression was induced by addition of 0.5 mM IPTG. After overnight growth, 3 L of cell culture were harvested by centrifugation (9000 rpm, 15 min, 4 °C), suspended in 20 ml buffer A (20 mM sodium phosphate pH 7.4, 0.5 M NaCl, 20 mM imidazole) and frozen at -20 °C. The cell pellets with recombinant MeT1 were thawed (60 min on ice) in the presence of 5 µg/mL lysozyme, 5 µg/mL DNAse I, 5 mM $MgCl_2$, 1 mM PMSF and EDTA-free protease inhibitor cocktail (Roche). The cell pellets containing recombinant MeT3 were thawed on ice and 20 µg/mL DNAse I and 5 mM $MgCl_2$ were added. The cells were disrupted by sonication on ice with three 40 Hz pulses of 20 s (10 s pause between pulses) per 7 mL of lysate. The supernatant was clarified by centrifugation (17000 rpm, 30 min, 4 °C), filtered through a 0.45 µm pore low protein binding filter (Millipore) and loaded onto a 5 mL HisTrap HP column (GE Healthcare), equilibrated with buffer A. The protein of interest was eluted with 200 mM imidazole in buffer B (20 mM sodium phosphate pH 7.4, 0.5 M NaCl, 500 mM imidazole) and its purity assessed by SDS-PAGE. Fractions containing the target protein were pooled and concentrated using a 10 kDa molecular weight cutoff centrifugal ultrafiltration device (Millipore), flash frozen in liquid nitrogen and stored at -80 °C. The protein content was determined with the Bradford assay kit (BioRad). All MeT1 variants used in this study were produced and purified using the protocol followed for the WT enzyme.

2.3. Expression and purification of SahH

The enzymatic assay to monitor MeT1 activity (see below) was based on the activity of a recombinant *S*-adenosyl-L-homocysteine hydrolase (SahH) from *M. smegmatis* (MSMEG_1843) whose gene was amplified from genomic DNA previously purified with SmartHelix DNAid Mycobacteria kit (Sekvenator, Slovenia) with KOD Hot-Start DNA polymerase (Novagen) using forward primer 5'-TAGGATCCATGACCGAACTCAAGGCC and reverse primer 5'-TATAAGCTTTCAGTAGCGGTAGTGCTCGGG that included *BamHI* and *HindIII* restriction sites (underlined), respectively. The amplification product was purified and cloned into pET30a to allow translation of a N-terminal 6xHis-tagged recombinant SahH, which was produced in *E. coli* BL21 (DE3) as described for MeT1. Cells were harvested 18 h post-induction by centrifugation (9000 rpm, 15 min, 4 °C), suspended in buffer A containing 2 mg/mL DNAse I, 5 mM $MgCl_2$ and disrupted by sonication on ice with three 40 Hz pulses of 20 s (10 s pause between pulses) per 7 mL of lysate, followed by centrifugation (17000 rpm, 30 min, 4 °C) to remove debris. The His-tagged recombinant SahH was purified with a 5 mL HisTrap HP column as described for MeT1 and the purest fractions as assessed by SDS-PAGE were pooled, dialyzed and concentrated by ultrafiltration and equilibrated with 10 mM BTP pH 7.5, 50 mM NaCl. The protein content was determined with the Bradford assay kit (BioRad).

2.4. Chemical synthesis, purification and NMR analysis of mannosides

The synthesis of compounds 3-*O*-methylmannose (sMetMan), 3,3'-di-*O*-methyl-4α-mannobiose ($sMetMan_2$) and 1,3,3'-tri-*O*-methyl-4α-mannobiose ($sMet_{1,3}Man_2$) were performed in collaboration with M. Rita Ventura (Bioorganic Chemistry Group, ITQB NOVA, Oeiras) and the chemical reactions and protocols required for their synthesis are described in Sequeira, 2015.

2.5. MeT1 substrate specificity

MeT1 specificity was examined using D-glucose, 3-*O*-methylglucose (Sigma), maltose, maltotetraose and maltotriose (Carbosynth), D-mannose (Man), 4α-mannobiose (Man_2, Dextra), sMetMan, $sMetMan_2$ and $sMet_{1,3}Man_2$ (all synthetized at ITQB NOVA) as acceptor substrates and *S*-adenosylmethionine (SAM) as donor group. Reaction containing pure enzyme MeT1 (7.9 µM), 25 mM BTP pH 7.5, 10 mM $MgCl_2$, 3 mM SAM and 2.5 mM of each of the potential acceptors were incubated at 37 °C for 1 h. Product formation was monitored by TLC on silica gel 60 plates (Merck) with a solvent system composed of chloroform:methanol:water (55:40:10, v/v/v) and stained with α-naphtol-sulfuric acid, followed by charring at 120 °C (Jacin and Mishkin, 1965).

2.6. MeT3 substrate specificity

The substrate specificity of MeT3 was examined using Man (Sigma), Man_2 (Dextra), $sMan_3$ and $sMan_4$ (section 2.3, chapter 3) as acceptor groups. The reaction mixtures containing pure MeT3 (6.2 µM), 25 mM BTP pH 7.5, 5 mM $MgCl_2$, 3 mM SAM and 2.5 mM of different sugars were incubated 37 °C during 2 h. Product formation was monitored by TLC on silica gel 60 plates (Merck) with a solvent system composed of chloroform:methanol:water (55:40:10, v/v/v) and revealed with α-naphtol solution as described above.

2.7. Biochemical characterization of MeT1 activity

MeT1 activity was measured with both discontinuous and continuous methods through indirect quantification of released *S*-adenosylhomocysteine (SAH). A *S*-adenosylhomocysteine hydrolase (SahH) (Lozada-Ramírez et al., 2006; Singhal et al., 2013), which was cloned and purified as described above, converted SAH into adenosine and homocysteine and the latter was quantified with Ellman's reagent (Lozada-Ramírez et al., 2006) by monitoring product formation with the increase of absorbance at 412 nm. This enzyme activity is dependent on NAD^+ (Singhal et al., 2013) and has a residual activity with degraded SAM in solution. Thus, we performed the appropriate control reactions, only with SahH, to avoid errors in enzyme activity quantification.

A series of discontinuous assays were performed to determine the enzyme's pH and temperature profiles. The assays were initiated by addition of MeT1 (3.9 µM) to reaction mixtures containing the appropriate buffer (50 mM), 10 mM $MgCl_2$, 2.5 mM $sMetMan_2$ and 3 mM SAM. Cooling on ethanol-ice stopped the reaction and inactivation of the enzyme was achieved by addition of 1.5 µL of 1 N HCl. The pH was stabilized with 50 µL of 100 mM sodium phosphate pH 7.8, followed by addition of 500 µM NAD^+, 500 µM DTNB (5,5′-dithiobis-2-nitrobenzoic acid, Ellman's Reagent), and 1.7 µM SahH. The reactions were incubated at 37 °C for 15 min and the absorbance at 412 nm measured. The effect of pH was determined at 37 °C in 50 mM MES (pH 6.0 to 6.5), BTP (pH 6.5 to 9.0), sodium phosphate (pH 7.0 to 7.8) and CAPSO (pH 9.0 to 10.0) buffers. The temperature profile was determined between 25 and 70 °C in 50 mM sodium phosphate pH 7.5. The influence of divalent cations on enzyme activity was examined by incubating the reaction mixture with the chloride salts of Mg^{2+}, Mn^{2+}, Co^{2+}, Fe^{2+}, Ca^{2+}, Cu^{2+}, Zn^{2+} (2.5 mM) and without cations, or in the presence of 10 mM EDTA, at 37 °C for 1 h. The reactions were analysed by TLC, as described above.

The MeT1 activity was quantified in the presence of $MgCl_2$ and $MnCl_2$ through a continuous method, varying the cation concentration between 0.1-10 mM ($MgCl_2$) and 0.1-1 mM ($MnCl_2$). Due to the characteristic colour of Mn^{2+} in solution, it was not possible to test equivalent concentrations of $MnCl_2$ and $MgCl_2$. The continuous assays were performed in 96-well microtiter

plates and reactions mixtures were prepared with 50 mM sodium phosphate buffer pH 7.5, 2.5 mM $sMetMan_2$, 3 mM SAM, 500 µM DTNB, 500 µM NAD^+ and 1.7 µM SahH. Reactions were initiated by addition of enzyme (1.9 µM) and product formation was monitored at 412 nm, measuring the amount of SAH released. Control reactions were performed to account for vestigial activity of SahH, without the presence of MeT1. All experiments were performed in triplicate.

2.8. Kinetic parameters

The kinetic parameters for MeT1 were determined under optimal conditions at 37 and 50 °C through continuous and discontinuous methods, respectively, due to limitations of the coupled enzyme quantification assay (SahH) at high temperatures.

Reactions were performed in 50 mM sodium phosphate buffer pH 7.5 and 100 µM $MnCl_2$ and initiated by the addition of MeT1 (1.97 µM at 37 °C and 0.98 µM at 50 °C). The K_m and V_{max} values were determined for SAM and $sMetMan_2$, using a fixed saturating concentration of each substrate (1 mM of SAM for both temperatures and 3.5 mM and 6 mM of $sMetMan_2$ at 37 and 50 °C, respectively). All experiments were performed in triplicate with appropriated controls. Kinetic parameters were calculated with GraphPad Prism software (version 5.00).

2.9. Analysis of reaction product by NMR

For NMR analysis of $Met_{1,3}Man_2$, the product was obtained in 0.5 mL reactions with 50 mM sodium phosphate pH 7.5, 100 µM $MnCl_2$, 2.5 mM $sMetMan_2$, 2 mM SAM and 0.2 µM MeT1 at 37 °C with overnight incubation. The reactions were spotted on TLC plates and product formation was monitored using a solvent system composed of chloroform:methanol:water (55:40:10, v/v/v). After staining the marginal lanes of the TLC plates and identifying the product spots, the products were obtained by scraping the corresponding region in the inner unstained lanes of the TLC plate, followed by product extraction from the silica gel with ultrapure water (Maranha et al., 2015). The sample was analysed by NMR in collaboration with M. Rita Ventura (Bioorganic Chemistry Group, ITQB NOVA, Oeiras) and compared with the synthetic standard.

2.10. MeT1 activity with products of MmpH

The reaction products of MmpH were used as substrates of MeT1 activity and the results analysed by TLC as described above (section 2.5). The products were obtained as previously described (section 2.8, chapter 2) and the mixtures were prepared with 25 mM BTP pH 7.5, 5 mM $MgCl_2$, 1.5 mM SAM, 2.5 mM of each hydrolytic product and 3.2 µM MeT1, incubating 2 h at 37 °C.

The activity was also quantified through a continuous method as described above (section 2.7), comparing the activity between synthetic and biological substrates. The assays were initiated by addition of MeT1 (1.9 μM) to reaction mixtures containing 50 mM BTP pH 7.5, 1.5 mM acceptor substrate, 1 mM SAM, 100 μM $MnCl_2$, 500 μM DTNB, 500 μM NAD^+ and 1.7 μM SahH. Product formation was monitored at 412 nm, measuring the amount of SAH released. All experiments were performed with appropriate controls.

2.11. Structure determination of MeT1 and analysis of the activity of MeT1 mutants

The structure determination of MeT1 was performed by members of the Macromolecular Structure Group at IBMC/i3S/UP (Porto) and all procedures are described in Ripoll-Rozada et al., 2019. To confirm the identity of the residues involved in the catalytic mechanism of the enzyme, MeT1-E78A, MeT1-H79A and MeT1-H144A variants were created by Jorge Ripoll-Rozada (IBMC/i3S, Porto). The activity of the three variants was analysed under the conditions considered optimal for activity of the WT MeT1. Each reaction containing 50 mM sodium phosphate buffer pH 7.5, 100 μM $MnCl_2$, 3.5 mM $sMetMan_2$, 1 mM SAM and 3.9 μM of enzyme was incubated at 37 °C and 50 °C for 1 h. The results were monitored by TLC as described above. The kinetic parameters were determined for the active variants H79A and E78A and reactions were performed as described for the WT enzyme at 37 °C, using a fixed saturating concentration of each substrate (1 mM of SAM for both variants and 2 mM and 2.5 mM of $sMetMan_2$ for MeT1-E78A and MeT1-H79A, respectively). Reactions were initiated by adding of enzyme (19.7 μM).

2.12. Size exclusion chromatography

The oligomeric state of WT MeT1 and of variants MeT1-E78A, MeT1-H79A, and MeT1-H144A in solution was analysed by size exclusion chromatography (by Jorge Ripoll-Rozada, IBMC/i3S/UP, Porto). Purified proteins (50 μL of a 40 μM solution) were loaded onto a Superdex 200 Increase 5/150 GL column (GE Healthcare) previously equilibrated with 10 mM BTP pH 7.5, 50 mM NaCl and eluted at a flow rate of 0.2 mL/min. The column was calibrated using four molecular weight standards (GE Healthcare): ferritin (440 kDa), aldolase (158 kDa), ovalbumin (43 kDa) and ribonuclease A (13.7 kDa).

3. Results

3.1. Identification of the MTases in the MMP cluster

The two MTases present in the MMP cluster (blue and green genes in figure 2.3 of chapter 2) are annotated as SAM-dependent MTases and we hypothesized that these genes could encode the enzymes involved in methylation reactions of MMP, one involved in methylation at position 3 and the other in methylation at position 1. The first MTase gene considered to be a 1-*O*-methltransferase, herein designated *meT1*, is a 654 bp gene (WP_005631133.1) that is divergently oriented in relation to the other three genes in the *M. hassiacum* genomic cluster (blue gene). The other MTase gene has 723 bp (WP_005631136.1) and is the third gene of the cluster in the *M. hassiacum* genome (green) that was designated *met3* for its anticipated function (3-*O*-methylation). The enzymes were purified to homogeneity as His-tagged recombinant proteins (figure 4.1) from *E. coli* cell-free extracts and MeT1 was obtained in bioactive form, at approximately 150 mg protein per litre of culture, whereas MeT3 did not display activity in any of the conditions tested (see below).

Both MTases have high amino acid sequence identity with other putative MTases from NTM (>70%) and related actinobacteria, such as *Streptomyces griseus* and *Nocardia otitidiscaviarum* (figure 2.3, chapter 2). However, they show only moderate amino acid sequence identity (30%) with the two putative MTases, Rv3030 and Rv3037c, proposed to be involved in MGLP biosynthesis in *M. tuberculosis*.

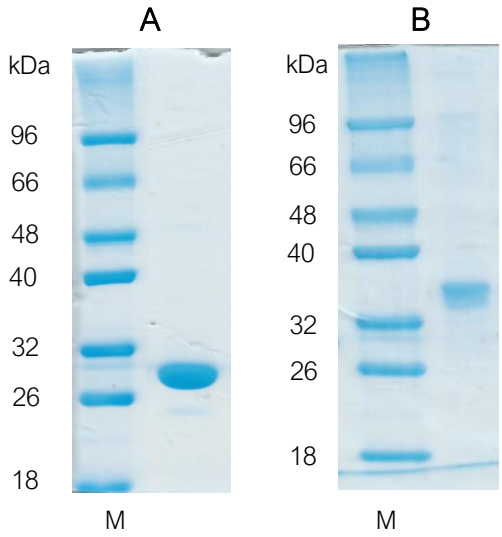

Figure 4.1 – SDS-PAGE analysis of the purified recombinant proteins. A) Purified recombinant MeT1 from *M. hassiacum*. B) Purified recombinant MeT3 from *M. hassiacum*. Lane M – molecular weight marker.

3.2. Substrate specificity of MTases

The MeT3 activity was tested with unmethylated acceptors ranging from the monomers to all tetramannosides available, but, unfortunately, this enzyme was unable to methylate the substrates in the conditions tested (figure 4.2). Eventually, despite apparent successful purification, this enzyme was not recovered in bioactive form, possibly because its correct folding failed or it lacks some cofactors need for its activity (Schein, 1991). It is possible that this can be solved through the use of other expression systems, such as expression in *M. smegmatis*, since this is an organism closely related to the native *M. hassiacum*.

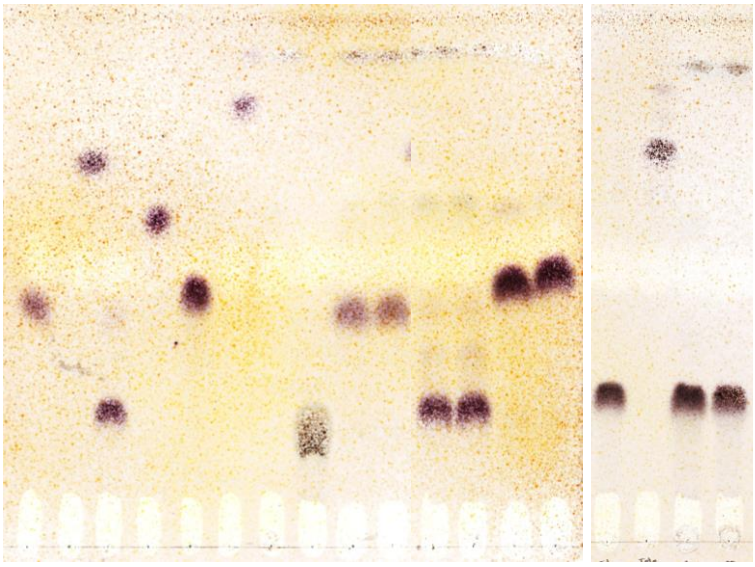

Figure 4.2 – TLC analysis of MeT3 activity. Lane 1 – Man; lane 2 – sMetMan; lane 3 – Man_2; lane 4 – $sMetMan_2$; lane 5 – $sMan_3$; lane 6 – $sMetMan_3$; lane 7 – SAM; lane 8 – SAH; lane 9 – MeT3 reaction with Man; lane 10 – MeT3 reaction with Man_2; lane 11 – MeT3 reaction with $sMan_3$; lane 12 – $sMan_4$; lane 13 – $sMetMan_4$; lane 14 – MeT3 reaction with $sMan_4$; lane Ct- – control without enzyme.

Regarding the other MTase in the cluster, MeT1, among the differentially methylated mono- and dimannoside substrates tested (synthetized at ITQB NOVA figure 4.3 A), the enzyme was very selective towards the specific position to which it transfers the methyl group. The enzyme methylates the 1-OH position of $sMetMan_2$ yielding $sMet_{1,3}Man_2$ (figure 4.3 B, lane 8) in the presence of SAM. The enzyme was not active towards un- or methylated monosaccharides nor unmethylated disaccharides (figure 4.3 B), requiring the methylation at position 3-OH and at least two mannoses to recognize the substrate. The methylation site was confirmed using synthetic $sMet_{1,3}Man_2$ as standard by TLC as well as by ^{1}H-NMR (figure 4.4).

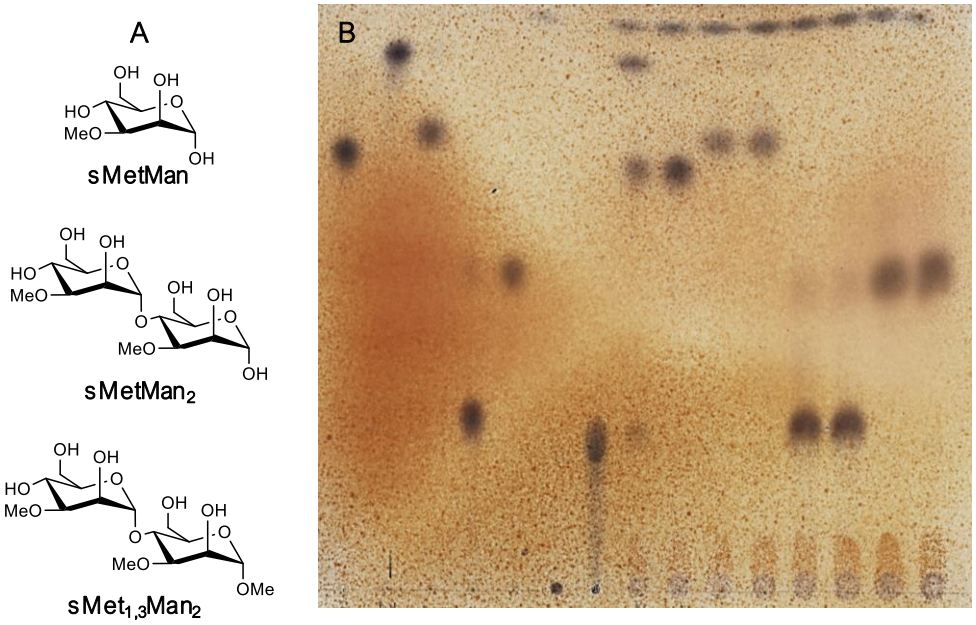

Figure 4.3 – A) Schematic representation of the structures of the mannosyl substrates synthesized at ITQB NOVA. B) TLC analysis of MeT1 activity. Lane 1 – sMetMan$_2$; lane 2 – sMet$_{1,3}$Man$_2$; lane 3 – sMetMan; lane 4 – Man$_2$; lane 5 – Man; lane 6 – SAM; lane 7 – SAH; lane 8 – MeT1 reaction with sMetMan$_2$; lane 9 – MeT1 reaction with sMet$_{1,3}$Man$_2$; lane 10 – MeT1 reaction with Man$_2$; lane 11 – MeT1 reaction with Man; lane Ct- – control without enzyme.

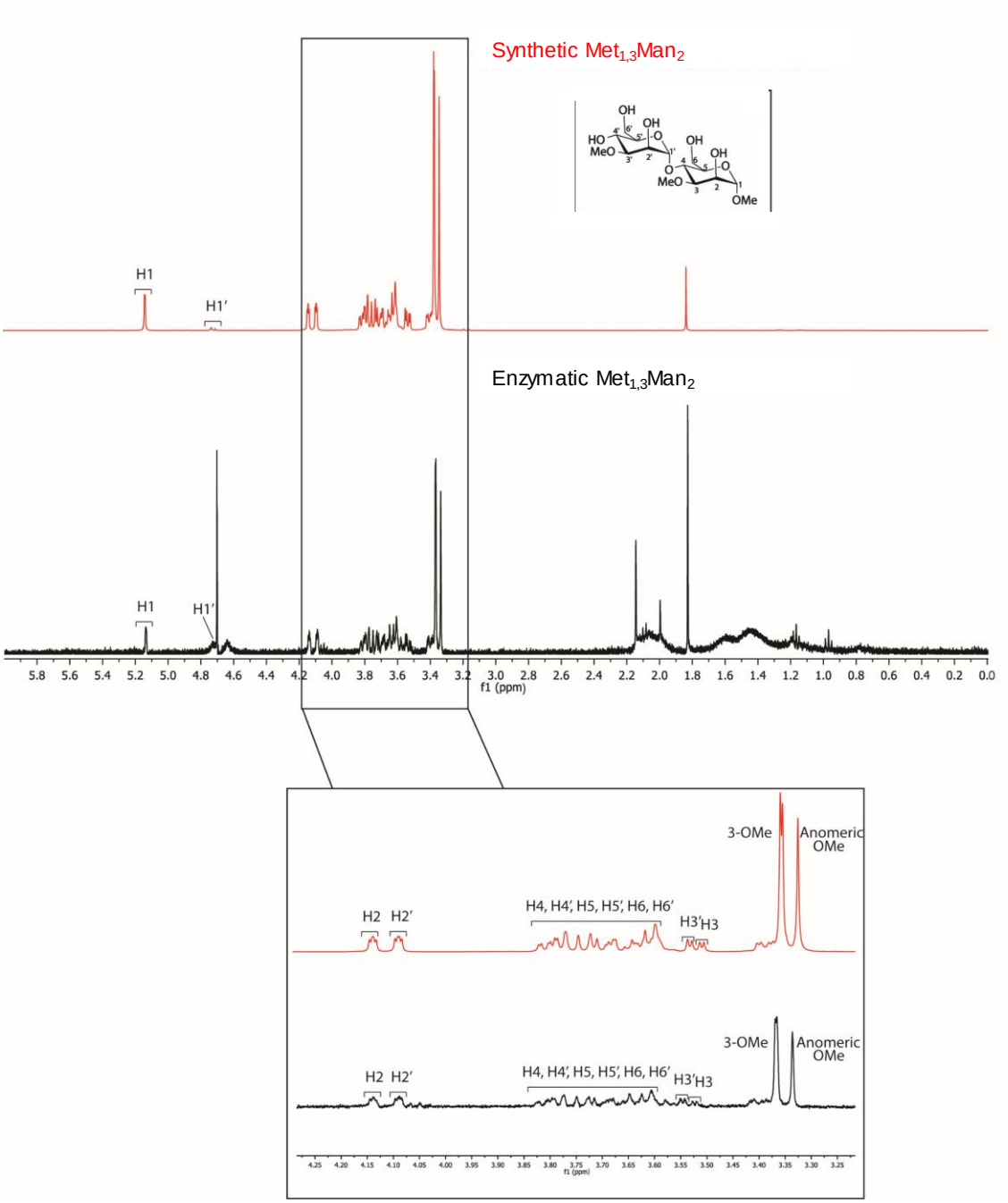

Figure 4.4 – ^{1}H-NMR spectra comparing the synthetic (red) and the natural (black) $Met_{1,3}Man_2$ synthesized by MeT1. Figure prepared by M. Rita Ventura at ITQB NOVA and adapted from Ripoll-Rozada et al., 2019.

3.3. Biochemical and kinetic characterization of MeT1

Recombinant MeT1 displayed maximum activity between 50 and 55 °C (figure 4.5 A) and, although MeT1 was active *in vitro* across a broad pH interval (pH 6.5 - 9.5), its activity peaked at pH 7.5 with both buffers tested, BTP and sodium phosphate (figure 4.5 B). This enzyme is dependent on divalent cations due to loss of activity in the presence of 10 mM EDTA and the

activity is improved in the presence of 10 mM Mg^{2+} and 100 µM Mn^{2+} (figure 4.5 C). Inhibition is an issue in the presence of 250 µM of $MnCl_2$ or higher, while in the presence of $MgCl_2$ it did not show inhibition. Testing $MnCl_2$ concentrations above 1 mM was not possible, because the colour of Mn^{2+} at high concentrations precluded absorbance readings at 412 nm, affecting the quantification assay.

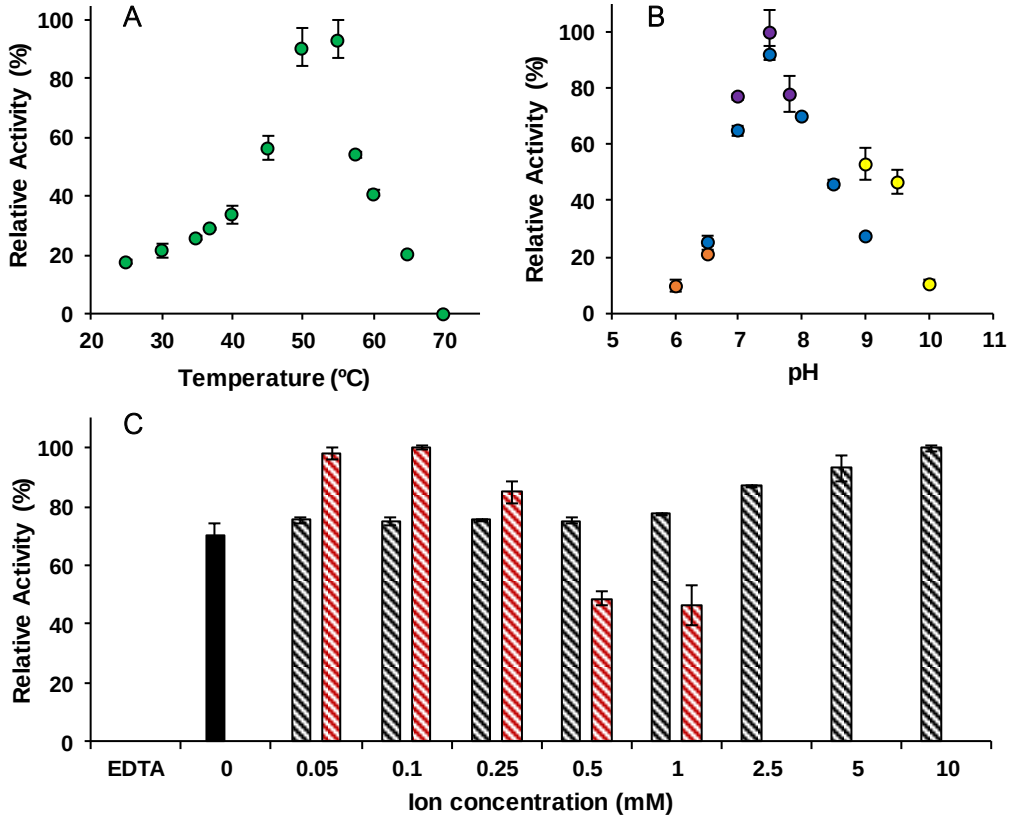

Figure 4.5 – Biochemical properties of recombinant *M. hassiacum* MeT1. A) Temperature profile. B) pH profile with MES buffer (orange), BTP buffer (blue), sodium phosphate buffer (purple) and CAPSO (yellow). C) Effect of divalent ions on MeT1 activity: in absence of added ions (black bar) and with $MnCl_2$ (patterned red bars) and $MgCl_2$ (patterned black bars). Error bars in all graphics represent standard deviation.

The kinetic characterization of MeT1 was performed with varying concentrations of SAM and $sMetMan_2$ at 37 and 50 °C, exhibiting a Michaelis-Menten behaviour (figure 4.5 A-D). From 37 to 50 °C, the values of V_{max} and K_m increased seven- and six-fold, respectively, for both substrates and the enzyme turnover at 50 °C is four-fold higher than at 37 °C. However, at both temperatures the catalytic efficiencies (k_{cat}/K_m) and enzyme turnover (k_{cat}) obtained are very low (table 4.1). This might be due to acceptor group used being a chemically synthetized compound and probably slightly different from the enzyme's biological substrate *in vivo*.

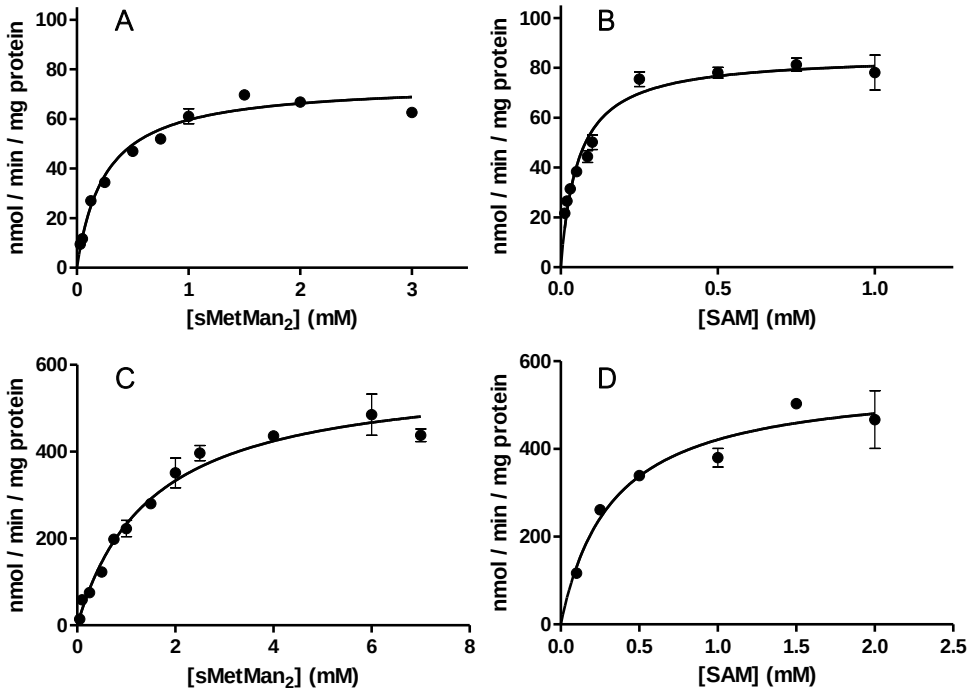

Figure 4.6 – Kinetic properties of recombinant MeT1. A and B) Michaelis-Menten curve of MeT1 activity as a function of sMetMan$_2$ and SAM, respectively, at 37 °C. C and D) Michaelis-Menten curve of MeT1 activity as a function of sMetMan$_2$ and SAM, respectively, at 50 °C. Error bars represent standard error of the mean.

Table 4.1 – Kinetic parameters of recombinant MeT1 from *M. hassiacum.*

T (°C)	Substrate	K_m (mM)	V_{max} (µmol/min/mg)	k_{cat} (min^{-1})	k_{cat}/K_m ($mM^{-1}.min^{-1}$)
37	sMetMan$_2$	0.25 ± 0.03	74.64 ± 2.37	0.037 ± 0.001	0.15 ± 0.02
	SAM	0.06 ± 0.01	85.17 ± 3.09	0.043 ± 0.001	0.77 ± 0.14
50	sMetMan$_2$	1.51 ± 0.19	584.7 ± 28.20	0.144 ± 0.006	0.095 ± 0.01
	SAM	0.33 ± 0.08	559.8 ± 38.54	0.137 ± 0.001	0.42 ± 0.10

3.4. Structure of MeT1

MeT1 shows a dimeric structure in solution with a Rossmann-like fold, containing seven β-strands (β1 to β7) that form a central predominantly parallel β-sheet domain core, surrounded by seven α-helices (αA to αG) (Ripoll-Rozada et al., 2019). These secondary structure elements, mostly in an α-β-α arrangement, are connected by loops that form the exterior surface of the protein. Through structural homology between MeT1 and other MTases, a putative catalytic residue, His144, was identified, as well as two possible residues involved in substrate-stabilization, His79 and Glu78. Hence, variants of each residue, MeT1-H144A, MeT1-H79A and MeT1-E78A, were produced (by Jorge Ripoll-Rozada, IBMC/i3S, Porto) in order to validate their functional importance. Although the H144A amino acid substitution did not alter the oligomeric

state or secondary structure of MeT1, the catalytic activity was completely abolished (figure 4.7), demonstrating that His144 acts as the active site base. For both MeT1-H79A and MeT1-E78A, the amino acid substitutions led to significantly lower catalytic activity, about 85% and 87% reduction, respectively (figure 4.7). The kinetic parameters of the mutants were also altered in relation to the WT enzyme: the K_m became approximately three-fold higher for $sMetMan_2$ at 37 °C, underscoring their contribution to substrate affinity (figure 4.8 and table 4.2); and the affinity for SAM was also affected in these variants, with a five-fold (MeT1-H79A) or nine-fold (MeT1-E78A) decrease over MeT1 WT (figure 4.8 and table 4.2).

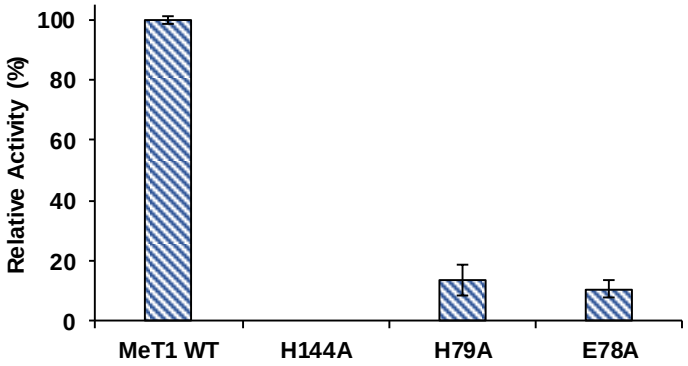

Figure 4.7 – Effect of the three single amino acid substitutions on the catalytic activity of MeT1. Error bars represent standard deviation.

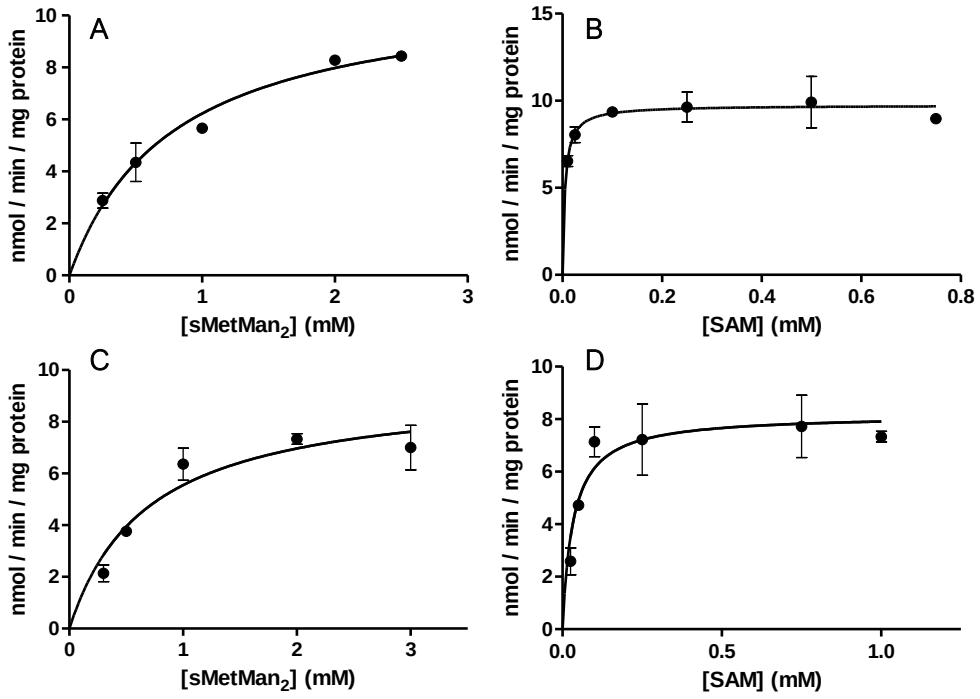

Figure 4.8 – Kinetic properties of MeT1-H79A and MeT1-E78A at 37 °C. A and B) Michaelis-Menten curve of MeT1-H79A activity as a function of $sMetMan_2$ and SAM, respectively. C and D) Michaelis-Menten curve of MeT1-E78A activity as a function of $sMetMan_2$ and SAM, respectively. Error bars represent standard error of the mean.

Table 4.2– Kinetic parameters of MeT1-H79A and MeT1-E78A at 37 °C.

MeT1 variant	Substrate	K_m (mM)	V_{max} (µmol/min/mg)
H79A	$sMetMan_2$	0.78 ± 0.19	11.1 ± 1.08
	SAM	0.005 ± 0.001	9.74 ± 0.41
E78A	$sMetMan_2$	0.68 ± 0.25	9.35 ± 0.68
	SAM	0.033 ± 0.01	8.17 ± 0.58

3.5. MeT1 activity with reaction products of MmpH

Recombinant *M. hassiacum* MeT1 showed activity with only two of the four hydrolytic products obtained with MmpH activity, the products **c** and **d** as can be observed in figure 4.9. An increase in hydrophobicity such as the addition of methyl groups makes substrates migrate further on TLC. As can be seen in lanes 3 and 4, the migration pattern of the reaction of MeT1 using products **c** and **d** as substrates is consistent with an increase in hydrophobicity when compared to the negative control (figure 4.9 A).

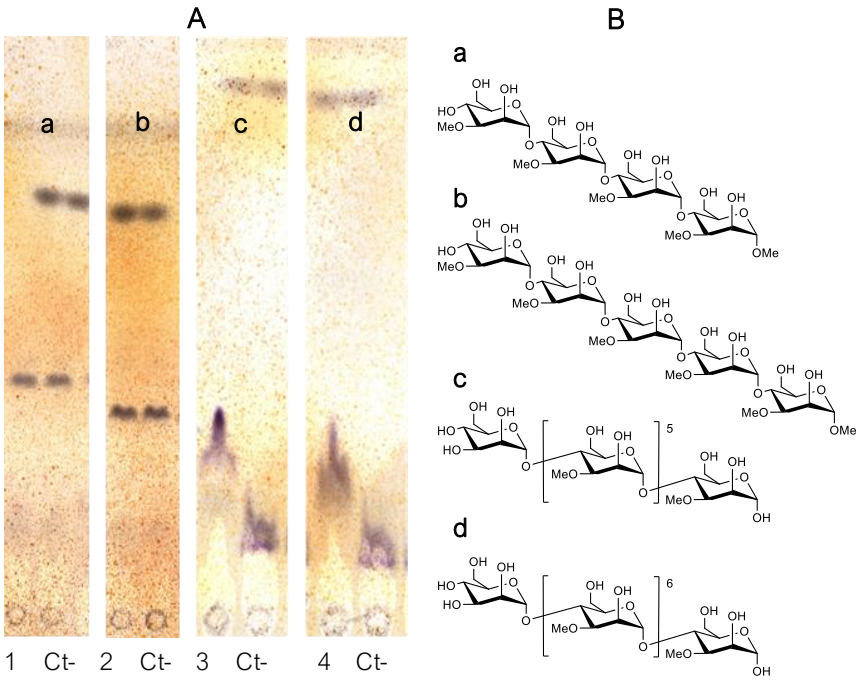

Figure 4.9 – A) TLC analysis of MeT1 activity with four MmpH hydrolytic products (**a**-**d**). B) Structure of four products **a**-**d** obtained from MmpH activity upon MMP. Lane 1 – reaction of MeT1 with product **a**; lane 2 – reaction of MeT1 with product **b**; lane 3 – reaction of MeT1 with product **c**; lane 4 – reaction of MeT1 with product **d**; lane Ct- – control without enzyme.

As stated in chapter 2, the 1-OH position of products **c** and **d** is unmodified (figure 4.9 B), since MmpH hydrolysed the C1-C4 bond and the anomeric position is deprotected, while products **a** and **b** possess the methyl-protected reducing end of MMP. Thus, MeT1 was able to methylate products **c** and **d**, while **a** and **b** are not used as substrates. The activity of MeT1against synthetic sMetMan$_2$ and the two biological substrates were compared. The relative activity of MeT1 was similar for the three compounds, with a slight preference for product **d** (figure 4.10).

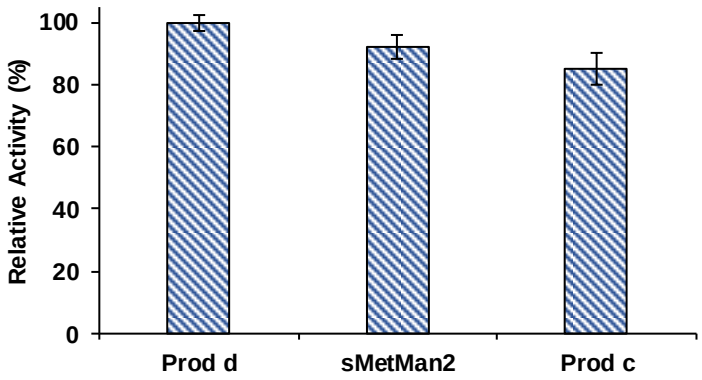

Figure 4.10 – Relative activity of MeT1 in the presence of synthetic sMetMan$_2$ and biological 4α-oligomannosides obtained by MmpH hydrolytic activity. Error bars represent standard deviation.

4. Discussion

Although MTase genes are abundant in mycobacterial genomes and several glycoconjugates with important structural and functional roles are known to be methylated to variable extent, several of the corresponding enzymes, including those required for MGLP and MMP biosynthesis, await characterization. Considering the rareness of the glycosidic bonds and methylation pattern of MMP, we sought to characterize both MTases present in the proposed MMP genetic cluster, which are candidates for methylation of the 3-OH of the MMP main backbone of and the 1-*O*-MTase required to block the MMP reducing end.

In this chapter, we identified and functionally characterized a unique MTase from *M. hassiacum*, designated MeT1, which blocks the reducing end of MMP. MeT1 was able to methylate the 1-OH position of $sMetMan_2$ but was not active towards un- or methylated monosaccharides nor unmethylated disaccharides (figure 4.3), requiring at least two mannoses and the methylation in position 3-OH to recognize the substrate.

The biochemical characterization of this enzyme revealed maximal activity at 50 °C (figure 4.5 A), in accordance with *M. hassiacum* being the most thermophilic of the known species in this genus (Tiago et al., 2012). The activity was dependent on divalent ions and improved in the presence of 100 µM Mn^{2+} or 10 mM Mg^{2+} (figure 4.5 C). The kinetic properties of the enzyme confirmed higher affinities and reaction velocity at the highest temperature with K_m and V_{max} six and seven-times higher when compared to 37 °C, respectively (figure 4.6 and table 4.1). Catalytic efficiency with synthetic $sMetMan_2$ was low, probably due to slight differences in relation to the enzyme's biological substrate, but the minute quantities of biological products **c** and **d** obtained did not allow to perform a full assessment of the kinetic parameters. Comparing the enzymatic activity in the presence of biological products obtained from MMP hydrolysis versus the synthetic substrate was fundamental to confirm the huge selectively of this enzyme towards 3-OH methylated mannosides longer than two mannoses. MeT1 methylated products **c** and **d**, the hydrolytic products of MmpH that have a free 1-OH group (section 3.3, chapter 2), utilizing with very similar efficiency the biological substrates and the synthetic one. As expected, this enzyme does not show activity with products **a** and **b** that after MMP cleavage retains the polysaccharide's reducing end (figure 4.9 A).

Comparison of MeT1 with its structural homologues suggested a catalytic base role for His144 in the methyl transfer reaction. In agreement, the MeT1-H144A variant was devoid of catalytic activity, but its affinity for the cofactor was essentially unchanged. On the other hand, the significant impact of the MeT1-H79A and MeT1-E78A on enzymatic activity corroborate the functional role of these residues in contributing to correct substrate orientation (Ripoll-Rozada et al., 2019).

Unfortunately, the second MTase identified in the genetic cluster, MeT3, still lacks activity confirmation, since it was purified in inactive form not able to methylate the acceptor substrates tested. However, as MeT1 is specific for 3-*O*-methylated oligomannosides, a crucial possible involvement of MeT3 in the addition of 3-OH methyl groups is anticipated.

In summary, the third enzyme of the 4-gene cluster for MMP biosynthesis was identified and characterized as a unique 1-OH MTase responsible for blocking the reducing end of MMP.

Chapter 5:
General Discussion

Tuberculosis is an ancient nightmare that remains the cause of many deaths (WHO, 2018). Although in the last decades its prevalence has been attenuated in developed countries, in recent years an increase of infections by opportunist nontuberculous mycobacteria (NTM) and the synergy with diseases, such as HIV and diabetes, has intensified the urgency to fight not only TB but all mycobacterial diseases (Behr et al., 2018; Claeys and Robinson, 2018). Furthermore, drug resistant cases have also been increasing with some mycobacterial strains already totally resistant to existing antibiotics (Hameed et al., 2018).

The mycobacterial cell envelope is one of the most peculiar features of these organisms that with its meticulous arrangement of different components confers them resistance and survival capacity in inhospitable environments, contributing to their pathogenicity and virulence (Singh et al., 2018). Mycobacteria synthesize two unique and rare intracellular polymethylated polysaccharides (PMPS) of 6-*O*-methylglucose (MGLP) and 3-*O*-methylmannose (MMP), which were both proposed to modulate fatty acid metabolism and, indirectly, the assembly of cell envelope lipids and glycoconjugates (Lee, 1966; Gray and Ballou, 1971; Ilton et al., 1971). PMPS have a particular distribution across mycobacterial species: MGLP appears to be synthetized by all known mycobacteria and MMP was only isolated from rapidly growing mycobacteria (RGM) (Mendes et al., 2012). As such, some questions have emerged about the importance of MMP and its possible contribution to mycobacterial fitness in the environment or during infection. Furthermore, PMPS could be the target of new innovative therapeutic approaches urgently needed to replace the dated and largely ineffective antibiotics in use against NTM diseases.

The presence of MGLP in strictly pathogenic mycobacteria rendered its biosynthetic pathway an attractive target of most studies, with some enzymes involved in the pathway already identified through mutagenesis approaches, while others were also functionally and structurally characterized (Stadthagen et al., 2007; Empadinhas et al., 2008; Pereira et al., 2008; Kaur et al., 2009; Mendes et al., 2011; Alarico et al., 2014; Maranha et al., 2015; Cereija et al., 2017). The enzymes also attracted increasing attention, because the corresponding genes had been considered essential for *M. tuberculosis* growth (Sassetti et al., 2003; Griffin et al., 2011; Mendes et al., 2012). The first studies on MMP synthesis date back from 1984 when it was proposed that MMP polymerization would occur through alternating mannosylation and methylation reactions, catalysed by a mannosyltransferase (ManT) and a methyltransferase (MTase), respectively (Weisman and Ballou, 1984a, 1984b). In those studies, ManT activity was detected in cell membrane extracts of *M. smegmatis* and in the presence of methylated tetra- to dodeca-mannosides ($Met_{1,3}Man_4$-$Met_{1,3}Man_{12}$) with a sharp decrease in affinity above $Met_{1,3}Man_6$ (Weisman and Ballou, 1984b), but smaller mannosides (<$Met_{1,3}Man_3$) were not used as acceptors. This is not surprising, since when isolating *M. smegmatis* MMP the authors

mentioned that the smallest precursors found were pentamannosides, suggesting the existence of a separate mechanism for the early biosynthetic steps originating the MMP precursors, different from the mechanism for the elongation (Yamada et al., 1979; Weisman and Ballou, 1984b). MTase activity was also detected in extracts, with broader activity when compared to ManT, methylating oligomannosides ranging from two to eleven mannose residues long but more active with the smaller ones (Weisman and Ballou, 1984a). Furthermore, these authors proposed that the MMP termination reaction and the presence of the last unmethylated mannose could be related with MTase activity. In this, the affinity towards the acceptors would decrease with elongation of the mannose chain, in addition to the presence of fatty acyl-CoA, which could induce the formation of a complex that would also lower the affinity of the MMP towards its biosynthetic enzymes (Weisman and Ballou, 1984a). Seven years ago, another study where ManT activity was also detected in membrane fractions of *M. smegmatis* suggested an alternative biosynthetic pathway wherein mannosylations reactions would be independent of methylations (Xia et al., 2012). These authors also identified the *manT* gene in *M. smegmatis* using bioinformatic tools but were faced with difficulties to purify the enzyme (Xia, 2013). However, using *E. coli* extracts with recombinant ManT they verified that this enzyme produced hexa- and heptamannosides from a methylated tetramannoside as acceptor substrate (Xia, 2013).

In this work, we propose that a 4-gene cluster encoding a 1-*O*-methyltransferase (MeT1), a MMP hydrolase (MmpH), an α-(1→4)-mannosyltransferase (ManT) and a putative SAM-dependent 3-*O*-methyltransferase (pMeT3) is responsible for MMP biosynthesis (figure 5.1). The functions of three enzymes were identified and characterized in this work, while a fourth enzyme could not be characterized although we predict it to be the MTase for methylation of mannoses at 3-OH positions. As would be expected, this cluster is detected in all RGM but, surprisingly, also in genomes of several slowly growing mycobacteria (SGM) such as *M. ulcerans*, *M. avium* and *M. xenopi* (figure 5.1). The PMPS isolation method optimized in our laboratory (by Ana Maranha) should make it easier to investigate whether these SGM actually synthesize MMP. On the other hand, in agreement with previous reports, this cluster is absent of the genomes of members of *M. tuberculosis* complex (figure 5.1).

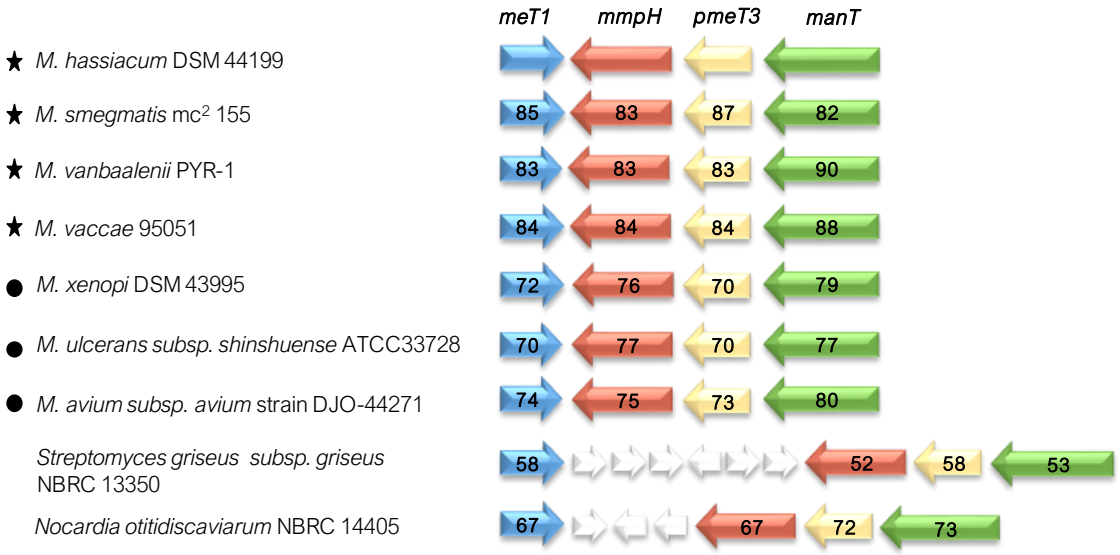

Figure 5.1 – Genomic organization of the MMP cluster in mycobacteria and other actinobacteria after identification and functional characterization of 1-*O*-methyltransferase (MeT1), MMP hydrolase (MmpH) and α-(1→4)-mannosyltransferase (ManT) activities. Cluster with four genes (arrows) drawn to scale. *meT1* (blue) 1-*O*-methyltransferase gene. *mmpH* (pink) MMP hydrolase gene. *pmeT3* (yellow) putative 3-*O*-methyltransferase gene. *manT* (green) α-(1→4)-mannosyltransferase gene. Black star, RGM; Black circle, SGM. The percentage of amino acid identity in relation to the *M. hassiacum* protein sequences is indicated inside the arrows.

In this work, we were able to extract a pure heterogeneous sample of MMP from *M. smegmatis*, isolating MMP with four different polymerization degrees that range from MMP_{11}, with nine 3-*O*-methylmannoses plus the reducing and nonreducing ends, to MMP_{14} with twelve 3-*O*-methyl mannoses and both terminal mannoses. This result was not unexpected, since it was in agreement with previous results with *M. smegmatis* where heterogenous MMP differing in one methylated mannose were isolated (Maitra and Ballou, 1977; Yamada et al., 1979). Our extraction method was fundamental to identify the function of MmpH, revealing it as a unique glycosyl hydrolase that cleaves internally the main backbone of MMP and acts as an α-(1→4)-mannanase, releasing oligomannosides that match the opposing ends of MMP. The oligomannosides identified were tetra- and pentamannosides with the MMP reducing end, as well as hepta- and octamannosides possessing the nonreducing terminus. Due to the heterogeneity of the purified MMP, it was difficult to describe in detail the hydrolytic mechanism of this enzyme. However, the production of the pentamannoside with the reducing end and the nonreducing octamannoside purified in higher amounts hint that these products may be produced preferentially by MmpH. As the combination of these two products results in MMP_{13}, this also suggests that MMP_{13} is the form preferentially hydrolysed by MmpH. Curiously, the shorter precursor isolated in earlier studies was a pentamannoside, which could be the result of MmpH activity (Yamada et al., 1979).

ManT characterized in this work transfers mannose residues from GDP-mannose and catalyses the formation of unusual α-(1→4) glycosidic bonds, a type of linkage that has not been reported among the mannans identified in nature (Moreira and Filho, 2008). The activity of this enzyme was reported as being associated to membrane extracts of *M. smegmatis* (Weisman and Ballou, 1984b; Xia et al., 2012). However, we could purify recombinant ManT in soluble form from *E. coli* cell-free extracts and it used GDP-mannose as donor group, which is a substrate described as a cytoplasmatic mannose donor in mycobacteria (Yokoyama and Ballou, 1989). We also found that ManT uses mannosides with three or more mannoses as substrates, methylated or not at position 3, the former being preferred. However, the presence of 3-*O*-methylation is not enough for ManT to display activity with mono and dimannosides, as was already found in previous studies (Weisman and Ballou, 1984b; Xia et al., 2012; Xia, 2013). This enzyme had activity with synthetic substrates, as well with the hydrolytic products of MmpH, showing equivalent preference for the synthetic methylated tetramannoside ($sMetMan_4$) and biological pentamannoside **b**, despite the additional mannose. This fact can be related to the presence of a propyl group at the 1-OH position of the $sMetMan_4$ that can mimic one extra mannose. The same artefact could occur with synthetic methylated trimannoside ($sMetMan_3$), since ManT has shown similar activity with $sMetMan_3$ and the biological tetramannoside **a**. However, confirmation of whether ManT is actually active in the presence of trisaccharides or if the low activity observed is an artefact resulting from the presence of an allyl group in the reducing end is still missing. Regarding ManT activity with oligomannosides matching the MMP nonreducing end (product **c** and **d**), it was lower than with other biological substrates, but corroborates the previous study where a decrease in activity using substrates longer than hexamannosides was observed (Weisman and Ballou, 1984b).

MeT1 is a very specific enzyme that methylates the 1-OH position of deprotected 3-*O*-methylated mannosides, both synthetic 3,3'-di-*O*-methyl-4α-mannobiose ($sMetMan_2$) and biological hepta- and octamannoside products of MmpH matching the MMP nonreducing end. A unique feature of this enzyme is that the presence of 3-*O*-methyl groups and at least two mannoses are required for a sugar to be recognized as substrate, since activity was not observed in the absence of methylation or using differentially methylated mono- and dimannosides. However, as expected, MeT1 was not active with oligomannosides matching the 1-*O*-methylated MMP reducing end (product **a** and **b**).

The identification and characterization of these three enzymes point to a unique mechanism for MMP biogenesis, where MmpH seems to serve as a recycling enzyme, hydrolysing the mature MMP chain into products that will be the precursors of new MMP chains polymerized by ManT and blocked by MeT1 at position 1-OH. MmpH therefore appears to be able to promote formation of new MMP chains from a pre-existing MMP without requiring mannose monomers,

oligosaccharides smaller than four mannoses or its corresponding activated donors. In this version of the biosynthetic pathway, the new MMP molecules are produced through the combined activities of ManT, MeT1 and pMeT3 (figure 5.2 A). This hypothesis is sustained by previous studies where the mannosylation activity was only detected in mannosides longer than four units, independently of the presence or not of methyl groups, and also by the fact that the smallest MMP precursor isolated from *M. smegmatis* was a pentamannoside (Yamada et al., 1979; Weisman and Ballou, 1984b; Xia et al., 2012; Xia, 2013). Furthermore, a mechanism such as this would allow the cell to spend less energy and to produce MMP faster, which would probably contribute to the rapid growth of mycobacteria that possess this polysaccharide and to the extreme versatility of mycobacteria under environmentally adverse conditions. Although the extension of a trimannoside by ManT and methylation of a dimannoside $sMetMan_2$ by MeT1 *in vitro* as determined in this work, indicate a broader range for their activities than what would be expected in light of the mechanism proposed, none of these observations excludes the possibility of a MMP recycling mechanism, because the *in vitro* specificity of the enzymes is usually much broader than *in vivo* (Maranha et al., 2015).

Although it is conceivable that the MMP recycling mechanism proposed in this thesis may represent a regulatory mechanism integrated into a broader biosynthetic scheme (figure 5.2 B), the activities encoded in the MMP cluster, three of them now experimentally confirmed, are enough for biogenesis of a mature MMP from pre-existing MMP molecules (figure 5.2 A). The identity of the MMP genes now disclosed will definitely allow deeper investigation of how this polysaccharide is involved in survival or resistance of mycobacteria under environmental stress or even during infection, which will also unequivocally put us closer to devise new strategies to fight infections by these opportunistic pathogens.

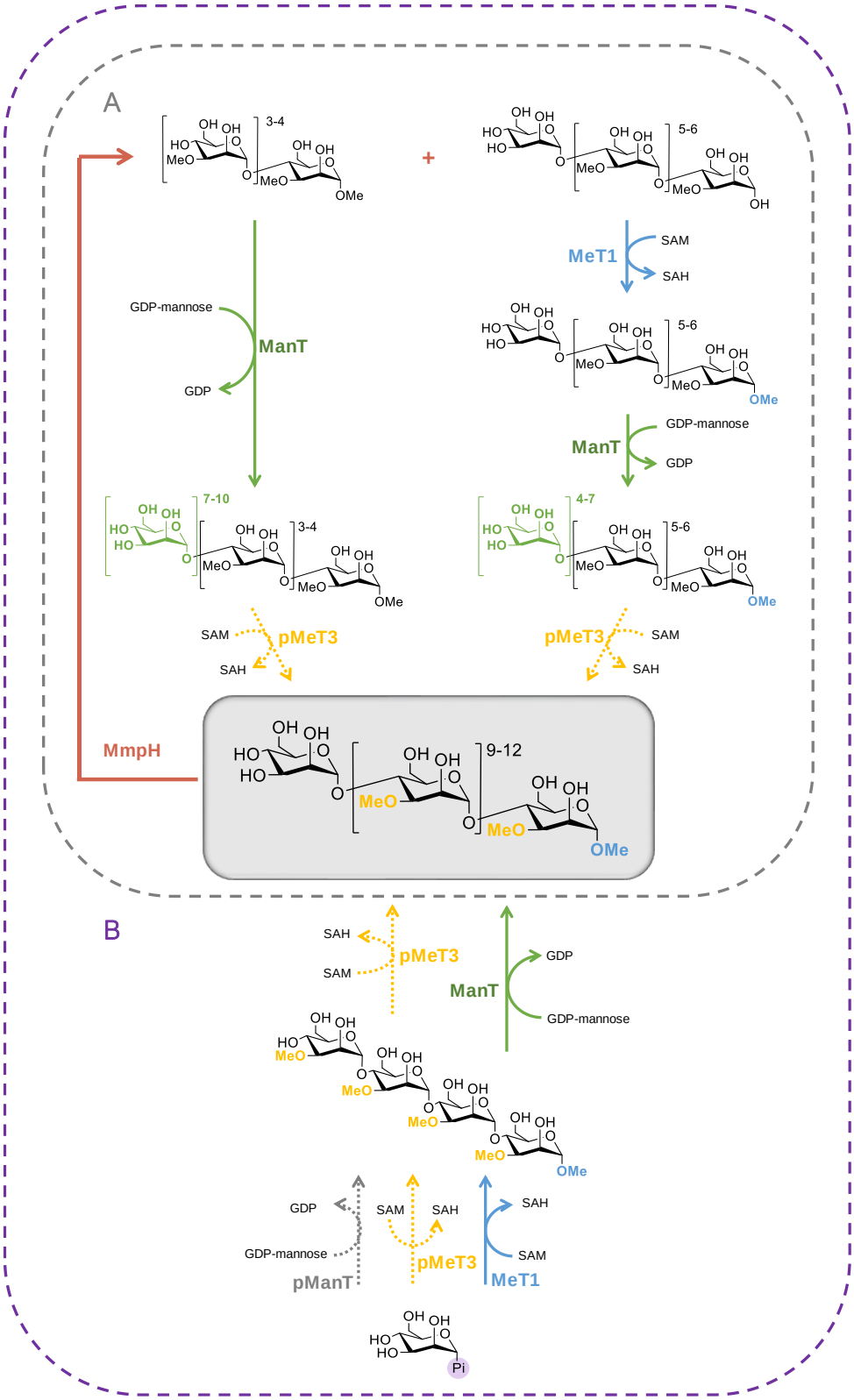

Figure 5.2 – Schematic representation of the proposed MMP biosynthetic pathways. A) Recycling mechanism based on the MMP hydrolytic activity of MmpH, followed by the synthesis of new MMP chains by ManT, MeT1 and pMeT3. B) Proposed MMP biosynthetic pathway from an activated mannose unit where synthesis occurs through the activity of at least four enzymes and in which MmpH acts as a regulatory enzyme. MmpH, MMP hydrolase (pink); ManT, α-(1→4)-mannosyltransferase (green); MeT1, 1-*O*-methyltransferase (blue); pMeT3, putative 3-*O*-methyltransferase; pManT, putative unknown mannosyltransferase (grey).

This main biosynthetic pathway would hypothetically start from mannosyl units and require the intervention of a second putative and unknown ManT (pManT) to establish the first mannose linkages in an oligomannoside to which pMeT3 and MeT1 would add methyl groups at position 3-OH and 1-OH, respectively, forming $Met_{1,3}Man_4$ (figure 5.2 B). As the structure of $Met_{1,3}Man_4$ is quite similar to the synthetic $sMetMan_3$ and $sMetMan_4$, which are substrates for ManT, we know that this enzyme would be capable of elongating the MMP backbone, together with pMeT3 that would add methyl groups at position 3-OH. The intervention of two different enzymes with similar activity but at different moments of the pathway is common in the assembling process and synthesis of other mannosides such as PIM, LM and LAM (Kremer et al., 2002; Kaur et al., 2007; Mishra et al., 2007, 2008; Guerin et al., 2009). In this scenario, MmpH would play an eventual regulatory role, acting as a secondary mechanism for *de novo* synthesis of MMP (figure 5.2 B). This enzyme could be active in situations, such as growth under stress or for adaptation to unknown environmental conditions, regulating MMP synthesis, reducing cellular energy expenditure and eventually, avoiding the consumption of mannose that could be essential to other biosynthetic pathways.

To investigate the real contribution of MmpH to MMP biosynthesis *in vivo*, a knockout mutant of MmpH would be a suitable initial approach. If MmpH indeed has a regulatory activity, expected changes in MMP content will most likely be observed under stress conditions such as temperature or pH variations or osmotic stress, while if the recycling mechanism relies solely on MmpH as the key enzyme to produce new MMP molecules, the synthesis will be completely abolished, since the precursors for ManT, MeT1 and pMeT3 activities will not be produced in such mutant.

The new mechanisms for MMP synthesis proposed in this work complement previous observations of other groups, not replacing but consolidating them with identification of a dedicated 4-gene cluster and also with the characterization of three enzymes, MmpH, ManT and MeT1, collectively introducing a new perspective on the MMP biosynthetic pathway.

References

REFERENCES

Abrahams, K. A.; Besra, G. S. Mycobacterial cell wall biosynthesis: a multifaceted antibiotic target. *Parasitology* 2018, *145*, 116–133.

Alarico, S.; Costa, M.; Sousa, M. S.; Maranha, A.; Lourenço, E. C.; Faria, T. Q.; Ventura, M. R.; Empadinhas, N. *Mycobacterium hassiacum* recovers from nitrogen starvation with up-regulation of a novel glucosylglycerate hydrolase and depletion of the accumulated glucosylglycerate. *Sci. Rep.* 2014, *4*, 6766.

Alderwick, L. J.; Lloyd, G. S.; Ghadbane, H.; May, J. W.; Bhatt, A.; Eggeling, L.; Fü Tterer, K.; Besra, G. S. The C-terminal domain of the arabinosyltransferase *Mycobacterium tuberculosis* EmbC is a lectin-like carbohydrate binding module. *PLoS Pathog.* 2011, *7* (2), e1001299.

Appelmelk, B. J.; den Dunnen, J.; Driessen, N. N.; Ummels, R.; Pak, M.; Nigou, J.; Larrouy-Maumus, G.; Gurcha, S. S.; Movahedzadeh, F.; Geurtsen, J.; et al. The mannose cap of mycobacterial lipoarabinomannan does not dominate the *Mycobacterium*-host interaction. *Cell. Microbiol.* 2008, *10* (4), 930–944.

Armarego, W. L. F.; Chain, C. *Purification of Laboratory Chemicals*, 5th ed.; Butterworth-Heinemann, 2003.

Ballou, C. E. Specific interaction of mycobacterial polymethypolysaccharides with long-chain fatty acids and acoyl-coenzyme A derivatives. *Pure Appl. Chem.* 1981, *53*, 107–112.

Ballou, C. E.; Vilkas, E.; Laderer, E. Structural studies on the myo-inositol phospholipids of *Mycobacterium tuberculosis* (var. *bovis*, strain BCG). *J. Biol. Chem.* 1963, *238* (1), 69–76.

Banis, R. J.; Peterson, D. O.; Bloch, K. *Mycobacterium smegmatis* fatty acid synthetase: polysaccharide stimulation of the rate-limiting step. *J. Biol. Chem.* 1977, *252* (16), 5740–5744.

Barry III, C. E.; Lee, R. E.; Mdluli, K.; Sampson, A. E.; Schroeder, B. G.; Slayden, R. A.; Yuan, Y.; Anderson, R. J. Mycolic acids: structure, biosynthesis and physiological functions. *Prog. Lipid Res.* 1998, *37* (2/3), 143–179.

Basille, D.; Jounieaux, V.; Andréjak, C. Treatment of other nontuberculous mycobacteria. *Semin. Respir. Crit. Care Med.* 2018, *39* (3), 377–382.

Bastos, H. N.; Osório, N. S.; Gagneux, S.; Comas, I.; Saraiva, M. The troika host-pathogen-extrinsic factors in tuberculosis: modulating inflammation and clinical outcomes. *Front. Immunol.* 2018, *8*, 1948.

Behr, M. A.; Edelstein, P. H.; Ramakrishnan, L. Revisiting the timetable of tuberculosis. *BMJ* 2018, *362*, k2738.

Berg, S.; Kaur, D.; Jackson, M.; Brennan, P. J. The glycosyltransferases of *Mycobacterium tuberculosis* - roles in the synthesis of arabinogalactan, lipoarabinomannan, and other glycoconjugates. *Glycobiology* 2007, *17* (6), 35R–56R.

Bergeron, R.; Machida, Y.; Bloch, K. Complex formation between mycobacterial

polysaccharides or cyclodextrins and palmitoyl coenzyme A. *J. Biol. Chem.* 1975, *250* (4), 1223–1230.

Besra, G. S.; Morehouse, C. B.; Rittner, C. M.; Waechter, C. J.; Brennan, P. J. Biosynthesis of mycobacterial lipoarabinomannan. *J. Biol. Chem.* 1997, *272* (29), 18460–18466.

Birch, H. L.; Alderwick, L. J.; Bhatt, A.; Rittmann, D.; Krumbach, K.; Singh, A.; Bai, Y.; Lowary, T. L.; Eggeling, L.; Besra, G. S. Biosynthesis of mycobacterial arabinogalactan: identification of a novel α-(1→3) arabinofuranosyltransferase. *Mol. Microbiol.* 2008, *69* (5), 1191–1206.

Bloch, K.; Vance, D. Control mechanisms in the synthesis of saturated fatty acids. *Annu. Rev. Biochem.* 1977, *46*, 268–298.

Brennan, P.; Ballou, C. E. Biosynthesis of mannophosphoinositides by *Mycobacterium phlei*: the family of dimannophosphoinositides. *J. Biol. Chem.* 1967, *242* (13), 3046–3056.

Brennan, P.; Ballou, C. E. Biosynthesis of mannophosphoinositides by *Mycobacterium phlei*: enzymatic acilation of the dimannophosphoinositides. *J. Biol. Chem.* 1968, *243* (11), 2975–2984.

Breton, C.; Fournel-Gigleux, S.; Palcic, M. M. Recent structures, evolution and mechanisms of glycosyltransferases. *Curr. Opin. Struct. Biol.* 2012, *22* (5), 540–549.

Brown-Elliott, B. A.; Philley, J. V. Rapidly growing mycobacteria. *Microbiol. Spectr.* 2017, *5* (1), 1–19.

Buurman, E. T.; Westwater, C.; Hube, B.; Brown, A. J. P.; Odds, F. C.; Gow, N. A. R. Molecular analysis of CaMnt1p, a mannosyl transferase important for adhesion and virulence of *Candida albicans*. *Proc. Natl. Acad. Sci. U. S. A.* 1998, *95* (13), 7670–7675.

Candy, D.; Baddiley, J. 3-*O*-methyl-D-mannose from *Streptomyces griseus*. *Biochem. J.* 1966, *98* (1), 15–18.

Cantarel, B. I.; Coutinho, P. M.; Rancurel, C.; Bernard, T.; Lombard, V.; Henrissat, B. The Carbohydrate-Active EnZymes database (CAZy): an expert resource for glycogenomics. *Nucleic Acids Res.* 2009, *37* (Database issue), D233–D238.

Cao, B.; Williams, S. J. Chemical approaches for the study of the mycobacterial glycolipids phosphatidylinositol mannosides, lipomannan and lipoarabinomannan. *Nat. Prod. Rep.* 2010, *27* (6), 919–947.

Cashmore, T. J.; Klatt, S.; Yamaryo-Botte, Y.; Brammananth, R.; Rainczuk, A. K.; McConville, M. J.; Crellin, P. K.; Coppel, R. L. Identification of a membrane protein required for lipomannan maturation and lipoarabinomannan synthesis in *Corynebacterineae*. *J. Biol. Chem.* 2017, *292* (12), 4976–4986.

Cereija, T. B.; Alarico, S.; Empadinhas, N.; Pereira, P. J. B. Production, crystallization and structure determination of a mycobacterial glucosylglycerate hydrolase. *Acta Crystallogr. F Struct. Biol. Commun.* 2017, *73* (9), 536–540.

Chan, E. D.; Iseman, M. D. Slender, older women appear to be more susceptible to nontuberculous mycobacterial lung disease. *Gend. Med.* 2010, *7* (1), 5–18.

Chan, E. D.; Iseman, M. D. Underlying host risk factors for nontuberculous mycobacterial lung disease. *Semin. Respir. Crit. Care Med.* 2013, *34* (1), 110–123.

Chandra, G.; Chater, K. F.; Bornemann, S. Unexpected and widespread connections between bacterial glycogen and trehalose metabolism. *Microbiology* 2011, *157* (6), 1565–1572.

Chauhan, P. S.; Gupta, N. Insight into microbial mannosidases: a review. *Crit. Rev. Biotechnol.* 2017, *37* (2), 190–201.

Chen, L.; Kong, F. A practical synthesis of α-D-Manp-(1→3)-α-D-Manp-(1→2)-[α-D-Glcp-(1→3)]-α-D-Manp-(1→2)-α-D-Manp-(1→2)-α-D-Manp, an *O*-specific heterohexasaccharide fragment of *Citrobacter braakii* O7a, 3b, 1c. *Carbohydr. Res.* 2003, *338* (21), 2169–2175.

Chen, S.-T.; Li, J.-Y.; Zhang, Y.; Gao, X.; Cai, H. Recombinant MPT83 derived from *Mycobacterium tuberculosis* induces cytokine production and upregulates the function of mouse macrophages through TLR2. *J. Immunol.* 2012, *188* (2), 668–677.

Claeys, T. A.; Robinson, R. T. The many lives of nontuberculous mycobacteria. *J. Bacteriol.* 2018, *200* (11), e00739-17.

Cooper, H. N.; Gurcha, S. S.; Nigou, J.; Brennan, P. J.; Belisle, J. T.; Besra, G. S.; Young, D. Characterization of mycobacterial protein glycosyltransferase activity using synthetic peptide acceptors in a cell-free assay. *Glycobiology* 2002, *12* (7), 427–434.

Daffé, M. The cell envelope of tubercle bacilli. *Tuberculosis* 2015, *95* (S1), S155–S158.

Daffé, M.; Crick, D. C.; Jackson, M. Genetics of capsular polysaccharides and cell envelope (glyco)lipids. *Microbiol. Spectr.* 2014, *2* (4), MGM2-0021-2013.

Davis, B. G.; Fairbanks, A. J. *Carbohydrate Chemistry (Oxford Chemistry Primers)*, Second.; OUP Higher Education Division, 2002.

Dinadayala, P.; Kaur, D.; Berg, S.; Amin, A. G.; Vissa, V. D.; Chatterjee, D.; Brennan, P. J.; Crick, D. C. Genetic basis for the synthesis of the immunomodulatory mannose caps of lipoarabinomannan in *Mycobacterium tuberculosis*. *J. Biol. Chem.* 2006, *281* (29), 20027–20035.

Dobos, K. M.; Swiderek, K.; Khoo, K.; Brennan, P. J.; Belisle, J. T. Evidence for glycosylation sites on the 45-kilodalton glycoprotein of *Mycobacterium tuberculosis*. *Infect. Immun.* 1995, *63* (8), 2846–2853.

Dobos, K. M.; Khoo, K.; Swiderek, K. M.; Brennan, P. J.; Belisle, J. T. Definition of the full extent of glycosylation of the 45-kilodalton glycoprotein of *Mycobacterium tuberculosis*. *J. Bacteriol.* 1996, *178* (9), 2498–2506.

Ehrt, S.; Schnappinger, D.; Rhee, K. Y. Metabolic principles of persistence and pathogenicity in *Mycobacterium tuberculosis*. *Nat. Rev. Microbiol.* 2018, *16* (8), 496–507.

Elbein, A. D.; Pastuszak, I.; Tackett, A. J.; Wilson, T.; Pan, Y. T. Last step in the conversion of trehalose to glycogen: a mycobacterial enzyme that transfers maltose from maltose 1-phosphate to glycogen. *J. Biol. Chem.* 2010, *285* (13), 9803–9812.

Empadinhas, N.; Albuquerque, L.; Mendes, V.; Macedo-Ribeiro, S.; Da Costa, M. S. Identification of the mycobacterial glucosyl-3-phosphoglycerate synthase. *FEMS Microbiol. Lett.* 2008, *280* (2), 195–202.

Empadinhas, N.; Costa, M.; Maranha, A.; Mendes, V.; Alarico, S.; Costa, D.; Gonçalves, T.; Ventura, M. R.; Ripoll-Rozada, J.; Pereira, P. J. B.; et al. Biosynthesis of rare methylmannose polysaccharides in nontuberculous mycobacteria. 2012, Grant PTDC/BIA-MIC/2779/2012.

Ernst, J. D. Mechanisms of *M. tuberculosis* immune evasion as challenges to TB vaccine design. *Cell Host Microbe* 2018, *24* (1), 34–42.

Esteban, J.; Muñoz-Egea, M.-C. *Mycobacterium bovis* and other uncommon members of the *Mycobacterium tuberculosis* complex. *Microbiol. Spectr.* 2016, *4* (6), 1–11.

Falkinham III, J. O. Surrounded by mycobacteria: nontuberculous mycobacteria in the human environment. *J. Appl. Microbiol.* 2009, *107* (2), 356–367.

Falkinham III, J. O. Environmental sources of nontuberculous mycobacteria. *Clin. Chest Med.* 2015, *36* (1), 35–41.

Falkinham III, J. O. Challenges of NTM drug development. *Front. Microbiol.* 2018, *9*, 1613.

Ferguson, J. A.; Ballou, C. E. Biosynthesis of a mycobacterial lipopolysaccharide: properties of the polysaccharide methyltransferase. *J. Biol. Chem.* 1970, *245* (16), 4213–4223.

Field, S. K. Bedaquiline for the treatment of multidrug-resistant tuberculosis: great promise or disappointment? *Ther. Adv. Chronic Dis.* 2015, *6* (4), 170–184.

Fukuda, T.; Matsumura, T.; Ato, M.; Hamasaki, M.; Nishiuchi, Y.; Murakami, Y.; Maeda, Y.; Yoshimori, T.; Matsumoto, S.; Kobayashi, K.; et al. Critical roles for lipomannan and lipoarabinomannan in cell wall integrity of mycobacteria and pathogenesis of tuberculosis. *MBio* 2013, *4* (1), 8–10.

Gagneux, S. Ecology and evolution of *Mycobacterium tuberculosis*. *Nat. Rev. Microbiol.* 2018, *16* (4), 202–213.

Gago, G.; Diacovich, L.; Gramajo, H. Lipid metabolism and its implication in mycobacteria-host interaction. *Curr. Opin. Microbiol.* 2018, *41*, 36–42.

Ghazaei, C. *Mycobacterium tuberculosis* and lipids: insights into molecular mechanisms from persistence to virulence. *J. Res. Med. Sci.* 2018, *23* (1), 63.

Goren, M. B. Mycobacterial lipids: selected topics. *Bacteriol. Rev.* 1972, *36* (1), 33–64.

Gray, G. R.; Ballou, C. E. Isolation and characterization of a polysaccharide containing 3-*O*-methyl-D-mannose from *Mycobacterium phlei*. *J. Biol. Chem.* 1971, *246* (22), 6835–6842.

Griffin, J. E.; Gawronski, J. D.; DeJesus, M. A.; Ioerger, T. R.; Akerley, B. J.; Sassetti, C. M.

High-resolution phenotypic profiling defines genes essential for mycobacterial growth and cholesterol catabolism. *PLoS Pathog.* 2011, *7* (9), 1–9.

Griffith, D. E.; Aksamit, T.; Brown-Elliott, B. A.; Catanzaro, A.; Daley, C.; Gordin, F.; Holland, S. M.; Horsburgh, R.; Huitt, G.; Iademarco, M. F.; et al. An official ATS/IDSA statement: diagnosis, treatment, and prevention of nontuberculous mycobacterial diseases. *Am. J. Respir. Crit. Care Med.* 2007, *175* (4), 367–416.

Grover, S.; Gupta, P.; Kahlon, P. S.; Goyal, S.; Grover, A.; Dalal, K.; Sabeeha; Ehtesham, N. Z.; Hasnain, S. E. Analyses of methyltransferases across the pathogenicity spectrum of different mycobacterial species point to an extremophile connection. *Mol. Biosyst.* 2016, *12* (5), 1615–1625.

Guerin, M. E.; Korduláková, J.; Schaeffer, F.; Svetlikova, Z.; Buschiazzo, A.; Giganti, D.; Gicquel, B.; Mikusova, K.; Jackson, M.; Alzari, P. M. Molecular recognition and interfacial catalysis by the essential phosphatidylinositol mannosyltransferase PimA from mycobacteria. *J. Biol. Chem.* 2007, *282* (28), 20705–20714.

Guerin, M. E.; Kaur, D.; Somashekar, B. S.; Gibbs, S.; Gest, P.; Chatterjee, D.; Brennan, P. J.; Jackson, M. New insights into the early steps of phosphatidylinositol mannoside biosynthesis in mycobacteria: PimB′ is an essential enzyme of *Mycobacterium smegmatis*. *J. Biol. Chem.* 2009, *284* (38), 25687–25696.

Guerin, M. E.; Korduláková, J.; Alzari, P. M.; Brennan, P. J.; Jackson, M. Molecular basis of phosphatidyl-*myo*-inositol mannoside biosynthesis and regulation in mycobacteria. *J. Biol. Chem.* 2010, *285* (44), 33577–33583.

Gupta, R. S.; Lo, B.; Son, J. Phylogenomics and comparative genomic studies robustly support division of the genus *Mycobacterium* into an emended genus *Mycobacterium* and four novel genera. *Front. Microbiol.* 2018, *9*, 67.

Hameed, H. M. A.; Islam, M. M.; Chhotaray, C.; Wang, C.; Liu, Y.; Tan, Y.; Li, X.; Tan, S.; Delorme, V.; Yew, W. W.; et al. Molecular targets related drug resistance mechanisms in MDR-, XDR- and TDR-Mycobacterium tuberculosis strains. *Front. Cell. Infect. Microbiol.* 2018, *8*, 114.

Harris, L. S.; Gray, G. R. Acetylated methylmannose polysaccharide of *Streptomyces griseus*. *J. Biol. Chem.* 1977, *252* (8), 2470–2477.

Hartmans, S.; de Bont, J. A.; Stachebrandt, E. The genus *Mycobacterium* - nonmedical. *Prokaryotes* 2006, *3*, 889–918.

Holt, M. R.; Kasperbauer, S. Management of extrapulmonary nontuberculous mycobacterial infections. *Semin. Respir. Crit. Care Med.* 2018, *39* (3), 399–410.

Hunter, S. W.; Murphy, R. C.; Clay, K.; Gorent, M. B.; Brennan, P. J. Trehalose-containing lipooligosaccharides: a new class of species-specific antigens from *Mycobacterium*. *J. Biol.*

Chem. 1983, *258* (17), 10481–10487.

Hunter, S. W.; Gaylor, H.; Brennan, P. J. Structure and antigenicity of the phosphorylated lipopolysaccharide antigens from the leprosy and tubercle bacilli. *J. Biol. Chem.* 1986, *261* (26), 12345–12351.

Ilton, M.; Jevans, A. W.; McCarthy, E. D.; Vance, D.; White, H. B.; Bloch, K. Fatty acid synthetase activity in *Mycobacterium phlei*: regulation by polysaccharides. *Proc. Natl. Acad. Sci.* 1971, *68* (1), 87–91.

Jacin, H.; Mishkin, A. Separation of carbohydrates on borate-impregnated silica gel G plates. *J Chromatogr* 1965, *18*, 170–173.

Jackson, M.; Brennan, P. J. Polymethylated polysaccharides from *Mycobacterium* species revisited. *J. Biol. Chem.* 2009, *284* (4), 1949–1953.

Jankute, M.; Cox, J. A. G.; Harrison, J.; Besra, G. S. Assembly of the mycobacterial cell wall. *Annu. Rev. Microbiol.* 2015, *69* (1), 405–423.

Källenius, G.; Correia-Neves, M.; Buteme, H.; Hamasur, B.; Svenson, S. B. Lipoarabinomannan, and its related glycolipids, induce divergent and opposing immune responses to *Mycobacterium tuberculosis* depending on structural diversity and experimental variations. *Tuberculosis* 2016, *96*, 120–130.

Kalscheuer, R.; Syson, K.; Veeraraghavan, U.; Weinrick, B.; Biermann, K. E.; Liu, Z.; Sacchettini, J. C.; Besra, G.; Bornemann, S.; Jacobs, W. R. Self-poisoning of *Mycobacterium tuberculosis* by targeting GlgE in an α-glucan pathway. *Nat. Chem. Biol.* 2010, *6* (5), 376–384.

Kamisango, K.; Dell, A.; Ballou, C. E. Biosynthesis of the mycobacterial *O*-methylglucose lipopolysaccharide: characterization of putative intermediates in the initiation, elongation and termination reactions. *J. Biol. Chem.* 1987, *262* (10), 4580–4586.

Karcher, U.; Schroder, H.; Haslinger, E.; Allmaier, G.; Schreiner, R.; Wieland, F.; Haselbeck, A.; Konig, H. Primary structure of the heterosaccharide of the surface glycoprotein of *Methanothermus fervidus*. *J. Biol. Chem.* 1993, *268* (36), 26821–26826.

Kari, B. E.; Gray, G. R. Acetylated methylmannose polysaccharide of *Streptomyces griseus*: locations of the acetyl groups. *J. Biol. Chem.* 1979, *254* (9), 3354–3357.

Kaur, D.; Berg, S.; Dinadayala, P.; Gicquel, B.; Chatterjee, D.; McNeil, M. R.; Vissa, V. D.; Crick, D. C.; Jackson, M.; Brennan, P. J. Biosynthesis of mycobacterial lipoarabinomannan: role of a branching mannosyltransferase. *Proc. Natl. Acad. Sci. U. S. A.* 2006, *103* (37), 13664–13669.

Kaur, D.; McNeil, M. R.; Khoo, K. H.; Chatterjee, D.; Crick, D. C.; Jackson, M.; Brennan, P. J. New insights into the biosynthesis of mycobacterial lipomannan arising from deletion of a conserved gene. *J. Biol. Chem.* 2007, *282* (37), 27133–27140.

Kaur, D.; Obregón-Henao, A.; Pham, H.; Chatterjee, D.; Brennan, P. J.; Jackson, M. Lipoarabinomannan of *Mycobacterium*: mannose capping by a multifunctional terminal

mannosyltransferase. *Proc. Natl. Acad. Sci. U. S. A.* 2008, *105* (46), 17973–17977.

Kaur, D.; Pham, H.; Larrouy-Maumus, G.; Rivière, M.; Vissa, V.; Guerin, M. E.; Puzo, G.; Brennan, P. J.; Jackson, M. Initiation of methylglucose lipopolysaccharide biosynthesis in mycobacteria. *PLoS One* 2009, *4* (5), e5447.

Kiho, T.; Ballou, C. E. Thermodynamic parameters and shape of the mycobacterial polymethylpolysaccharide-fatty acid complex. *Biochemistry* 1988, *27* (15), 5824–5828.

Komaniecka, I.; Choma, A.; Zamlynska, K.; Sroka-Bartnicka, A.; Sowinski, P. Structure of *O*-specific polysaccharide of *Oligotropha carboxidovorans* OM5 - a wastewater bacterium. *Carbohydr. Res.* 2017, *439*, 30–34.

Konrad, B. Control mechanisms for fatty acid synthesis in *Mycobacterium smegmatis*. *Adv. Enzymol. Relat. Areas Mol. Biol.* 1977, *45*, 1–84.

Korduláková, J.; Gilleron, M.; Mikusová, K.; Puzo, G.; Brennan, P. J.; Gicquel, B.; Jackson, M. Definition of the first mannosylation step in phosphatidylinositol mannoside synthesis: PimA is essential for growth of mycobacteria. *J. Biol. Chem.* 2002, *277* (35), 31335–31344.

Korduláková, J.; Gilleron, M.; Puzo, G.; Brennan, P. J.; Gicquel, B.; Mikušová, K.; Jackson, M. Identification of the required acyltransferase step in the biosynthesis of the phosphatidylinositol mannosides of *Mycobacterium* species. *J. Biol. Chem.* 2003, *278* (38), 36285–36295.

Kremer, L.; Gurcha, S. S.; Bifani, P.; Hitchen, P. G.; Baulard, A.; Morris, H. R.; Dell, A.; Brennan, P. J.; Besra, G. S. Characterization of a putative α-mannosyltransferase involved in phosphatidylinositol trimannoside biosynthesis in *Mycobacterium tuberculosis*. *Biochem. J.* 2002, *363* (Pt3), 437–447.

Ladevèze, S.; Laville, E.; Despres, J.; Mosoni, P.; Potocki-Véronèse, G. Mannoside recognition and degradation by bacteria. *Biol. Rev.* 2017, *92* (4), 1969–1990.

Lairson, L. L.; Henrissat, B.; Davies, G. J.; Withers, S. G. Glycosyltransferases: structures, functions, and mechanisms. *Annu. Rev. Biochem.* 2008, *77* (1), 521–555.

Lea-Smith, D. J.; Martin, K. L.; Pyke, J. S.; Tull, D.; McConville, M. J.; Coppel, R. L.; Crellin, P. K. Analysis of a new mannosyltransferase required for the synthesis of phosphatidylinositol mannosides and lipoarabinomannan reveals two lipomannan pools in *Corynebacterineae*. *J. Biol. Chem.* 2008, *283* (11), 6773–6782.

Lee, S. H. Tuberculosis infection and latent tuberculosis. *Tuberc. Respir. Dis. (Seoul).* 2016, *79* (4), 201–206.

Lee, Y. C. Isolation and characterization of lipopolysaccharides containing 6-*O*-methyl-D-glucose from *Mycobacterium* species. *J. Biol. Chem.* 1966, *241* (8), 1899–1908.

Lee, Y. C.; Ballou, C. E. Complete structures of the glycophospholipids of mycobacteria. *Biochemistry* 1965, *4* (7), 1395–1404.

Lever, M. A new reaction for colorimetric determination of carbohydrates. *Anal. Biochem.* 1972,

47, 273–279.

Liang, D. M.; Liu, J. H.; Wu, H.; Wang, B. Bin; Zhu, H. J.; Qiao, J. J. Glycosyltransferases: mechanisms and applications in natural product development. *Chem. Soc. Rev.* 2015, *44* (22), 8350–8374.

Liao, W.; Lu, D. Synthesis of a hexasaccharide acceptor corresponding to the reducing terminus of mycobacterial 3-*O*-methylmannose polysaccharide (MMP). *Carbohydr. Res.* 1996, *296*, 171–182.

Liu, C.-F.; Tonini, L.; Malaga, W.; Beau, M.; Stella, A.; Bouyssié, D.; Jackson, M. C.; Nigou, J.; Puzo, G.; Guilhot, C.; et al. Bacterial protein-*O*-mannosylating enzyme is crucial for virulence of *Mycobacterium tuberculosis*. *Proc. Natl. Acad. Sci. U. S. A.* 2013, *110* (16), 6560–6565.

Liu, L.; Siuda, I.; Richards, M.; Renaud, J.; Kitova, E.; Mayer, P.; Tieleman, P.; Lowary, T.; Klassen, J. S. Structure and stability of carbohydrate-lipid interactions. Methylmannose polysaccharide-fatty acid complexes. *ChemBioChem* 2016, *17* (16), 1571–1578.

Lozada-Ramírez, J. D.; Martínez-Martínez, I.; Sánchez-Ferrer, A.; García-Carmona, F. A colorimetric assay for *S*-adenosylhomocysteine hydrolase. *J. Biochem. Biophys. Methods* 2006, *67*, 131–140.

Lundemo, P. *Transglycosylation by Glycoside Hydrolases - Production and Modification of Alkyl Glycosides*; 2015.

Machelart, A.; Song, O.-R. O. R.; Hoffmann, E.; Brodin, P. Host-directed therapies offer novel opportunities for the fight against tuberculosis. *Drug Discov. Today* 2017, *22* (8), 1250–1257.

Machida, Y.; Bloch, K. Complex formation between mycobacterial polysaccharides and fatty acyl-CoA derivatives. *Proc. Natl. Acad. Sci.* 1973, *70* (4), 1146–1148.

Machida, Y.; Bergeron, R.; Bloch, K. Effects of cyclodextrins on fatty acid synthesis. *J. Biol. Chem.* 1973, *248*, 6246–6247.

Maggio, J. E. Structure of a mycobacterial polysaccharide-fatty acyl-CoA complex: nuclear magnetic resonance studies. *Proc. Natl. Acad. Sci. U. S. A.* 1980, *77* (5), 2582–2586.

Maitra, S. K.; Ballou, C. E. Heterogeneity and refined structures of 3-*O*-methyl-D-mannose polysaccharides from *Mycobacterium smegmatis*. *J. Biol. Chem.* 1977, *252* (8), 2459–2469.

Malgas, S.; van Dyk, J. S.; Pletschke, B. I. A review of the enzymatic hydrolysis of mannans and synergistic interactions between β-mannanase, β-mannosidase and α-galactosidase. *World J. Microbiol. Biotechnol.* 2015, *31* (8), 1167–1175.

Maranha, A.; Moynihan, P. J.; Miranda, V.; Correia Lourenço, E.; Nunes-Costa, D.; Fraga, J. S.; Pereira, P. J. B.; Macedo-Ribeiro, S.; Ventura, M. R.; Clarke, A. J.; et al. Octanoylation of early intermediates of mycobacterial methylglucose lipopolysaccharides. *Sci. Rep.* 2015, *5*, 13610.

Martiniano, S. L.; Nick, J. A. Nontuberculous mycobacterial infections in cystic fibrosis. *Clin. Chest Med.* 2015, *36* (1), 101–115.

Maruyama, Y.; Nakajima, T. The aman6 gene encoding a yeast mannan backbone degrading 1,6-α-D-mannanase in *Bacillus circulans*: cloning, sequence analysis and expression. *Biosci. Biotechnol. Biochem.* 2000, *64* (9), 2018–2020.

Matsuda, K.; Kurakata, Y.; Miyazaki, T.; Matsuo, I.; Ito, Y.; Nishikawa, A.; Tonozuka, T. Heterologous expression, purification, and characterization of an α-mannosidase belonging to glycoside hydrolase family 99 of *Shewanella amazonensis*. *Biosci. Biotechnol. Biochem.* 2011, *75* (4), 797–799.

Mellitzer, A.; Glieder, A.; Weis, R.; Reisinger, C.; Flicker, K. Sensitive high-throughput screening for the detection of reducing sugars. *Biotechnol. J.* 2012, *7* (1), 155–162.

Mendes, V.; Maranha, A.; Lamosa, P.; da Costa, M. S.; Empadinhas, N. Biochemical characterization of the maltokinase from *Mycobacterium bovis* BCG. *BMC Biochem.* 2010, *11*, 21.

Mendes, V.; Maranha, A.; Alarico, S.; da Costa, M. S.; Empadinhas, N. *Mycobacterium tuberculosis* Rv2419c, the missing glucosyl-3-phosphoglycerate phosphatase for the second step in methylglucose lipopolysaccharide biosynthesis. *Sci. Rep.* 2011, *1* (177), 1–8.

Mendes, V.; Maranha, A.; Alarico, S.; Empadinhas, N. Biosynthesis of mycobacterial methylglucose lipopolysaccharides. *Nat Prod Rep* 2012, *29* (8), 834–844.

Michell, S. L.; Whelan, A. O.; Wheeler, P. R.; Panico, M.; Easton, R. L.; Etienne, A. T.; Haslam, S. M.; Dell, A.; Morri, H. R.; Reason, A. J.; et al. The MPB83 antigen from *Mycobacterium bovis* contains *O*-linked mannose and (1→3)-mannobiose moieties. *J. Biol. Chem.* 2003, *278* (18), 16423–16432.

Mirsaeidi, M.; Sadikot, R. T. Gender susceptibility to mycobacterial infections in patients with non-CF bronchiectasis. *Int J Mycobacteriol* 2015, *4* (2), 92–96.

Mishra, A. K.; Alderwick, L. J.; Rittmann, D.; Tatituri, R. V. V.; Nigou, J.; Gilleron, M.; Eggeling, L.; Besra, G. S. Identification of an α-(1→6) mannopyranosyltransferase (MptA), involved in *Corynebacterium glutamicum* lipomanann biosynthesis, and identification of its orthologue in *Mycobacterium tuberculosis*. *Mol. Microbiol.* 2007, *65* (6), 1503–1517.

Mishra, A. K.; Alderwick, L. J.; Rittmann, D.; Wang, C.; Bhatt, A.; Jacobs, W. R.; Takayama, K.; Eggeling, L.; Besra, G. S. Identification of a novel α-(1→6) mannopyranosyltransferase MptB from *Corynebacterium glutamicum* by deletion of a conserved gene, NCgl1505, affords a lipomannan- and lipoarabinomannan-deficient mutant. *Mol. Microbiol.* 2008, *68* (6), 1595–1613.

Mishra, A. K.; Driessen, N. N.; Appelmelk, B. J.; Besra, G. S. Lipoarabinomannan and related glycoconjugates: structure, biogenesis and role in *Mycobacterium tuberculosis* physiology and host-pathogen interaction. *FEMS Immunol. Med. Microbiol.* 2011, *35* (6), 1126–1157.

Moreira, L. R. S.; Filho, E. X. F. An overview of mannan structure and mannan-degrading enzyme

systems. *Appl. Microbiol. Biotechnol.* 2008, *79* (2), 165–178.

Morita, Y. S.; Patterson, J. H.; Billman-Jacobe, H.; McConville, M. J. Biosynthesis of mycobacterial phosphatidylinositol mannosides. *Biochem. J.* 2004, *378* (2), 589–597.

Morita, Y. S.; Velasquez, R.; Taig, E.; Waller, R. F.; Patterson, J. H.; Tull, D.; Williams, S. J.; Billman-Jacobe, H.; McConville, M. J. Compartmentalization of lipid biosynthesis in mycobacteria. *J. Biol. Chem.* 2005, *280* (22), 21645–21652.

Morita, Y. S.; Sena, C. B. C.; Waller, R. F.; Kurokawa, K.; Sernee, M. F.; Nakatani, F.; Haites, R. E.; Billman-Jacobe, H.; McConville, M. J.; Maeda, Y.; et al. PimE is a polyprenol-phosphate-mannose-dependent mannosyltransferase that transfers the fifth mannose of phosphatidylinositol mannoside in mycobacteria. *J. Biol. Chem.* 2006, *281* (35), 25143–25155.

Murphy, H. N.; Stewart, G. R.; Mischenko, V. V.; Apt, A. S.; Harris, R.; McAlister, M. S. B.; Driscoll, P. C.; Young, D. B.; Robertson, B. D. The OtsAB pathway is essential for trehalose biosynthesis in *Mycobacterium tuberculosis*. *J. Biol. Chem.* 2005, *280* (15), 14524–14529.

Naka, T.; Nakata, N.; Maeda, S.; Yamamoto, R.; Doe, M.; Mizuno, S.; Niki, M.; Kobayashi, K.; Ogura, H.; Makino, M.; et al. Structure and host recognition of serotype 13 glycopeptidolipid from *Mycobacterium intracellulare*. *J. Bacteriol.* 2011, *193* (20), 5766–5774.

Nakajima, T.; Maitra, S. K.; Clinton, B. E. An endo-α-1,6-D-mannanase from a soil bacterium: purification, properties and mode of action. *J. Biol. Chem.* 1976, *251* (1), 174–181.

Nakajima, T.; Maruyama, Y.; Sato, A.; Matsumoto, T.; Suenaga, M.; Ichishima, E. Purification and characterization of an endo α-1,3-D-mannanase from *Flavobacterium* sp. AS-9. *Biosci. Biotechnol. Biochem.* 1996, *60* (10), 1743–1746.

Nandakumar, S.; Kannanganat, S.; Dobos, K. M.; Lucas, M.; Spencer, J. S.; Fang, S.; McDonald, M. A.; Pohl, J.; Birkness, K.; Chamcha, V.; et al. *O*-mannosylation of the *Mycobacterium tuberculosis* adhesin Apa is crucial for T cell antigenicity during infection but is expendable for protection. *PLoS Pathog.* 2013, *9* (10).

Nobre, A.; Alarico, S.; Maranha, A.; Mendes, V.; Empadinhas, N. The molecular biology of mycobacterial trehalose in the quest for advanced tuberculosis therapies. *Microbiology* 2014, *160*, 1547–1570.

Nunes-Costa, D.; Alarico, S.; Dalcolmo, M. P.; Correia-Neves, M.; Empadinhas, N. The looming tide of nontuberculous mycobacterial infections in Portugal and Brazil. *Tuberculosis* 2016, *96*, 107–119.

O'Brien, D. P.; Jeanne, I.; Blasdell, K.; Avumegah, M.; Athan, E. The changing epidemiology worldwide of *Mycobacterium ulcerans*. *Epidemiol. Infect.* 2019, *147*, E19.

Ortalo-Magné, A.; Lemassu, A.; Lanéelle, M. A.; Bardou, F.; Silve, G.; Gounon, P.; Marchal, G.; Daffé, M. Identification of the surface-exposed lipids on the cell envelopes of *Mycobacterium*

tuberculosis and other mycobacterial species. *J. Bacteriol.* 1996, *178* (2), 456–461.

Parish, T.; Liu, J.; Nikaido, H.; Parish, T.; Liu, J. U. N.; Nikaido, H. A *Mycobacterium smegmatis* mutant with a defective inositol monophosphate phosphatase gene homolog has altered cell envelope permeability. *J. Bacteriol.* 1997, *179* (24), 7827–7833.

Patterson, J. H.; Waller, R. F.; Jeevarajah, D.; Billman-Jacobe, H.; McConville, M. J. Mannose metabolism is required for mycobacterial growth. *Biochem. J.* 2003, *372* (Pt 1), 77–86.

Pereira, P. J. B.; Empadinhas, N.; Albuquerque, L.; Sá-Moura, B.; Da Costa, M. S.; Macedo-Ribeiro, S. *Mycobacterium tuberculosis* glucosyl-3-phosphoglycerate synthase: structure of a key enzyme in methylglucose lipopolysaccharide biosynthesis. *PLoS One* 2008, *3* (11), 1–12.

Peterson, D. O.; Bloch, K. *Mycobacterium smegmatis* fatty acid synthetase: long chain transacylase chain length specificity. *J. Biol. Chem.* 1977, *252* (16), 5735–5739.

Pitarque, S.; Larrouy-Maumus, G.; Payré, B.; Jackson, M.; Puzo, G.; Nigou, J. The immunomodulatory lipoglycans, lipoarabinomannan and lipomannan, are exposed at the mycobacterial cell surface. *Tuberculosis* 2008, *88* (6), 560–565.

Poláková, M.; Roslund, M. U.; Ekholm, F. S.; Saloranta, T.; Leino, R. Synthesis of β-(1→2)-linked oligomannosides. *European J. Org. Chem.* 2009, No. 6, 870–888.

Pommier, M.-T. T.; Michel, G. Isolation and characterization of an *O*-methylglucose-containing lipopolysaccharide produced by *Nocardia otitidis-caviarum*. *J. Gen. Microbiol.* 1986, *132* (9), 2433–2441.

Pontali, E.; Sotgiu, G.; D'Ambrosio, L.; Centis, R.; Migliori, G. B. Bedaquiline and multidrug-resistant tuberculosis: a systematic and critical analysis of the evidence. *Eur. Respir. J.* 2016, *47* (2), 394–402.

Poole, J.; Day, C. J.; von Itzstein, M.; Paton, J. C.; Jennings, M. P. Glycointeractions in bacterial pathogenesis. *Nat. Rev. Microbiol.* 2018, *16* (7), 440–452.

Procop, G. W. HIV and mycobacteria. *Semin. Diagn. Pathol.* 2017, *34* (4), 332–339.

Ragas, A.; Roussel, L.; Puzo, G.; Rivière, M. The *Mycobacterium tuberculosis* cell-surface glycoprotein apa as a potential adhesin to colonize target cells via the innate immune system pulmonary C-type lectin surfactant protein A. *J. Biol. Chem.* 2007, *282* (8), 5133–5142.

Raju, R. M.; Raju, S. M.; Zhao, Y.; Rubin, E. J. Leveraging advances in tuberculosis diagnosis and treatment to address nontuberculous mycobacterial disease. *Emerg. Infect. Dis.* 2016, *22* (3), 365–369.

Ripoll-Rozada, J.; Costa, M.; Manso, J. A.; Maranha, A.; Miranda, V.; Sequeira, A.; Ventura, M. R.; Macedo-Ribeiro, S.; Pereira, P. J. B.; Empadinhas, N. Biosynthesis of mycobacterial methylmannose polysaccharides requires a unique 1-*O*-methyltransferase specific for 3-*O*-methylated mannosides. *Proc. Natl. Acad. Sci. U. S. A.* 2019, *116* (3), 835–844.

Roxas, B. A. P.; Li, Q. Acid stress response of a mycobacterial proteome: insight from a gene

ontology analysis. *Int. J. Clin. Exp. Med.* 2009, *2* (4), 309–328.

Russell, D. G.; Barry, C. E.; Flynn, J. L. Tuberculosis: what we don't know can, and does, hurt us. *Russell J. Bertrand Russell Arch.* 2010, *328* (5980), 852–856.

Saier, M. H.; Ballou, C. E. The 6-*O*-methylglucose-containing lipopolysaccharide of *Mycobacterium phlei*: complete structure of the polysaccharide. *J. Biol. Chem.* 1968a, *243* (16), 4332–4341.

Saier, M. H.; Ballou, C. E. The 6-*O*-methylglucose-containing lipopoplysaccharide of *Mycobacterium phlei*: identification of D-glyceric acid and 3-*O*-methyl-D-glucose in the polysaccharide. *J. Biol. Chem.* 1968b, *243* (5), 992–1003.

Sambou, T.; Dinadayala, P.; Stadthagen, G.; Barilone, N.; Bordat, Y.; Constant, P.; Levillain, F.; Neyrolles, O.; Gicquel, B.; Lemassu, A.; et al. Capsular glucan and intracellular glycogen of *Mycobacterium tuberculosis*: biosynthesis and impact on the persistence in mice. *Mol. Microbiol.* 2008, *70* (3), 762–774.

Sancho-Vaello, E.; Albesa-Jové, D.; Rodrigo-Unzueta, A.; Guerin, M. E. Structural basis of phosphatidyl-myo-inositol mannosides biosynthesis in mycobacteria. *Biochim. Biophys. Acta* 2017, *1862* (11), 1355–1367.

Sassetti, C. M.; Boyd, D. H.; Rubin, E. J. Genes required for mycobacterial growth defined by high density mutagenesis. *Mol Microbiol* 2003, *48* (1), 77–84.

Schein, C. H. Optimizing protein folding to the native state in bacteria. *Curr. Opin. Biotechnol.* 1991, *2* (5), 746–750.

Seaworth, B. J.; Griffith, D. E. Therapy of multidrug-resistant and extensively drug-resistant tuberculosis. *Microbiol. Spectr.* 2017, *5* (2), 25–32.

Sequeira, A. Synthesis of precursors of the rare 3-*O*-methylmannose polysaccharides present in nontuberculous mycobacteria, Universidade Nova de Lisboa - Master Thesis, 2015.

Shi, L.; Berg, S.; Lee, A.; Spencer, J. S.; Zhang, J.; Vissa, V.; McNeil, M. R.; Khoo, K.-H.; Chatterjee, D. The carboxy terminus of EmbC from *Mycobacterium smegmatis* mediates chain length extension of the arabinan in lipoarabinomannan. *J. Biol. Chem.* 2006, *281* (28), 19512–19526.

Shibata, N.; Okawa, Y. Enzymatic synthesis of new oligosaccharides using mannosyltransferases from *Candida* species and their NMR assignments. *Biol. Pharm. Bull.* 2010, *33* (5), 895–899.

Simner, P. J.; Woods, G. L.; Wengenack, N. L. Mycobacteria. *Microbiol. Sprectrum* 2016, *4* (4), DMIH2-0016-2015.

Singh, P.; Rameshwaram, N. R.; Ghosh, S.; Mukhopadhyay, S. Cell envelope lipids in the pathophysiology of *Mycobacterium tuberculosis*. *Future Microbiol.* 2018, *13* (6), 689–710.

Singhal, A.; Arora, G.; Sajid, A.; Maji, A.; Bhat, A.; Virmani, R.; Upadhyay, S.; Nandicoori, V. K.;

Sengupta, S.; Singh, Y. Regulation of homocysteine metabolism by *Mycobacterium tuberculosis S*-adenosylhomocysteine hydrolase. *Sci. Rep.* 2013, *3* (2264).

Sood, G.; Parrish, N. Outbreaks of nontuberculous mycobacteria. *Curr. Opin. Infect. Dis.* 2017, *30* (4), 404–409.

Srivastava, P. K.; Kapoor, M. Production, properties, and applications of endo-β-mannanases. *Biotechnol. Adv.* 2017, *35* (1), 1–19.

Stadthagen, G.; Sambou, T.; Guerin, M.; Barilone, N.; Boudou, F.; Korduláková, J.; Charles, P.; Alzari, P. M.; Lemassu, A.; Daffé, M.; et al. Genetic basis for the biosynthesis of methylglucose lipopolysaccharides in *Mycobacterium tuberculosis*. *J. Biol. Chem.* 2007, *282* (37), 27270–27276.

Staudacher, E. Methylation - an uncommon modification of glycans. *Biol. Chem.* 2012, *393* (8), 675–685.

Stoop, E. J. M.; Mishra, A. K.; Driessen, N. N.; van Stempvoort, G.; Bouchier, P.; Verboom, T.; van Leeuwen, L. M.; Sparrius, M.; Raadsen, S. A.; van Zon, M.; et al. Mannan core branching of lipo(arabino)mannan is required for mycobacterial virulence in the context of innate immunity. *Cell. Microbiol.* 2013, *15* (12), 2093–2108.

Supply, P.; Marceau, M.; Mangenot, S.; Roche, D.; Rouanet, C.; Khanna, V.; Majlessi, L.; Criscuolo, A.; Tap, J.; Pawlik, A.; et al. Genome analysis of smooth tubercle bacilli provides insights into ancestry and pathoadaptation of the etiologic agent of tuberculosis. *Nat. Genet.* 2013, *45* (2), 172–179.

Takayama, K.; Wang, C.; Besra, G. S. Pathway to synthesis and processing of mycolic acids in *Mycobacterium tuberculosis*. *Clin. Microbiol. Rev.* 2005, *18* (1), 81–101.

Thompson, A. J.; Williams, R. J.; Hakki, Z.; Alonzi, D. S.; Wennekes, T.; Gloster, T. M.; Songsrirote, K.; Thomas-Oates, J. E.; Wrodnigg, T. M.; Spreitz, J.; et al. Structural and mechanistic insight into N-glycan processing by endo-mannosidase. *Proc. Natl. Acad. Sci. U. S. A.* 2012, *109* (3), 781–786.

Tiago, I.; Maranha, A.; Mendes, V.; Alarico, S.; Moynihan, P. J.; Clarke, A. J.; Macedo-Ribeiro, S.; Pereira, P. J. B.; Empadinhas, N. Genome sequence of *Mycobacterium hassiacum* DSM 44199, a rare source of heat-stable mycobacterial proteins. *J. Bacteriol.* 2012, *194* (24), 7010–7011.

Tian, X. X.; Li, A.; Farrugia, I. V.; Mo, X.; Crich, D.; Groves, M. J. Isolation and identification of poly-α-(1→4)-linked 3-*O*-methyl-D-mannopyranose from a hot-water extract of *Mycobacterium vaccae*. *Carbohydr. Res.* 2000, *324* (1), 38–44.

Trofimov, V.; Costa-Gouveia, J.; Hoffmann, E.; Brodin, P. Host–pathogen systems for early drug discovery against tuberculosis. *Curr. Opin. Microbiol.* 2017, *39*, 143–151.

Tuffal, G.; Ponthus, C.; Picard, C.; Rivière, M.; Puzo, G. Structural elucidation of novel

methylglucose-containing polysaccharides from *Mycobacterium xenopi*. *Eur. J. Biochem.* **1995**, *233* (1), 377–383.

Tuffal, G.; Albigot, R.; Rivière, M.; Puzo, G. Newly found 2-*N*-acetyl-2,6-dideoxy-β-glucopyranose containing methyl glucose polysaccharides in *M. bovis* BCG: revised structure of the mycobacterial methyl glucose lipopolysaccharides. *Glycobiology* **1998**, *8* (7), 675–684.

Vance, D. E.; Mitsuhashi, O.; Bloch, K. Purification and properties of the fatty acid synthetase from *Mycobacterium phlei*. *J. Biol. Chem.* **1973**, *248* (7), 2303–2309.

VanderVen, B. C.; Harder, J. D.; Crick, D. C.; Belisle, J. T. Export-mediated assembly of mycobacterial glycoproteins parallels eukaryotic pathways. *Science (80-.).* **2005**, *309* (5736), 941–943.

Walsh, C. T.; Tu, B. P.; Tang, Y. Eight kinetically stable but thermodynamically activated molecules that power cell metabolism. *Chem. Rev.* **2018**, *118* (4), 1460–1494.

Wassilew, N.; Hoffmann, H.; Andrejak, C.; Lange, C. Pulmonary disease caused by non-tuberculous mycobacteria. *Respiration* **2016**, *91*, 386–402.

Weber, P. L.; Gray, G. R. Structural and immunochemical characterization of the acidic arabinomannan of *Mycobacterium smegmatis*. *Carbohydr. Res.* **1979**, *74* (1), 259–278.

van de Weerd, R.; Boot, M.; Maaskant, J.; Sparrius, M.; Verboom, T.; van Leeuwen, L. M.; Burggraaf, M. J.; Paauw, N. J.; Dainese, E.; Manganelli, R.; et al. Inorganic phosphate limitation modulates capsular polysaccharide composition in mycobacteria. *J. Biol. Chem.* **2016**, *291* (22), 11787–11799.

Weisman, L. S.; Ballou, C. E. Biosynthesis of the mycobacterial methylmannose polysaccharide: identification of a 3-*O*-methyltransferase. *J. Biol. Chem.* **1984a**, *259* (6), 3464–3469.

Weisman, L. S.; Ballou, C. E. Biosynthesis of the mycobacterial methylmannose polysaccharide: identification of an α-(1→4)-mannosyltransferase. *J. Biol. Chem.* **1984b**, *259* (6), 3457–3463.

WHO, W. H. O. *Global Tuberculosis Report 2018*; 2018.

Wood, W. L.; Peterson, D. O.; Bloch, K. *Mycobacterium smegmatis* fatty acid synthetase: a mechanism based on steady state rates and product distributions. *J. Biol. Chem.* **1977**, *252* (16), 5745–5749.

Xia, L. Studies of a mycobacterial α-(1→4)-mannosyltransferase involved in 3-O-methyl-mannose polysaccharide biosynthesis, University of Alberta - PhD Thesis, **2013**.

Xia, L.; Zheng, R. B.; Lowary, T. L. Revisiting the specificity of an α-(1→4)-mannosyltransferase involved in mycobacterial methylmannose polysaccharide biosynthesis. *ChemBioChem* **2012**, *13* (8), 1139–1151.

Yabusaki, K. K.; Ballou, C. E. Interaction of mycobacterial polymethylpolysaccharides with paranaric acid and palmitoyl-coenzyme A : Structural specificity and monomeric dissociation constants. *Proc. Natl. Acad. Sci. U. S. A.* **1978**, *75* (2), 691–695.

Yabusaki, K. K.; Ballou, C. E. Effect of polymethylpolysaccharides on the hydrolysis of palmitoyl coenzyme A by a thioesterase from *Mycobacterium smegmatis*. *J. Biol. Chem.* **1979**, *254* (24), 12314–12317.

Yabusaki, K. K.; Cohen, R. E.; Ballou, C. E. Conformational changes associated with complex formation between a mycobacterial polymethylpolysaccharide and palmitic acid. *J. Biol. Chem.* **1979**, *254* (15), 7282–7286.

Yamada, H.; Cohen, R. E.; Ballou, C. E. Characterization of 3-*O*-methyl-D-mannose polysaccharide precursors in *Mycobacterium smegmatis*. *J. Biol. Chem.* **1979**, *254* (6), 1972–1979.

Yokoyama, K.; Ballou, C. E. Synthesis of α-(1→6)-mannooligosaccharides in *Mycobacterium smegmatis*: function of β-mannosylphosphoryldecaprenol as the mannosyl donor. *J. Biol. Chem.* **1989**, *264* (36), 21621–21628.

Zaia, J. Mass spectrometry of oligosaccharides. *Mass Spectrom. Rev.* **2004**, *23* (3), 161–227.

Annex 1

Characterization of all compounds synthesized in this work

Mannose carbon numeration:

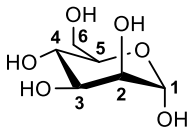

Monomer's identification used on NMR description:

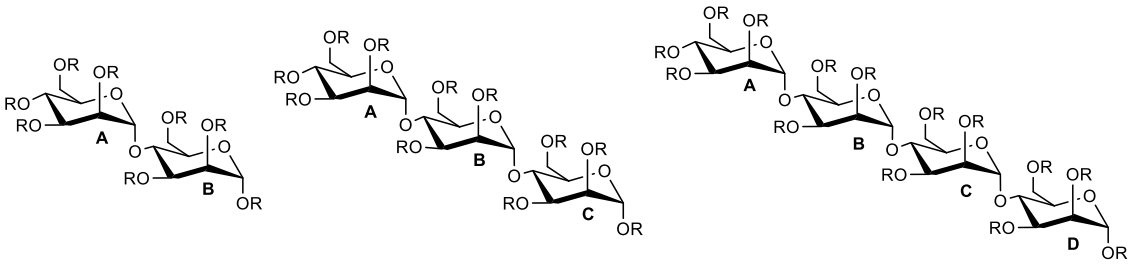

Allyl α-D-mannopyranoside (5)

FTIR (ATR): 3383.79 (O-H), 1647.0 (C=C), 1060.48 (C-O) cm^{-1}.

The NMR data for the α-anomer was in accordance to that described in the literature: M. Poláková, M.U. Roslund, F.S. Ekholm, T. Saloranta, R. Leino; *Euro. J. Org. Chem.* **2009**, 870-888.

Allyl 4,6-*O*-benzylidene-α-D-mannopyranoside (6)

FTIR (ATR): 3384.58 (O-H), 1647.06 (C=C), 1094.67-1027.72 (C-O) cm^{-1}.

NMR data for the α-anomer was in accordance to that described in the literature: M. Poláková, M.U. Roslund, F.S. Ekholm, T. Saloranta, R. Leino; *Euro. J. Org. Chem.* **2009**, 870-888.

Allyl 2,3-di-*O*-acetyl-4,6-*O*-benzylidene-α-D-mannopyranoside (7)

NMR data for the α-anomer was in accordance to that described in the literature: M. Poláková, M.U. Roslund, F.S. Ekholm, T. Saloranta, R. Leino; *Euro. J. Org. Chem.* **2009**, 870-888.

Allyl 2,3-di-*O*-acetyl-6-*O*-benzyl-α-D-mannopyranoside (8)

FTIR (ATR): 3467.5 (O-H), 1746.9 (C=O) cm^{-1}.

^{1}H-NMR ($CDCl_3$): δ 7.39 – 7.27 (m, 5H, Ar), 6.00 - 5.77 (m, 1H, $OCH_2C\underline{H}=CH_2$), 5.39 – 5.15 (m, 4H, H-2, H-3 and $OCH_2CH=C\underline{H}_2$), 4.84 (s, 1H, H-1), 4.62 (dd, 1H, *J* = 24.0 Hz, *J* = 12.0 Hz, $OC\underline{H}_2Ph$), 4.23 – 3.97 (m, 3H, H-4 and $OC\underline{H}_2CH=CH_2$), 3.91 – 3.72 (m, 3H, H-5 and H-6), 2.12 (s, 3H, $OCOC\underline{H}_3$), 2.07 (s, 3H, $OCOC\underline{H}_3$) ppm.

^{13}C-NMR ($CDCl_3$): δ 170.8 (C=O), 170.1 (C=O), 137.8 (C_q), 133.2 ($OCH_2\underline{C}H=CH_2$), 128.4 (Ar), 127.8 (Ar), 127.7 (Ar), 118.0 ($OCH_2CH=\underline{C}H_2$), 96.6 (C-1), 73.7 ($O\underline{C}H_2Ph$), 71.9 (C-3), 71.0 (C-5), 70.0 (C-6), 69.8 (C-2), 68.3 ($O\underline{C}H_2CH=CH_2$), 67.2 (C-4), 20.9 ($OCO\underline{C}H_3$), 20.9 ($OCO\underline{C}H_3$) ppm.

Allyl 2,3-di-*O*-acetyl-6-*O*-benzyl-4-*O*-*tert*-butyldimethylsilyl-α-D-mannopyranoside (9)

FTIR (ATR): 1750.8 (C=O) cm^{-1}.

^{1}H-NMR ($CDCl_3$): δ 7.40 – 7.19 (m, 5H, Ar), 5.95 – 5.83 (m, 1H, $OCH_2C\underline{H}=CH_2$), 5.33 – 5.06 (m, 4H, H-2, H-3 and $OCH_2CH=C\underline{H}_2$), 4.81 (d, 1H, *J* = 1.5 Hz, H-1), 4.62 (t, 2H, *J* = 12.7 Hz, $OC\underline{H}_2Ph$), 4.20 (dd, 1H, *J* = 7.8 Hz, *J* = 5.1 Hz, 1x$OC\underline{H}_2CH=CH_2$), 4.05 – 3.95 (m, 2H, H-4 and 1x$OC\underline{H}_2CH=CH_2$), 3.84 – 3.79 (m, 1H, H-5), 3.70 (d, 2H, *J* = 3.4 Hz, H-6), 2.09 (s, 3H, $OCOC\underline{H}_3$), 2.00 (s, 3H, $OCOC\underline{H}_3$), 0.79 (s, 9H, $SiC(C\underline{H}_3)_3$), 0.07 (d, 6H, *J* = 6.7 Hz, $Si(C\underline{H}_3)_2$) ppm.

^{13}C-NMR ($CDCl_3$): δ 133.5 ($OCH_2\underline{C}H=CH_2$), 128.3 (Ar), 127.9 (Ar), 127.5 (Ar), 127.4 (Ar), 117. 9 ($OCH_2CH=\underline{C}H_2$), 96.4 (C-1), 74.9, 74. 6, 73.8, 73.3 ($O\underline{C}H_2Ph$), 72.7 (C-3), 72.5 (C-5), 69.9, 69.6, 69.1 (C-6), 68.2 ($O\underline{C}H_2CH=CH_2$), 66.2 (C-4), 25.7 ($SiC(\underline{C}H_3)_3$), 21.1 ($OCO\underline{C}H_3$), 20.7 ($OCO\underline{C}H_3$), -4.2 ($Si(\underline{C}H_3)_2$) ppm.

2,3-di-*O*-acetyl-6-*O*-benzyl-4-*O*-*tert*-butyldimethylsilyl-α-D-mannopyranoside (10)

FTIR (ATR): 3419.1 (O-H), 1747.3 (C=O) cm^{-1}.

^{1}H-NMR ($CDCl_3$) δ 7.41 – 7.25 (m, 5H, Ar), 5.33 – 5.28 (m, 1H, H-2), 5.22 – 5.15 (m, 2H, H-1 and H-3), 4.69 – 4.52 (m, 2H, $OC\underline{H}_2Ph$), 4.14 – 4.06 (m, 1H, H-5), 3.96 – 3.88 (m, 1H, H-4), 3.76 – 3.61 (m, 2H, H-6), 2.12 (s, 3H, $OCOC\underline{H}_3$), 2.03 (s, 3H, $OCOC\underline{H}_3$), 0.80 (s, 9H, $SiC(C\underline{H}_3)_3$), 0.05 – 0.01 (m, 6H, $Si(C\underline{H}_3)_2$) ppm.

^{13}C-NMR ($CDCl_3$): δ 170.2 (C=O), 137.7 (C_q), 128.47 (Ar), 128.0 (Ar), 127. 8 (Ar), 92.2 (C-1), 73.4 ($O\underline{C}H_2Ph$), 72.3 (C-3), 72.1 (C-5), 70.3 (C-2), 69.3 (C-6), 66.6 (C-4), 25.6 ($SiC(\underline{C}H_3)_3$), 21.0 ($OCO\underline{C}H_3$), 20.9 ($OCO\underline{C}H_3$), -4.2 ($Si(\underline{C}H_3)_2$) ppm.

2,3-di-*O*-acetyl-6-*O*-benzyl-4-*O*-*tert*-butyldimethylsilyl-α-D-mannopyranosyl trichloroacetamidate (11)

$[\alpha]_D^{20}$ +45.4 (c 0.5, CH_2Cl_2).

FTIR (ATR): 3320.1 (N-H), 1754.5 (C=O) cm^{-1}.

^{1}H-NMR ($CDCl_3$): δ 8.69 (s, 1H, $OC(N\underline{H})CCl_3$), 7.40 – 7.22 (m, 5H, Ar), 6.26 (s, 1H, H-1), 5.50 – 5.47 (m, 1H, H-2), 5.18 (dd, 1H, *J* = 6.3 Hz, *J* = 3.2 Hz, H-3), 4.61 (s, 2H, $OC\underline{H}_2Ph$), 4.19

(t, 1H, *J* = 9.5 Hz, H-4), 4.00 (dd, 1H, *J* = 6.6 Hz, *J* = 2.9, H-5), 3.83 – 3.69 (m, 2H, H-6), 2.14 (s, 3H, OCOC$\underline{H}_3$), 2.03 (s, 3H, OCOC$\underline{H}_3$), 0.83 (s, 9H, SiC(C$\underline{H}_3$)$_3$), 0.06 (d, 6H, *J* = 3.6 Hz, Si(C$\underline{H}_3$)$_2$) ppm.

^{13}C-NMR ($CDCl_3$): δ 170.0 (C=O), 169.8 (C=O), 160.1 (C=O), 138.3 (C_q), 128.3 (Ar), 127.5 (Ar), 127.4 (Ar), 95.1 (C-1), 75.7 (C-5), 73.3 (O$\underline{C}$H$_2$Ph), 72.3 (C-3), 68.4 (C-6), 68.1 (C-2), 65.4 (C-4), 25.7 (SiC($\underline{C}$H$_3$)$_3$), 21.0 (OCO$\underline{C}$H$_3$), 20.7 (OCO$\underline{C}$H$_3$), -4.3 (Si($\underline{C}$H$_3$)$_2$ ppm.

Allyl 2,3-di-*O*-acetyl-6-*O*-benzyl-4-*O*-*tert*-butyldimethylsilyl-α-D-mannopyranosyl-(1→4)-2,3-di-*O*-acetyl-6-*O*-benzyl-α-D-mannopyranoside (12)

FTIR (ATR): 1747.6 (C=O) cm^{-1}.

^{1}H-NMR ($CDCl_3$) δ 7.39 – 7.21 (m, 10H, Ar), 5.96 – 5.84 (m, 1H, OCH$_2$C$\underline{H}$=CH$_2$), 5.37 – 5.24 (m, 3H, H-2 B, H-3 B and 1xOCH$_2$CH=C$\underline{H}_2$), 5.24 – 5.17 (m, 2H, H-2 A and 1xOCH$_2$CH=C$\underline{H}_2$), 5.05 – 4.97 (m, 2H, H-1 A and H-3 A), 4.87 – 4.81 (m, 1H, H-1 B), 4.64 – 4.48 (m, 4H, OC$\underline{H}_2$Ph A-B), 4.23 – 4.08 (m, 2H, H-4 B and 1xOC$\underline{H}_2$CH=CH$_2$), 4.07 – 3.96 (m, 2H, H-4 A and 1xOC$\underline{H}_2$CH=CH$_2$), 3.96 – 3.73 (m, 3H, H-5 A-B and H-6 B), 3.64 – 3.51 (m, 2H, H-6 A), 2.17 (s, 3H, OCOC$\underline{H}_3$), 2.11 – 2.03 (m, 6H, (OCOC$\underline{H}_3$)$_2$), 2.00 (s, 3H, OCOC$\underline{H}_3$), 0.82 (s, 9H, SiC(C$\underline{H}_3$)$_3$), 0.03 (s, 6H, Si(C$\underline{H}_3$)$_2$) ppm.

^{13}C-NMR ($CDCl_3$): δ 170.1 (C=O), 170.0 (C=O), 169.8 (C=O), 138.5 (C_q), 138.2 (C_q), 133.2 (OCH$_2$$\underline{C}$H=CH$_2$), 128.3 (Ar), 128.2 (Ar), 127.4 (Ar), 118.1 (OCH$_2$CH=$\underline{C}$H$_2$), 100.0 (C-1 A), 96.4 (C-1 B), 74.3 (C-4 B), 73.8 (C-5 A), 73.3 (O$\underline{C}$H$_2$Ph A or B), 73.2 (O$\underline{C}$H$_2$Ph A or B), 72.3 (C-3 A), 71.5 (C-3 B), 71.04 (C-5 B), 70.0 (C-2 A), 69.8 (C-2 B), 69.1 (C-6 B), 68.9 (C-6 A), 68.4 (O$\underline{C}$H$_2$CH=CH$_2$), 65.9 (C-4 A), 25.7 (SiC($\underline{C}$H$_3$)$_3$), 21.0 (OCO$\underline{C}$H$_3$), 20.9 (OCO$\underline{C}$H$_3$), 20.8 (OCO$\underline{C}$H$_3$), 20.7 (OCO$\underline{C}$H$_3$), -4.3 (Si($\underline{C}$H$_3$)$_2$) ppm.

Allyl 2,3-di-*O*-acetyl-6-*O*-benzyl-α-D-mannopyranosyl-(1→4)-2,3-di-*O*-acetyl-6-*O*-benzyl-α-D-mannopyranoside (13)

FTIR (ATR): 3479.7 (O-H), 1746.7 (C=O) cm^{-1}.

^{1}H-NMR ($CDCl_3$): δ 7.39 – 7.20 (m, 10H, Ar), 5.90 (m, 1H, OCH$_2$C$\underline{H}$=CH$_2$), 5.38 – 5.17 (m, 4H, OCH$_2$CH=C$\underline{H}_2$, H-2 B and H-3 B), 5.17 – 5.00 (m, 3H, H-1 A, H-2 A and H-3 A), 4.83 (d, 1H, *J* = 1.5 Hz, H-1 B), 4.55 (d, 3H, *J* = 12.5 Hz, OC$\underline{H}_2$Ph A, 1xOC$\underline{H}_2$Ph B), 4.44 (d, 1H, *J*=11.9 Hz, 1xOC$\underline{H}_2$Ph B), 4.29 – 4.07 (m, 2H, H-4 B and 1xOC$\underline{H}_2$CH=CH$_2$), 4.07 – 3.70 (m, 6H, H-4 A, 1xC$\underline{H}_2$Ph, H-5 B, H-5 A and H-6 B), 3.68 - 3.62 (m, 1H, 1xH-6 A), 3.60 – 3.54 (m, 1H, 1xH-6 A), 2.13 – 2.03 (m, 12H, (OCOC$\underline{H}_3$)$_4$) ppm.

^{13}C-NMR ($CDCl_3$): δ 170.1 (C=O), 137.8 (C_q), 133.6 (OCH$_2$$\underline{C}$H=CH$_2$), 128.4 (Ar), 128.3 (Ar), 127.7 (Ar), 127.4 (Ar), 118.2 (OCH$_2$CH=$\underline{C}$H$_2$), 99.4 (C-1 A), 96.4 (C-1 B), 73.7 (O$\underline{C}$H$_2$Ph B),

73.3 (C-4), 72.1 (O<u>C</u>H_2Ph A),72.2 (C-5 A), 71.8 (C-3 B), 71.4 (C-2 A or C-3 A), 70.9 (C-5 B), 69.9 (C-2 A or C-3 A), 69.5 (C-6 A), 69.1 (C-6 B), 68.4 (O<u>C</u>H_2CH=CH_2), 67.1 (C-4 A), 20.9 (OCO<u>C</u>H_3), 20.8 (OCO<u>C</u>H_3) ppm.

Allyl 2,3,4-tri-*O*-acetyl-6-*O*-benzyl-α-D-mannopyranosyl-(1→4)-2,3-di-*O*-acetyl-6-*O*-benzyl-α-D-mannopyranoside (14)

FTIR (ATR): 1747.1 (C=O) cm^{-1}.

^{1}H-NMR ($CDCl_3$): δ 7.39 – 7.22 (m, 10H, Ar), 5.96 – 5.84 (m, 1H, OCH$_2$C<u>H</u>=CH$_2$), 5.38 – 5.05 (m, 8H, H-1 A, H-2 A-B, H-3 A-B, H-4 A and OCH$_2$CH=C<u>H$_2$</u>), 4.84 (s, 1H, H-1 B), 4.54 (d, 3H, *J* = 13.1 Hz, OC<u>H$_2$</u>Ph A and 1xOC<u>H$_2$</u>Ph B), 4.37 (d, 1H, *J* = 11.9 Hz, 1xOC<u>H$_2$</u>Ph B), 4.23 – 4.09 (m, 2H, H-4 B and 1xOC<u>H$_2$</u>CH=CH$_2$), 4.06 – 3.82 (m, 4H, 1xOC<u>H$_2$</u>CH=CH$_2$, H-5 A-B and 1xH-6 B), 3.75 (d, 1H, *J* = 10.2 Hz, 1xH-6 B), 3.46 – 3.35 (m, 2H, H-6 A), 2.15 – 2.08 (m, 9H, (OCOC<u>H$_3$</u>)$_3$), 1.98 (s, 3H, OCOC<u>H$_3$</u>), 1.91 (s, 3H, OCOC<u>H$_3$</u>) ppm.

^{13}C-NMR ($CDCl_3$): δ 170.0 (C=O), 169.7 (C=O), 138.4 (C_q), 133.2 (OCH$_2$<u>C</u>H=CH$_2$), 128.3 (Ar), 128.3 (Ar), 127.9 (Ar), 127.7 (Ar), 127.4 (Ar), 118.2 (OCH$_2$CH=<u>C</u>H$_2$), 99.4 (C-1 A), 96.4 (C-1 B), 73.9 (C-4 B), 73.5 (O<u>C</u>H$_2$Ph B), 73.3 (O<u>C</u>H$_2$Ph A), 71.6 (C-3 B), 71.0 (C-5 B), 70.6 (C-5 A), 69.9 (C-2 B), 69.8 (C-2 A), 69.1 (C-6 B), 68.9 (C-3 A), 68.7 (O<u>C</u>H$_2$CH=CH$_2$), 68.5 (C-6 A), 66.6 (C-4 A), 20.9 (OCO<u>C</u>H$_3$), 20.8 (OCO<u>C</u>H$_3$), 20.7 (OCO<u>C</u>H$_3$), 20.6 (OCO<u>C</u>H$_3$) ppm.

2,3,4-tri-*O*-acetyl-6-*O*-benzyl-α-D-mannopyranosyl-(1→4)-2,3-di-*O*-acetyl-6-*O*-benzyl-α-D-mannopyranoside (15)

FTIR (ATR): 3467.0 (O-H), 1746.9 (C=O) cm^{-1}.

^{1}H-NMR ($CDCl_3$): δ 7.38 – 7.20 (m, 10H, Ar), 5.37 (dd, 1H, *J* = 6.2 Hz, *J* = 3.3 Hz, H-3 B), 5.35 – 5.27 (m, 1H, H-4 A), 5.25 – 5.18 (m, 3H, H-1 B, H-2 B and H-3 A), 5.15 – 5.11 (m, 1H, H-2 A), 5.07 (d, 1H, *J* = 2.0 Hz, H-1 A), 4.59 – 4.49 (m, 3H, OC<u>H$_2$</u>Ph A and 1xOC<u>H$_2$</u>Ph B), 4.38 (d, 1H, *J* = 12.0 Hz, 1xOC<u>H$_2$</u>Ph B), 4.19 – 4.04 (m, 2H, H-4 B and H-5 B), 3.94 – 3.87 (m, 1H, H-5 A), 3.85 – 3.79 (m, 1H, 1xH-6 B), 3.78 – 3.73 (m, 1H, 1xH-6 B), 3.40 (dd, 1H, *J* = 7.9Hz, *J* = 4.7 Hz, 1xH-6 A), 3.34 (dd, 1H, *J* = 7.9 Hz, *J* = 2.8 Hz, 1xH-6 A), 2.11 (d, 6H, *J* = 6.7 Hz, (OCOC<u>H$_3$</u>)$_2$), 2.05 (s, 3H, OCOC<u>H$_3$</u>), 1.98 (s, 3H, OCOC<u>H$_3$</u>), 1.92 (s, 3H, OCOC<u>H$_3$</u>) ppm.

^{13}C-NMR ($CDCl_3$): δ 170.1 (C=O), 170.0 (C=O), 169.8 (C=O), 169.70 (C=O), 138.2 (C_q), 137.7 (C_q), 128.3 (Ar), 127.9 (Ar), 127.7 (Ar), 127.6 (Ar), 127.6 (Ar) 99.4 (C-1 A), 92.1 (C-1 B), 74.1 (C-4 B), 73.5 (O<u>C</u>H$_2$Ph B), 73.4 (O<u>C</u>H$_2$Ph B), 71.17 (C-3 B), 70.8 (C-5 B), 70.7 (C-5 A), 70.1 (C-2 B), 69.8 (C-2 A), 69.4 (C-6 B), 68.9 (C-3 A), 68.5 (C-6 A), 66.6 (C-4 A), 20.9 (OCO<u>C</u>H$_3$), 20.8 (OCO<u>C</u>H$_3$), 20.7 (OCO<u>C</u>H$_3$), 20.6 (OCO<u>C</u>H$_3$) ppm.

2,3,4-tri-*O*-acetyl-6-*O*-benzyl-α-D-mannopyranosyl-(1→4)-2,3-di-*O*-acetyl-6-*O*-benzyl-α-D-mannopyranosyl trichloroacetamidate (16)

$[\alpha]_D^{20}$ +76.0 (c 0.33, CH_2Cl_2).

FTIR (ATR): 3350.5 (N-H), 1748.2 (C=O) cm^{-1}.

^{1}H-NMR ($CDCl_3$): δ 8.71 (s, 1H, OC(N<u>H</u>)CCl_3), 7.36 – 7.23 (m, 5H, Ar), 6.26 (d, 1H, *J* = 1.5 Hz, H-1 B), 5.51 – 5.47 (m, 1H, H-2 B), 5.40 – 5.29 (m, 2H, H-3 B and H-4 A), 5.24 (dd, 1H, *J* = 3.1 Hz, H-3 A), 5.18 – 5.13 (m, 2H, H-2 A and H-1 A), 4.59 – 4.50 (s, 3H, OC<u>H</u>$_2$Ph A and 1xOC<u>H</u>$_2$Ph B), 4.34 (d, 1H, *J* = 11.0 Hz, 1xOC<u>H</u>$_2$Ph B), 4.39 – 4.29 (m, 2H, 1xOC<u>H</u>$_2$Ph B and H-4 B), 4.11 – 4.05 (m, 1H, H-5 B), 3.99 – 3.89 (m, 2H, H-5 A and 1xH-6 B), 3.76 (d, 1H, *J* = 11.6 Hz, 1xH-6 B), 3.45 – 3.35 (m, 2H, H-6 A), 2.15 – 2.11 (m, 6H, (OCOC<u>H</u>$_3$)$_2$), 2.06 (s, 3H, OCOC<u>H</u>$_3$), 1.98 (s, 3H, OCOC<u>H</u>$_3$), 1.90 (s, 3H, OCOC<u>H</u>$_3$) ppm.

^{13}C-NMR ($CDCl_3$): δ 170.0 (C=O), 169.9 (C=O), 169.7 (C=O), 160.1 (C_q), 138.4 (C_q), 137.7 (C_q), 128.3 (Ar), 127.9 (Ar), 127.7 (Ar), 127.5 (Ar), 99.4 (C-1 A), 94.8 (C-1 B), 74.0 (C-5 B), 73.5 (O<u>C</u>H_2Ph B), 73.4 (O<u>C</u>H_2Ph A), 72.5 (C-4 B), 71.2 (C-3 B), 70.7 (C-5 A), 69.7 (C-2 A), 69.0 (C-3 A), 68.7 (C-6 A) 68.5 (C-6 B), 68.1 (C-2 B), 66.5 (C-4 A), 20.9 (OCO<u>C</u>H_3), 20.8 (OCO<u>C</u>H_3), 20.7 (OCO<u>C</u>H_3), 20.6 (OCO<u>C</u>H_3) ppm.

Allyl 2,3,4-tri-*O*-acetyl-6-*O*-benzyl-α-D-mannopyranosyl-(1→4)-2,3-di-*O*-acetyl-6-*O*-benzyl-α-D-mannopyranosyl-(1→4)-2,3-di-*O*-acetyl-6-*O*-benzyl-α-D-mannopyranosyl-(1→4)-2,3-di-*O*-acetyl-6-*O*-benzyl-α-D-mannopyranoside (17)

FTIR (ATR): 1747.1 (C=O) cm^{-1}.

^{1}H-NMR ($CDCl_3$): δ 7.37 – 7.21 (m, 20H, Ar), 5.97 – 5.84 (m, 1H, OCH_2C<u>H</u>$=CH_2$), 5.36 – 5.02 (m, 16H, H-1 A-C, H-2 A-D, H-3 A-D, H-4 A-C, $OCH_2CH=C$<u>H</u>$_2$), 4.84 (d, 1H, *J* = 1.3 Hz, H-1 D), 4.63 – 4.30 (m, 8H, OC<u>H</u>$_2$Ph A-D), 4.23 – 3.68 (m, 12H, H-4 D, H-5 A-D, 5xH-6, OC<u>H</u>$_2$CH=CH_2), 3.54 (d, 1H, *J* = 11.6 Hz, 1xH-6), 3.42 – 3.31 (m, 2H, H-6), 2.13 – 1.88 (m, 27H, (OCOC<u>H</u>$_3$)$_9$) ppm.

^{13}C-NMR ($CDCl_3$): δ 170.0 (C=O), 169.9 (C=O), 169.8 (C=O), 169.8 (C=O), 169.7 (C=O), 138.5 (C_q) 138.4 (C_q), 138.3 (C_q), 137.7 (C_q), 133.2 (OCH_2<u>C</u>H$=CH_2$), 128.4 (Ar), 128.3 (Ar), 128.2 (Ar), 127.9 (Ar), 127.7 (Ar), 127.5 (Ar), 127.4 (Ar), 118.2 ($OCH_2CH=$<u>C</u>H_2), 99.4 (C-1 A or B or C), 99.2 (C-1 A or B or C), 99.1 (C-1 A or B or C), 96.4 (C-1 D), 73.9, 73.6 (<u>C</u>H_2Ph A or B or C or D), 73.5 (<u>C</u>H_2Ph A or B or C or D), 73.3 (<u>C</u>H_2Ph A or B or C or D), 73.2 (<u>C</u>H_2Ph A or B or C or D), 73.2, 73.1, 72.2, 72.0, 71.7, 71.4, 71.2, 71.1, 70.9, 70.6, 70.0, 69.9, 69.8, 68.9 (C-6), 68.6 (C-6), 68.4 (C-6), 66.7, 20.9 (OCO<u>C</u>H_3), 20.8 (OCO<u>C</u>H_3), 20.7 (OCO<u>C</u>H_3), 20.6 (OCO<u>C</u>H_3) ppm.

Allyl 6-*O*-benzyl-α-D-mannopyranosyl-(1→4)-6-*O*-benzyl-α-D-mannopyranosyl-(1→4)-6-*O*-benzyl-α-D-mannopyranosyl-(1→4)-6-*O*-benzyl-α-D-mannopyranoside (18)

FTIR (ATR): 3396.0 (O-H) cm^{-1}.

^{1}H-NMR (MeOD): δ 7.37 – 7.21 (m, 20H, Ar), 6.02 – 5.91 (m, 1H, $OCH_2C\underline{H}=CH_2$), 5.34 – 5.17 (m, 5H, H-1 A-C and $OCH_2CH=C\underline{H}_2$), 4.80 (d, 1H, *J* = 1.7 Hz, H-1 D), 4.58 – 4.30 (m, 8H, $OC\underline{H}_2Ph$ A-C), 4.25 – 4.18 (m, 1H, $1xOC\underline{H}_2CH=CH_2$), 4.06 – 3.99 (m, 2H, H-4 A and $1xOC\underline{H}_2CH=CH_2$), 3.95 – 3.64 (m, 23H, H-2 A-D, H-3 A-D, H-4 B-D, H-5 A-D and H-6 A or B or C or D), 3.57 (s, 2H, H-6 A or B or C or D) ppm.

^{13}C-NMR (MeOD): δ 138.2 (C_q), 134.0 ($OCH_2\underline{C}H=CH_2$), 128.1 (Ar), 127.9 (Ar), 127.7 (Ar), 127.6 (Ar), 127.4 (Ar), 127.2 (Ar), 116.0 ($OCH_2CH=\underline{C}H_2$), 102.1 (C-1 A or B or C), 101.7 (C-1 A or B or C) 101.5 (C-1 A or B or C), 99.2 (C-1 D), 74.9, 74.7, 74.4, 73.2 ($O\underline{C}H_2Ph$ A or B or C or D), 73.1 ($O\underline{C}H_2Ph$ A or B or C or D), 73.0 ($O\underline{C}H_2Ph$ A or B or C or D), 72.8 ($O\underline{C}H_2Ph$ A or B or C or D), 71.9, 71.6, 71.5, 71.3, 71.2, 70.9, 70.6, 70.0 (C-6 A or B or C or D), 69.9 (C-6 A or B or C or D), 69.7 (C-6 A or B or C or D), 67.6 ($O\underline{C}H_2CH=CH_2$), 67.4 (C-4 A) ppm.

Propyl α-D-mannopyranosyl-(1→4)-α-D-mannopyranosyl-(1→4)-α-D-mannopyranosyl-(1→4)-α-D-mannopyranoside (1)

FTIR (ATR): 3350.6 (O-H) cm^{-1}.

^{1}H-NMR (D_2O): δ 5.18 – 5.13 (m, 3H, H-1 A-C), 4.78 (s, 1H, H-1 D), 4.00 – 3.91 (m, 3H, H-2 A-C), 3.90 – 3.54 (m, 22H, H-2 D, H-3 A-D, H-4 A-D, H-5 A-D, H-6 A-D and $1xOC\underline{H}_2CH_2CH_3$), 3.47 – 3.39 (m, 1H, $1xOC\underline{H}_2CH_2CH_3$), 1.59 – 1.47 (m, 2H, $OCH_2C\underline{H}_2CH_3$), 0.84 (t, 3H, *J* = 7.4 Hz, $OCH_2CH_2C\underline{H}_3$) ppm.

^{13}C-NMR (D_2O): δ 101.4 (C-1 A or B or C), 101.3 (C-1 A or B or C), 99.5 (C-1 D), 74.3, 74.1, 74.1, 73.7, 72.2, 72.2, 71.1, 70.8, 70.7, 70.5, 70.3, 70.2, 69.6 ($O\underline{C}H_2CH_2CH_3$), 66.5, 61.0 (C-6 A or B or C or D) 60.9 (C-6 A or B or C or D), 60.8 (C-6 A or B or C or D), 21.9 ($OCH_2\underline{C}H_2CH_3$), 9.9 ($OCH_2CH_2\underline{C}H_3$) ppm.

HR-MS: calcd. for $C_{27}H_{49}O_{21}$ $[M + H]^+$: 709.2761; found: 709.2763.

Allyl 2,3,4-tri-*O*-acetyl-6-*O*-benzyl-α-D-mannopyranosyl-(1→4)-2,3-di-*O*-acetyl-6-*O*-benzyl-α-D-mannopyranosyl-(1→4)-2,3-di-*O*-acetyl-6-*O*-benzyl-α-D-mannopyranose (19)

FTIR (ATR): 3478.9 (O-H), 1747.2 (C=O) cm^{-1}.

^{1}H-NMR ($CDCl_3$): δ 7.38 – 7.20 (m, 15H, Ar), 5.97 – 5.83 (m, 1H, $OCH_2C\underline{H}=CH_2$), 5.36 – 5.28 (m, 3H, H-2 C, H-3 C, $1xOCH_2CH=C\underline{H}_2$), 5.24 – 5.17 (m, 3H, H-2 A ou B, H-3 A ou B, $1xOCH_2CH=C\underline{H}_2$), 5.13 – 5.01 (m, 4H, H-1 A-B, H-2 A or B, H-3 A or B), 4.84 (d, 1H, *J* = 1.4

Hz, H-1 C), 4.59 – 4.39 (m, 6H, OC$\underline{H}_2$Ph A-C), 4.24 – 4.08 (m, 3H, H-4 A ou B, H-4 C, 1xOC$\underline{H}_2$CH=CH$_2$), 4.05 – 3.85 (m, 5H, H-4 A or B, H-5 C, H-6 A ou B, 1xOC$\underline{H}_2$CH=CH$_2$), 3.80 – 3.59 (m, 4H, H-5 A-B and H-6 C), 3.54 (dd, 2H, *J* = 10.1 Hz, *J* = 4.1 Hz, H-6 A or B), 2.11 – 2.00 (m, 21H, (OCOC$\underline{H}_3$)$_7$) ppm.

^{13}C NMR (CDCl$_3$): δ 169.8 (C=O), 133.2 (OCH$_2\underline{C}$H=CH$_2$), 128.4 (Ar), 128.3 (Ar), 127.8 (Ar), 127.7 (Ar), 127.4 (Ar), 127.3 (Ar), 118.2 (OCH$_2$CH=$\underline{C}$H$_2$), 99.5 (C-1 A or B), 99.1 (C-1 A or B), 96.4 (C-1 C), 74.0, 73.7 (O$\underline{C}$H$_2$Ph A or B or C), 73.3 (O$\underline{C}$H$_2$Ph A or B or C), 72.7, 71.9, 71.6, 71.4, 70.9, 70.0, 68.9, 68.4 (O$\underline{C}$H$_2$CH=CH$_2$), 20.9 (OCO$\underline{C}$H$_3$), 20.8 (OCO$\underline{C}$H$_3$), 20.7 (OCO$\underline{C}$H$_3$) ppm.

Allyl 6-*O*-benzyl-α-D-mannopyranosyl-(1→4)-6-*O*-benzyl-α-D-mannopyranosyl-(1→4)-6-*O*-benzyl-α-D-mannopyranoside (20)

FTIR (ATR): 3401.1 (O-H) cm^{-1}.

^{1}H-NMR (MeOD): δ 7.39 – 7.21 (m, 15H, Ar), 6.01 – 5.90 (m, 1H, OCH$_2$C$\underline{H}$=CH$_2$), 5.34 – 5.16 (m, 4H, H-1 A-B and OCH$_2$CH=C$\underline{H}_2$), 4.79 (d, 1H, *J* = 1.6 Hz, H-1 C), 4.56 – 4.36 (m, 6H, OC$\underline{H}_2$Ph A-C), 4.21 (dd, 1H, *J* = 7.9 Hz, *J* = 5.1 Hz, 1xOC$\underline{H}_2$CH=CH$_2$), 4.06 – 3.62 (m, 19H, 1xOC$\underline{H}_2$CH=CH$_2$, H-2 A-C, H-3 A-C, H-4 A-C, H-5 A-C and H-6 A-C) ppm.

^{13}C-NMR (MeOD): δ 138.3 (C$_q$), 134.0 (OCH$_2\underline{C}$H=CH$_2$), 128.0 (Ar), 127.9 (Ar), 127.7 (Ar), 127.6 (Ar), 127.5 (Ar), 127.3 (Ar), 127.2 (Ar), 116.0 (OCH$_2$CH=$\underline{C}$H$_2$), 102.0 (C-1 A or B), 101.7 (C-1 A or B), 99.2 (C-1 C), 74.9, 74.8, 73.2 (O$\underline{C}$H$_2$Ph A or B or C), 73.0 (O$\underline{C}$H$_2$Ph A or B or C), 72.9, 72.8 (O$\underline{C}$H$_2$Ph A or B or C), 71.8, 71.5, 71.3, 71.2, 71.1, 70.8, 70.7, 70.0 (C-6 A or B or C), 69.7 (C-6 A or B or C), 67.6 (O$\underline{C}$H$_2$CH=CH$_2$), 67.3 ppm.

Propyl-α-D-mannopyranosyl-(1→4)-α-D-mannopyranosyl-(1→4)-α-D-mannopyranoside (2)

FTIR (ATR): 3306.5 (O-H) cm^{-1}.

^{1}H-NMR (D$_2$O): δ 5.16 (d, *J* = 1.9 Hz, 2H, H-1 A and B), 4.78 (d, 1H, *J* = 1.1 Hz, H-1 C), 4.00 – 3.91 (m, 2H, H-2 A-B), 3.88 – 3.54 (m, 17H, H-2 C, H-3 A-C, H-4 A-C, H-5 A-C, H-6 A-C and 1xOC$\underline{H}_2$CH$_2$CH$_3$), 3.47 – 3.39 (m, 1H, 1xOC$\underline{H}_2$CH$_2$CH$_3$), 1.59 – 1.47 (m, 2H, OCH$_2$C$\underline{H}_2$CH$_3$), 0.83 (t, 3H, *J* = 7.4 Hz, OCH$_2$CH$_2$C$\underline{H}_3$) ppm.

^{13}C-NMR (D$_2$O): δ 101.4 (C-1 A or B), 101.3 (C-1 A or B), 99.5 (C-1 C), 74.3, 74.0, 73.7, 72.2, 71.1, 70.8, 70.7, 70.5 (C-2 C), 70.3 (C-2 A or B), 70.2 (C-2 A or B), 69.6 (O$\underline{C}$H$_2$CH$_2$CH$_3$), 66.5, 61.0 (C-6 A or B or C), 60.9 (C-6 A or B or C), 60.8 (C-6 A or B or C), 21.90 (OCH$_2\underline{C}$H$_2$CH$_3$), 9.84 (OCH$_2$CH$_2\underline{C}$H$_3$) ppm.

HR-MS: calcd. for C$_{21}$H$_{38}$NaO$_{16}$ [M + Na]$^+$: 569.2052; found: 569.2056.

Allyl 4,6-*O*-benzylidene-3-*O*-methyl-α-D-mannopyranoside (21)

FTIR (ATR): 3461.67 (O-H), 1646.98 (C=C), 1093.78-1034.83 (C-O) cm^{-1}.

NMR data for the α-anomer described according to the literature: W. Liao, D. Lu; *Carbohydr. Res.* **1996**, 296, 171-182.

Allyl 2,4-di-*O*-acetyl-4,6-*O*-benzylidene-3-*O*-methyl-α-D-mannopyranoside (22)

FTIR (ATR): 1746.45 (C=O), 1646.97 (C=C) cm^{-1}.

NMR data for the α-anomer described according to the literature: J. Ripoll-Rozada, M. Costa, J. A. Manso, A. Maranha, V. Miranda, A. Sequeira, M. R. Ventura, S. Macedo-Ribeiro, P. J. B. Pereira, N. Empadinhas; *Proc. Natl. Acad. Sci. U. S. A.* **2019**, 116 (3), 835-844.

Allyl 2-*O*-acetyl-6-*O*-benzyl-3-*O*-methyl-α-D-mannopyranoside (23)

FTIR (ATR): 3467.07 (O-H), 1744.5 (C=O), 1646.98 (C=C) cm^{-1}.

NMR data for the α-anomer described according to the literature: J. Ripoll-Rozada, M. Costa, J. A. Manso, A. Maranha, V. Miranda, A. Sequeira, M. R. Ventura, S. Macedo-Ribeiro, P. J. B. Pereira, N. Empadinhas; *Proc. Natl. Acad. Sci. U. S. A.* **2019**, 116 (3), 835-844.

Allyl 2-*O*-acetyl-6-*O*-benzyl-4-*O*-*tert*-butyldimethylsilyl-3-*O*-methyl-α-D-mannopyranoside (24)

FTIR (ATR): 1747.5 (C=O) cm^{-1}.

^{1}H-NMR ($CDCl_3$): δ 7.38 – 7.23 (m, 5H, Ar), 5.98 – 5.86 (m, 1H, $OCH_2C\underline{H}=CH_2$), 5.32 (s, 1H, H-2), 5.28 (d, 1H, *J* = 1.4 Hz, 1x$OCH_2CH=C\underline{H}_2$), 5.21 (d, 1H, *J* = 11.1 Hz, 1x$OCH_2CH=C\underline{H}_2$), 4.86 (s, 1H, H-1), 4.60 (q, 2H, *J* = 8 Hz, *J* = 12 Hz, $C\underline{H}_2Ph$), 4.21 (dd, 1H, *J* = 7.6 Hz, *J* = 5.2 Hz, 1x$OC\underline{H}_2CH=CH_2$), 4.05 – 3.97 (m, 1H, 1x$OC\underline{H}_2CH=CH_2$), 3.82 – 3.72 (m, 3H, H-4 and H-6), 3.72 – 3.66 (m, 1H, H-5), 3.46 – 3.40 (m, 1H, H-3), 3.30 (s, 3H, $OC\underline{H}_3$), 2.10 (s, 3H, $OCOC\underline{H}_3$), 0.87 (s, 9H, $SiC(C\underline{H}_3)_3$), 0.03 (d, *J* = 21.1 Hz, 6H, $Si(C\underline{H}_3)_2$) ppm.

^{13}C-NMR ($CDCl_3$): δ 170.5 (C=O), 138.5 (C_q), 133.6 ($OCH_2\underline{C}H=CH_2$) 128.4 (Ar), 128.3 (Ar), 127.9 (Ar), 127.7 (Ar), 127.4 (Ar), 117.8 ($OCH_2CH=\underline{C}H_2$) 96.8 (C-1), 79.8 (C-3), 73.2 ($\underline{C}H_2Ph$), 72.8 (C-5), 69.6 (C-6), 68.2 ($O\underline{C}H_2CH=CH_2$), 67.9 (C-4), 67.7 (C-2), 56.8 ($O\underline{C}H_3$), 26.0 ($SiC(\underline{C}H_3)_3$), 21.0 ($OCO\underline{C}H_3$), -4.05 ($Si(\underline{C}H_3)_2$) ppm.

2-*O*-acetyl-6-*O*-benzyl-4-*O*-*tert*-butyldimethylsilyl-3-*O*-methyl-α-D-mannopyranoside (25)

^{1}H-NMR ($CDCl_3$): δ 7.40 – 7.26 (m, 5H, Ar), 5.35 (dd, 1H, *J* = 1.2 Hz, *J* = 2 Hz, H-2), 5.23 (s, 1H, H-1), 4.70 – 4.61 (m, 1H, 1x$OC\underline{H}_2Ph$), 4.59 – 4.52 (m, 1H, 1x$OC\underline{H}_2Ph$), 4.05 – 3.99 (m, 1H, H-5), 3.78 (dd, 1H, *J* = 8.4 Hz, *J* = 2 Hz, 1xH-6), 3.72 – 3.57 (m, 2H, H-4 and 1xH-6), 3.49 (dd, 1H, *J* = 6 Hz, *J* = 3.2 Hz, H-3), 3.32 (s, 3H, $OC\underline{H}_3$), 2.12 (s, 3H, $OCOC\underline{H}_3$), 0.82 (s, 9H, $SiC(C\underline{H}_3)_3$), 0.05 (m, 6H, $Si(C\underline{H}_3)_2$) ppm.

^{13}C-NMR ($CDCl_3$): δ 170.4 (C=O), 138.0 (C_q), 128.4 (Ar), 127.8 (Ar), 127.7 (Ar), 92.5 (C-1), 79.3 (C-3), 73.4 (O$\underline{C}H_2$Ph), 72.5 (C-5), 69.9 (C-6), 68.2 (C-4), 67.9 (C-2), 56.8 (O$\underline{C}H_3$), 25.9 (SiC($\underline{C}H_3)_3$), 21.0 (OCO$\underline{C}H_3$), -4.1 (Si($\underline{C}H_3)_2$) ppm.

2-*O*-acetyl-6-*O*-benzyl-4-*O*-*tert*-butyldimethylsilyl-3-*O*-methyl-α-D-mannopyranoside trichloroacetamidate (26)

^{1}H-NMR ($CDCl_3$): δ 8.69 (s, 1H, OC(N$\underline{H}$)CCl_3), 7.38 – 7.23 (m, 5H, Ar), 6.29 (d, 1H, *J* = 1.6 Hz, H-1), 5.51 – 5.48 (m, 1H, H-2), 4.59 (s, 2H, OC$\underline{H}_2$Ph), 4.00 - 3.91 (m, 2H, H-4 and H-5), 3.75 (d, 2H, *J* = 2.2 Hz, H-6), 3.47 (dd, 1H, *J* = 5.6 Hz, *J* = 2.8 Hz, H-3), 3.33 (s, 3H, OC$\underline{H}_3$), 2.13 (s, 3H, OCOC$\underline{H}_3$), 0.84 (s, 9H, SiC(C$\underline{H}_3)_3$), 0.05 (d, 6H, *J* = 19.5 Hz, Si(C$\underline{H}_3)_2$) ppm.

^{13}C-NMR ($CDCl_3$): δ 170.1 (C=O), 160.0 (C=O), 138.4 (C_q), 128.4 (Ar), 128.2 (Ar), 127.8 (Ar), 127.7 (Ar), 127.6 (Ar), 127.4 (Ar), 95.4 (C-1), 79.9 (C-3), 75.8 (C-5), 73.2 (O$\underline{C}H_2$Ph), 68.9 (C-6), 67.1 (C-4), 66.1 (C-2), 57.0 (O$\underline{C}H_3$), 26.0 (SiC($\underline{C}H_3)_3$), 20.9 (OCO$\underline{C}H_3$), -4.1 (Si($\underline{C}H_3)_2$) ppm.

Allyl 2,4-di-*O*-acetyl-6-*O*-benzyl-3-*O*-methyl-α-D-mannopyranoside (27)

FTIR (ATR): 1743.29 (C=O), 1647.14 (C=C) cm^{-1}.

NMR data for the α-anomer described according to the literature: J. Ripoll-Rozada, M. Costa, J. A. Manso, A. Maranha, V. Miranda, A. Sequeira, M. R. Ventura, S. Macedo-Ribeiro, P. J. B. Pereira, N. Empadinhas; *Proc. Natl. Acad. Sci. U. S. A.* **2019**, 116 (3), 835-844.

2,4-Di-*O*-acetyl-6-*O*-benzyl-3-*O*-methyl-(α/β)-D-mannopyranoside (28)

FTIR (ATR): 3419.51 (O-H), 1743.65 (C=O) cm^{-1}.

NMR data for the α-anomer described according to the literature: J. Ripoll-Rozada, M. Costa, J. A. Manso, A. Maranha, V. Miranda, A. Sequeira, M. R. Ventura, S. Macedo-Ribeiro, P. J. B. Pereira, N. Empadinhas; *Proc. Natl. Acad. Sci. U. S. A.* **2019**, 116 (3), 835-844.

2,4-Di-*O*-acetyl-6-*O*-benzyl-3-*O*-methyl-α-D-mannopyranosyl trichloroacetamidate (29)

$[\alpha]_D^{20}$ +38.8 (c 0.95, CH_2Cl_2).

FTIR (ATR): 3316.9 (N-H), 1748.9 (C=O) cm^{-1}.

NMR data for the α-anomer described according to the literature: J. Ripoll-Rozada, M. Costa, J. A. Manso, A. Maranha, V. Miranda, A. Sequeira, M. R. Ventura, S. Macedo-Ribeiro, P. J. B. Pereira, N. Empadinhas; *Proc. Natl. Acad. Sci. U. S. A.* **2019**, 116 (3), 835-844.

Allyl 2-*O*-acetyl-6-*O*-benzyl-3-*O*-methyl-α-D-mannopyranosyl-(1→4)-2-*O*-acetyl-6-*O*-benzyl-3-*O*-methyl-α-D-mannopyranoside (30)

FTIR (ATR): 3468.2 (O-H), 1743.5 (C=O) cm^{-1}.

^{1}H-NMR ($CDCl_3$): δ 7.38 – 7.20 (m, 10H, Ar), 5.98 – 5.83 (m, 1H, $OCH_2C\underline{H}=CH_2$), 5.36 (dd, 1H, *J* = 1.2 Hz, *J* = 2.0 Hz, H-2 A), 5.34 – 5.27 (m, 2H, H-2 B and 1x$OCH_2CH=C\underline{H}_2$), 5.24 (d, 1H, *J* = 1.6 Hz, H-1 A), 5.21 (d, 2H, *J* = 1.6 Hz, 1x$OCH_2CH=C\underline{H}_2$), 4.86 (d, 1H, *J* = 1.6 Hz, H-1 B), 4.60 – 4.44 (m, 4H, $OC\underline{H}_2$Ph A-B), 4.24 – 4.15 (m, 1H, 1x$OC\underline{H}_2CH=CH_2$), 4.05 – 3.98 (m, 1H, 1x$OC\underline{H}_2CH=CH_2$), 3.96 – 3.73 (m, 6H, H-4 A-B, H-5 A-B and H-6 B), 3.70 – 3.65 (m, 1H, H-3 B), 3.65 – 3.55 (m, 2H, H-6 A), 3.48 – 3.44 (m, 1H, H-3 A), 3.42 (s, 3H, $OC\underline{H}_3$ A or B), 3.40 (s, 3H, $OC\underline{H}_3$ A or B), 2.08 (d, 6H, *J* = 0.8 Hz, $(OCOC\underline{H}_3)_2$) ppm.

^{13}C-NMR ($CDCl_3$): δ 170.3 (C=O), 170.1 (C=O), 138.4 (C_q), 138.1 (C_q), 133.4 ($OCH_2\underline{C}H=CH_2$), 128.6 (Ar), 128.3 (Ar), 127.6 (Ar), 127.4 (Ar), 118.0 ($OCH_2CH=\underline{C}H_2$), 99.7 (C-1 A), 96.7 (C-1 B), 80.1 (C-3 B), 79.1 (C-3 A), 73.6 ($O\underline{C}H_2$Ph A or B), 73.5 (C-4 B), 73.3 ($O\underline{C}H_2$Ph A or B), 72.0 (C-5 A or B), 70.9 (C-5 A or B), 70.1 (C-6 A), 69.6 (C-6 B), 68.4 ($O\underline{C}H_2CH=CH_2$), 67.6 (C-4 A), 67.6 (C-2 B), 67.3 (C-2 A), 57.4 ($O\underline{C}H_3$ A or B), 57.2 ($O\underline{C}H_3$ A or B), 21.0 ($OCO\underline{C}H_3$) ppm.

Allyl 2,4-di-*O*-acetyl-6-*O*-benzyl-3-*O*-methyl-α-D-mannopyranosyl-(1→4)-2-*O*-acetyl-6-*O*-benzyl-3-*O*-methyl-α-D-mannopyranoside (31)

FTIR (ATR): 1746.63 (C=O), 1652.68 (C=C) cm^{-1}.

NMR data for the α-anomer described according to the literature: J. Ripoll-Rozada, M. Costa, J. A. Manso, A. Maranha, V. Miranda, A. Sequeira, M. R. Ventura, S. Macedo-Ribeiro, P. J. B. Pereira, N. Empadinhas; *Proc. Natl. Acad. Sci. U. S. A.* **2019**, 116 (3), 835-844.

2,4-Di-*O*-acetyl-6-*O*-benzyl-3-*O*-methyl-α-D-mannopyranosyl-(1→4)-2-*O*-acetyl-6-*O*-benzyl-3-*O*-methyl-α-D-mannopyranose (32)

FTIR (ATR): 3418.6 (O-H),1743.5 (C=O) cm^{-1}.

NMR data for the α-anomer described according to the literature: J. Ripoll-Rozada, M. Costa, J. A. Manso, A. Maranha, V. Miranda, A. Sequeira, M. R. Ventura, S. Macedo-Ribeiro, P. J. B. Pereira, N. Empadinhas; *Proc. Natl. Acad. Sci. U. S. A.* **2019**, 116 (3), 835-844.

2,4-Di-*O*-acetyl-6-*O*-benzyl-3-*O*-methyl-α-D-mannopyranosyl-(1→4)-2-*O*-acetyl-6-*O*-benzyl-3-*O*-methyl-α-D-mannopyranosyl trichloroacetamidate (33)

$[\alpha]_D^{20}$ +28.8 (c 1, CH_2Cl_2).

FTIR (ATR): 3302.9 (O-H), 1747.1 (C=O) cm^{-1}.

^{1}H-NMR ($CDCl_3$): δ 8.74 (s, 1H, OC(N<u>H</u>)CCl_3), 7.35 – 7.21 (m, 10H, Ar), 6.29 (d, 1H, *J* = 1.6 Hz, H-1 B), 5.51 – 5.46 (m, 1H, H-2 B), 5.41 – 5.38 (m, 1H, H-2 A), 5.30 (d, 1H, *J* = 2 Hz, H-1 A), 5.19 (t, 1H, *J* = 10.0 Hz, H-4 B), 4.60 – 4.36 (m, 4H, OC<u>H</u>$_2$Ph A- B), 4.08 – 3.97 (m, 2H, H-4 A and H-5 A), 3.91 – 3.82 (m, 1H, H-5 B), 3.82 – 3.73 (m, 2H, H-6 A), 3.71 (dd, 1H, *J* = 5.6 Hz, *J* = 3.4 Hz, H-3 A), 3.58 (dd, 1H, *J* = 6.4 Hz, *J* = 3.2 Hz, H-3 B), 3.49 – 3.40 (m, 5H, H-6 B and OC<u>H</u>$_3$ A or B), 3.39 – 3.33 (m, 3H, OC<u>H</u>$_3$ A or B), 2.11 (d, 6H, *J* = 3.4 Hz, (OCOC<u>H</u>$_3$)$_2$), 1.97 (s, 3H, OCOC<u>H</u>$_3$) ppm.

^{13}C-NMR ($CDCl_3$): δ 170.2 (C=O), 169.9 (C=O), 138.4 (C_q), 138.0 (C_q), 128.5 (Ar), 128.3 (Ar), 128.2 (Ar), 127.8 (Ar), 127.6 (Ar), 127.5 (Ar), 99.4 (C-1 A), 95.1 (C-1 B), 80.0 (C-3 A), 76.7 (C-3 B), 73.9 (C-5 A), 73.5 (O<u>C</u>H$_2$Ph A or B), 73.3 (O<u>C</u>H$_2$Ph A or B), 72.6 (C-4 A), 70.8 (C-5 B), 69.3 (C-6 A), 69.2 (C-6 B), 68.2 (C-4 A), 67.7 (C-2 A), 66.0 (C-2 B), 57.6 (O<u>C</u>H$_3$ A or B), 57.2 (O<u>C</u>H$_3$ A or B), 21.0 (OCO<u>C</u>H$_3$), 20.9 (OCO<u>C</u>H$_3$), 20.8 (OCO<u>C</u>H$_3$) ppm.

Allyl 2,4-di-*O*-acetyl-6-*O*-benzyl-3-*O*-methyl-α-D-mannopyranosyl-(1→4)-2-*O*-acetyl-6-*O*-benzyl-3-*O*-methyl-α-D-mannopyranosyl-(1→4)-2-*O*-acetyl-6-*O*-benzyl-3-*O*-methyl-α-D-mannopyranosyl-(1→4)-2-*O*-acetyl-6-*O*-benzyl-3-*O*-methyl-α-D-mannopyranoside (34)

FTIR (ATR): 1743.3 (C=O) cm^{-1}.

^{1}H-NMR ($CDCl_3$): δ 7.40 – 7.17 (m, 20H, Ar), 5.98 – 5.85 (m, 1H, OCH_2C<u>H</u>$=CH_2$), 5.43 – 5.14 (m, 10H, H-1 A-C, H-2 A-D, H-4 A, $OCH_2CH=C$<u>H</u>$_2$), 4.86 (d, 1H, *J* = 1.6 Hz, H-1 D), 4.65 – 4.37 (m, 8H, OC<u>H</u>$_2$Ph A-D) 4.21 (dd, 1H, *J* = 7.2 Hz, *J* = 5.6 Hz, 1xOC<u>H</u>$_2$CH=CH$_2$), 4.02 (dd, 1H, *J* = 12.8 Hz, *J* = 6.2 Hz, 1xOC<u>H</u>$_2$CH=CH$_2$), 3.96 – 3.51 (m, 17H, H-3 A-D, H-4 A-D, H-5 A-D and H-6 A-C), 3.47 – 3.27 (m, 14H, H-6 D and OC<u>H</u>$_3$ A-D), 2.16 – 1.95 (m, 15H, (OCOC<u>H</u>$_3$)$_5$) ppm.

^{13}C-NMR ($CDCl_3$): δ 170.3 (C=O), 170.1 (C=O), 170.0 (C=O), 169.9 (C=O), 169.8 (C=O), 138.5 (C_q), 138.0 (C_q), 133.4 (OCH_2<u>C</u>H$=CH_2$), 128.5 (Ar), 128.4 (Ar), 128.3 (Ar), 128.2 (Ar), 128.1 (Ar), 127.8 (Ar), 127.7 (Ar), 127.6 (Ar), 127.5 (Ar), 127.4 (Ar), 118.1 ($OCH_2CH=$<u>C</u>H$_2$), 99.7 (C-1 A or B or C), 99.6 (C-1 A or B or C), 99.4 (C-1 A or B or C), 96.7 (C-1 D), 79.9 (C-3 A or B or C or D), 79.7 (C-3 A or B or C or D), 79.0 (C-3 A or B or C or D), 76.9 (C-3 A or B or C or D), 74.7, 74.2, 73.6, 73.5 (O<u>C</u>H$_2$Ph A or B or C or D), 73.4 (O<u>C</u>H$_2$Ph A or B or C or D), 73.3 (O<u>C</u>H$_2$Ph A or B or C or D), 73.2 (O<u>C</u>H$_2$Ph A or B or C or D), 71.9, 71.8, 71.1, 70.8, 70.0 (C-6 A or B or C or D), 69.9 (C-6 A or B or C or D), 69.8 (C-6 A or B or C or D), 69.4 (C-6 A or B or C or D), 68.5 (O<u>C</u>H$_2$CH=CH$_2$), 68.3 (C-4 A), 67.7 (C-2 A or B or C or D), 67.5 (C-2 A or B or C or D), 67.4 (C-2 A or B or C or D), 67.3 (C-2 A or B or C or D), 57.5 (O<u>C</u>H$_3$ A or B or C or D), 57.2 (O<u>C</u>H$_3$ A or B or C or D), 57.1 (O<u>C</u>H$_3$ A or B or C or D), 57.0 (O<u>C</u>H$_3$ A or B or C or D), 21.0 (OCO<u>C</u>H$_3$), 20.9 (OCO<u>C</u>H$_3$) ppm.

Allyl 6-*O*-benzyl-3-*O*-methyl-α-D-mannopyranosyl-(1→4)-6-*O*-benzyl-3-*O*-methyl-α-D-mannopyranosyl-(1→4)-6-*O*-benzyl-3-*O*-methyl-α-D-mannopyranosyl-(1→4)-6-*O*-benzyl-3-*O*-methyl-α-D-mannopyranoside (35)

FTIR (ATR): 3422.7 (O-H) cm^{-1}.

^{1}H-NMR (MeOD): δ 7.41 – 7.16 (m, 20H, Ar), 6.03 – 5.92 (m, 1H, $OCH_2C\underline{H}=CH_2$), 5.32 (dd, 1H, *J* = 15.6 Hz, *J* = 1.6 Hz, 1x$OCH_2CH=C\underline{H}_2$), 5.23 – 5.16 (m, 4H, H-1 A-C and 1x$OCH_2CH=C\underline{H}_2$), 4.85 (s, 1H, H-1 D), 4.58 – 4.31 (m, 8H, $OC\underline{H}_2$Ph A-D), 4.23 (dd, 1H, *J* = 8 Hz, *J* = 5 Hz, 1x$OC\underline{H}_2CH=CH_2$), 4.17 – 4.00 (m, 5H, 1x$OC\underline{H}_2CH=CH_2$ and H-2 A-D) 3.97 – 3.64 (m, 15H, H-4 A-D, H-5 A-D, H-6 A or B or C or D), 3.57 (d, 1H, *J* = 4.1 Hz, 1xH-6 A or B or C or D), 3.55 – 3.49 (m, 2H, H-3 A or B or C or D), 3.49 – 3.38 (m, 14H, $OC\underline{H}_3$ A-D and H-3 A or B or C or D) ppm.

^{13}C-NMR (MeOD): δ 128.1 (Ar) 127.9 (Ar), 127.7 (Ar), 127.6 (Ar), 127.2 (Ar), 116.3 ($OCH_2CH=\underline{C}H_2$), 102.4 (C-1 A or B or C), 102.0 (C-1 A or B or C), 101.8 (C-1 A or B or C), 99.1 (C-1 D), 81.9 (C-3 A or B or C or D), 81.5 (C-3 A or B or C or D), 80.8 (C-3 A or B or C or D) 73.6, 73.4, 73.3, 73.2 ($O\underline{C}H_2$Ph A or B or C or D), 73.1 ($O\underline{C}H_2$Ph A or B or C or D), 73.0 ($O\underline{C}H_2$Ph A or B or C or D), 72.8 ($O\underline{C}H_2$Ph A or B or C or D), 71.8, 71.6, 71.5, 70.7, 70.0 (C-6 A or B or C or D), 69.9 (C-6 A or B or C or D), 67.8 ($O\underline{C}H_2CH=CH_2$), 66.7 (C-2 A or B or C or D), 66.3 (C-2 A or B or C or D), 66.1 (C-2 A or B or C or D), 56.0 ($O\underline{C}H_3$ A or B or C or D), 55.3 ($O\underline{C}H_3$ A or B or C or D) 55.2 ($O\underline{C}H_3$ A or B or C or D) ppm.

Propyl 3-*O*-methyl-α-D-mannopyranosyl-(1→4)-3-*O*-methyl-α-D-mannopyranosyl-(1→4)-3-*O*-methyl-α-D-mannopyranosyl-(1→4)-3-*O*-methyl-α-D-mannopyranoside (3)

FTIR (ATR): 3306.2 (O-H) cm^{-1}.

^{1}H-NMR (D_2O): δ 5.14 (s, 3H, H-1 A-C), 4.83 (d, 1H, *J* = 1.5 Hz, H-1 D), 4.20 – 4.04 (m, 4H, H-2 A-D), 3.86 – 3.56 (m, 20H, H-4 A-D, H-5 A-D, H-6 A-D, 1x$OC\underline{H}_2CH_2CH_3$, H-3 A or B or C or D), 3.48 – 3.32 (m, 14H, $OC\underline{H}_3$ A-D, 1x$OC\underline{H}_2CH_2CH_3$ and H-3 A or B or C or D), 1.59 – 1.46 (m, 2H, $OCH_2C\underline{H}_2CH_3$), 0.85 (t, 3H, *J* = 7.6 Hz, $OCH_2CH_2C\underline{H}_3$) ppm.

^{13}C-NMR (D_2O): δ 101.3 (C-1 A or B or C), 101.2 (C-1 A or B or C), 101.1 (C-1 A or B or C), 99.4 (C-1 D), 81.0, 80.7, 79.7, 73.7, 72.6, 72.3, 72.2, 72.1, 71.0, 69.7 ($O\underline{C}H_2CH_2CH_3$), 66.1 (C-2 A or B or C or D), 66.0 (C-2 A or B or C or D), 65.8 (C-2 A or B or C or D), 65.4 (C-2 A or B or C or D), 60.9 (C-6 A or B or C or D), 60.8 (C-6 A or B or C or D), 56.1 ($O\underline{C}H_3$ A-D), 21.9 ($OCH_2\underline{C}H_2CH_3$), 9.7 ($OCH_2CH_2\underline{C}H_3$) ppm.

HR-MS: calcd. for $C_{31}H_{57}O_{21}$ $[M + H]^+$: 765.3387; found: 765.3388.

Allyl 2,4-di-*O*-acetyl-6-*O*-benzyl-3-*O*-methyl-α-D-mannopyranosyl-(1→4)-2-*O*-acetyl-6-*O*-benzyl-3-*O*-methyl-α-D-mannopyranosyl-(1→4)-2-*O*-acetyl-6-*O*-benzyl-3-*O*-methyl-α-D-mannopyranoside (36)

FTIR (ATR): 1743.8 (C=O) cm^{-1}.

^{1}H-NMR ($CDCl_3$): δ 7.36 – 7.21 (m, 15H, Ar), 5.99 – 5.83 (m, 1H, $OCH_2C\underline{H}=CH_2$), 5.40 – 5.36 (m, 2H, H-2 A-B), 5.34 – 5.30 (m, 1H, H-2 C), 5.29 (d, 1H, *J* = 1.5 Hz, 1x$OCH_2CH=C\underline{H}_2$), 5.24 (s, 1H, H-1 A or B), 5.23 – 5.21 (m, 1H, 1x$OCH_2CH=C\underline{H}_2$), 5.17 (dd, 2H, *J* = 2 Hz, *J* = 4 Hz, H-1 A or B and H-4 A), 4.86 (d, 1H, *J* = 1.7 Hz, H-1 C) , 4.66 – 4.38 (m, 6H, $OC\underline{H}_2$Ph A-C), 4.25 – 4.18 (m, 1H, 1x$OC\underline{H}_2CH=CH_2$), 4.02 (dd, 1H, *J* = 6.4 Hz, *J* = 6.4 Hz, 1x$OC\underline{H}_2CH=CH_2$), 3.94 – 3.54 (m, 12H, H-3 A-C, H-4 B-C, H-5 A-C and H-6 A or B or C), 3.49 – 3.31 (m, 11H, $OC\underline{H}_3$ A-C and H-6 A or B or C), 2.12 – 2.04 (m, 9H, $(OCOC\underline{H}_3)_3$), 1.98 (s, 3H, $OCOC\underline{H}_3$) ppm.

^{13}C-NMR ($CDCl_3$): δ 170.1 (C=O), 170.0 (C=O), 138.5 (C_q), 138.0 (C_q), 133.4 ($OCH_2\underline{C}H=CH_2$), 128.3 (Ar), 128.2 (Ar), 127.8 (Ar), 127.6 (Ar), 127.4 (Ar), 118.0 ($OCH_2CH=\underline{C}H_2$), 99.7 (C-1 A or B), 99.4 (C-1 A or B), 96.7 (C-1 C), 79.9 (C-3 A or B or C), 79.8 (C-3 A or B or C), 76.8 (C-3 A or B or C), 74.6, 73.6, 73.5 ($O\underline{C}H_2$Ph A or B or C), 73.4 ($O\underline{C}H_2$Ph A or B or C), 73.3 ($O\underline{C}H_2$Ph A or B or C), 71.9, 71.0, 70.8, 69.9 (C-6 A or B or C), 69.4 (C-6 A or B or C), 68.5 ($O\underline{C}H_2CH=CH_2$), 68.3 (C-4 A), 67.7 (C-2 A or B or C), 67.5 (C-2 A or B or C), 67.4 (C-2 A or B or C), 57.6 ($O\underline{C}H_3$ A or B or C), 57.2 ($O\underline{C}H_3$ A or B or C), 57.1 ($O\underline{C}H_3$ A or B or C), 21.0 ($OCO\underline{C}H_3$), 20.9 ($OCO\underline{C}H_3$) ppm.

Allyl 6-*O*-benzyl-3-*O*-methyl-α-D-mannopyranosyl-(1→4)-6-*O*-benzyl-3-*O*-methyl-α-D-mannopyranosyl-(1→4)-6-*O*-benzyl-3-*O*-methyl-α-D-mannopyranoside (37)

FTIR (ATR): 3415.7 (O-H) cm^{-1}.

^{1}H-NMR (MeOD): δ 7.42 – 7.22 (m, 15H, Ar), 6.03 – 5.90 (m, 1H, $OCH_2C\underline{H}=CH_2$), 5.43 – 5.12 (m, 4H, H-1 A-B and $OCH_2CH=C\underline{H}_2$), 4.84 (d, 1H, *J* = 1.6 Hz, H-1 C), 4.69 – 4.35 (m, 6H, $OC\underline{H}_2$Ph A-C), 4.26 – 4.16 (m, 1H, 1x$OC\underline{H}_2CH=CH_2$), 4.15 – 3.99 (m, 4H, H-2 A-C and 1x$OC\underline{H}_2CH=CH_2$), 3.95 – 3.61 (m, 12H, H-4 A-C, H-5 A-C and H-6 A-C), 3.59 – 3.36 (m, 12H, OCH_3 A-C) ppm.

^{13}C-NMR (MeOD): δ 133.9 ($OCH_2\underline{C}H=CH_2$), 128.0 (Ar), 127.9 (Ar), 127.6 (Ar), 127.5 (Ar), 127.3 (Ar), 127.2 (Ar), 127.1 (Ar), 116.3 ($OCH_2CH=\underline{C}H_2$), 102.3 (C-1 A or B), 102.0 (C-1 A or B), 99.1 (C-1 C), 81.8 (C-3 A or B or C), 81.5 (C-3 A or B or C), 80.7 (C-3 A or B or C), 73.7, 73.5, 73.2 ($O\underline{C}H_2$Ph A or B or C), 73.1 ($O\underline{C}H_2$Ph A or B or C), 72.9 ($O\underline{C}H_2$Ph A or B or C), 71.8, 70.8, 69.9 (C-6 A or B or C), 69.8 (C-6 A or B or C), 69.6 (C-6 A or B or C), 67.8 ($O\underline{C}H_2CH=CH_2$), 66.7 (C-2 A or B or C), 66.4 (C-2 A or B or C), 66.1 (C-2 A or B or C), 66.0, 55.9 ($O\underline{C}H_3$ A or B or C), 55.3 ($O\underline{C}H_3$ A or B or C) ppm.

Propyl 3-*O*-methyl-α-D-mannopyranosyl-(1→4)-3-*O*-methyl-α-D-mannopyranosyl-(1→4)-3-*O*-methyl-α-D-mannopyranoside (4)

FTIR (ATR): 3351.8 (O-H) cm^{-1}.

^{1}H-NMR (D_2O): δ 5.15 – 5.12 (m, 2H, H-1 A and B), 4.87 – 4.82 (m, 1H, H-1 C), 4.16 – 4.09 (m, 3H, H-2 A-C), 3.83 – 3.53 (m, 17H, H-3 A-C, H-4 A-C, H-5 A-C, H-6 A-C and $OC\underline{H}_2CH_2CH_3$), 3.47 – 3.33 (m, 9H, $OC\underline{H}_3$ A-C), 1.58 – 1.51 (m, 2H, $OCH_2C\underline{H}_2CH_3$), 0.85 (dd, 3H, *J* = 12.4 Hz, *J* = 5.1 Hz, $OCH_2CH_2C\underline{H}_3$).

^{13}C-NMR (D_2O): δ 101.3 (C-1 A or B), 101.2 (C-1 A or B), 99.4 (C-1 C), 81.0, 80.7, 80.2, 80.0, 79.7, 73.7, 72.7, 72.3, 72.2, 71.0, 69.7 ($O\underline{C}H_2CH_2CH_3$), 69.5, 66.1, 66.0, 65.8, 65.4, 60.9 (C-6 A or B or C), 60.8 (C-6 A or B or C), 56.2 ($O\underline{C}H_3$ A or B or C), 56.1 ($O\underline{C}H_3$ A or B or C), 56.0 ($O\underline{C}H_3$ A or B or C), 21.9 ($OCH_2\underline{C}H_2CH_3$), 9.9 ($OCH_2CH_2\underline{C}H_3$).

HR-MS: calcd for $C_{24}H_{44}NaO_{16}$ $[M + Na]^+$: 611.2522; found: 611.2521.

NMR spectra of newly synthetized compounds

^{1}H-NMR (400 MHz) spectrum of allyl 2,3-di-*O*-acetyl-6-*O*-benzyl-α-D-mannopyranoside (8)

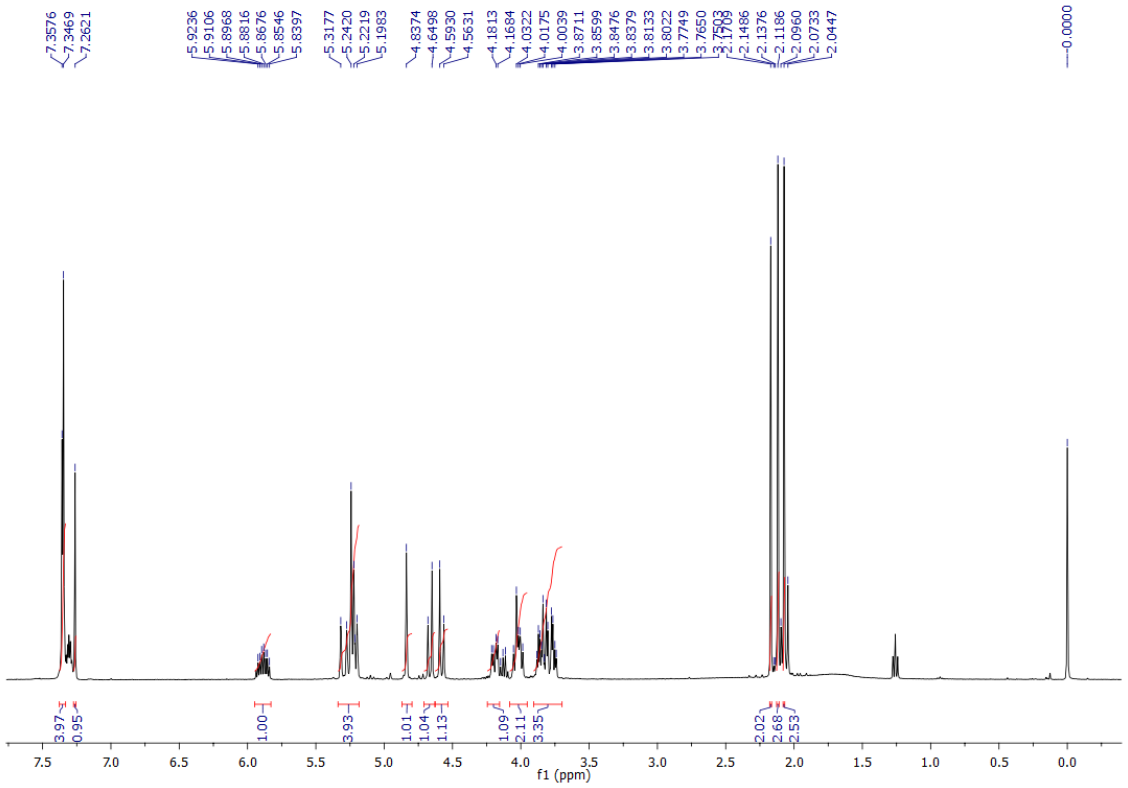

^{13}C-NMR (100.61 MHz) spectrum of allyl 2,3-di-*O*-acetyl-6-*O*-benzyl-α-D-mannopyranoside (8)

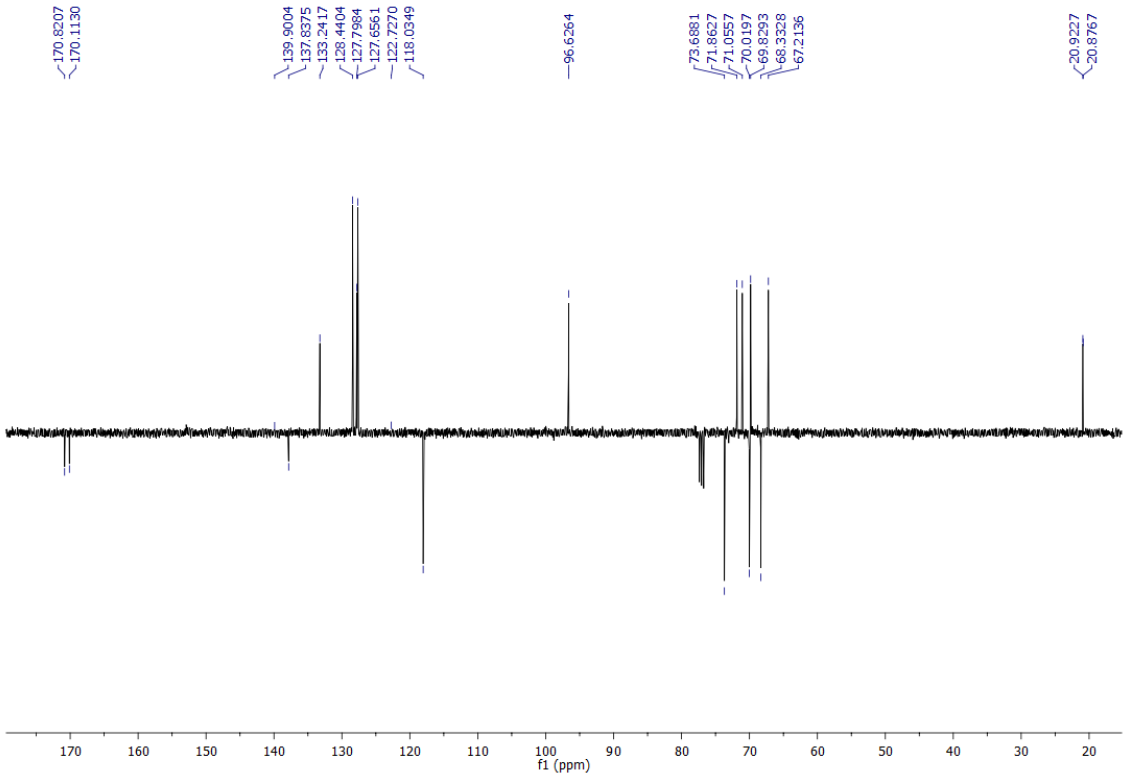

^{1}H-NMR (400 MHz) spectrum of allyl 2,3-di-*O*-acetyl-6-*O*-benzyl-4-*O*-tert-butyldimethylsilyl-α-D-mannopyranoside (9)

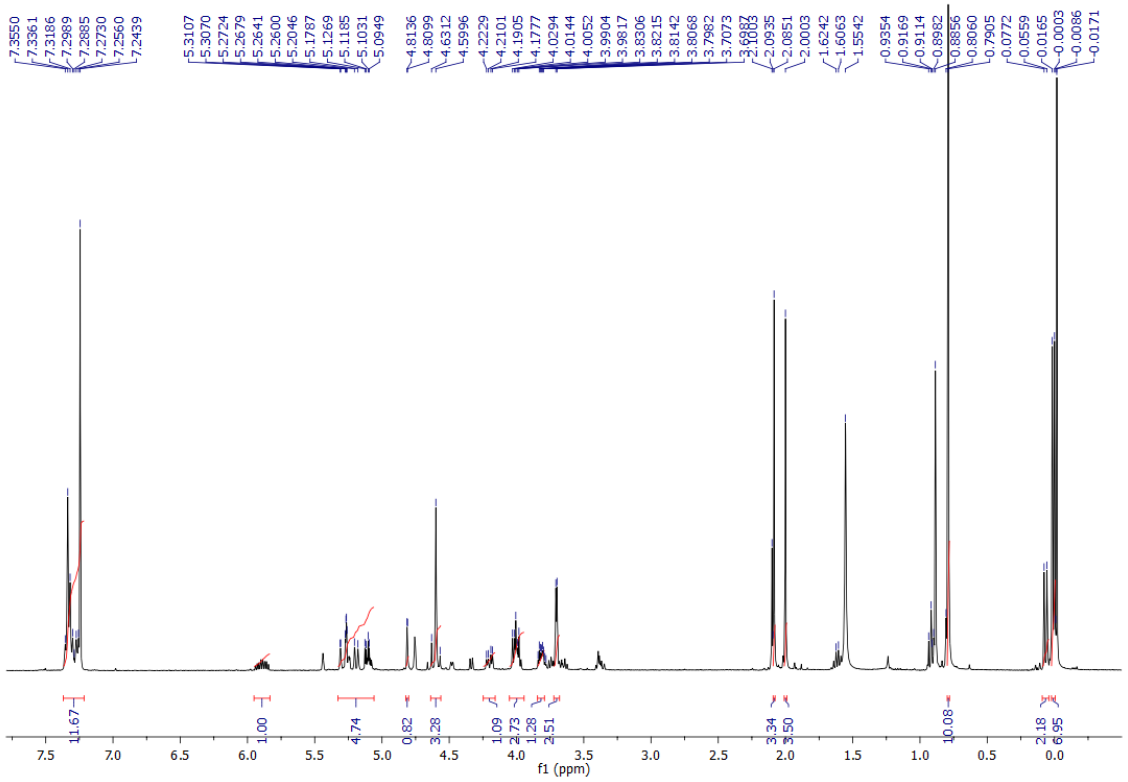

^{13}C-NMR (100.61 MHz) spectrum of allyl 2,3-di-*O*-acetyl-6-*O*-benzyl-4-*O*-tert-butyldimethylsilyl-α-D-mannopyranoside (9)

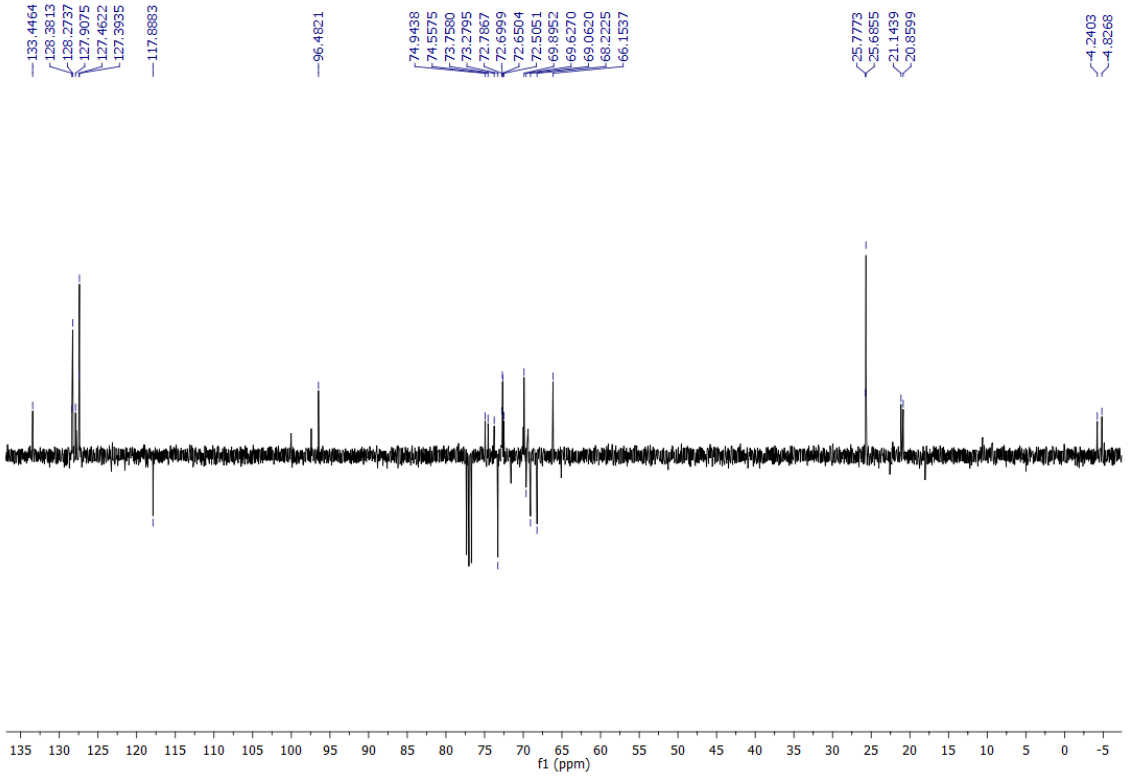

^{1}H-NMR (400 MHz) spectrum of 2,3-di-*O*-acetyl-6-*O*-benzyl-4-*O*-tert-butyldimethylsilyl-α-D-mannopyranoside (10)

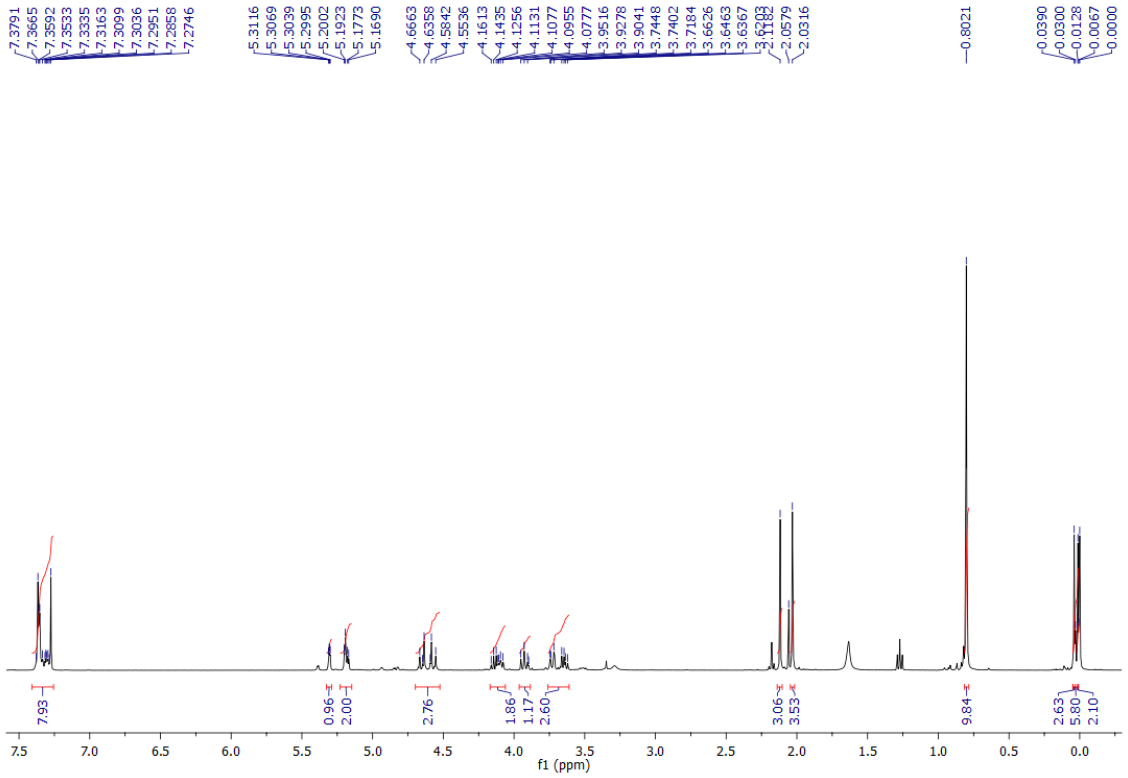

^{13}C-NMR (100.61 MHz) spectrum of 2,3-di-*O*-acetyl-6-*O*-benzyl-4-*O*-tert-butyldimethylsilyl-α-D-mannopyranoside (10)

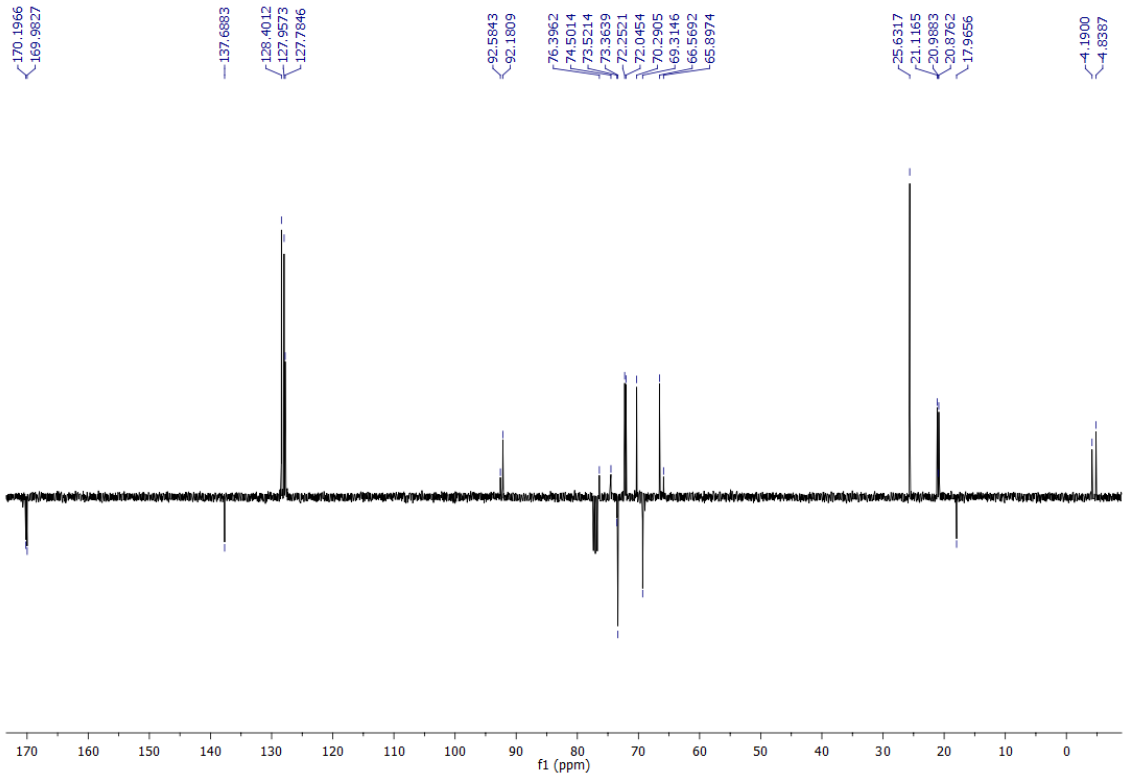

^{1}H-NMR (400 MHz) spectrum of 2,3-di-*O*-acetyl-6-*O*-benzyl-4-*O*-tert-butyldimethylsilyl-α-D-mannopyranosyl trichloroacetamidate (11)

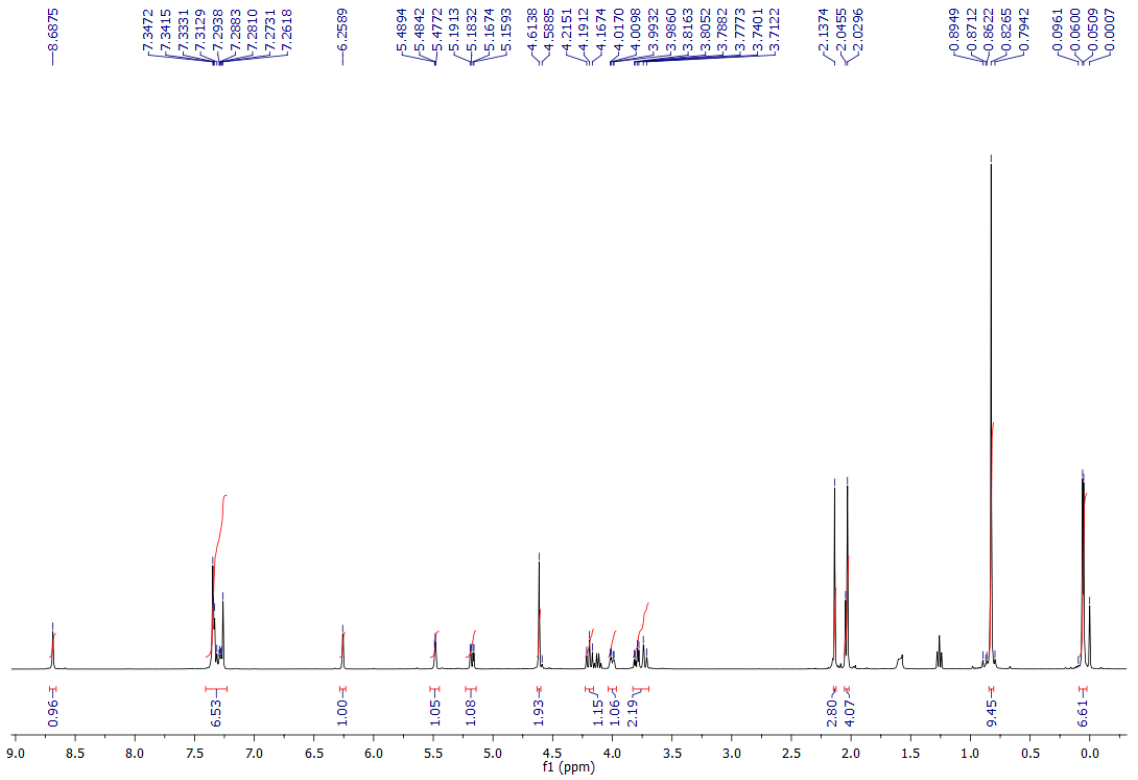

^{13}C-NMR (100.61 MHz) spectrum of 2,3-di-*O*-acetyl-6-*O*-benzyl-4-*O*-tert-butyldimethylsilyl-α-D-mannopyranosyl trichloroacetamidate (11)

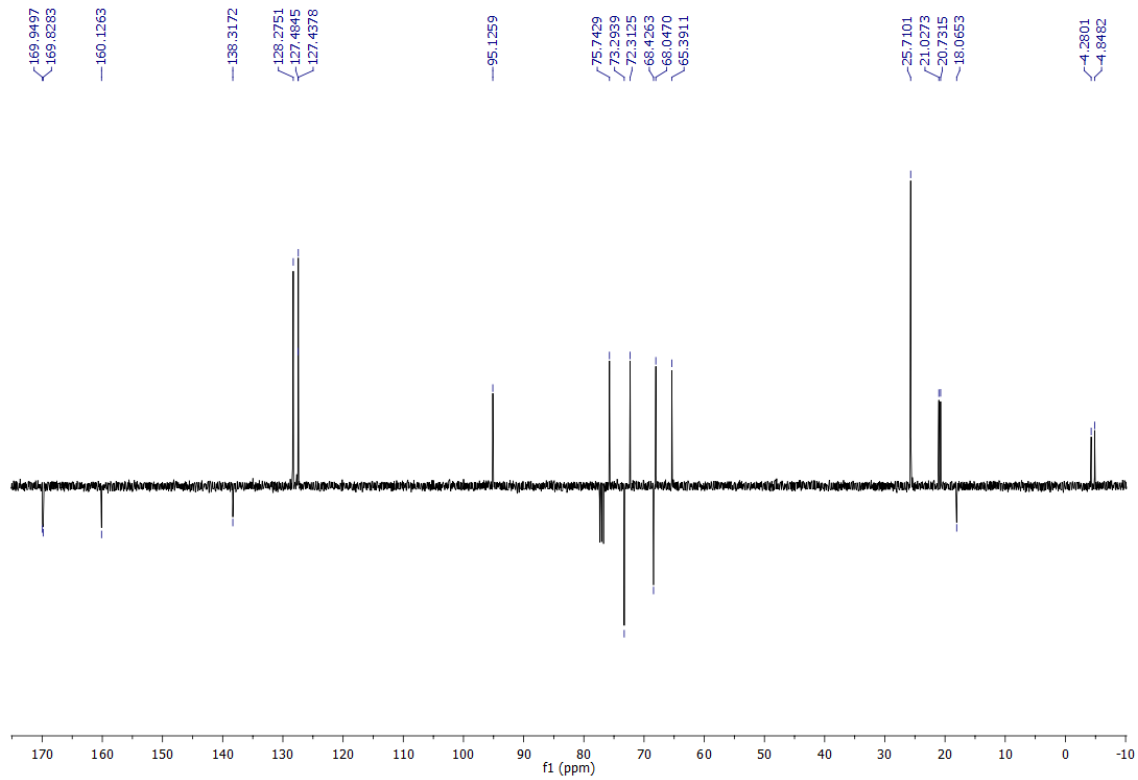

^{1}H-NMR (400 MHz) spectrum of allyl 2,3-di-*O*-acetyl-6-*O*-benzyl-4-*O*-*tert*-butyldimethylsilyl-α-D-mannopyranosyl-(1→4)-2,3-di-*O*-acetyl-6-*O*-benzyl-α-D-mannopyranoside (12)

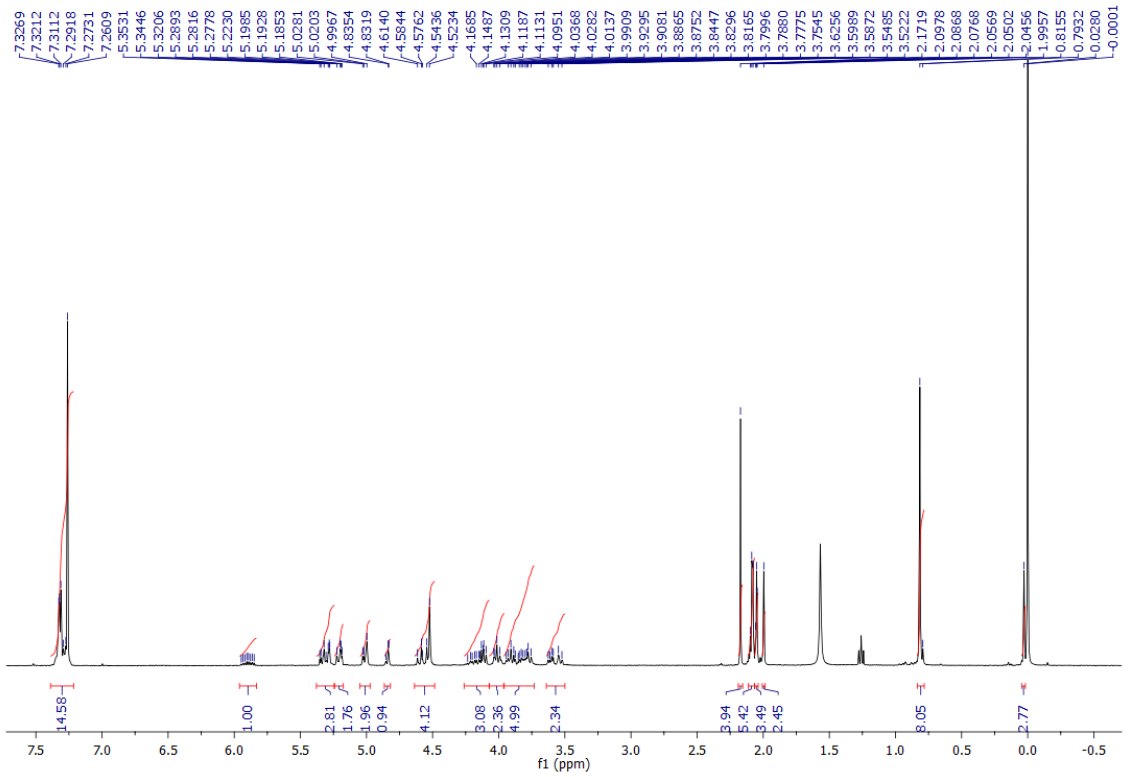

^{13}C-NMR (100.61 MHz) spectrum of allyl 2,3-di-*O*-acetyl-6-*O*-benzyl-4-*O*-*tert*-butyldimethylsilyl-α-D-mannopyranosyl-(1→4)-2,3-di-*O*-acetyl-6-*O*-benzyl-α-D-mannopyranoside (12)

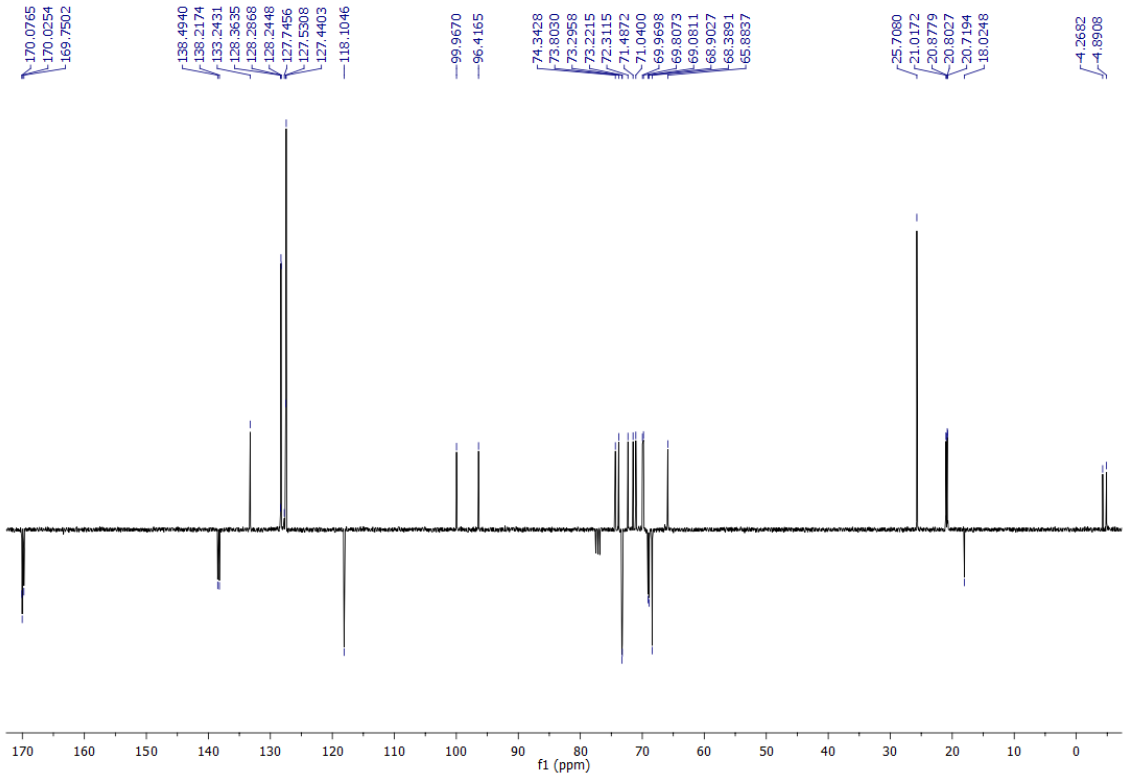

^{1}H-NMR (400 MHz) spectrum of allyl 2,3-di-*O*-acetyl-6-*O*-benzyl-α-D-mannopyranosyl-(1→4)-2,3-di-*O*-acetyl-6-*O*-benzyl-α-D-mannopyranoside (13)

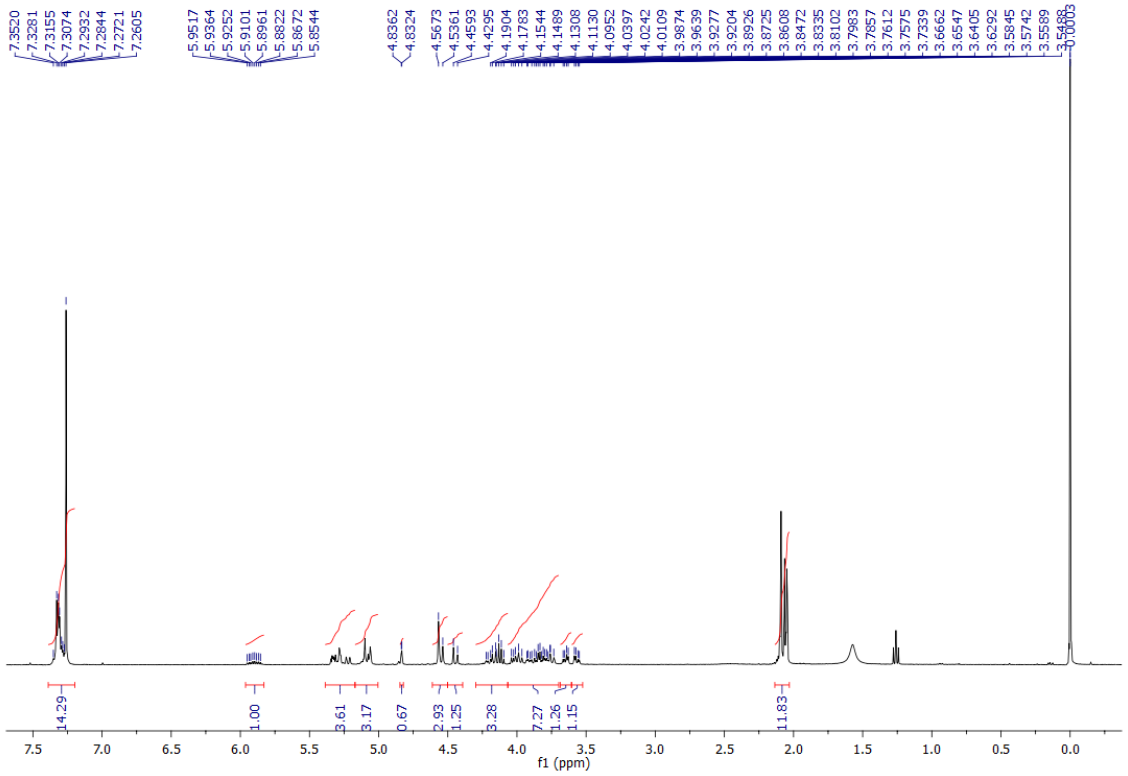

^{13}C-NMR (100.61 MHz) spectrum of allyl 2,3-di-*O*-acetyl-6-*O*-benzyl-α-D-mannopyranosyl-(1→4)-2,3-di-*O*-acetyl-6-*O*-benzyl-α-D-mannopyranoside (13)

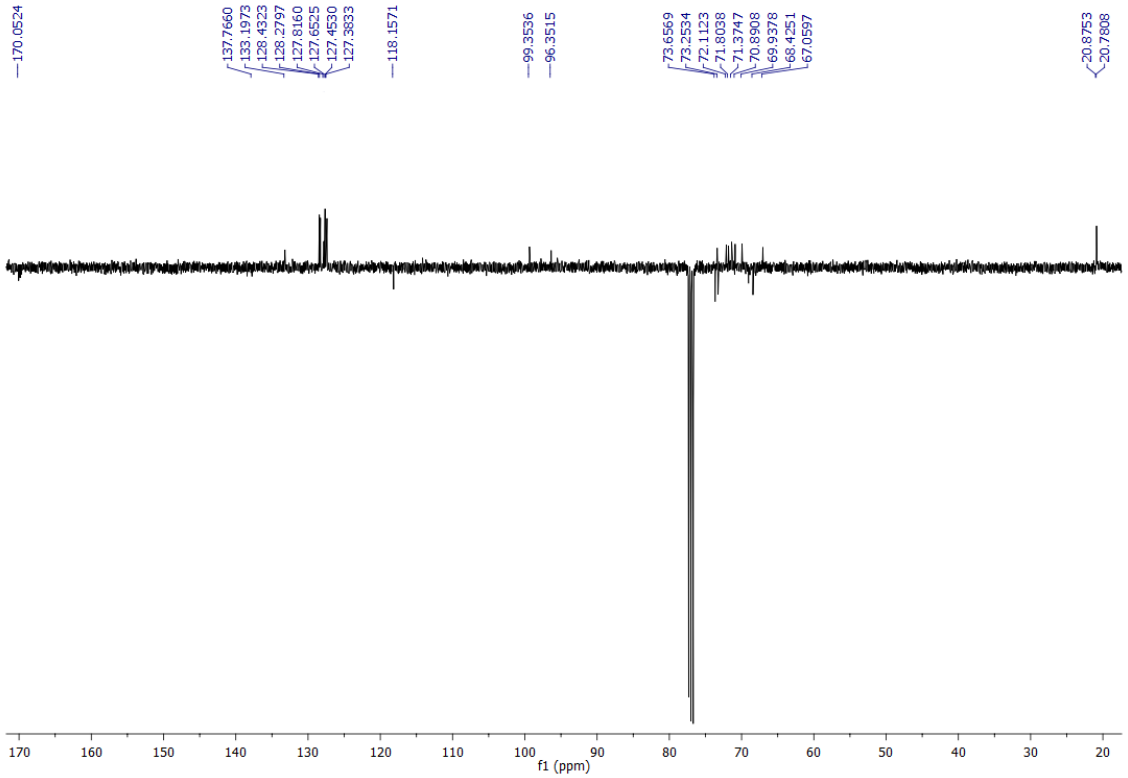

^{1}H-NMR (400 MHz) spectrum of allyl 2,3,4-tri-*O*-acetyl-6-*O*-benzyl-α-D-mannopyranosyl-(1→4)-2,3-di-*O*-acetyl-6-*O*-benzyl-α-D-mannopyranoside (14)

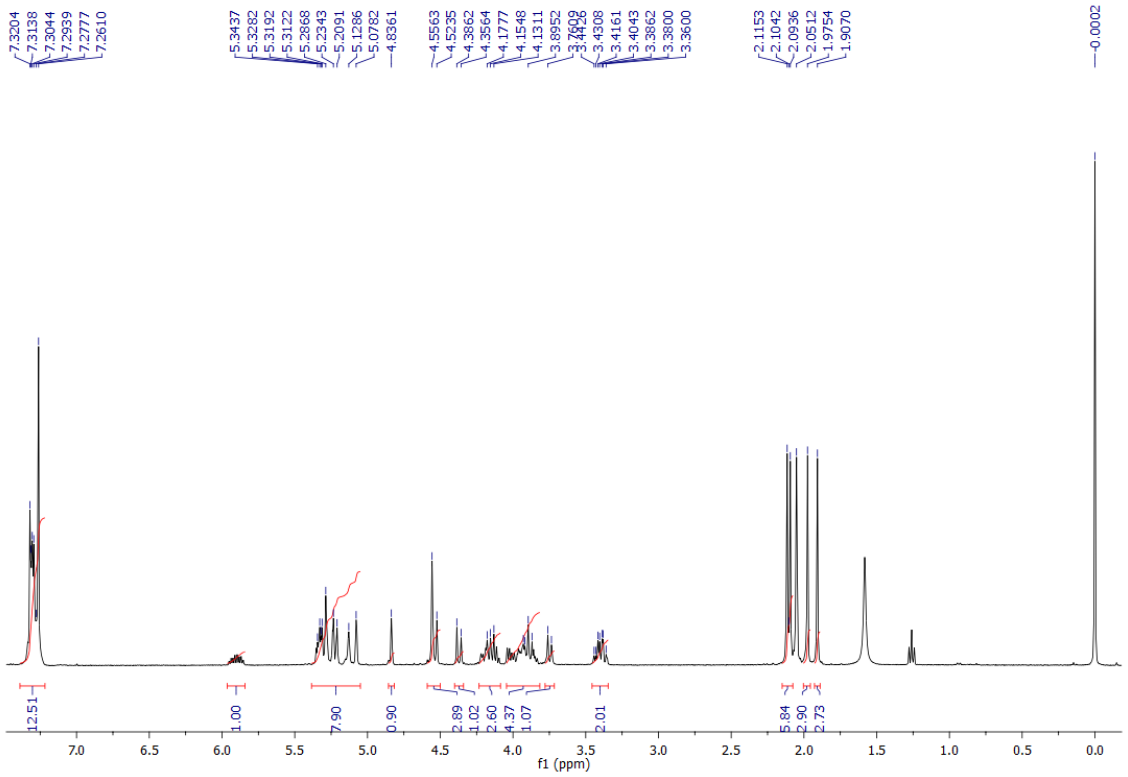

^{13}C-NMR (100.61 MHz) spectrum of allyl 2,3,4-tri-*O*-acetyl-6-*O*-benzyl-α-D-mannopyranosyl-(1→4)-2,3-di-*O*-acetyl-6-*O*-benzyl-α-D-mannopyranoside (14)

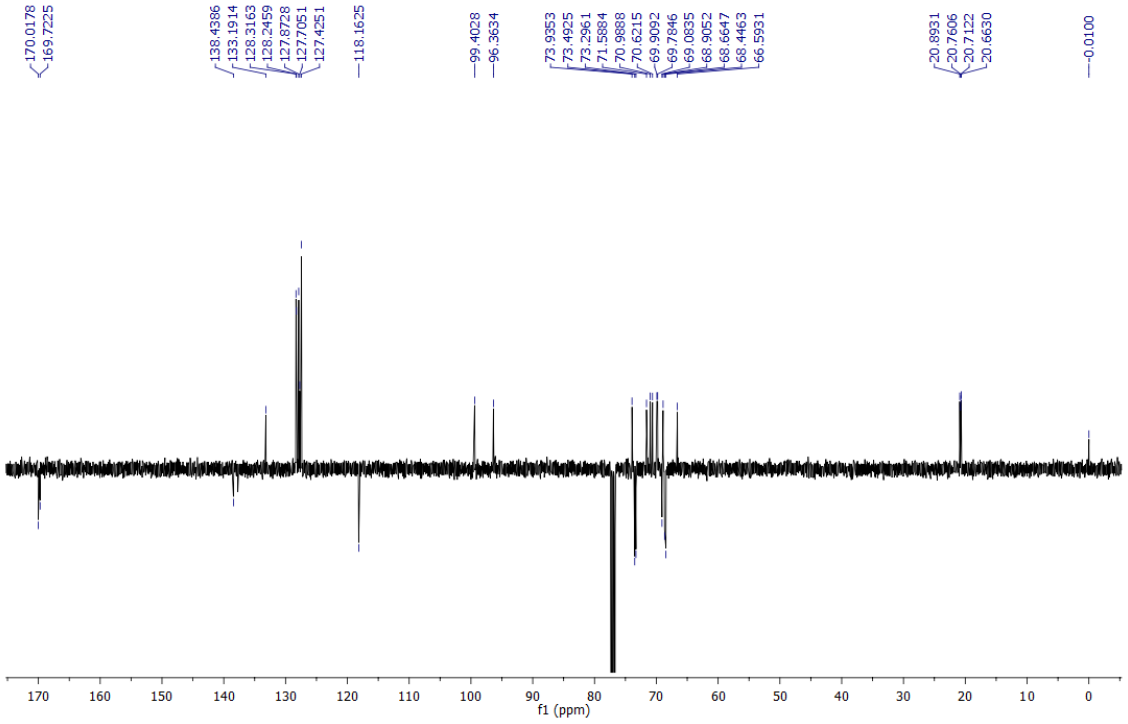

^{1}H-NMR (400 MHz) spectrum of 2,3,4-tri-*O*-acetyl-6-*O*-benzyl-α-D-mannopyranosyl-(1→4)-2,3-di-*O*-acetyl-6-*O*-benzyl-α-D-mannopyranoside (15)

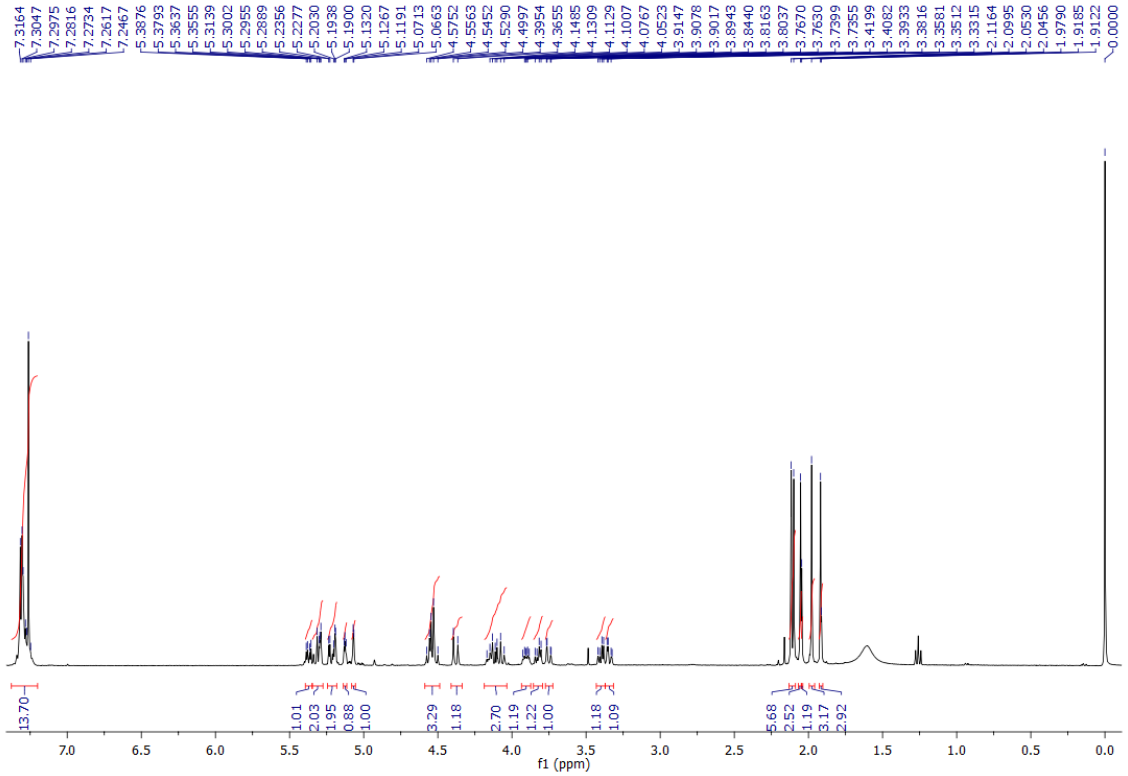

^{13}C-NMR (100.61 MHz) spectrum of 2,3,4-tri-*O*-acetyl-6-*O*-benzyl-α-D-mannopyranosyl-(1→4)-2,3-di-*O*-acetyl-6-*O*-benzyl-α-D-mannopyranoside (15)

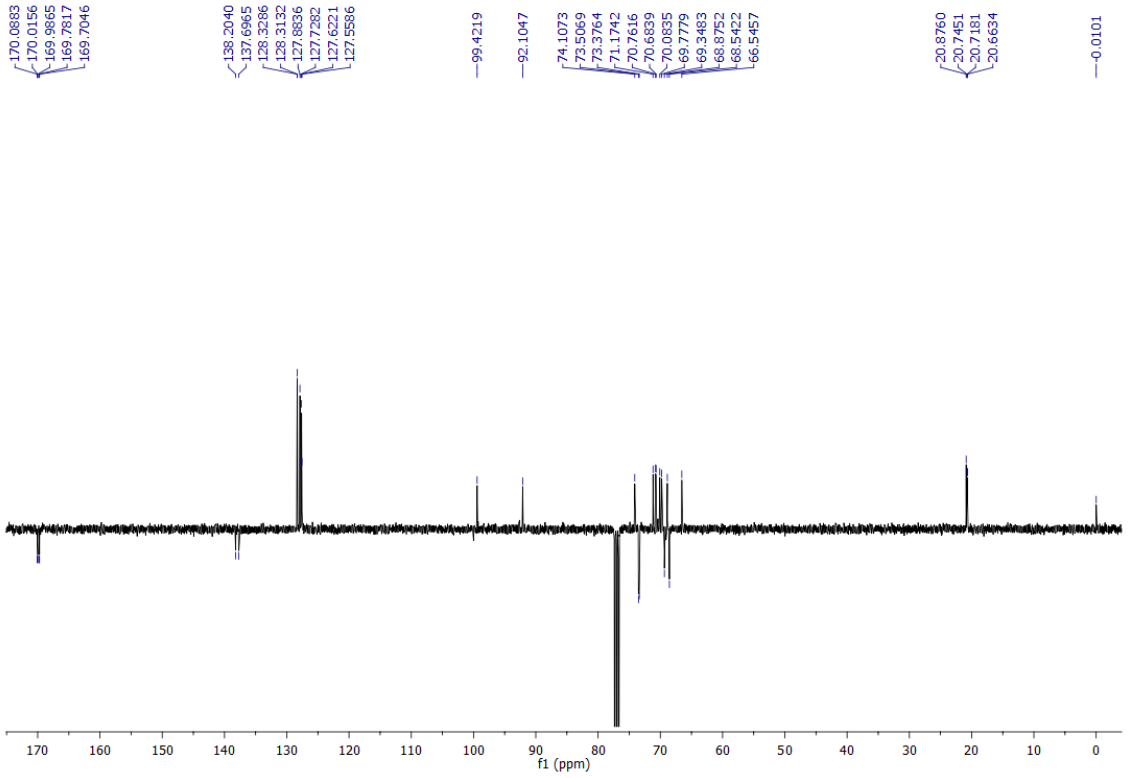

^{1}H-NMR (400 MHz) spectrum of 2,3,4-tri-*O*-acetyl-6-*O*-benzyl-α-D-mannopyranosyl-(1→4)-2,3-di-*O*-acetyl-6-*O*-benzyl-α-D-mannopyranosyl trichloroacetamidate (16)

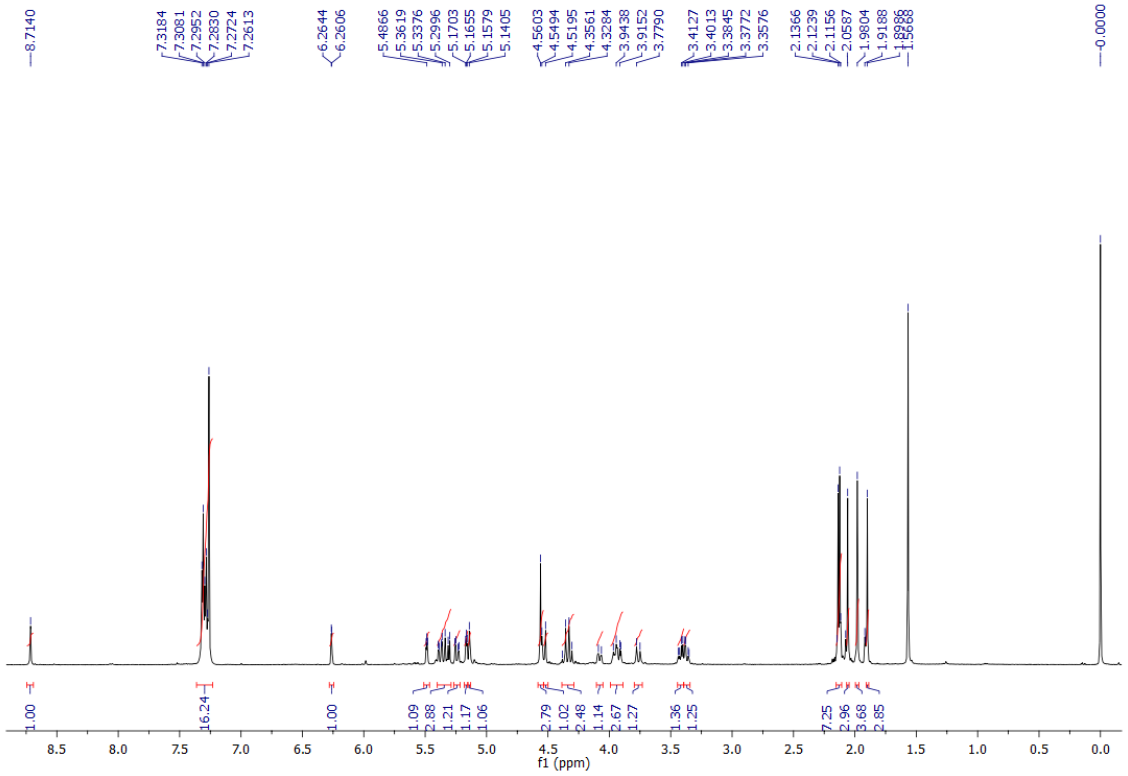

^{13}C-NMR (100.61 MHz) spectrum of 2,3,4-tri-*O*-acetyl-6-*O*-benzyl-α-D-mannopyranosyl-(1→4)-2,3-di-*O*-acetyl-6-*O*-benzyl-α-D-mannopyranosyl trichloroacetamidate (16)

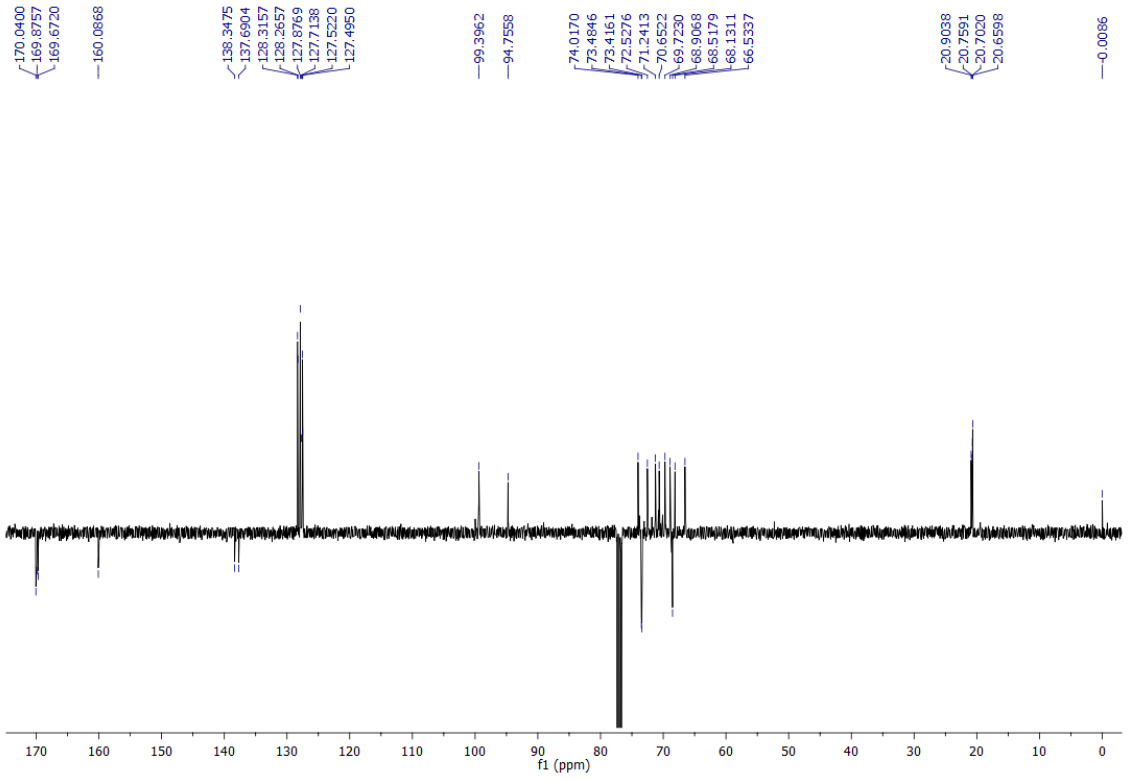

^{1}H-NMR (400 MHz) spectrum of allyl 2,3,4-tri-*O*-acetyl-6-*O*-benzyl-α-D-mannopyranosyl-(1→4)-2,3-di-*O*-acetyl-6-*O*-benzyl-α-D-mannopyranosyl-(1→4)-2,3-di-*O*-acetyl-6-*O*-benzyl-α-D-mannopyranosyl-(1→4)-2,3-di-*O*-acetyl-6-*O*-benzyl-α-D-mannopyranoside (17)

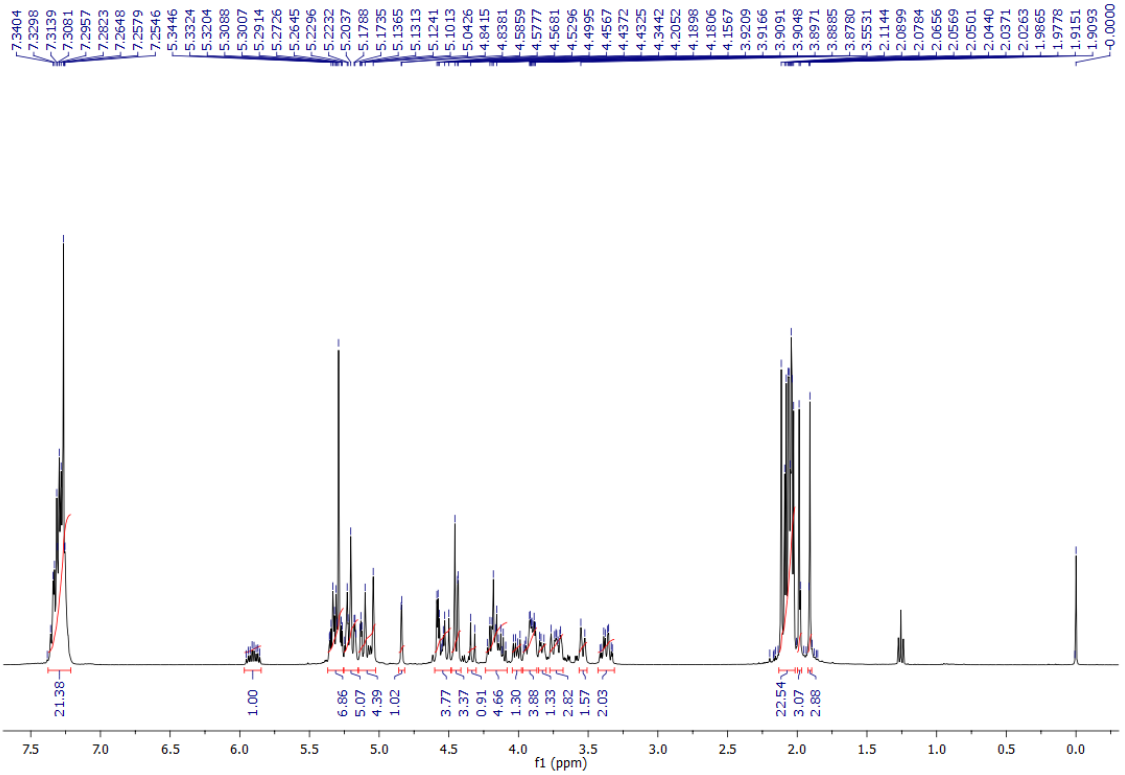

^{13}C-NMR (100.61 MHz) spectrum of allyl 2,3,4-tri-*O*-acetyl-6-*O*-benzyl-α-D-mannopyranosyl-(1→4)-2,3-di-*O*-acetyl-6-*O*-benzyl-α-D-mannopyranosyl-(1→4)-2,3-di-*O*-acetyl-6-*O*-benzyl-α-D-mannopyranosyl-(1→4)-2,3-di-*O*-acetyl-6-*O*-benzyl-α-D-mannopyranoside (17)

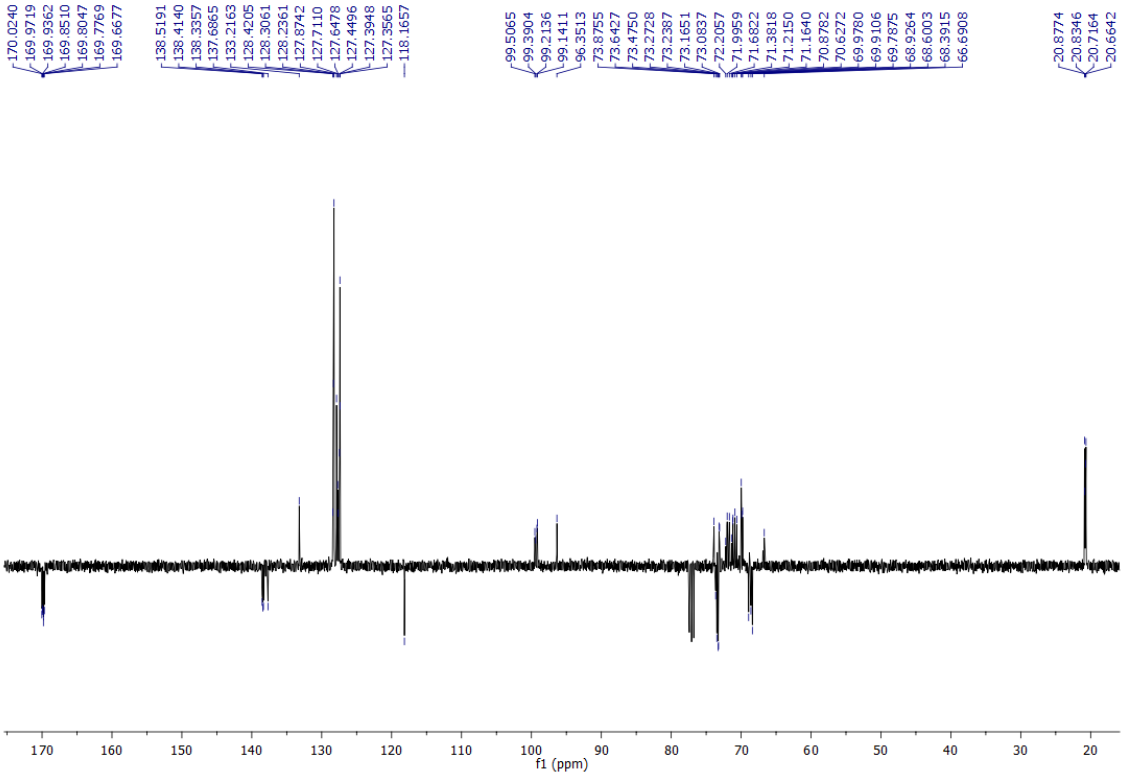

^{1}H-NMR (400 MHz) spectrum of allyl 6-*O*-benzyl-α-D-mannopyranosyl-(1→4)-6-*O*-benzyl-α-D-mannopyranosyl-(1→4)-6-*O*-benzyl-α-D-mannopyranosyl-(1→4)-6-*O*-benzyl-α-D-mannopyranoside (18)

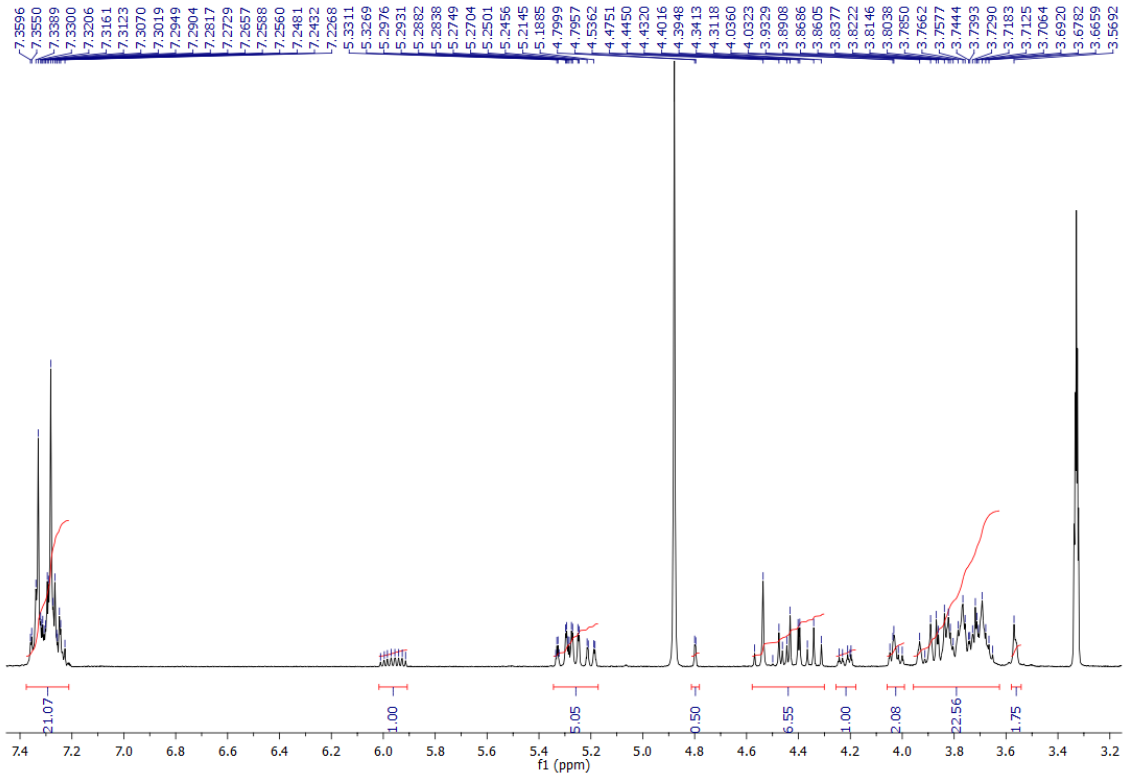

^{13}C-NMR (100.61 MHz) spectrum of allyl 6-*O*-benzyl-α-D-mannopyranosyl-(1→4)-6-*O*-benzyl-α-D-mannopyranosyl-(1→4)-6-*O*-benzyl-α-D-mannopyranosyl-(1→4)-6-*O*-benzyl-α-D-mannopyranoside (18)

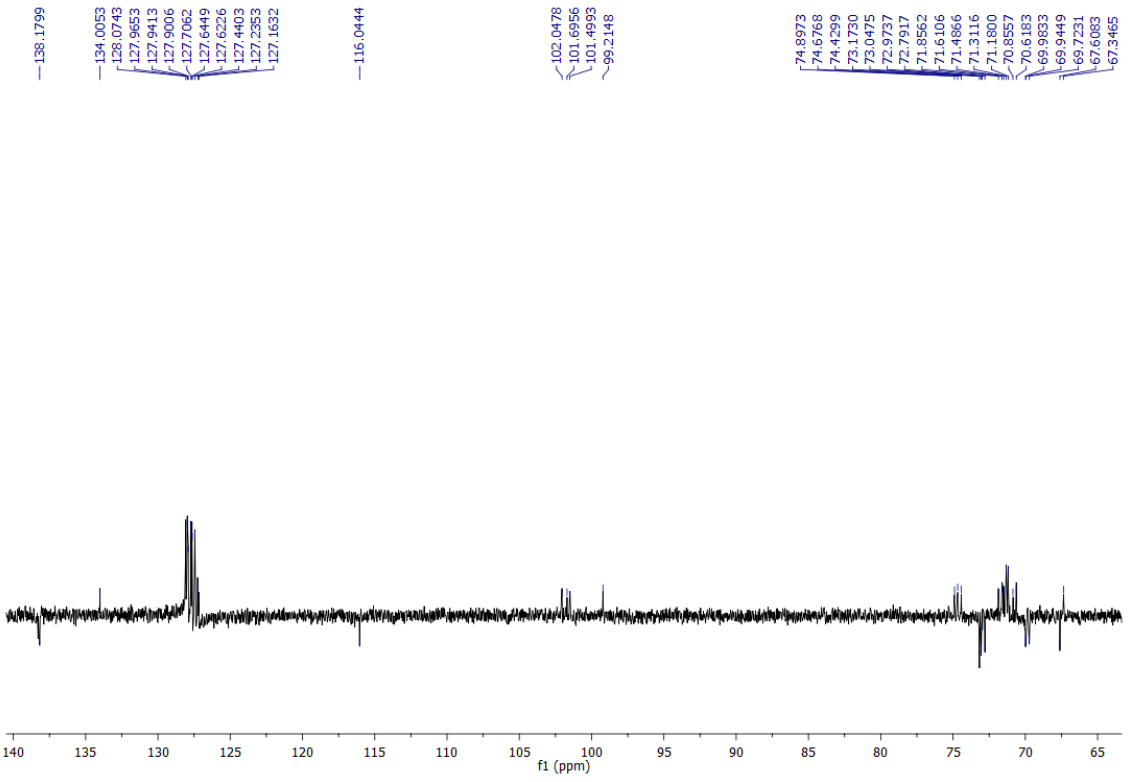

^{1}H-NMR (400 MHz) spectrum of propyl α-D-mannopyranosyl-(1→4)-α-D-mannopyranosyl-(1→4)-α-D-mannopyranosyl-(1→4)-α-D-mannopyranoside (1)

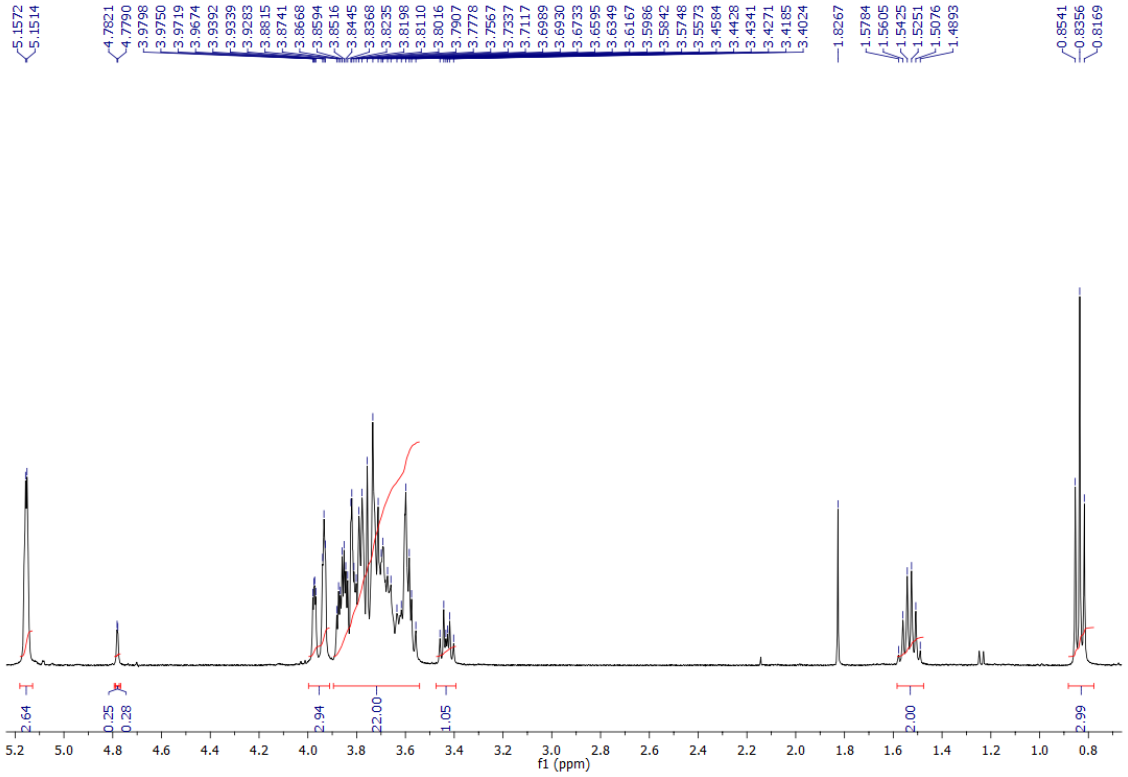

^{13}C-NMR (100.61 MHz) spectrum of propyl α-D-mannopyranosyl-(1→4)-α-D-mannopyranosyl-(1→4)-α-D-mannopyranosyl-(1→4)-α-D-mannopyranoside (1)

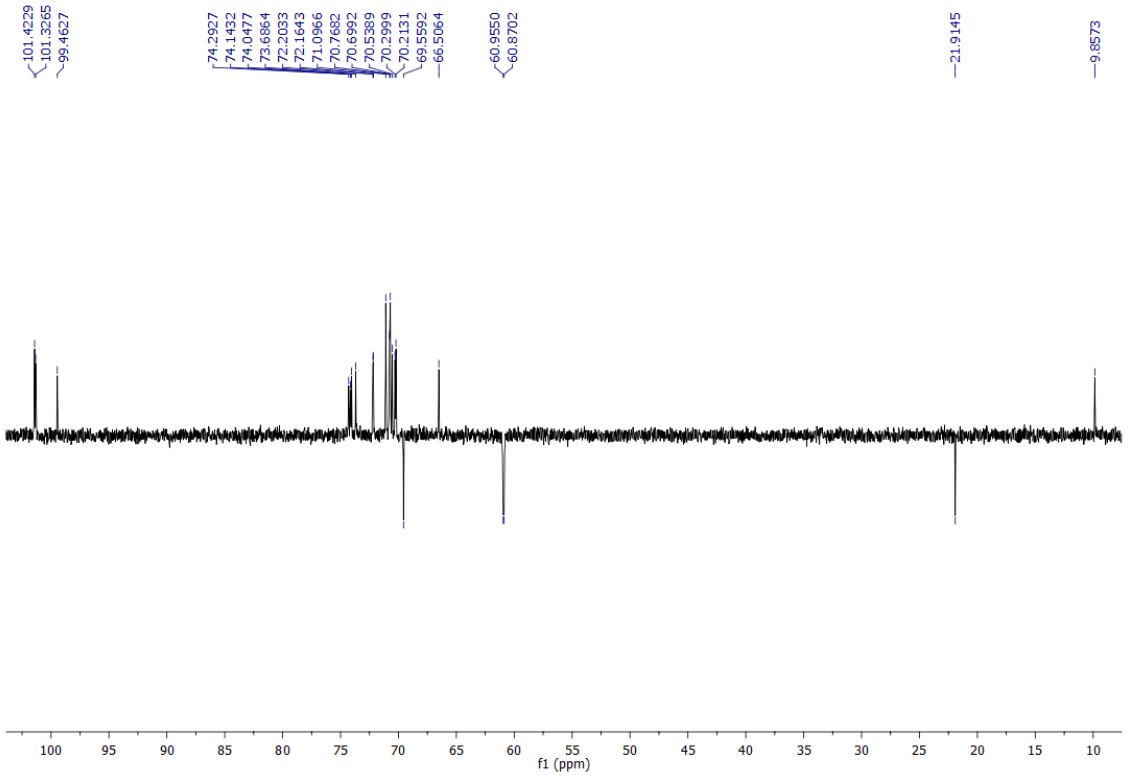

^{1}H-NMR (400 MHz) spectrum of allyl 2,3,4-tri-*O*-acetyl-6-*O*-benzyl-α-D-mannopyranosyl-(1→4)-2,3-di-*O*-acetyl-6-*O*-benzyl-α-D-mannopyranosyl-(1→4)-2,3-di-*O*-acetyl-6-*O*-benzyl-α-D-mannopyranose (19)

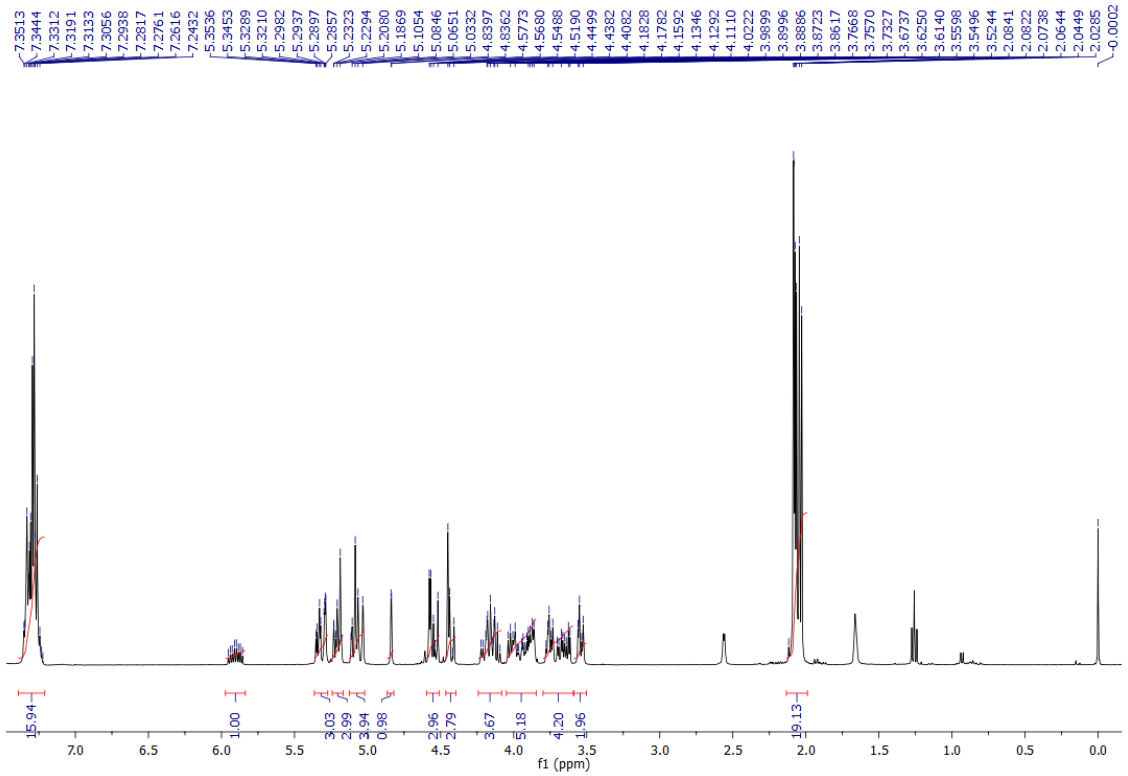

^{13}C-NMR (100.61 MHz) spectrum of allyl 2,3,4-tri-*O*-acetyl-6-*O*-benzyl-α-D-mannopyranosyl-(1→4)-2,3-di-*O*-acetyl-6-*O*-benzyl-α-D-mannopyranosyl-(1→4)-2,3-di-*O*-acetyl-6-*O*-benzyl-α-D-mannopyranose (19)

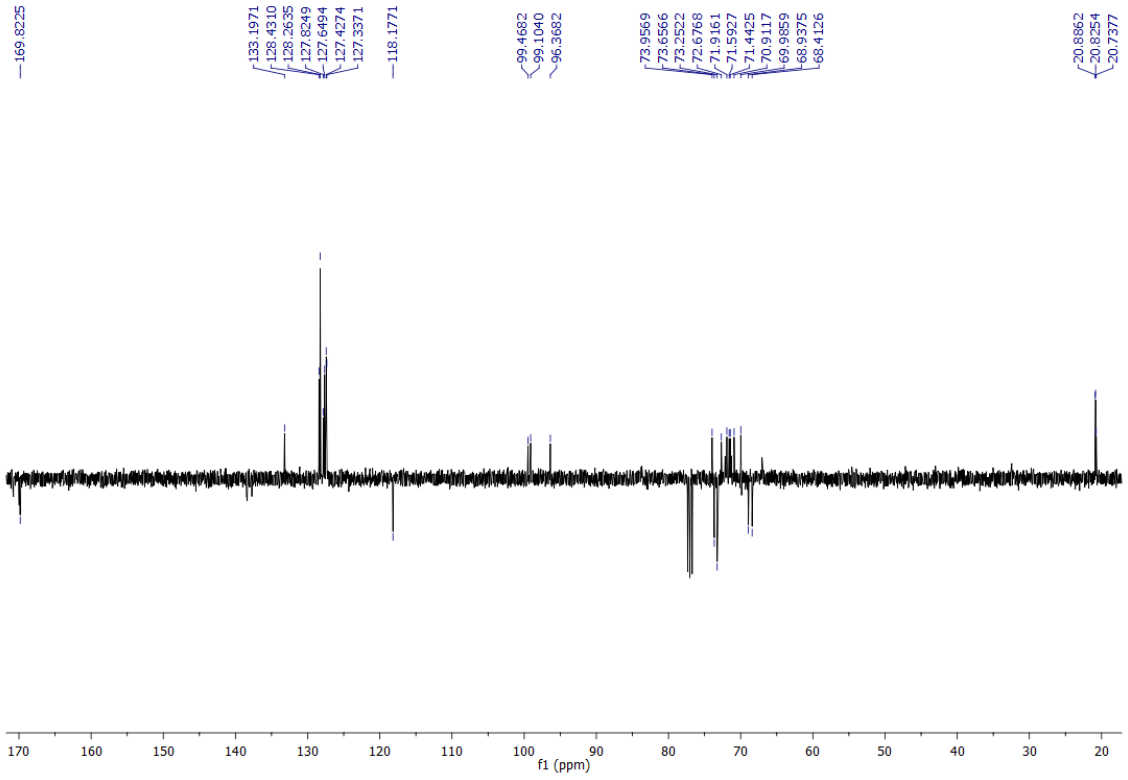

^{1}H-NMR (400 MHz) spectrum of allyl 6-O-benzyl-α-D-mannopyranosyl-(1→4)-6-O-benzyl-α-D-mannopyranosyl-(1→4)-6-O-benzyl-α-D-mannopyranoside (20)

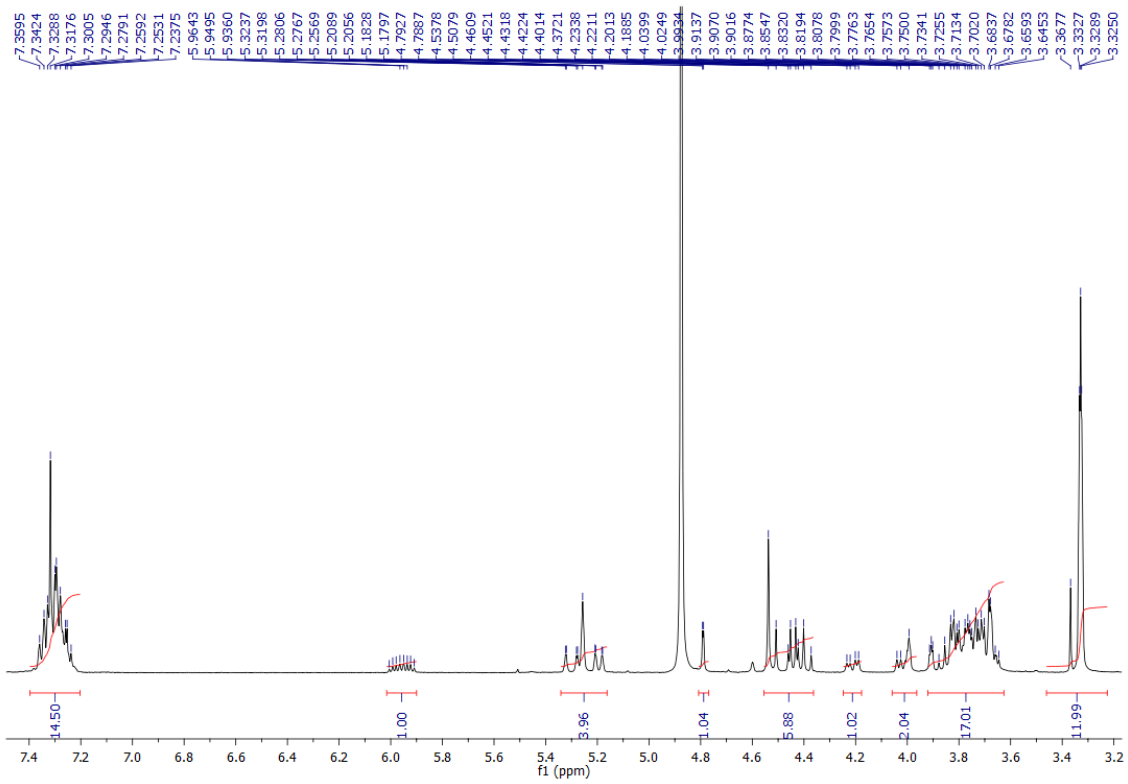

^{13}C-NMR (100.61 MHz) spectrum of allyl 6-O-benzyl-α-D-mannopyranosyl-(1→4)-6-O-benzyl-α-D-mannopyranosyl-(1→4)-6-O-benzyl-α-D-mannopyranoside (20)

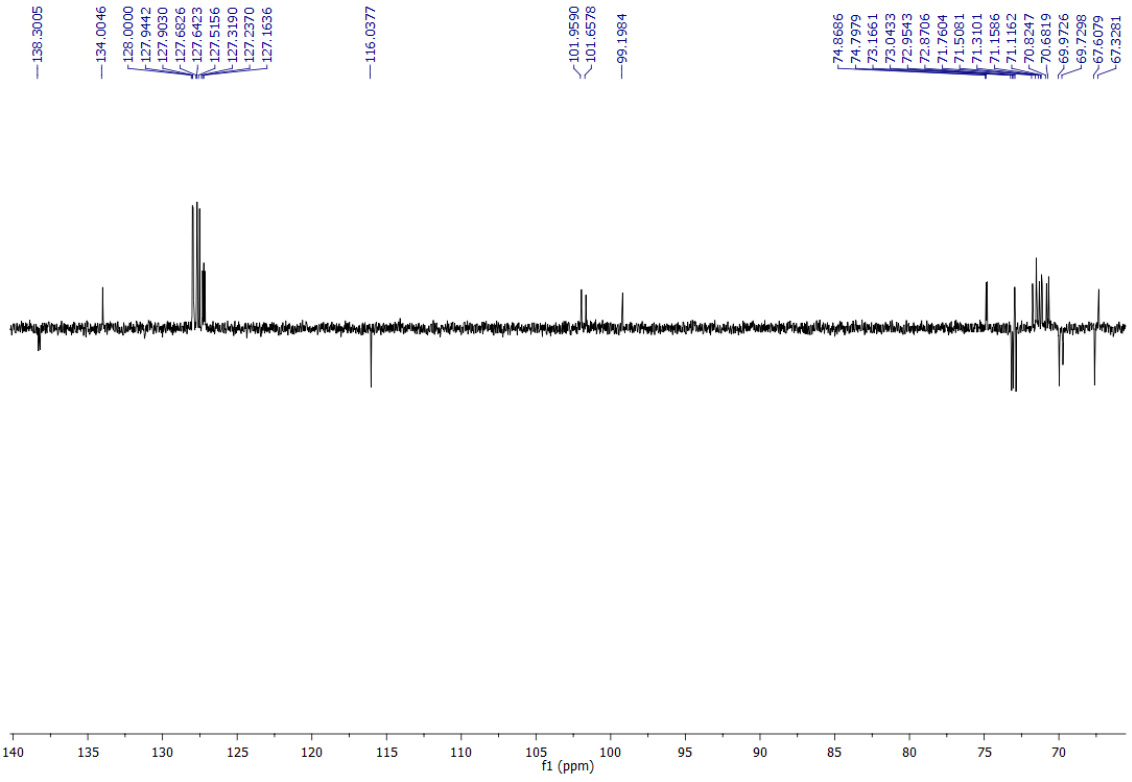

^{1}H-NMR (400 MHz) spectrum of propyl-α-D-mannopyranosyl-(1→4)-α-D-mannopyranosyl-(1→4)-α-D-mannopyranoside (2)

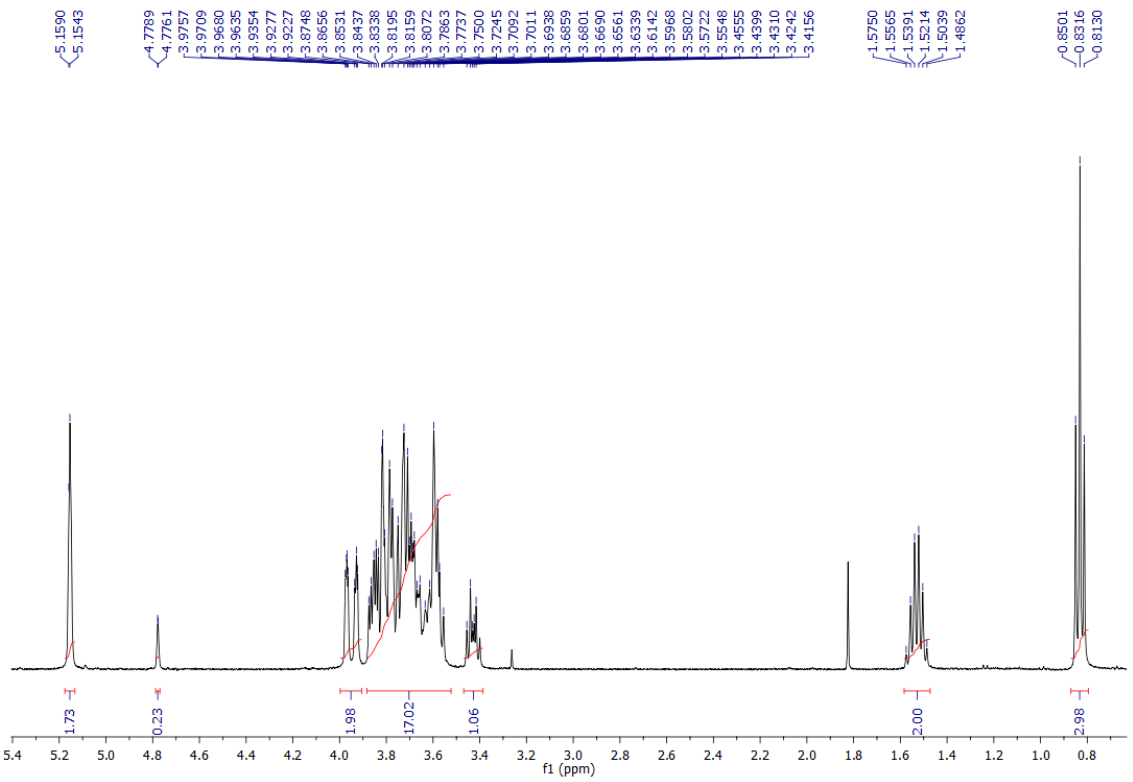

^{13}C-NMR (100.61 MHz) spectrum of propyl-α-D-mannopyranosyl-(1→4)-α-D-mannopyranosyl-(1→4)-α-D-mannopyranoside (2)

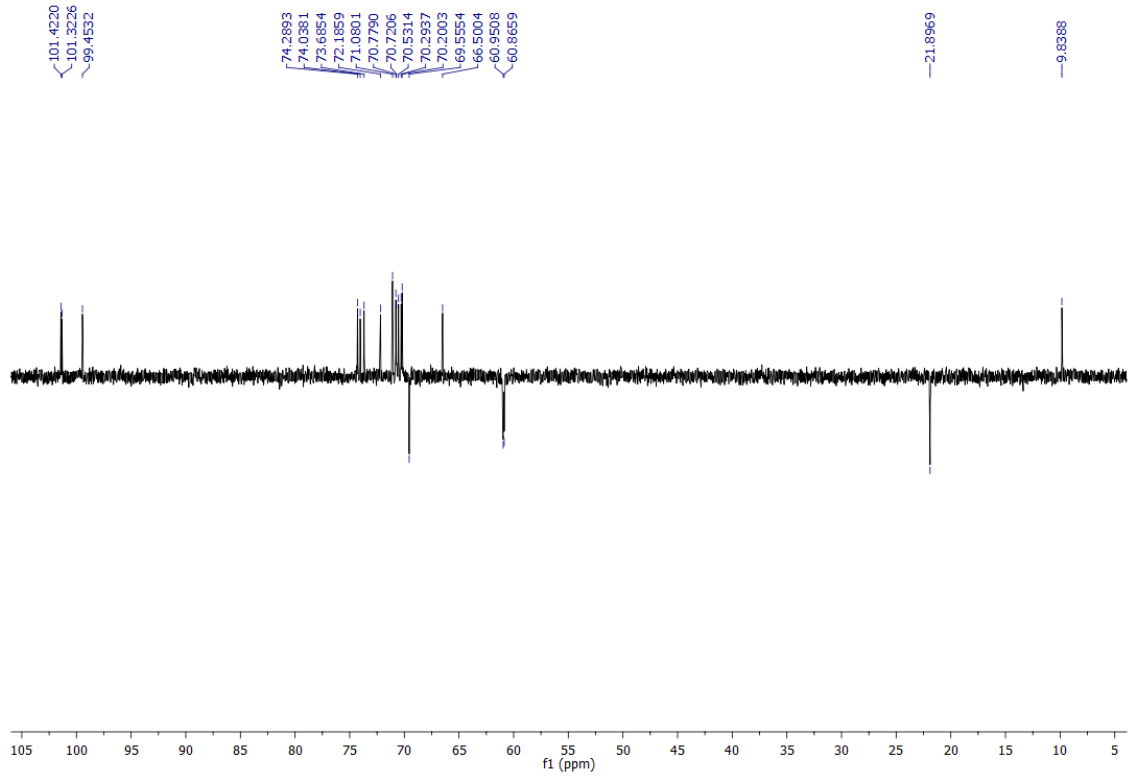

^{1}H-NMR (400 MHz) spectrum of allyl 2-*O*-acetyl-6-*O*-benzyl-4-*O*-*tert*-butyldimethylsilyl-3-*O*-methyl-α-D-mannopyranoside (24)

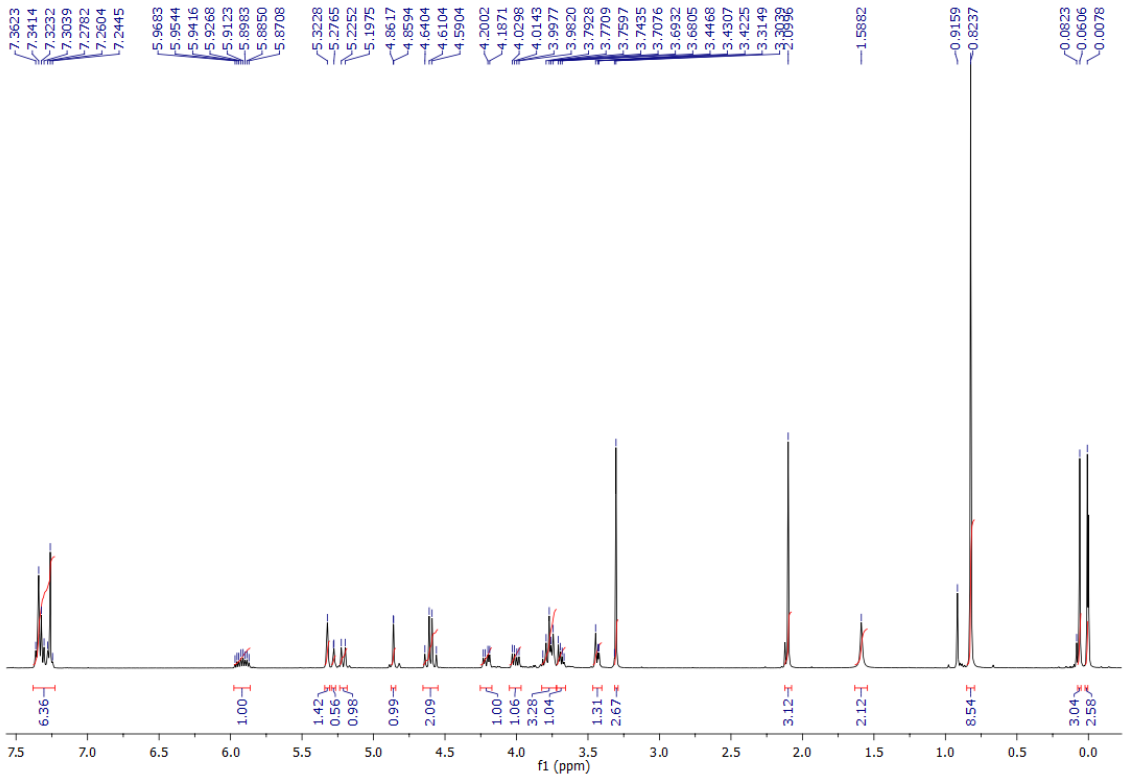

^{13}C-NMR (100.61 MHz) spectrum of allyl 2-*O*-acetyl-6-*O*-benzyl-4-*O*-*tert*-butyldimethylsilyl-3-*O*-methyl-α-D-mannopyranoside (24)

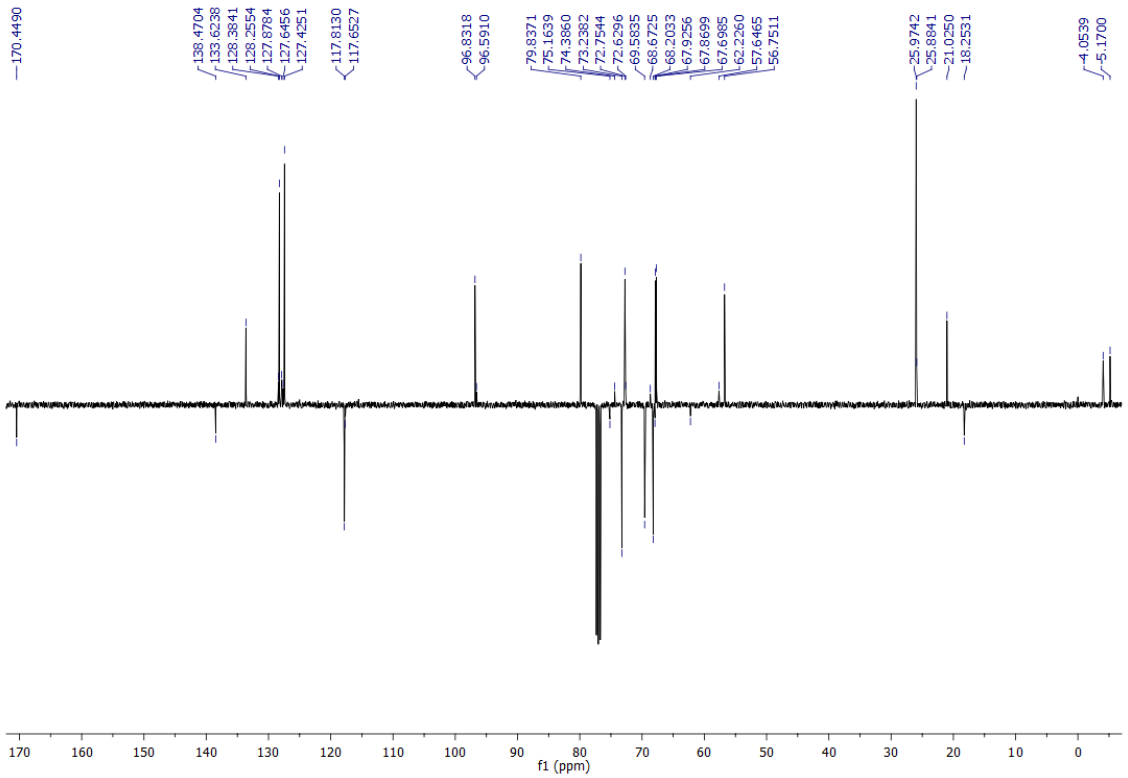

^{1}H-NMR (400 MHz) spectrum of 2-*O*-acetyl-6-*O*-benzyl-4-*O*-tert-butyldimethylsilyl-3-*O*-methyl-α-D-mannopyranoside (25)

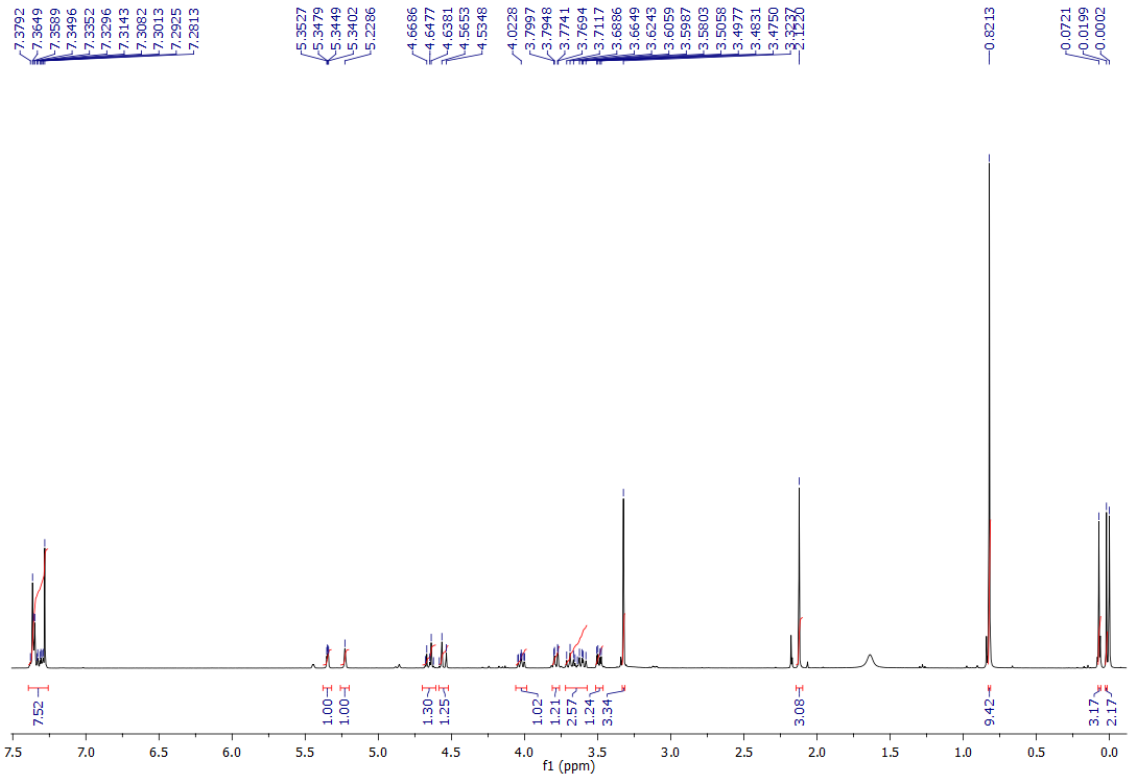

^{13}C-NMR (100.61 MHz) spectrum of 2-*O*-acetyl-6-*O*-benzyl-4-*O*-tert-butyldimethylsilyl-3-*O*-methyl-α-D-mannopyranoside (25)

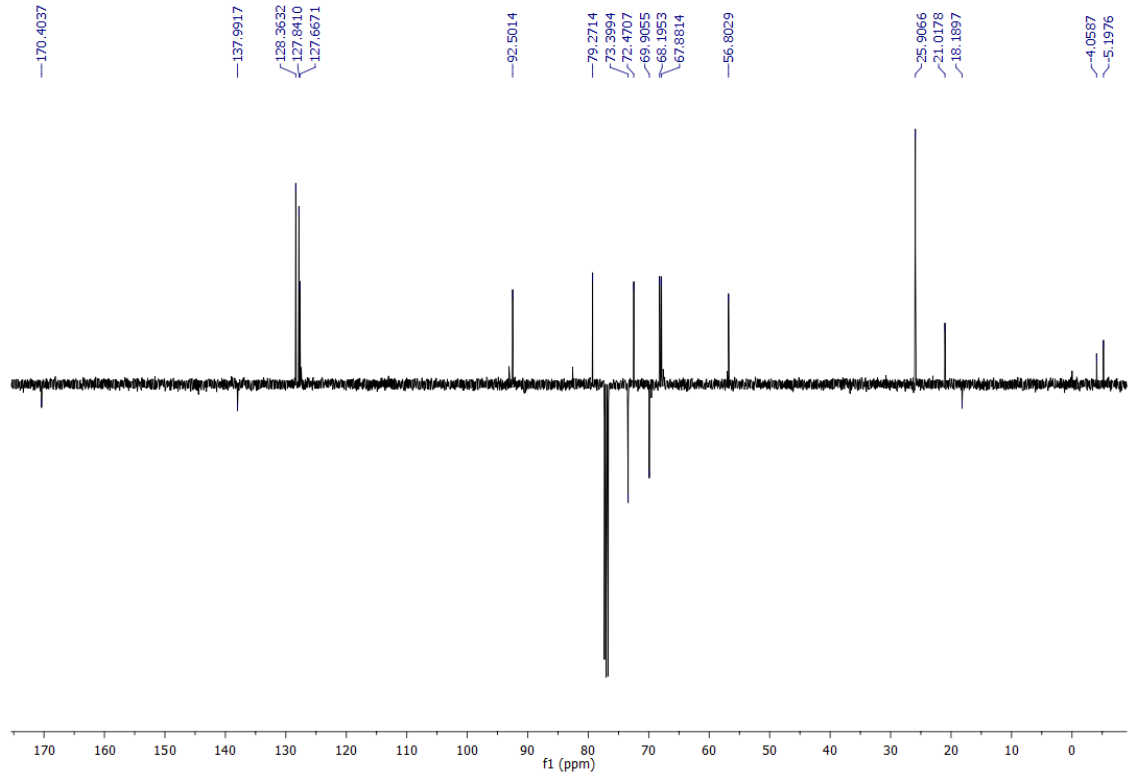

^{1}H-NMR (400 MHz) spectrum of 2-*O*-acetyl-6-*O*-benzyl-4-*O*-*tert*-butyldimethylsilyl-3-*O*-methyl-α-D-mannopyranoside trichloroacetamidate (26)

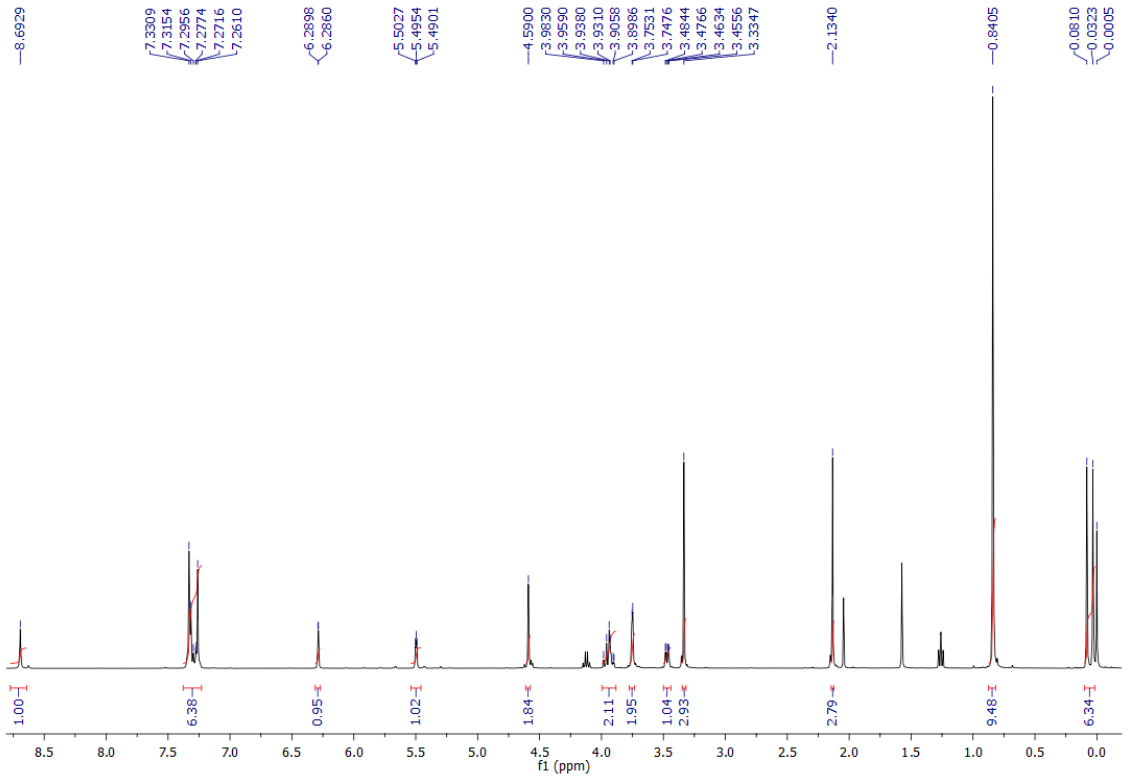

^{13}C-NMR (100.61 MHz) spectrum of 2-*O*-acetyl-6-*O*-benzyl-4-*O*-*tert*-butyldimethylsilyl-3-*O*-methyl-α-D-mannopyranoside trichloroacetamidate (26)

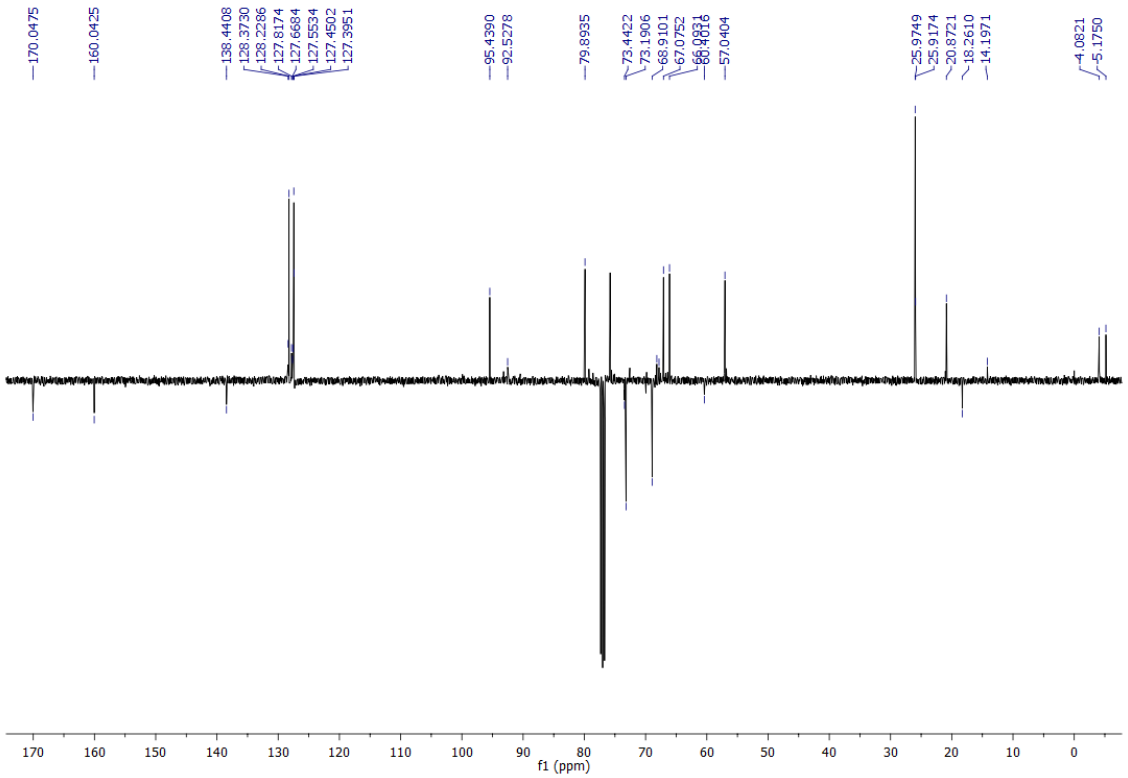

^{1}H-NMR (400 MHz) spectrum of allyl 2-*O*-acetyl-6-*O*-benzyl-3-*O*-methyl-α-D-mannopyranosyl-(1→4)-2-*O*-acetyl-6-*O*-benzyl-3-*O*-methyl-α-D-mannopyranoside (30)

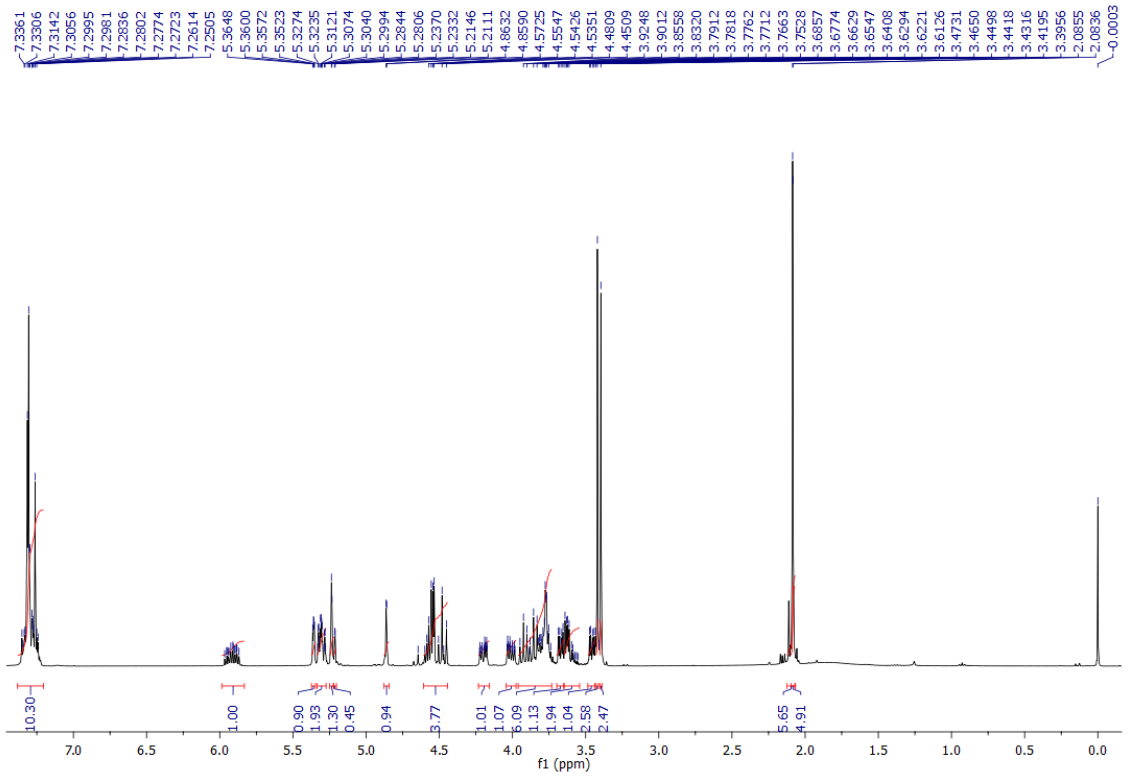

^{13}C-NMR (100.61 MHz) spectrum of allyl 2-*O*-acetyl-6-*O*-benzyl-3-*O*-methyl-α-D-mannopyranosyl-(1→4)-2-*O*-acetyl-6-*O*-benzyl-3-*O*-methyl-α-D-mannopyranoside (30)

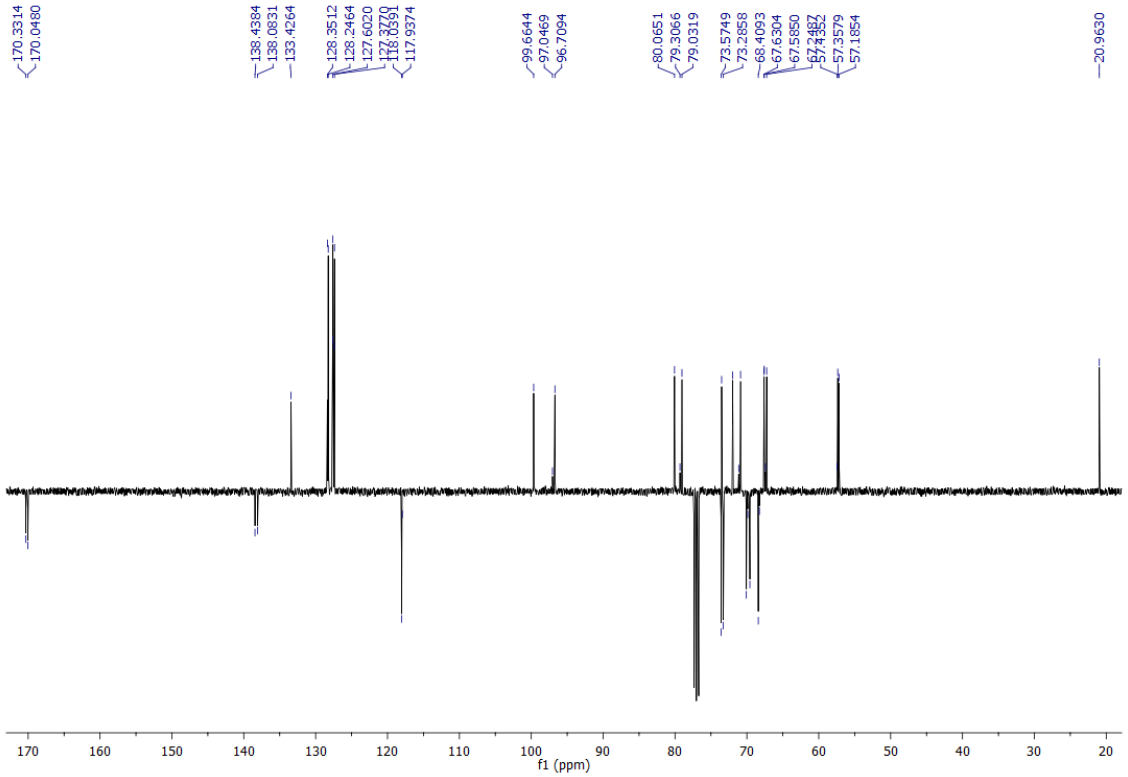

^{1}H-NMR (400 MHz) spectrum of 2,4-Di-*O*-acetyl-6-*O*-benzyl-3-*O*-methyl-α-D-mannopyranosyl-(1→4)-2-*O*-acetyl-6-*O*-benzyl-3-*O*-methyl-α-D-mannopyranosyl trichloroacetamidate (33)

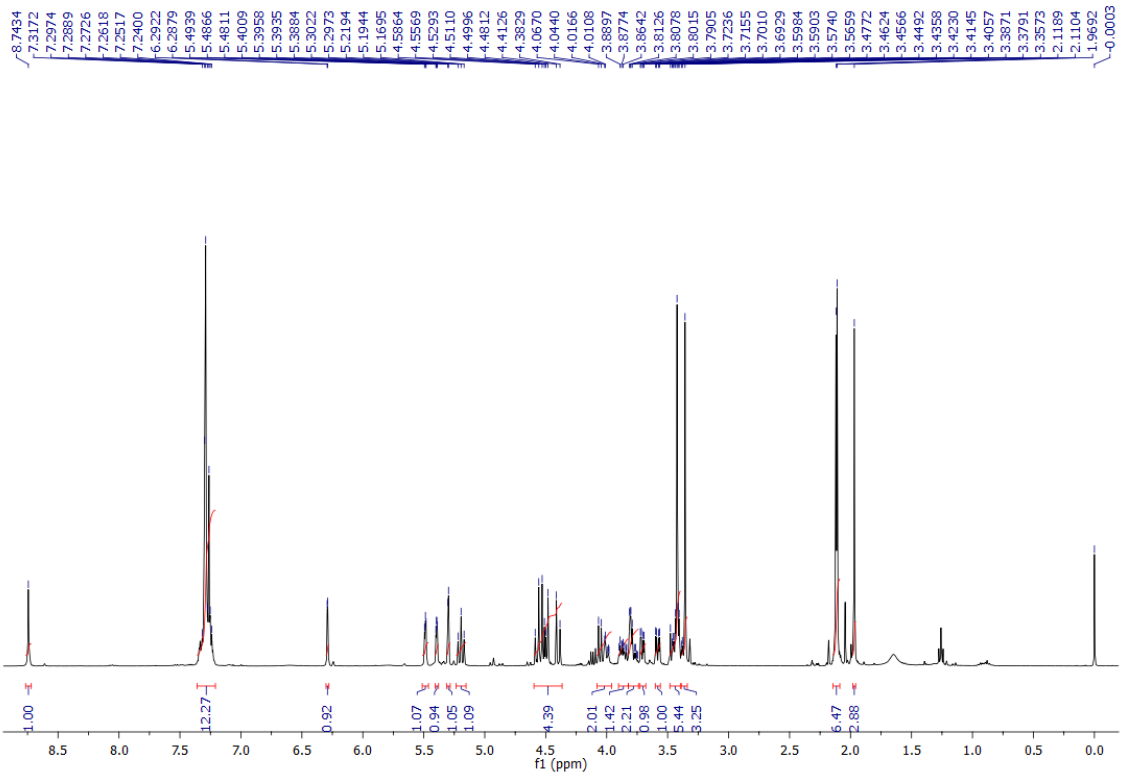

^{13}C-NMR (100.61 MHz) spectrum of 2,4-Di-*O*-acetyl-6-*O*-benzyl-3-*O*-methyl-α-D-mannopyranosyl-(1→4)-2-*O*-acetyl-6-*O*-benzyl-3-*O*-methyl-α-D-mannopyranosyl trichloroacetamidate (33)

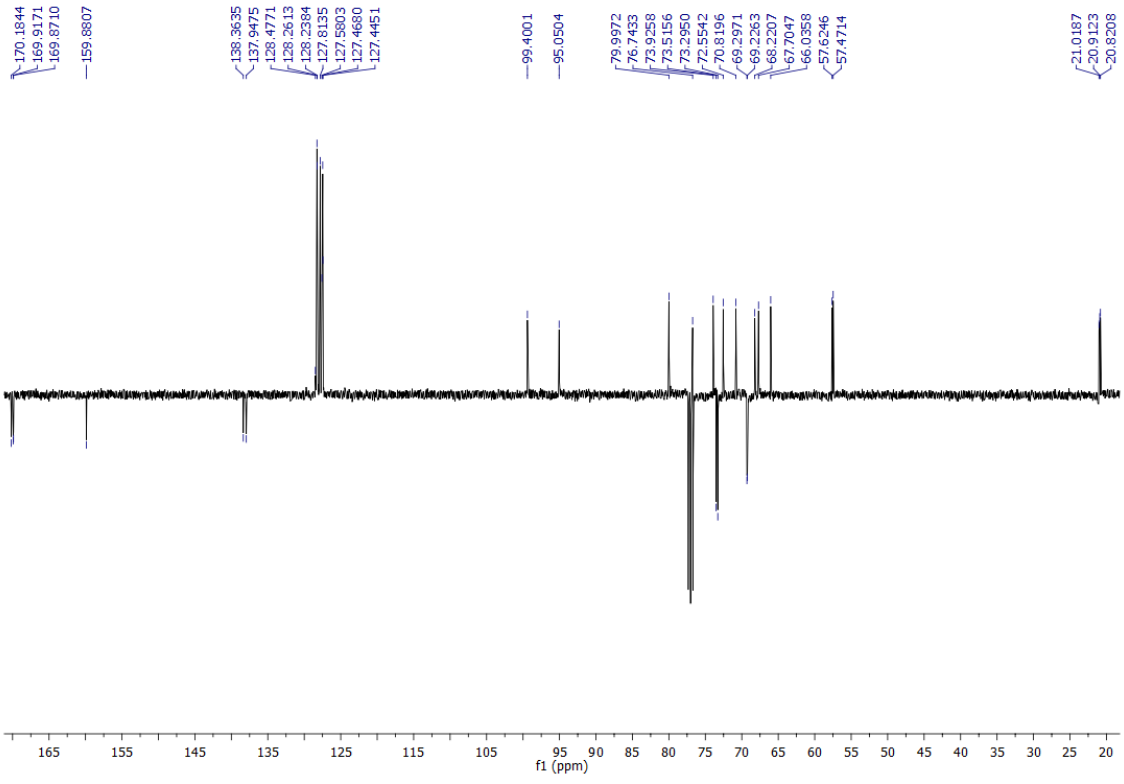

^{1}H-NMR (400 MHz) spectrum of allyl 2,4-di-*O*-acetyl-6-*O*-benzyl-3-*O*-methyl-α-D-mannopyranosyl-(1→4)-2-*O*-acetyl-6-*O*-benzyl-3-*O*-methyl-α-D-mannopyranosyl-(1→4)-2-*O*-acetyl-6-*O*-benzyl-3-*O*-methyl-α-D-mannopyranosyl-(1→4)-2-*O*-acetyl-6-*O*-benzyl-3-*O*-methyl-α-D-mannopyranoside (34)

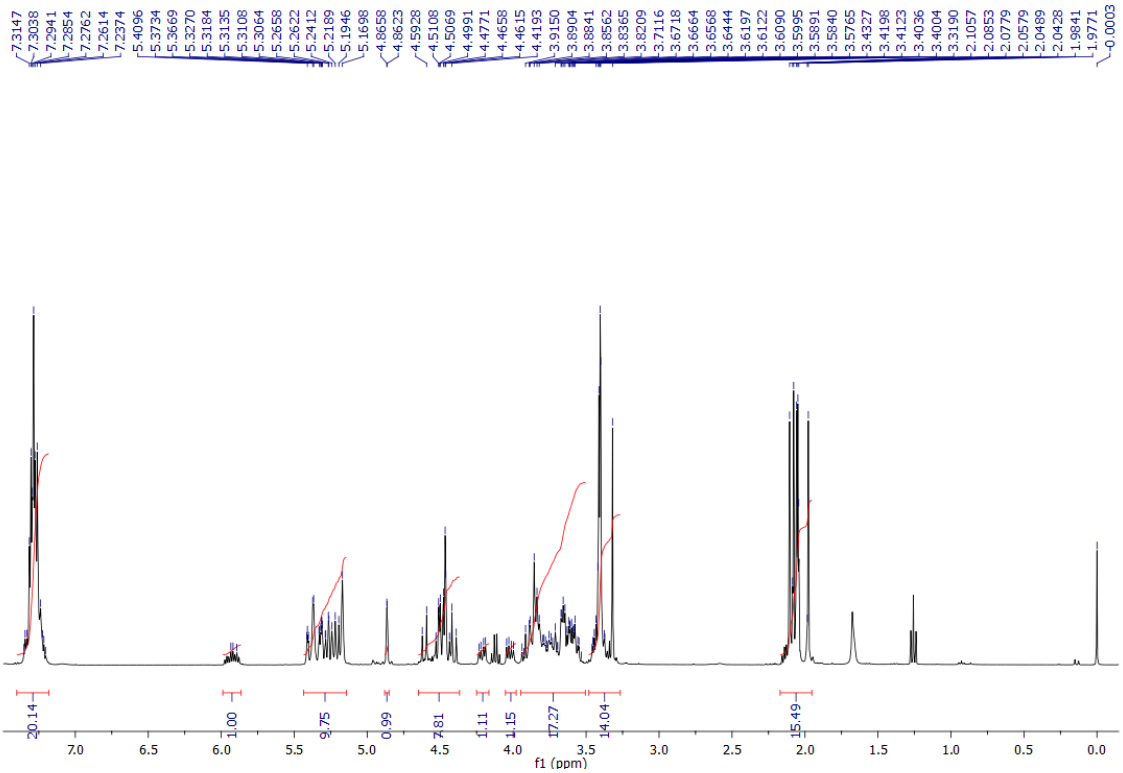

^{13}C-NMR (100.61 MHz) spectrum of allyl 2,4-di-*O*-acetyl-6-*O*-benzyl-3-*O*-methyl-α-D-mannopyranosyl-(1→4)-2-*O*-acetyl-6-*O*-benzyl-3-*O*-methyl-α-D-mannopyranosyl-(1→4)-2-*O*-acetyl-6-*O*-benzyl-3-*O*-methyl-α-D-mannopyranosyl-(1→4)-2-*O*-acetyl-6-*O*-benzyl-3-*O*-methyl-α-D-mannopyranoside (34)

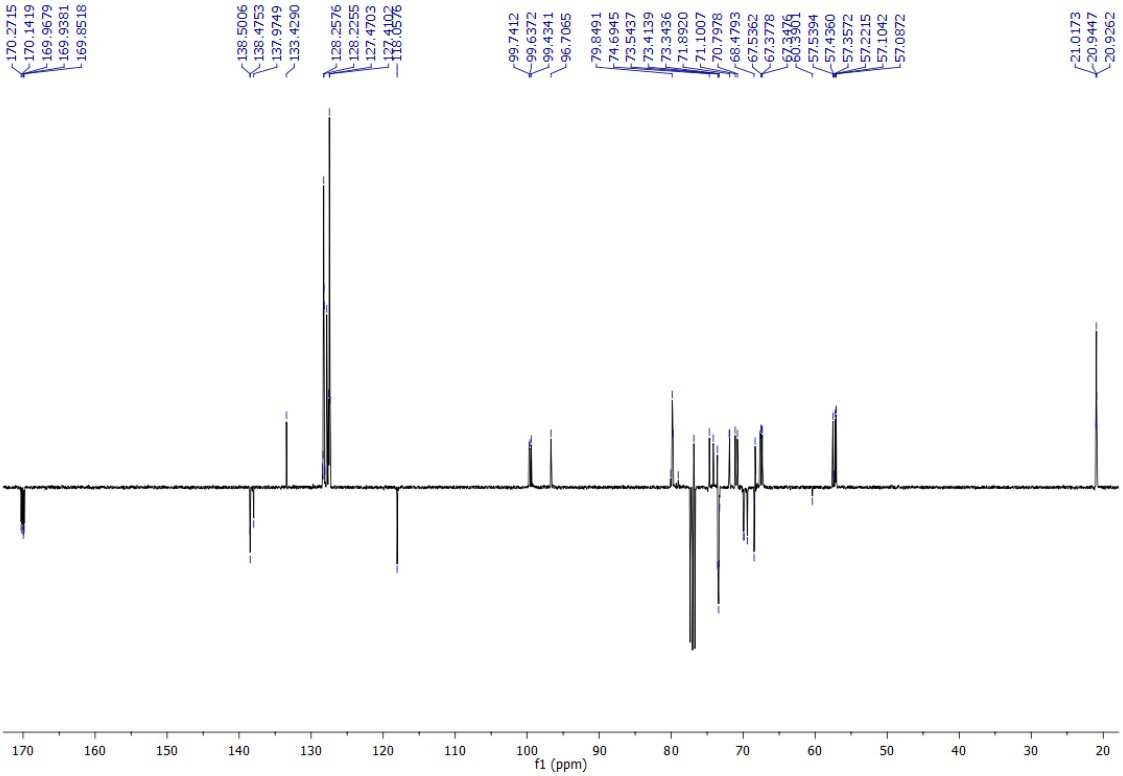

^{1}H-NMR (400 MHz) spectrum of allyl 6-*O*-benzyl-3-*O*-methyl-α-D-mannopyranosyl-(1→4)-6-*O*-benzyl-3-*O*-methyl-α-D-mannopyranosyl-(1→4)-6-*O*-benzyl-3-*O*-methyl-α-D-mannopyranosyl-(1→4)-6-*O*-benzyl-3-*O*-methyl-α-D-mannopyranoside (35)

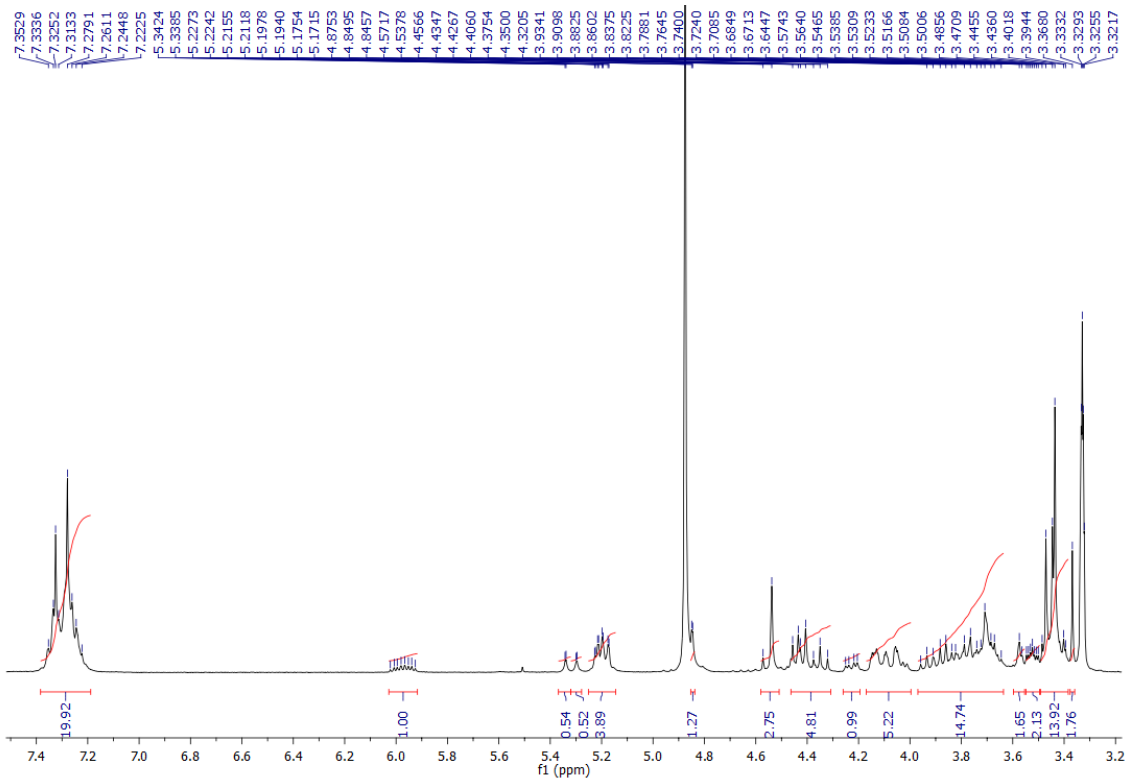

^{13}C-NMR (100.61 MHz) spectrum of allyl 6-*O*-benzyl-3-*O*-methyl-α-D-mannopyranosyl-(1→4)-6-*O*-benzyl-3-*O*-methyl-α-D-mannopyranosyl-(1→4)-6-*O*-benzyl-3-*O*-methyl-α-D-mannopyranosyl-(1→4)-6-*O*-benzyl-3-*O*-methyl-α-D-mannopyranoside (35)

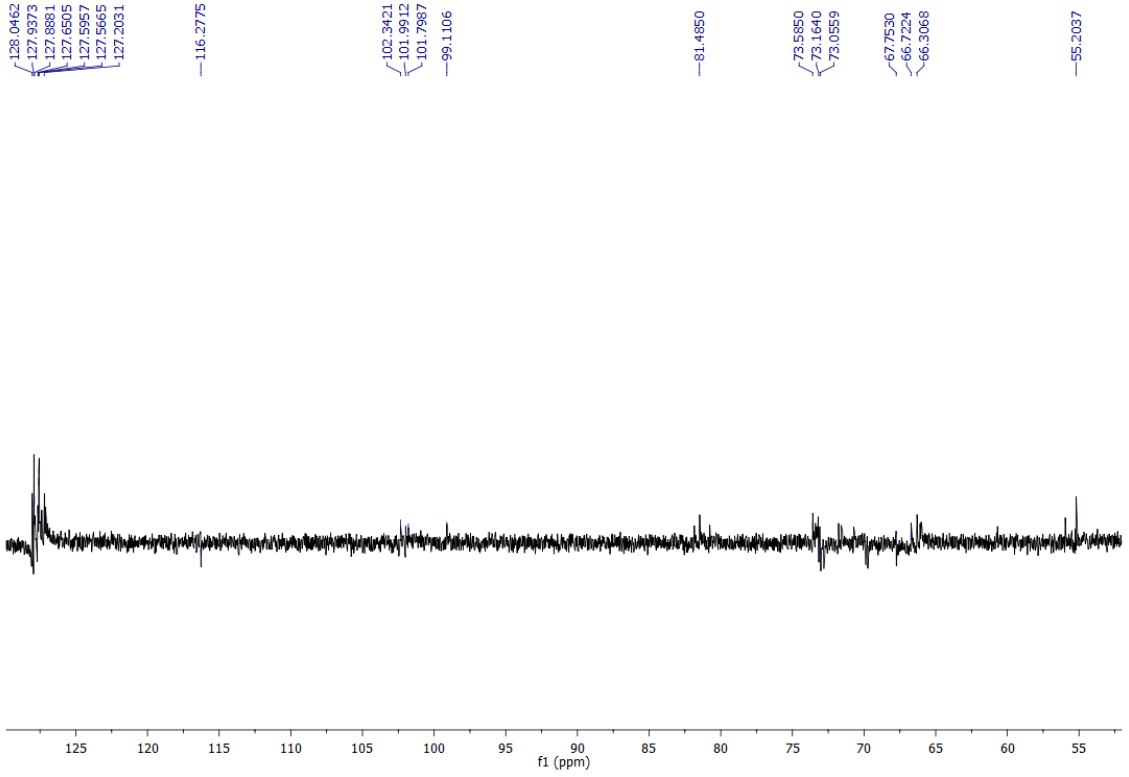

^{1}H-NMR (400 MHz) spectrum of propyl 3-*O*-methyl-α-D-mannopyranosyl-(1→4)-3-*O*-methyl-α-D-mannopyranosyl-(1→4)-3-*O*-methyl-α-D-mannopyranosyl-(1→4)-3-*O*-methyl-α-D-mannopyranoside (3)

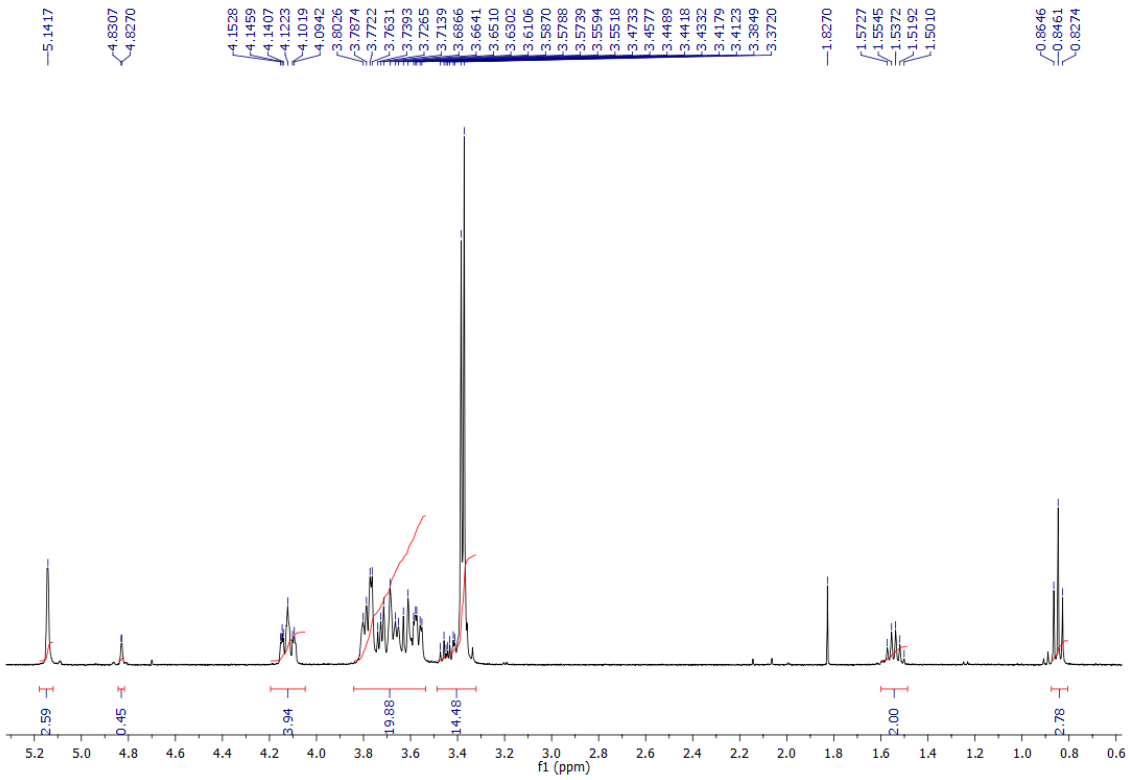

^{13}C-NMR (100.61 MHz) spectrum of propyl 3-*O*-methyl-α-D-mannopyranosyl-(1→4)-3-*O*-methyl-α-D-mannopyranosyl-(1→4)-3-*O*-methyl-α-D-mannopyranosyl-(1→4)-3-*O*-methyl-α-D-mannopyranoside (3)

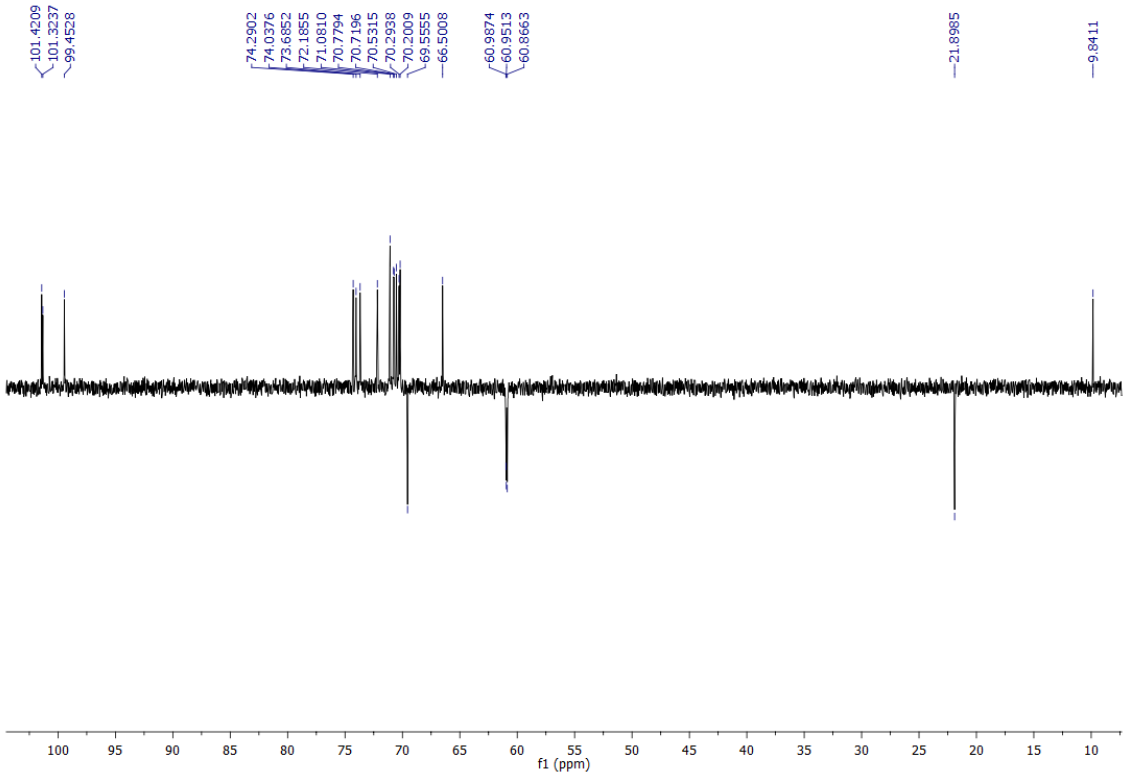

^{1}H-NMR (400 MHz) spectrum of allyl 2,4-di-*O*-acetyl-6-*O*-benzyl-3-*O*-methyl-α-D-mannopyranosyl-(1→4)-2-*O*-acetyl-6-*O*-benzyl-3-*O*-methyl-α-D-mannopyranosyl-(1→4)-2-*O*-acetyl-6-*O*-benzyl-3-*O*-methyl-α-D-mannopyranoside (36)

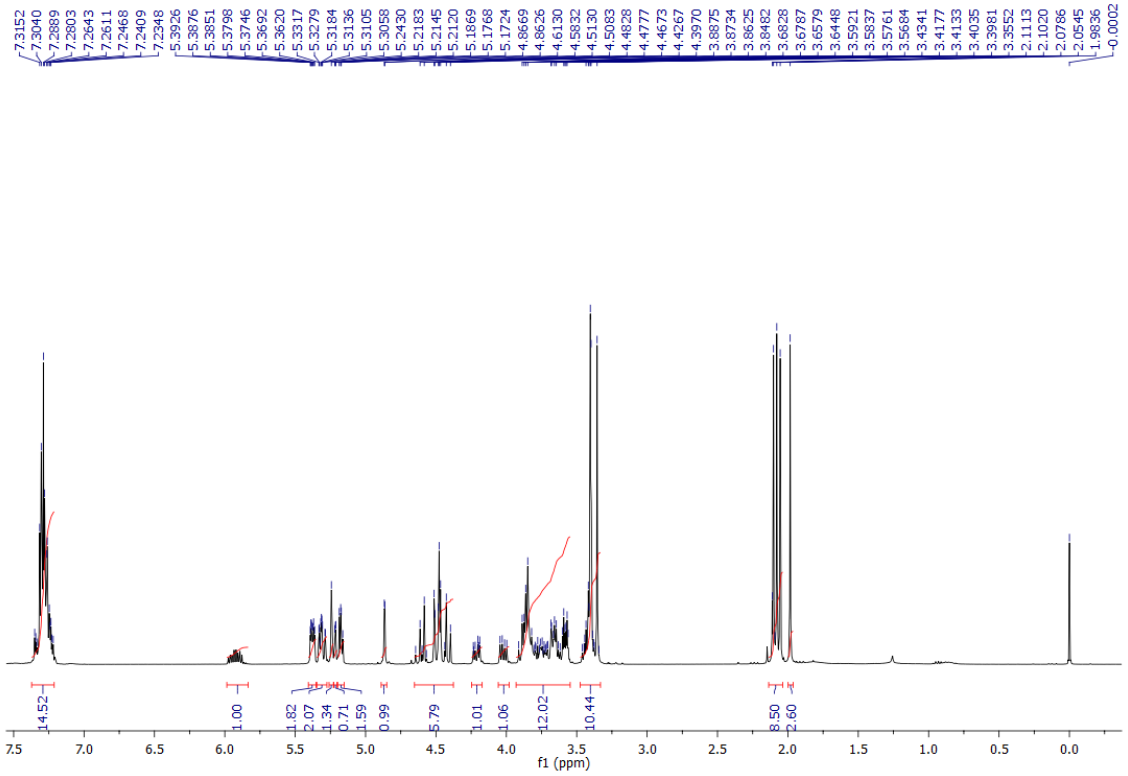

^{13}C-NMR (100.61 MHz) spectrum of allyl 2,4-di-*O*-acetyl-6-*O*-benzyl-3-*O*-methyl-α-D-mannopyranosyl-(1→4)-2-*O*-acetyl-6-*O*-benzyl-3-*O*-methyl-α-D-mannopyranosyl-(1→4)-2-*O*-acetyl-6-*O*-benzyl-3-*O*-methyl-α-D-mannopyranoside (36)

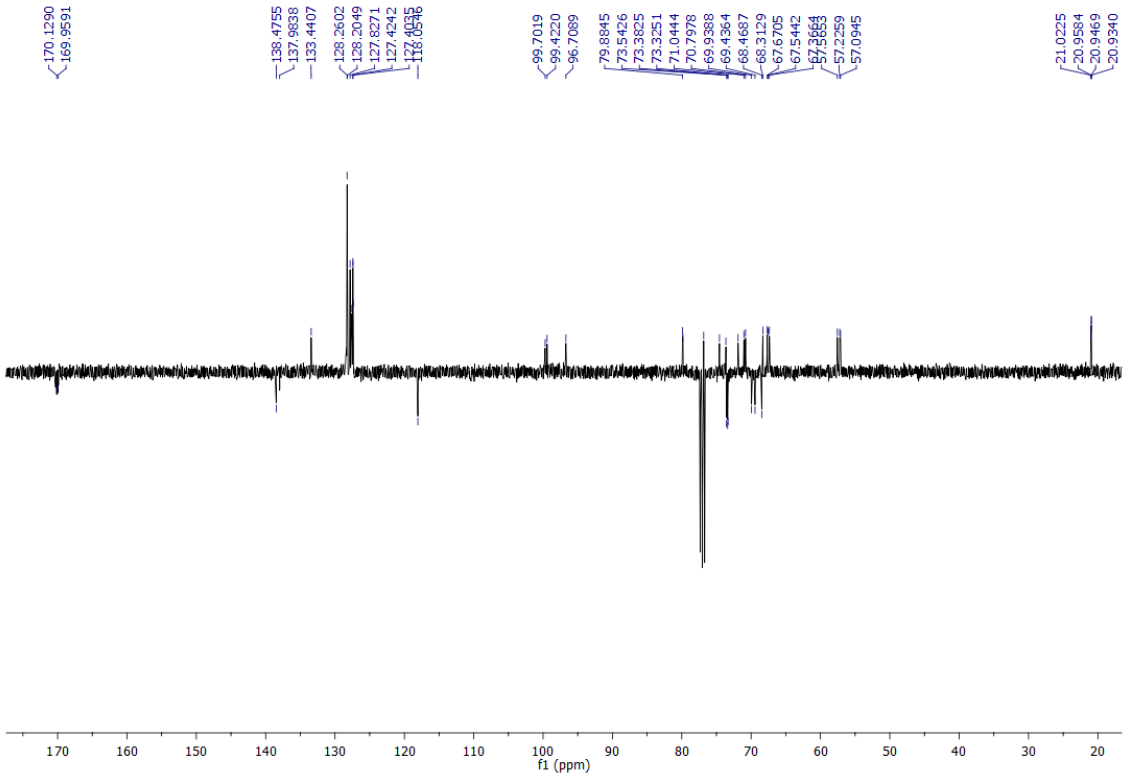

^{1}H-NMR (400 MHz) spectrum of allyl 6-*O*-benzyl-3-*O*-methyl-α-D-mannopyranosyl-(1→4)-6-*O*-benzyl-3-*O*-methyl-α-D-mannopyranosyl-(1→4)-6-*O*-benzyl-3-*O*-methyl-α-D-mannopyranoside (37)

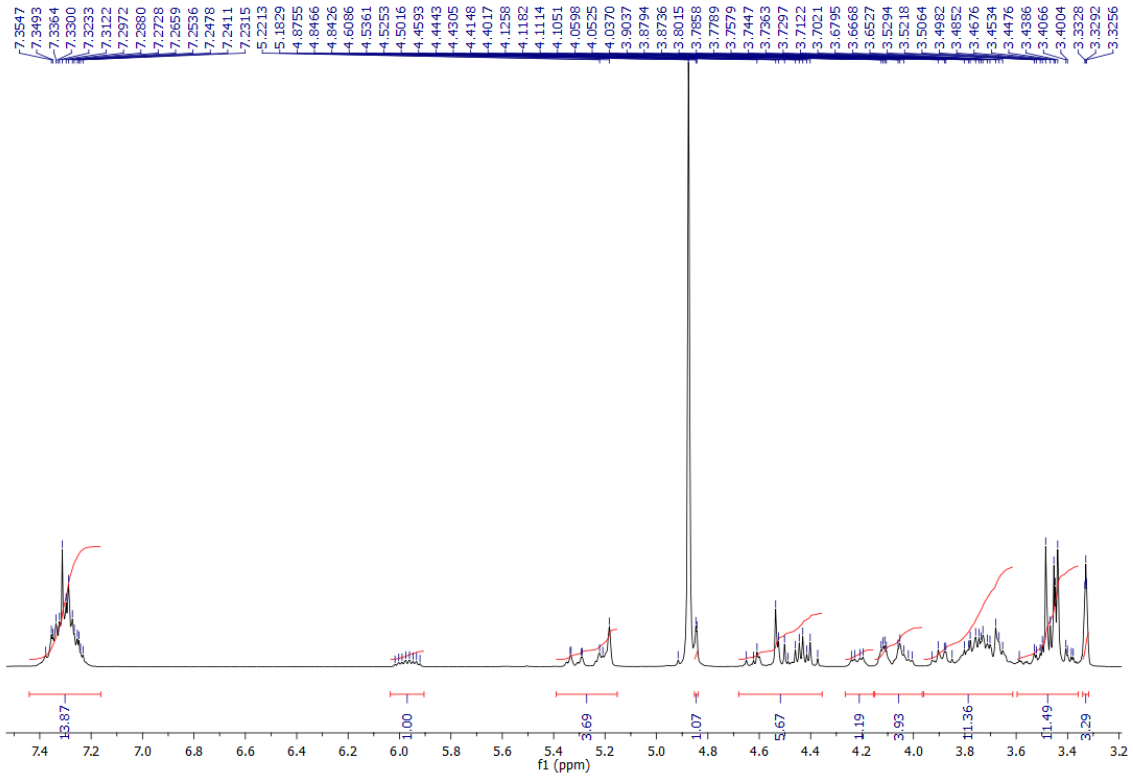

^{13}C-NMR (100.61 MHz) spectrum of allyl 6-*O*-benzyl-3-*O*-methyl-α-D-mannopyranosyl-(1→4)-6-*O*-benzyl-3-*O*-methyl-α-D-mannopyranosyl-(1→4)-6-*O*-benzyl-3-*O*-methyl-α-D-mannopyranoside (37)

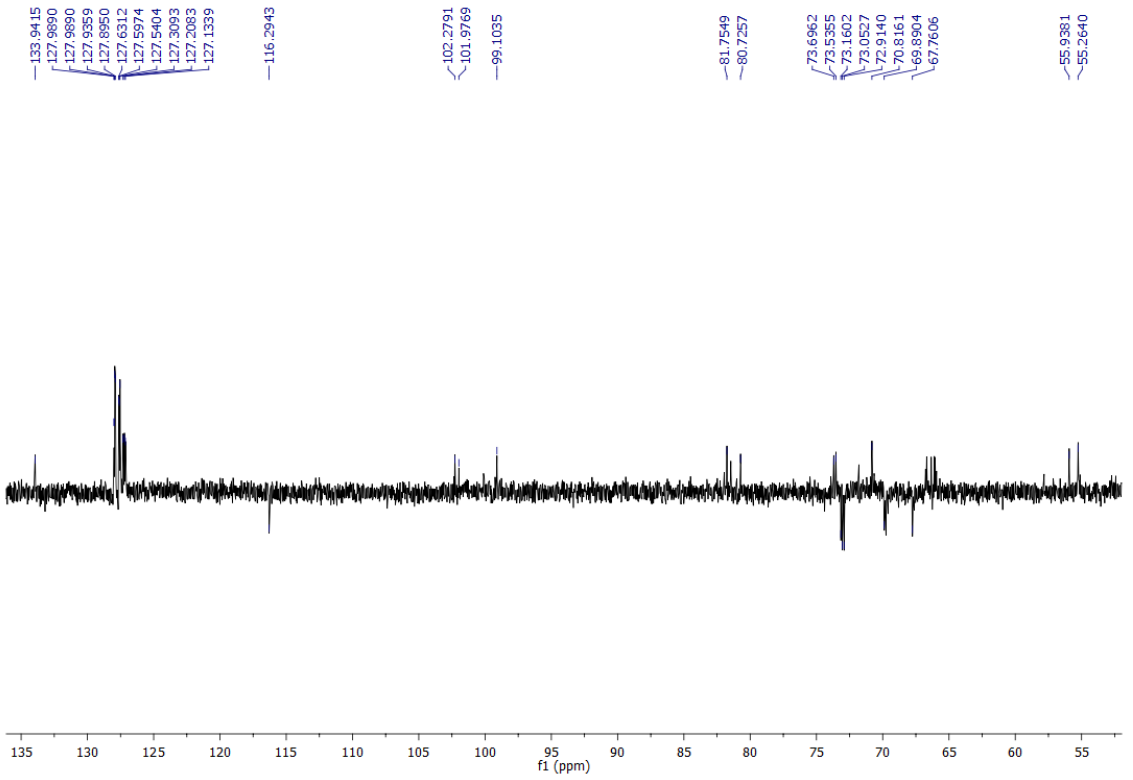

^{1}H-NMR (400 MHz) spectrum of propyl 3-*O*-methyl-α-D-mannopyranosyl-(1→4)-3-*O*-methyl-α-D-mannopyranosyl-(1→4)-3-*O*-methyl-α-D-mannopyranoside (4)

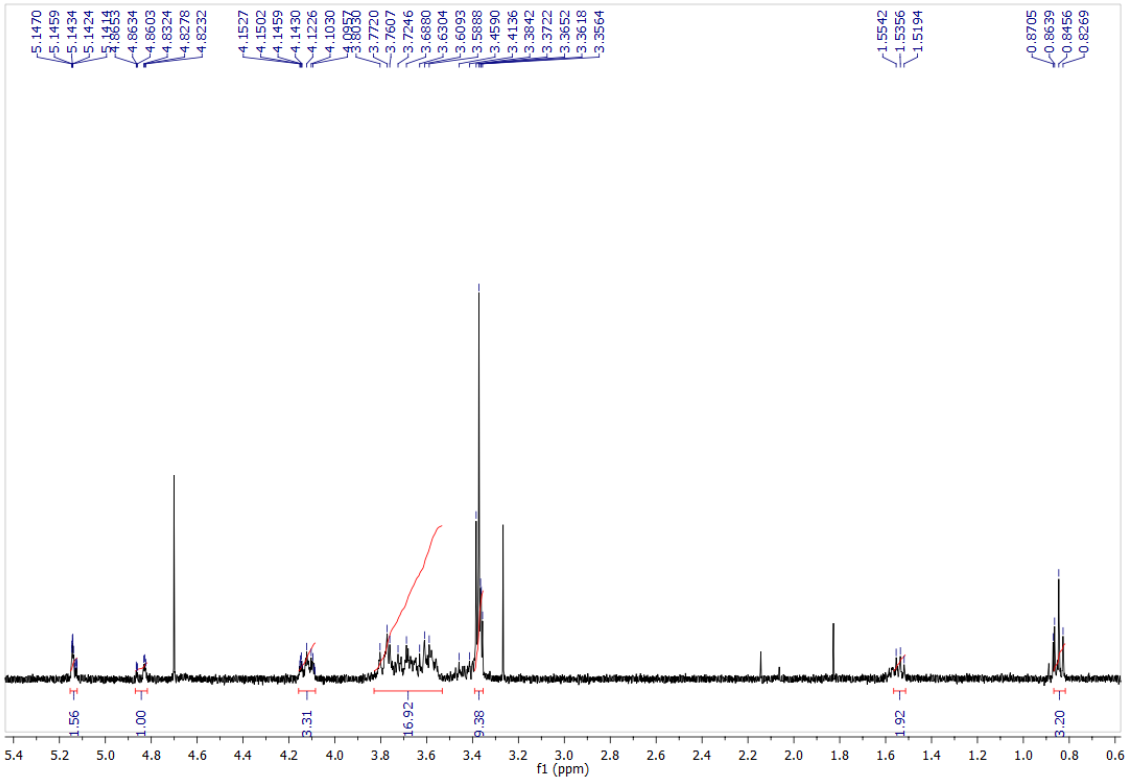

^{13}C-NMR (100.61 MHz) spectrum of propyl 3-*O*-methyl-α-D-mannopyranosyl-(1→4)-3-*O*-methyl-α-D-mannopyranosyl-(1→4)-3-*O*-methyl-α-D-mannopyranoside (4)